APRIL 2017

Ph.D in Civil Engineering

QAIS SAHIB BANYHUSSAN

UNIVERSITY OF GAZİANTEP

GRADUATE SCHOOL OF

NATURAL & APPLIED SCIENCES

DEVELOPMENT OF OPTIMAL DEFLECTION HARDENING CEMENTITIOUS COMPOSITES MIXTURE FOR HIGHWAY BRIDGE DECKS TO ADDRESS SHRINKAGE CRACKING PROBLEM

Ph.D THESIS

IN

CIVIL ENGINEERING

BY

QAIS SAHIB BANYHUSSAN

APRIL 2017

Development of Optimal Deflection Hardening Cementitious Composites Mixture for Highway Bridge Decks to Address Shrinkage Cracking Problem

Ph.D Thesis

in

Civil Engineering

University of Gaziantep

Supervisor

Prof. Dr. Mustafa GÜNAL

Co-Supervisor

Prof. Dr. Mustafa ŞAHMARAN

by

Qais Sahib BANYHUSSAN

April 2017

REPUBLIC OF TURKEY
UNIVERSITY OF GAZİANTEP
GRADUATE SCHOOL OF NATURAL & APPLIED SCIENCES
CIVIL ENGINEERING DEPARTMENT

Name of the thesis: Development of Optimal Deflection Hardening Cementitious Composites Mixture for Highway Bridge Decks to Address Shrinkage Cracking Problem

Name of the student: Qais Sahib BANYHUSSAN

Exam date: 07.04.2017

Approval of the Graduate School of Natural and Applied Sciences

Prof. Dr. Ahmet Necmeddin YAZICI
Director

I certify that this thesis satisfies all the requirements as a thesis for the degree of Doctor of Philosophy.

Prof. Dr. Abdulkadir ÇEVİK
Head of Department

This is to certify that we have read this thesis and that in our opinion it is fully adequate, in scope and quality, as a thesis for the degree of Doctor of Philosophy.

Co-Supervisor
Prof. Dr. Mustafa ŞAHMARAN

Supervisor
Prof. Dr. Mustafa GÜNAL

Examining Committee Members: Signature

Prof. Dr. İsmail Özgür YAMAN ----------

Prof. Dr. Mustafa GÜNAL ----------

Prof. Dr. Abdulkadir ÇEVİK ----------

Assist. Prof. Dr. Talha EKMEKYAPAR ----------

Assist. Prof. Dr. Gürkan YILDIRIM ----------

I hereby declare that all information in this document has been obtained and presented in accordance with academic rules and ethical conduct. I also declare that, as required by these rules and conduct, I have fully cited and referenced all material and results that are not original to this work.

Qais Sahib BANYHUSSAN

ABSTRACT

DEVELOPMENT OF OPTIMAL DEFLECTION HARDENING CEMENTITIOUS COMPOSITES MIXTURE FOR HIGHWAY BRIDGE DECKS TO ADDRESS SHRINKAGE CRACKING PROBLEM

BANYHUSSAN, QAIS SAHIB
Ph.D in Civil Engineering
Supervisor: Prof. Dr. Mustafa GÜNAL
Co-Supervisor: Prof. Dr. Mustafa ŞAHMARAN
April 2017
171 pages

The bridge deck concrete tends to crack more than other concrete structures due to shrinkage. This behavior is attributed to the fact that the shrinkage increases whenever the surface to-volume ratio increases. The production of High Performance Fiber Reinforced Concretes (HPFRC) based on a maximal amount of coarse aggregates and increasing use of industrial by-products (without sacrificing the deflection-hardening behavior) is the purpose of present study to contribute enhancing the mechanical and durability performance with increasing the cracking resistance. After a preliminary study, 24 HPFRC mixtures with a maximum aggregate size of 12 mm were developed with maximal variation in coarse aggregate contents without compromising deflection-hardening behavior. Three different fibers were used at a maximum of 2% of volume in single or hybrid systems: polyvinyl-alcohol (P), hooked-end steel (S) and nylo-mono (N) fibers. To function synergistically with different fiber types and high amounts of coarse aggregates, matrix properties were optimized by varying the proportions of fly ash to Portland cement (FA/PC ratios of 0.20, 0.45, and 0.70, by weight) and aggregate to binder (A/B ratios of 1.0, 1.5, and 2.0, by weight). The produced HPFRC mixtures were evaluated to find their performances under different tests such as bending, compression, free and restrained shrinkage, impact, slab panel, and freezing- thawing tests. Based on the obtained results from the above performed tests, all of produced mixtures were ranked depending on the performances rank analysis. The results revealed that, the overall mixtures' performance was clearly increased as mixtures having three types of fibers (i.e. hybrid fiber system with three types of fibers). The increasing trend in mixtures' performance was improved throughout increasing the A/B ratios especially at A/B ratio of 2.0.

Keywords: Deflection-hardening; HPFRC; Cracking Resistance; Coarse Aggregates; Impact Resistance; Energy Absorption.

ÖZET

OTOYOL KÖPRÜ TABLİYELERİNDEKİ RÖTRE ÇATLAK PROBLEMLERİNE ÇÖZÜM GETİRECEK ŞEKİL DEĞİŞTİRME SERTLEŞMESİ GÖSTEREN ÇİMENTO BAĞLAYICILI KOMPOZİTLERİN EN UYGUN KARIŞIM TASARIMI

BANYHUSSAN, QAIS SAHIB
Doktora Tezi, İnşaat Mühendisliği Bölümü
Tez Yöneticisi: Prof. Dr. Mustafa GÜNAL
Yardımcı Tez Yöneticisi: Prof. Dr. Mustafa ŞAHMARAN
Nisan 2017
171 sayfa

Köprü tabliyelerinde kullanılan beton malzemesi rötre sebebiyle diğer beton yapılara kıyasla daha yüksek çatlama eğilimi sergilemektedir. Bu durum yüzey-hacim oranının artması sonucu rötre oluşumunun artmasıyla ilişkilendirilmektedir. Tamamlanan tez çalışması kapsamında, mümkün olabilecek en yüksek miktarda iri agrega ve endüstriyel yan ürünlerin dahil edilmesiyle eğilme altında şekil değiştirme sertleşmesi davranışı sergileyen Yüksek Performanslı Lif Donatılı Beton (YPLDB) karışımları geliştirilmiş ve bu sayede yapıların çatlak oluşturma dirençlerinin arttırılarak daha üstün mekanik ve dayanıklılık özelliklerine sahip olabilmeleri amaçlanmıştır. Ön çalışmaların ardından, eğilme altında şekil değiştirme sertleşmesi davranışından ödün verilmeksizin maksimum tane boyutu 12 mm olan iri agregaları mümkün olabilecek en yüksek oranlarda kullanarak 24 farklı HPFRC karışımı geliştirilmiştir. Tekil ve hibrid (çoklu) sistemlerde karışım hacimlerinin maksimum %2'si oranında üç farklı türde (polivinil-alkol [P], çelik [Ç] ve naylon [N]) lif kullanılmıştır. Farklı türlerde lifler ve yüksek miktarlardaki iri agregalarla uyumluluk elde edilebilmesi amacıyla matris özellikleri ağırlıkça farklı uçucu kül-Portland çimentosu oranları (UK/PÇ=0,20, 0,45 ve 0,70) ve agrega-bağlayıcı malzeme oranları (A/B=1,0, 1,5 ve 2,0) kullanılarak optimize edilmiştir. Üretilen YPLDB karışımlarının performans analizleri eğilmede çekme, basınç dayanımı, serbest ve kısıtlanmış rötre, darbe dayanımı, plaka ve donma-çözülme deneyleri aracılığıyla analiz edilmiştir. Testlerin tamamlanmasıyla elde edilen sonuçlar kullanılarak üretilen numunelerin performansları sıralanmıştır. Elde edilen sonuçlar ışığında karışımlarda üç farklı lif türünün kullanıldığı durumlarda (hibrid sistemlerde) genel anlamda performansların daha üst seviyelerde olduğu sonucuna varılmıştır. Performanslardaki iyileşme A/B oranlarının daha yüksek seviyelere çekilmesiyle (A/B=2,0) daha belirgin bir hal almıştır.

***Anahtar Kelimeler*:** Eğilmede çekme şekil değiştirme davranışı; YPLDB; Çatlak Direnci; İri Agregalar; Darbe Dayanımı; Enerji Yutma.

To the souls of my parents

ACKNOWLEDGEMENT

Before everything unlimited praise to God. I do believe that one of the God's virtues manifested through sending some people to stand beside us. These people directly or indirectly give us the help.

I am grateful to my wise and knowledgeable supervisor, Prof. Dr. Mustafa GÜNAL. He is a wellspring of knowledge and an example to the humble scientist. I extend my sincere thanks for his time and effort toward the successful completion of this study. Also, I am indebted to my supervisor, Prof. Dr. Mustafa ŞAHMARAN, for his exemplary patience, guidance, and support. He taught me the approach to problems in research, inspired me to be patient when progress was slow, and to overcome all obstacles on my way toward completing my thesis. I would also like to extend my gratitude to my committee members, for their valuable suggestions and kind support.

I would like to acknowledge the Iraqi Ministry of Higher Education (MOHE-IRAQ), College of Engineering/Al-Mustansiriya University, and Highway and Transportation Department for their confidence through nominating me to study for a Ph.D. Also, I must acknowledge the assistance of the Scientific and Technical Council of Turkey.

I wish also to express my loyalty and thankfulness to every-one who guided, encouraged and supported me during the preparation of this work, especially Assist. Prof. Dr. Gürkan YILDIRIM. I am also grateful to Prof. Dr. Özgür Anıl, for taking the time and energy to help me throughout the research.

Special thanks to my faithful friend Ali AL-DAHAWI who has a great role in overcoming some problems and difficulties since beginning the study together until completing my thesis.

I want to thank all my friends who assisted me in my endeavors, with a special thanks to Yazin AL-NAJJAR, Farhad EMAMI, Mohammad SARWARY, Arash

HAMIDZADEH, and Mohammad BALAV for their invaluable support rendered during the progress of this thesis.

Finally, I would like to express my deepest gratitude to my family for all their love, support and encouragement throughout my life to this point. Without their guidance and encouragement this work would not have been possible. I especially want to thank my lovely sister Kahramane for her encouragement and patient that have provided through inspiring me to be more than I am.

TABLE OF CONTENTS

Page

LIST OF TABLES

Page

LIST OF FIGURES

Page

LIST OF SYMBOLS/ABBREVIATIONS

A/B	Aggregate to binder ratio
AASHTO	American Association of State Highway and Transportation Officials
ACI	American Concrete Institute
Al_2O_3	Aluminum oxide
ASTM	American Society for Testing and Materials
C/F	Coarse -to-Fine aggregate ratio
$Ca(OH)_2$	Calcium hydroxide
$CaCO_3$	Calcium carbonate
CaO	Calcium oxide
CH	Calcium hydroxide crystals
CO	Carbon monoxide
CO_2	Carbon dioxide
C-S-H	Calcium-silicate-hydroxide gel
D_{max}	Maximum particle size
d_e	Equivalent Diameter
DF	Durability Factor
d_i	Opening size of the i^{th} sieve
DOT	Department of Transportation
EFNARC	European federation of national associations of specialist contractors and material suppliers for the construction industry
EN	European norm (standard)
F/T	Freezing-and Thawing
FA	Fly Ash
Fe_2O_3	Iron oxide
FL	First Load
FRC	Fiber- Reinforced Concrete
GGBFS	Ground Granulated Blast Furnace Slag
GPa	Giga Pascal
h	Thickness of panel
HPC	High Performance Concrete
HPFRC	High Performance Fiber Reinforced Concrete

HPPF	High Performance Polypropylene Fiber
HRWRA	High Range Water Reducing Admixture
ITZ	Interfacial Transition Zone
J	Joules
K_2O	Potassium oxide
L	Liter
LVDT	Linear Variable Displacement Transducer
MAS	Maximum Aggregate Size
MgO	Magnesium oxide
MMFRC	Multi-Modal Fiber Reinforced Concrete
MOR	Modulus of Rupture
MPa	Mega Pascal
N	Nylo-mono fiber
n	Fundamental transverse frequency at 0 cycles
n_1	Fundamental transverse frequency after c cycles
Na_2O	Sodium oxide
NH	Ammonium ion hydroxide
P	Polyvinyl-alcohol fiber
PC	Portland Cement
PCA	Portland Cement Association
P_i	Performance of tested mixtures for i^{th} property
P_{max}	Maximum performances
P_{min}	Minimum performances
PP_i	Cumulative percent passing from i^{th} sieve
PVA	Polyvinyl-alcohol
R^2	Correlation coefficient
RDME	Relative Dynamic Modulus of Elasticity
RH	Relative Humidity
S	Hooked-end steel fiber
SCM	Supplementary Cementitious Material
SEM	Scanning Electron Microscopy
SF	Silica fume
SiO_2	Silicon dioxide
SP	Superplasticizer
SRA	Shrinkage Reducing Admixture
TRB	Transportation Research Board
UL	Ultimate Load

w/cm	Water to Cementitious materials ratio
μm	Micrometer
σ	Flexural tensile strength
^{o}C	Degrees Celsius
V_{agg}	Aggregate volume
ε_{con}	Concrete shrinkage strain
ε_{p}	Cement paste shrinkage strain

CHAPTER ONE

INTRODUCTION

1.1 Preface

Concrete is a universal construction material with wide-spread suitability which is used for relatively different applications, although it has two eye-catching drawbacks regarding its low tensile strength and strain. Its low tensile strain capacity accompanied with a high brittleness makes it more prone to cracking due to shrinkage or thermal stress, especially for highway structures such as pavements, bridge approach slab and bridge deck. These types of structures deteriorate in much faster rate than other concrete structures as a result of exposure to the environmental and traffic loads.

It was expected that using high quality concrete, such as High Performance Concrete (HPC), would directly minimize the cost, and decrease the maintenance periods of bridges (the latter due to a decrease in the time when the bridges are out of service). Unfortunately, HPC characteristics regarding with low permeability, high resistance to abrasion, and good durability do not intercede to reduce the potential for concrete to crack. This shortcoming is due to utilizing a high cementitious content such as cement, silica fume (SF) and ground granulated blast furnace slag (GGBFS). In addition, the low amount and size of aggregate leads to increase the tendency of a bridge deck to shrink; thus, it leads to cracking (Lee et al., 2006).

Cracks reduce the capacity of the carrying load leading to durability problems; they reduce service life and increase maintenance costs. Moreover, cracks increase the corrosion potential of steel bars because they provide a channel for the ingress of harmful fluids into the concrete. Therefore, the time for the onset of corrosion will significantly decrease (Boulfiza et al., 2003).

The bridge deck concrete tends to crack more than other concrete structures due to shrinkage. This behavior is attributed to the fact that the shrinkage increases whenever the surface to-volume ratio increases. Moreover, cracking in bridge decks has become a growing problem in recent years. Cracks may appear at the onset of bridge life; occasionally, even prior to a bridge being open to traffic (Morris, 2002). Thus, the development of concrete material for bridge decks that overcome unexpected brittle failure and low cracking resistance has become necessary for safety and economic reasons.

One possible way to remedy the concrete's shortcoming is to modify or develop concrete mixtures in which their behavior becomes more resistant to the shrinkage cracking potential while remaining their high-performance characteristics. Inclusion of fibers into HPC produces a type of concrete known as High-Performance Fiber Reinforced Concrete (HPFRC). Reinforcing the concrete with small, randomly distributed fibers has increasingly been used in many applications, especially highway structures. Increasing the energy absorption capacity and toughness is the main objective of adding the fibers. In addition, it contributes by increasing the tensile and flexural strength of the material. HPFRC response after first crack is a quasi strain-hardening, which mostly appears as multiple cracks and high energy absorption capacity. The main point of strain-hardening is that the post cracking strength is more than the first cracking strength, or elasto-plastic behavior. Additionally, in most of the instances, HPFRCs are produced with aggregates that are relatively small in size irrespective of the selected system of fibers (single or hybrid) (Şahmaran et al., 2012; Ahmed and Maalej, 2009). Although the selection of relatively fine aggregates helps contributing to a more uniform fiber distribution in HPFRC mixtures, it also leads to higher amounts of Portland cement to be included in cementitious systems as the main binder, increasing the cost and the chance for dimensional instability as compared to counterpart systems incorporating coarse aggregates. To minimize this effect, industrial by-products such as FA and GGBFS are commonly used in HPFRC mixtures for both environmental and economical reasons. Reduced matrix fracture toughness, obtained with the use of industrial by-products as supplementation to ordinary Portland cement, can also potentially inhibit higher matrix fracture toughness values that are going to be obtained when a large

amount of aggregate of a maximum possible size is used in cementitious systems (Şahmaran et al., 2012).

1.2 Objectives of the Study

The main goal of this thesis is to develop new generation cementitious composites with deflection- hardening capability that are able to address the shrinkage cracking problem which occurs in the concrete bridge deck. The study is organized into the following tasks:

1.2.1 Development of Varying Mixtures

The major purpose of this study is to develop fiber reinforced cementitious composites mixtures with deflection-hardening capability by proposing the incorporation of different fiber and matrix combinations with higher amounts of coarse aggregates. It is believed that the production of fiber reinforced cementitious composites based on a maximal amount of coarse aggregates and increasing use of industrial by-products (without sacrificing the deflection-hardening behavior) can contribute to enhanced greenness and superior dimensional, mechanical and durability performance (increasing the cracking resistance), as well as the widespread use of such materials in the field at reasonable prices.

At the same time, the developed concrete mixtures are used for the contribution in addressing the shrinkage cracking, especially drying shrinkage. A tight or crack-free concrete (i.e. concrete having cracks with width less than 100 μm) is the target of this study by controlling the crack width. The reason of developing this type of mixtures is to enhance the durability of concrete, and therefore, extend the service life of infrastructures.

1.2.2 Evaluation of Mixtures Performance

After developing mixtures have a deflection hardening behavior, the developed mixtures are evaluated regarding with mechanical, durability, slab and flexural impact tests. For mechanical properties, flexural and compressive strength are investigated. Moreover, durability properties with respect to the free and drying shrinkage tests are measured in addition to the freezing- and thawing durability. Structural properties of developed mixtures for impact test are experimentally and

numerically evaluated. Furthermore, slab panel test is performed to evaluate the energy absorption associated with the structural performance of the developed mixtures in present study.

The specific objectives of present study are shown below:

- To evaluate the addition of moderate volume of single and/or hybrid fibered system on the concrete performance.
- To investigate the use of different coarse aggregate contents with larger aggregate size.
- To document the effect of replacing cement by mineral admixtures such as FA and SF on the concrete mixture performance.

1.2.3 Normalization of Tests Results and Selection of Optimal Mixtures

Based on the results that will be obtained from the above tests, all of the investigated mixtures are ranked upon the performances rank analysis. In addition to the ranking of mixtures' performance, cement content effect also included where it is considered as a negative factor regarding the air pollution (CO_2 emission) during the production of the cement.

1.3 Scope of the Study

The structure of this thesis is systematized into five chapters, as outlined below;

Chapter One states a preface, objectives, and the scope of the study. Chapter Two includes i) Background of the main reasons causing the cracks in bridge deck slabs ii) Affecting factors on shrinkage and shrinkage cracking iii) Mechanism of crack formation in conventional reinforced concrete and high performance concrete iv) Affecting factors on high performance concrete behavior. Chapter Three shows the experimental work, material properties, and the detail of conducted tests. The results and of the experimental works are described and discussed in Chapter Four in addition to selecting the optimal mixture based on the a certain mixtures performance was done. Chapter Five presents the conclusions of the research.

CHAPTER TWO

BACKGROUND AND LITERATURE REVIEW

2.1 Introduction

Concrete is widely used in several types of highway structures such as bridge decks, approach slabs and pavements. Brittleness and dimensional instability are considered to be unfavorable properties in concrete. With regard to the bridge construction, bridge members may be pre-cast (e.g. girders) or cast in place (e.g. bridge decks) which have different ways and times of construction. Generally, due to the differences found in the properties of bridge members and their performance, especially in the coefficient of thermal expansion, a restraint in their movement will be found between them, and the more rigid members become restrainers. Therefore, girders and other supports restrain the free movement of bridge decks as a result of dimensional instability caused by shrinkage. When changes in the volume of a concrete deck are restrained, concrete may induce stresses that exceed its tensile capacity; thus, bridge deck cracks may appear (Whiting et al., 2000). There is general agreement that the maximum tensile strength is low in relation to its compressive strength which is equal to approximately one-tenth. Therefore, concrete is prone to cracking as long as there are stresses surpassing its tensile strength.

It is essential to take precautions to control the cracking in a bridge deck by eliminating, or at least reducing, these cracks, which can, and do, have a number of unsightly results. Cracks reduce the capacity of the carrying load leading to durability problems; they reduce service life and increase maintenance costs. Moreover, cracks increase the corrosion potential of steel bars because they provide a channel for the ingress of harmful fluids into the concrete. Therefore, the time for the onset of corrosion will significantly decrease (Boulfiza et al., 2003; Paulsson-Tralla and Silfwerbrand, 2002).

Regarding bridge decks, there are several factors that can affect the amount and rate of shrinkage such as concrete materials, construction techniques, bridge geometry and environmental conditions (Krauss and Rogalla, 1996). The bridge deck concrete tends to crack more than other concrete structures due to shrinkage. This behavior is attributed to the fact that the shrinkage increases whenever the surface-volume ratio increases. Moreover, cracking in bridge decks has become a growing problem in recent years. Cracks may appear at the onset of bridge life; occasionally, even prior to a bridge being open to traffic (Morris, 2002). Thus, the development of concrete material for bridge decks that overcome unexpected brittle failure and low cracking resistance has become necessary for safety and for economic reasons.

Nowadays, hopeful prospects have been opened for the construction industry with the development and application of a new type of concrete called high performance concrete (HPC) (Bloom and Bentur, 1995). Due to its high strength, high elastic modulus, low permeability, long-term durability and excellent workability, HPC has been widely used for bridge decks, pavements and other construction structures (Wan et al., 2010). For a given structure (e.g. bridge decks or pavements), HPC can efficiently reduce the required construction materials by reducing structural member reinforcement (e.g. area of steel) or minimizing slab thickness. Reductions occur due to an increase in the concrete's flexural strength (Ostertag and Blunt, 2008). On the other hand, Jansen et al., (1995) indicated that the increase in the compressive strength of concrete leads to more brittleness; thus, steeper post-peak behavior will occur (Figure 2.1). In other words, an increase in the brittleness of concrete may cause a sudden, catastrophic failure due to unexpected loads or dynamic forces.

In order to overcome the high fragility (i.e. brittleness) of HPC, the incorporation of fibers into the concrete is one way to remedy the concrete's shortcomings. The inclusion of suitable fibers into HPC produces a new type of concrete known as HPFRC. According to the degree of enhancement, fibers in hardened concrete have at least three significant effects. First, they may increase the fracture stress at which the concrete matrix initiates cracking. Second, they may tend to enhance strain capacity or ductility by preventing unexpected brittle failure. The third and final important effect is that the concrete is suspect to improve cracking resistance by minimizing crack width, delaying time-to-cracking and/or reducing the average crack spacing.

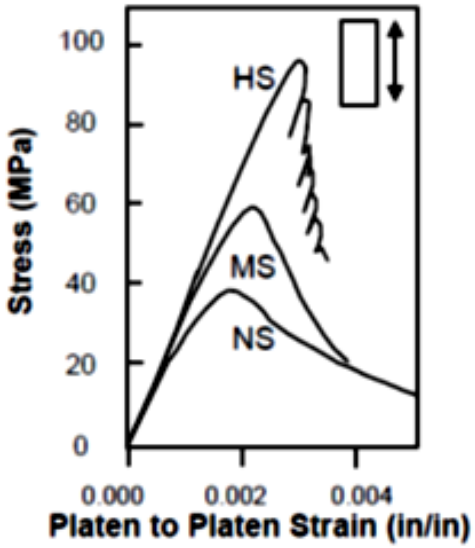

Figure 2.1 Effect of strength on the stress-strain response (Jansen et al., 1995)

2.2 Causes of Cracks in Bridge Deck Concrete

Cracking in bridge decks may cause considerable deterioration in the concrete. From a structural point of view, the presence of cracks in the concrete facilitates harmful agents and/or water to penetrate into the concrete thereby causing corrosion in the steel reinforcing, particularly at a full depth. Then, the ability of the steel reinforcing to carry the loads may decrease, thereby shortening the service life of the structure (Weiss et al., 1998). Moreover, cracks on the surface of the bridge deck are considered unsightly and they may cause a reduction in the functional performance of the bridge in terms of its ride quality.

It was expected that using high quality concrete, such as HPC, would directly minimize the cost of, and decrease the maintenance periods of, bridges (the latter due to a decrease in the time when the bridges are out of service). Unfortunately, HPC characteristics regarding low permeability, high resistance to abrasion, and good durability do not intercede to reduce the potential for concrete to crack. This shortcoming is due to utilizing a high cementitious materials content such as Portland cement, SF and GGBFS. In addition, the low amount and size of aggregate leads to increasing the tendency of a bridge deck to shrink; thus, it risks cracking (Lee et al., 2006).

As mentioned previously, plain concrete has a low tensile strength, equaling to one-tenth of its compressive strength. It is well known that shrinkage increases with time; therefore, when a concrete member is restrained, the shrinkage-induced stresses increase accordingly and the concrete also gains its strength. Cracking is a competition between the matrix's (plain concrete) tensile strength and the shrinkage-induced stress to show which will overcome the other. The time at which the tensile stress caused from restrained shrinkage exceeds the concrete strength is known as time-to-cracking (Figure 2.2).

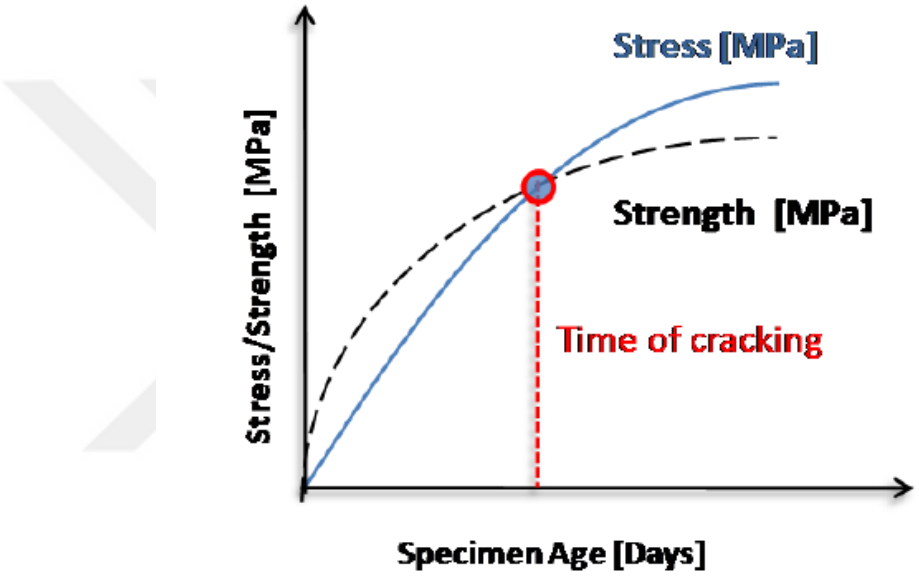

Figure 2.2 Relationship the concrete strength and time of cracking (Radlinska et al., 2007)

In addition to shrinkage cracking, mechanical loading, such as from early opening to traffic, overloading, and fatigue, can lead to cracking a bridge deck (Rajabipour et al., 2012). Furthermore, temperature gradients in the concrete caused by preferential cooling or drying between the concrete surface and its core may create non-uniform shrinkage strain profiles along the bridge deck depth. The strains may lead to the development of axial and bending stresses in the restrained concrete members.

Shrinkage cracking occurs when a structural element is restrained and when the concrete's tensile stress is greater than its tensile strength (Figure 2.3). For a bridge deck, the restraint of the deck may occur either via external means such as girders, or through internal resistance such as steel reinforcing bars and/or aggregates (the latter

of which may cause micro-cracking). The restraint that is created due to external conditions is dependent on factors such as structural design characteristics (e.g. girder type, length and space of girder, girder end support and deck slab thickness), the composite action between the deck and the girders (e.g. connecting studs), and the techniques used in the construction of the bridge deck.

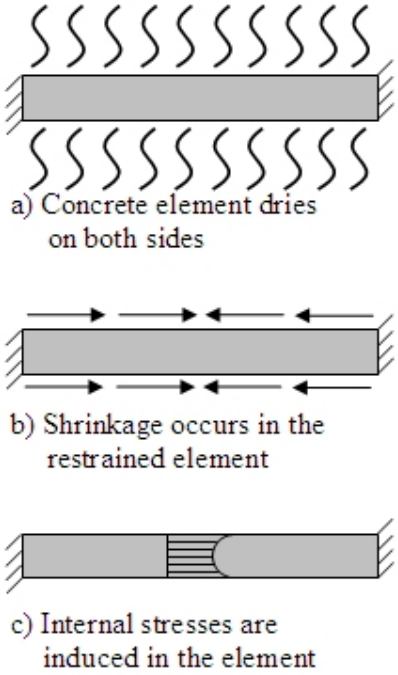

Figure 2.3 Stresses induced by restrained shrinkage (Mindess et al., 2003)

In general, there are several factors that can lead to cracking in bridge decks, including shrinkage and mechanical loading. Types of shrinkage include plastic shrinkage, chemical and autogenous shrinkage, drying shrinkage and carbonation shrinkage (Li, 2011), which are discussed in the next section.

2.2.1 Shrinkage

2.2.1.1 Plastic Shrinkage

Plastic shrinkage occurs in fresh concrete in a semi-fluid or plastic state, where the process of hydration is still beginning; therefore, much hydrating water fills the voids spread around the cement particles. The hydrating water may move out due either to exterior phenomena such as evaporation or bleeding on concrete surfaces. However, menisci are created when the rate of evaporation surpasses the rate of bleeding water, where the water is lifted up to the surface. Then, the menisci develop capillary

tension forces on the cement skeleton, resulting in a volumetric reduction that may occur, thereby resulting in plastic cracks (Cohen et al., 1990; Mindess et al., 2003; Radlinska et al., 2007). Cohen et al. (1990) reported that for High Strength Concrete (HSC) containing SF, an increase in water to cementitious materials ratio (w/cm) leads to an increase in the plastic shrinkage. Moreover, this behavior is attributed to the reduction in the bleeding water and/or to the pore size, which becomes smaller; thus, tensile stresses would increase.

2.2.1.2 Chemical and Autogenous Shrinkage

When water reacts with cement, the total volume produced will be lower than the original component volume (cement+ water) (Tazawa and Miyazawa, 1995). In other words, the volume of the resultant products (C-S-H gel, portlandite and other products) is lower than the volume of the reactants. This type of reduction is known as chemical shrinkage; its value roughly equals 1.77 in^3 per pound of Portland cement (Jensen and Hansen, 2001). As cement hydrates, more water in the pores is consumed. This type of shrinkage would significantly share in the total shrinkage of the concrete; therefore, the risk of cracking may increase (Holt, 2001). The chemical shrinkage is different from the autogenous shrinkage. The autogenous shrinkage is defined as an external macroscopic diminution occurring without moving the water to the external environment (Aitcin, 1998). Figure 2.4 depicts the relationship between chemical and autogenous shrinkages. This phenomenon is also known as self-desiccation (Mindess et al., 2003). Autogenous shrinkage is the most distinguished component for concrete with a w/cm ratio lower than 0.4 and with high cement content.

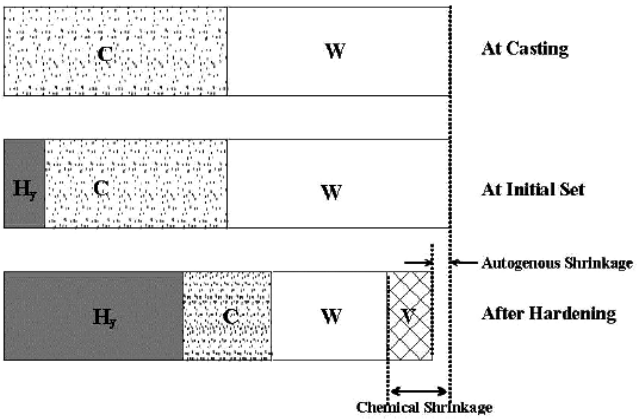

Figure 2.4 Relationship between chemical shrinkage and autogenous (Aitcin, 1998)

2.2.1.3 Drying Shrinkage

Drying shrinkage is a phenomenon occurring in concrete as a result of moisture loss due to concrete drying. Water moves from inside concrete matrix toward the surface; then, the water will evaporate from the surface of the concrete. Drying shrinkage occurs when the relative humidity of the surrounding environment is lower than the relative humidity of the hardened concrete (Radocea, 1992). Based on the Feldman-Sereda model (Feldman and Sereda, 1970), different types of water related to the saturated hydrate cement partials are stated, as shown in Figure 2.5. These types of water are illustrated below in more detail (Mehta and Monterio, 2006):

1- Capillary water: This is found in voids of sizes up to 0.05 micrometers. Furthermore, it may be divided into two kinds of water: free water, which is found in voids larger than 0.05 micrometers, which does not cause shrinking during its evaporation from the concrete since it has no chemical-physical bonds holding it to the cement particles. The second type of water is found in pores of size between 0.005 and 0.05 micrometers, which can cause volume changes after its removal.

2- Adsorbed water: This water exists close to the surface of hydrated cement and it is held on the surface of cement particles with a hydrogen bond. Due to this bonding, adsorbed water is responsible for creating the shrinkage of cement as a result of its ejection. Moreover, it may be dried at a Relative Humidity (RH) of less than 30%.

3- Interlayer water: This water is related to C-S-H structure. It is held by a strong hydrogen bond; therefore, it can be only removed by powerful drying such as RH values less than 11%. Consequently, the C-S-H structure undergoes an extreme reduction of volume due to interlayer water loss.

4- Chemical combined water: This is water that is an integral part of the microstructure of various cement hydration products. This water is not easily lost by drying. The concrete is desiccated by subjecting it to high heat such as burning.

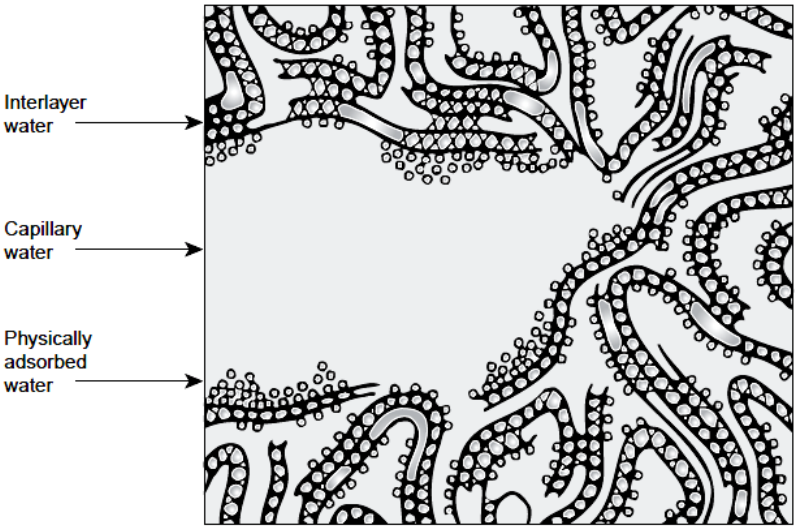

Figure 2.5 Diagrammatic model of the types of water related with hydrated cement (Feldman and Sereda, 1970)

Furthermore, Figure 2.6 shows two contiguous cement particles which are exposed to drying. Because of the water movement toward the outside, menisci will be formed followed by the development of stresses. Moreover, the stresses inside any capillary pores may increase whenever the capillary diameter decreases; therefore, the shrinkage also increases. In fact, the loss of water directly causes volume changes inside the concrete matrix. Moreover, the movement of water is controlled by several mechanisms, including capillary stress, disjoining pressure, and surface free energy (Rougelot et al., 2009).

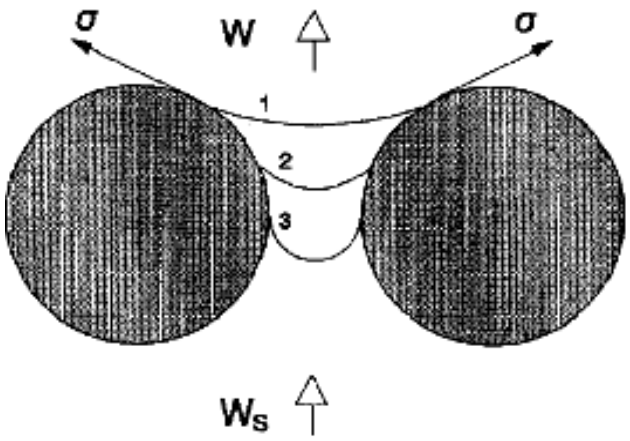

Figure 2.6 Stress pulling the water meniscus lower between two cement particles (Radocea, 1992)

It can be argued that aggregate content, w/cm, temperature and relative humidity surrounding a bridge deck are deemed to be the main parameters causing increases in the drying shrinkage of concrete. Aggregates play a decisive role in resisting the shrinkage of paste as the aggregate does not shrink (or shrinks very little) in comparison to the other concrete components (Almudaiheem and Hansen, 1987).

Pickett (1956) suggested a relationship between aggregate volume and cement paste shrinkage to estimate the total shrinkage of concrete (Equation 2.1).

$$\varepsilon_{con} = \varepsilon_p (1 - V_{agg})^n \quad (2.1)$$

where

ε_{con} is the concrete shrinkage strain (μm/m)

ε_p is the cement paste shrinkage strain (μm/m)

V_{agg} is the aggregate volume, and

the *n* parameter ranges from 1.2 to 1.7, depending upon aggregate and paste stiffness.

2.2.1.4 Carbonation Shrinkage

This kind of shrinkage is not accompanied by water loss or loss of any other materials from the concrete. In fact, carbonation occurs due to the presence of carbon dioxide (CO_2) in the ambient air and its interaction with the concrete. This interaction, actually, leads to an increase in the mass of the cement products. The carbonation reaction is illustrated in Equation 2.2.

$$\mathbf{Ca(OH)_2 + CO_2 \longrightarrow CaCO_3 + H_2O} \quad (2.2)$$

As mentioned in the above reaction, the solid volume increases approximately 3.29%. However, the shrinkage mechanism due to carbonation is not clearly known. One of the hypotheses showed that as a result of the presence of menisci generated in the cement paste, the menisci would apply a compressive stress on the $Ca(OH)_2$ crystals. The skeleton of these crystals is stable and they behave as a prop for the prevention of the C-S-H gel particles from breaking down. However, once carbonation takes place, the CH is dissolved, which results in a collapse of the gel particles, thus causing shrinkage. Due to the presence the CO_2 in the air, the total

resultant shrinkage is a combination of drying and carbonation shrinkages (Neville, 1995).

2.2.1.5 Thermal Contraction

Thermal contraction is another source of concrete shrinkage which leads to increasing the tendency of the concrete to crack. In a fresh state, the process of cement hydration is still continuing and accompanied by increasing heat, which results in a rise of concrete temperature. As mentioned in (ACI, 2010), the concrete sets at its peak temperature or near to its peak temperature, followed by a cooling process resulting in contraction of the concrete. In concrete, tensile stress develops and this leads to cracks due to thermal contraction. This can occur in external members such as girders that restrict the movement of the deck slab (TRB, 2006). Moreover, temperature gradients in both patterns (external and internal) lead to thermal cracking.

The external temperature gradients are generated when there are substantial differences in temperature between the maximum concrete temperature and the temperature of adjacent elements or supports (e.g. girders). Due to the support restraint to the deck during deck concrete cooling, a residual tensile stress is developed inside the concrete, thereby causing cracks in the bridge deck (TRB, 2006). Likewise, internal temperature gradients increase when there are non-uniform temperatures across the slab concrete profile. The difference in temperature of the concrete core and its temperature at its surface occurs when the rate of cooling or heating of the air is higher than the rate of temperature change in the concrete core (Mehta and Monterio, 2006).

To mitigate the heating caused by cement hydration, concrete constituents and their proportions have profound effects in its alleviation. Aggregate content and w/cm ratio are the significant factors that cause an increase in the thermal cracking due to the hydration temperature. This temperature increases, particularly with concretes with lower aggregate content and low w/cm ratios (ACI, 2010). Moreover, Supplementary Cementitious Material (SCM), such as FA and GGBFS, are used to decrease or suppress the temperature resulting from cement hydration.

2.2.2 Mechanical Load

A mechanical load, which is applied on the bridge deck, causes a minor tensile stress as compared to stresses formed by shrinkage (Schmitt and Darwin, 1995; Krauss and Rogalla, 1996; Frosch et al., 2003; Hadidi and Saadeghvaziri, 2005). The inauguration of a bridge for traffic or heavy weights can be controlled by gaining the minimum required strength of concrete. Moreover, several parts of a bridge deck normally are subjected to stresses formed by the early flow of traffic during maintenance work; thus, cracks will form particularly at the early stages (Issa, 1999). Insufficient casting cases in a bridge deck also create cracks during the construction period. For instance, cracking appears in cases of continuous multi-span bridges due to flexural negative moments. The flexural negative moments form cracks in the concrete deck at the piers of the bridge because of the dead loads of the concrete are subjected on the positive area (middle of a span). Hence, to mitigate these moments, the casting of the concrete should be placed firstly at the positive area. Then, other parts of the bridge deck are cast (Babaei and Hawkins, 1987; Issa, 1999). Furthermore, repetitive loads, such as traffic, may cause fatigue cracks as the concrete ages. Cracks begin as micro-cracks and develop into macro-cracks after a certain number of cycling loads. Obviously, a bridge deck subjected to fewer heavy vehicles and slower speeds exhibits fewer cracks compared decks or bridges with higher volumes and speed of traffic (Mc Keel Jr, 1985).

2.3 Factors Affecting Shrinkage and Cracking

Several previous studies have defined factors that enhance or decrease the cracking resistance in restrained bridge elements such as decks. These factors are classified into major categories, which include concrete properties and ingredients, structural design, environmental effects and construction factors (Shah et al., 1997; Nmai et al., 1998).

2.3.1 Effect of Cement

2.3.1.1 Type of Cement

Low temperatures resulting from the hydration of cement produce less thermal cracking and a lower elastic modulus value. For this, Type II cement produces

concrete with fewer cracks than other types of cement (Krauss and Rogalla, 1996; Brown et al., 2001). Conversely, using Type III cement in concrete increases the possibility of forming cracks due to the rapid setting time and high temperature which occurs because of the hydration process. Hence, utilizing Type II cement significantly reduces the shrinkage of concrete as compared to other types of cements (Darwin et al., 2007a). Indeed, shrinkage cracks can be minimized or even eliminated by using shrinkage-compensating concrete. Expansive cement is normally used to mitigate or eliminate shrinkage in concrete. It can be argued that using expansive cement tends to produce lower shrinkage in mortars. In this regard, the study conducted by Brown et al. (2001) showed that shrinkage cracks can be significantly reduced by using Type K cement in concrete. This is attributable to the shrinkage-compensating cement which can lead to equilibrium in the shrinkage caused by autogenous and drying shrinkage. Therefore, it is an expansive agent in concrete that prevents shrinkage cracking (Figure 2.7).

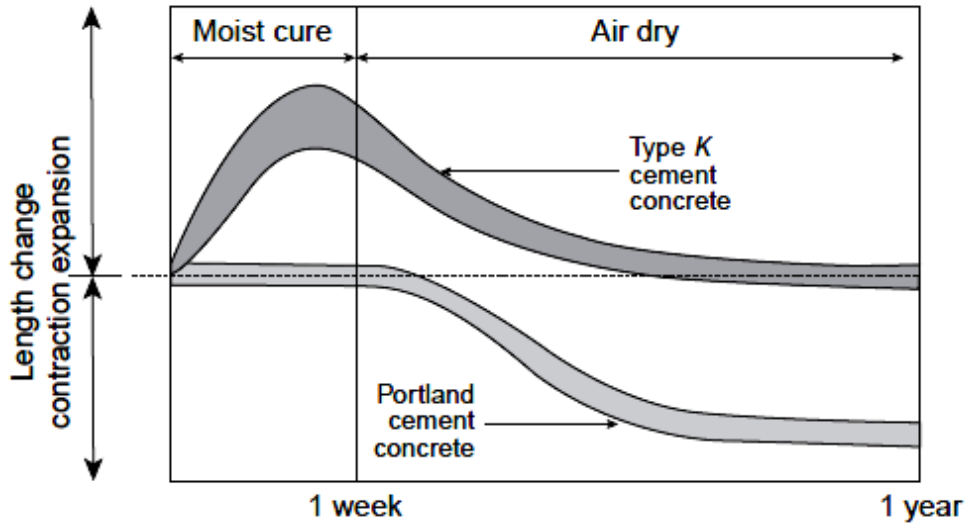

Figure 2.7 Comparison of length change between Portland cement and Type K cement concrete (Mehta and Monteiro, 2006)

2.3.1.2 Cement Content

As it is well known, concrete comprises aggregate, cement, water, and additives. Shrinkage clearly appears in the cement (but not the aggregate) during the phase when the concrete that is prone to shrinkage. In addition, cement paste is the phase that is mainly responsible for creating the heat of hydration. Therefore, increasing the amount of cement significantly influences the rate and the amount of shrinkage in

concrete (French et al., 1999). On the other hand, aggregate does not shrink and has volumetric stability.

In general, cracks in concrete are significantly affected by increasing the cement content (Schmitt and Darwin, 1999; Hadidi and Saadeghvaziri, 2005). For example, at high cement content and low w/cm concrete is more prone to cracking than other concretes (Krauss and Rogalla, 1996; Darwin et al., 2004). A study conducted by Tritsch et al. (2005) showed that an increase in cement content leads to an increase in total free shrinkage and tendency to crack. Moreover, the volume of concrete paste is deemed to be the main factor influencing the severity of shrinkage in bridge decks. Bissonnette et al. (1999) and Darwin et al. (2007b) concluded that whenever cement content is reduced, the free shrinkage of concrete decreases. Likewise, the volume of cement paste plays a substantial role in drying shrinkage (Hooton et al., 2009).

2.3.2 Effect of w/cm Ratio

In general, concrete with low w/cm has low resistance to cracking (Brown et al., 2001). This is mainly attributed to:

- Increased thermal stresses which are caused by the increase in the heat of hydration.
- Increased autogenous shrinkage and self-desiccation.
- Increased stiffness and the decrease in w/cm that leads to an increase in concrete strength.

The cracks in a bridge deck increase whenever concrete strength increases (Darwin et al., 2004). Moreover, concretes with low w/cm may be more prone to cracks due to the increase in autogenous shrinkage (Weiss et al., 2000). Hindy et al. (1994) observed that w/cm ratio significantly affects the drying shrinkage of HPC. In the same regard, Krauss and Rogalla (1996) and Nassif et al. (2007) indicated that high w/cm in concrete increases plastic, drying and carbonation shrinkage. Several previous studies estimated upper limits of w/cm ratio that should not be exceeded in order to avoid shrinkage. Kochanski et al. (1990) suggested that this ratio range from 0.40 to 0.48. Similarly, McLeod et al. (2009) proposed a ratio between 0.42 and 0.45.

However, other literature agreed that the w/cm ratio did not have a significant effect on the shrinkage of concrete (Bissonnette et al., 1999; Darwin et al., 2007a).

2.3.3 Effect of Aggregate

As mentioned previously, cracks are a clear threat to a bridge deck with regard to its durability, which decreases especially with the presence of harmful agents. The enhancement of concrete performance by reducing the shrinkage and increasing the cracking resistance may be achieved by selecting adequate concrete materials with respect to its ingredients and proportions. Aggregate is an effective factor in identifying the properties of concrete. Furthermore, as aggregates occupy 60% to 70% of the volume in concrete, they have an important role in both its mechanical and durability properties. Hence, the characteristics of the aggregate, such as particle size distribution, shape, texture, angularity, coarse-to-fine aggregate ratio (C/F), and packing density, play a pronounced significant role in fresh and hardened concrete.

2.3.3.1 Type of Aggregate

Several studies have attempted to increase the cracking resistance and/or mitigate shrinkage by using different types of aggregate due to an aggregate's restraining effect to shrinkage. In the terms of mineralogy, Babaei and Purvis (1995) studied the effect of utilizing different types of aggregate on concrete shrinkage. The results showed that concrete made with sandstone (a low stiffness aggregate) produced a higher drying shrinkage than concrete containing dolomite aggregate (high stiffness aggregate). However, Richard (1998) indicated that concrete containing limestone aggregate showed lower cracking potential than other types of aggregate. Concretes containing granites as coarse aggregate revealed lower shrinkage than concrete with a limestone coarse aggregate (Darwin et al., 2007a). Fu et al. (2016) reported that using limestone aggregate leads to an increase in the crack resistance of produced concrete from 4.2 days to 32 days with regard to time-to-cracking.

The characteristics and physical properties of aggregate have a significant effect on the mechanical properties of concrete. The physical properties of aggregate, such as its shape and surface texture, have an effect on the strength of the Interfacial Transition Zone (ITZ) by increasing or decreasing the interlock between the aggregate and other components of the concrete. For instance, limestone aggregate

particles have a rough surface texture and an angular shape; thus, the bond between the limestone and the cement paste might be stronger than other types of aggregate, thereby leading to a stronger ITZ. Indeed, high strength ITZ concretes lead to a lower possibility of cracks in the concrete. Additionally, the absorption capacity of aggregate also has an effect on the final shrinkage of concrete (Krauss and Rogalla, 1996). Previous literature suggests that the maximum absorption capacity should not exceed 0.5% and 1.5% for course and fine aggregate respectively (Babaei and Purvis, 1995). Moreover, utilizing fully saturated aggregate in concrete increases the shrinkage strain in comparison to a dry condition aggregate (Al-Attar, 2008).

2.3.3.2 Aggregate Content

As mentioned earlier, cement paste has the profound effect of increasing the rate and amount of shrinkage; thus, an increase in the risk of cracking is expected. One possible way to decrease this effect is by reducing the amount of cement. Following the same principle, an increase in aggregate content leads to a reduction of cement content. Therefore, with regard to the shrinkage, cement and aggregate have opposite influences (Figure 2.8).

As the aggregate content increases inside the concrete matrix, the ability of the concrete to resist shrinkage increases (Almudaiheem and Hansen, 1987). An increase of aggregate leads to a decrease in cement paste; thus, the shrinkage of the produced concrete will decrease. Several previous studies recommend that the maximum cement paste content should not exceed 27% (Schmitt and Darwin, 1995; Darwin et al., 2004). Moreover, an increase in the coarse/fine aggregate grade ratio of above 1.5 and utilizing more than 1110 kg/m^3 aggregate enhances the ability of the concrete to resist cracks (Nassif et al., 2007).

2.3.3.3 Aggregate Size

Without doubt, increasing the quantity and size of the concrete constituents, which have adverse influences on shrinkage, leads to lowering shrinkage and cracking. Aggregates are inherently hard or have a low tendency to shrink. As a result, the use of concrete made with coarser aggregates reduces the required cement volume; therefore, a reduction in ultimate shrinkage and an increase in cracking resistance are anticipated (Qiao et al., 2010). It can be argued that coarser aggregate sizes lead to

increasing the crack resistance of the produced concrete (Krauss and Rogalla, 1996). Aggregate provides a rigid structure inside concrete; thus, the aggregate tends to resist the free shrink of the cement paste. Delatte and Crowl (2012) reported that larger aggregate sizes in HPC enhance concrete properties with respect to shrinkage mitigation. With regard to bridge decks, design requirements limit the size of the aggregate, especially in the thinner slabs. Therefore, optimizing the aggregate size to match the design requirements with other uses, such as workability needs and shrinkage alleviation, is necessary. Furthermore, although coarser aggregate could lower drying shrinkage, it has an adverse effect by increasing the number of micro-cracks in the cement paste (Aitcin, 1998).

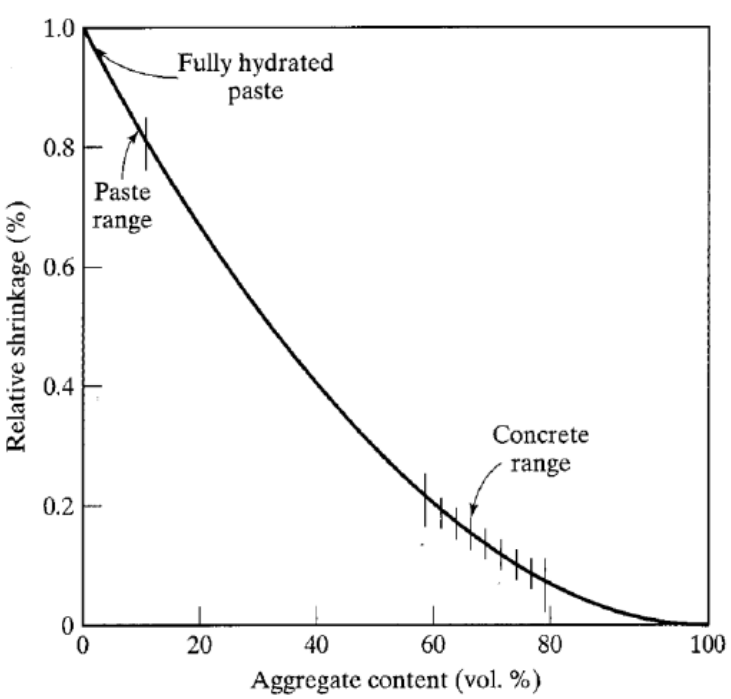

Figure 2.8 The effect of aggregate content on the drying shrinkage of concrete (Mindess et al., 2003)

2.3.3.4 Aggregate Packing

The well graded distribution of aggregate is a conclusive characteristic in the containment of the coarser aggregate with the finer aggregate; thus, more packing density is anticipated (Figure 2.9). A denser aggregate distribution can be obtained by aggregate optimization. One common method to increase aggregate packing is Fuller distribution (Fuller and Thompson, 1907). To obtain a concrete with high aggregate content leading to less cement paste content, aggregate packing

optimization and well particle gradation are important as recommended by several studies (Shilstone, 1990; McLeod, 2009; Lindquist, 2008; Darwin et al., 2010). Studies by De Larrard and Buil (1987) and Quiroga and Fowler, (2004) reported that when the components of a concrete mixture reached a maximum aggregate packing density, the behavior of the concrete showed a high comprehensive performance. Hwang and Khayat (2008) indicated that high stiffness of mixtures and low ultimate drying shrinkage may be gained by aggregate packing optimization and well particle size distribution. In general, blended aggregate as well-graded, rounded, and smooth particles require less paste volume to yield a given workability in comparison to aggregate with flat, elongated, angular, and rough particles. Therefore, the optimization of aggregate characteristics is a major factor in the production of low-cost, effective and durable concrete.

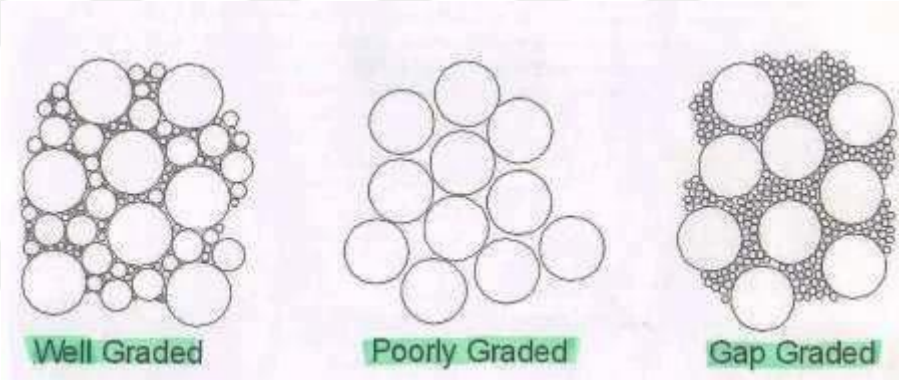

Figure 2.9 Aggregate density diagrams of different gradations

2.3.4 Effect of Chemical Admixture

Several previous studies have investigated the influence of concrete additives, also known as Shrinkage Reducing Admixtures (SRAs), on the durability of concrete, particularly in bridge decks. Folliard et al. (2003) studied the possibility of adding SRAs to concrete to control drying shrinkage cracks in bridge deck concrete. The study revealed that SRAs could be restricting the free drying shrinkage strain of concrete. Similarly, Tia et al. (2005) observed that incorporating SRAs in concrete considerably mitigated free shrinkage strain and shrinkage-induced stresses. Quangphu et al. (2008) also studied the effect of SRAs on the drying shrinkage of HPC. The authors reported that the use of SRAs in HPC can reduce the ultimate shrinkage strain by up to 41% compared to corresponding mixes without utilizing

SRAs. Other previous studies have estimated the percentage of decreases in shrinkage strain due to utilizing SRAs by more than 50% (Radlinska et al., 2008; Rajabipour et al., 2008). Moreover, several studies conducted on restrained concrete slabs have revealed that adding SRAs into concrete not only decreases the drying shrinkage, it also enhances the strength of concrete to enable it to resist cracks and decrease the crack width; thus, there is an increase in the durability of the concrete (Shah et al., 1997; Nmai et al., 1998; Weiss et al., 1998; Weiss et al., 2003; Hwang and Khayat, 2008). Lura et al. (2007) investigated the effect of utilizing SRAs on the plastic shrinkage of mortars. The results revealed that mortar with SRA tends to form fewer cracks at smaller widths as compared to similar mortars without SRAs. They attributed this to the positive effects of SRAs, leading to a decrease in the surface tension of the fluid in the pores of the concrete. Therefore, lower evaporation, a decrease in settlement, a reduction in capillary tension and less shrinkage-induced stress at the surface of mortar occurs.

Similarly, Shah et al. (1992) utilized different types and dosages of SRAs in concrete to estimate their effects on free and restrained shrinkage. The authors also reported that the incorporation of SRAs into concrete leads to a significant reduction in the shrinkage of concrete. Moreover, the reduction of shrinkage becomes more likely whenever the percentage of SRAs increases. Superplasticizers (SP) in concrete were also investigated by Darwin et al. (2007a). The results revealed that, at a certain amount of SP, the shrinkage of concrete may increase.

2.3.5 Effect of Mineral Admixtures

In general, mineral admixtures are incorporated in concretes and/or mortars because they behave as pozzolanic material and they affect the mechanical and durability properties of the concrete. Mineral admixtures, such as FA, GGBFS and SF used as a supplementary cementitious material, are replaced by cement content in the mix design.

The effects of utilizing SF in concrete were investigated by Cohen et al. (1990), Mindess et al. (2003), and Bentz and Jensen (2004). These studies revealed that, in case of plastic shrinkage, the deficiency of water bleeding encouraged the concrete to be prone to cracks. Moreover, SF concretes showed higher values of autogenous

shrinkage and cracks forming due to the reduction in pore size. Krauss and Rogalla (1996) indicated that concrete containing SF exhibited lower crack resistance than concrete without SF. Furthermore, the crack intensity on the surface of bridge decks increased due to the addition of SF to the concrete (Schmitt and Darwin, 1999). This is most likely due to the lack of bleeding water that was caused by adding SF. Similarly, Li et al. (1999) concluded that whenever cement was partially replaced by SF, the produced concrete showed less crack resistance and an increase in the width of the cracks. Drying shrinkage of HPC was studied by Lange et al. (2003). Their results revealed that the mixtures containing SF have higher values of drying shrinkage. The authors attributed this behavior to the fineness of particle size of SF.

Moreover, Tangtermsirikul (1995) and Babaei and Purvis (1995) utilized FA as a supplementary cementitious material in concrete and concluded that the concrete that was produced required less water for certain workability; thus, the concrete seemed to be less prone to shrinkage and had lower values of drying shrinkage. Lawler (2007) also reported that the use of mineral admixtures, such as FA, leads to a decrease in water demand of mixtures as well as the volume of cement. Therefore, the resistance of concrete to cracks also increases (Tia et al., 2005). On the other hand, utilizing Class C fly ash as a partial replacement material by volume of cement increases the shrinkage of the produced concrete (Darwin et al., 2007a).

As mentioned previously, using GGBFS as a supplementary cementitious material is similar to using other mineral admixtures such as SF and FA. It was reported that incorporating GGBFS causes an increase in early-age shrinkage strain of produced concrete (Qiao et al., 2010). Moreover, replacing 50% of the cement with GGBFS, results in an increase in the autogenous shrinkage of the constant w/cm (Lee et al., 2006). In contrast, Li et al. (1999) studied the effect of utilizing SF, FA and a calcium nitrite inhibitor on the durability aspects of concrete. The authors concluded that the cracking time increased and crack width opening decreased for concretes containing minerals. However, the values of the shrinkage strain did not significantly change when GGBFS was incorporated. Furthermore, the increase in packing density (microstructure density) and the reduction of capillary porosity lead to a decrease in the drying shrinkage for concretes containing GGBFS (Li and Yao, 2001).

2.3.6 Effect of Fibers

Although fibers have no significant effect on the shrinkage of concrete, they do considerably decrease the width of cracks in concrete (Grzybowski and Shah, 1990; Folliard et al., 2003). However, the drying shrinkage for fiber concrete and/or mortar still represent a major concern for some aspects of concrete durability (Kawashima and Shah, 2011). The inclusion of fibers in concrete may reduce the crack width and the formation of multiple cracks. Moreover, the degree of decrease depends on the type, volume and dosage of fibers used in the concrete. For instance, micro fibers are more effective than coarse fibers to control the cracks (Banthia et al., 1996). Hence, the orientation of fibers in concrete significantly mitigated the cracks formed due to plastic and settlement shrinkage (Krauss and Rogalla, 1996; Qi et al., 2003; Banthia and Gupta, 2006). The reasons for such behavior are mainly related to the mechanism of the fiber as restrictive components inside the concrete matrix (Sun et al., 2000; Banthia, 2000). Kim and Weiss (2003) agreed about the aforementioned behavior of fibers inside the concrete such that it not only increases the crack resistance of concrete, but it also reduces the crack width. In addition, macro-crack propagation in the concrete is significantly eliminated by adding fiber to concrete by bridging these cracks (Shah and Weiss, 2006). Figure 2.10 shows the influence of fiber reinforcement on maximum crack width and time to cracking due to drying.

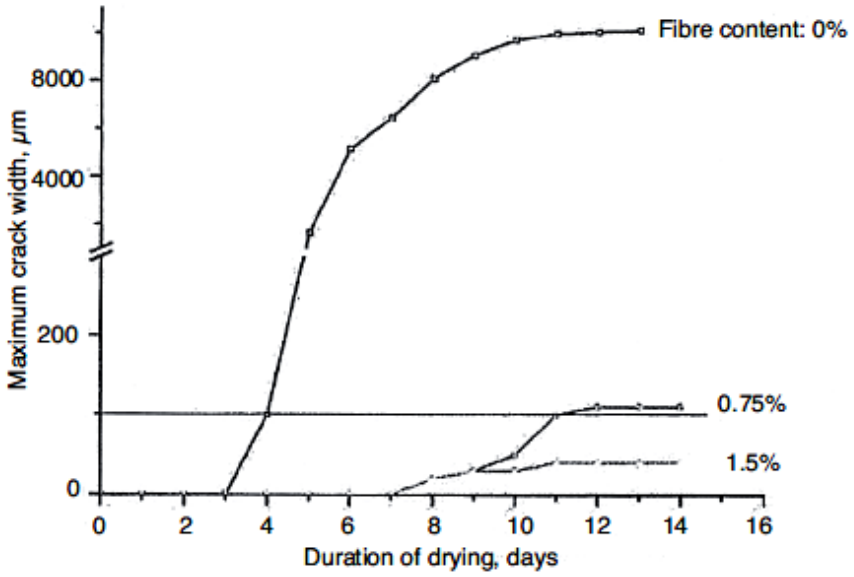

Figure 2.10 Influence of fiber reinforcement on maximum crack width (Shah and Weiss, 2006)

The effect of various types of fiber and shape geometry on the free shrinkage and crack resistance has been investigated by Voigt et al. (2004). The results revealed that whenever the numbers of fibers increases (i.e., a decrease in the specific gravity of the fiber), the strength of the concrete to resist cracks increases. With 30-millimeter length flat end, the steel fiber is able to extend the time required to form cracks as well as decrease crack width. Similarly, Hwang and Khayat (2008) utilized different types and volumes of fiber in the concrete and tested for restrained shrinkage. The authors used two types of fibers, 50-millimeter length circular cross section and 40-millimeter length rectangular cross section, to conduct the study. The results indicated that adding fibers at 0.25% and 0.50% showed an increase in crack resistance regardless of the type of fibers. Furthermore, Qi et al. (2003) and Passuello et al. (2009) indicated that the use of micro-fibers has a greater influence on reducing crack width than macro-fibers.

2.4 Effect of Environmental Conditions on Concrete Cracking

2.4.1 Ambient Relative Humidity

In hot weather, the rate of water evaporation from the surface of the concrete increases; this is especially when high temperatures are accompanied by low relative humidity and high wind speeds. Thus, the high rate of water evaporation leads to increasing the shrinkage and possibility of cracks in concrete.

Relative humidity is a ratio of the actual amount of water vapor (content) in the air in comparison to the maximum amount of water vapor that the air is able to contain (capacity) at the same temperature. It is expressed as a percentage (Equation 2.3). The warmer the air, the more moisture it can hold. The opposite is equally true such that the cooler the air, the less moisture it can hold.

$$RH = \frac{water\ vapor}{maximum\ water\ vapour} 100 \qquad (2.3)$$

The data in Table 2.1 indicate that warmer air has a higher saturation mixing ratio than cooler air at a constant atmospheric pressure. It is important to note that this relationship between temperature and water vapor content in the air is exponential, not linear. In other words, for each 10-degree increase in temperature, the saturation mixing ratio increases by a larger quantity.

Table 2.1 Maximum water vapor capacity (Pidwirny, 2006)

Temperature Degree (^{o}C)	Water Vapor Capacity (g) per Kilogram of dry air
50	88.12
40	49.81
30	27.69
20	14.85
10	7.76
0	3.84

In cases of not adding, or removing, any water to the air, an increase in temperature leads to an increase of the air's capacity to hold more moisture (Table 2.1); thus, the RH will decrease accordingly (Figure 2.11).

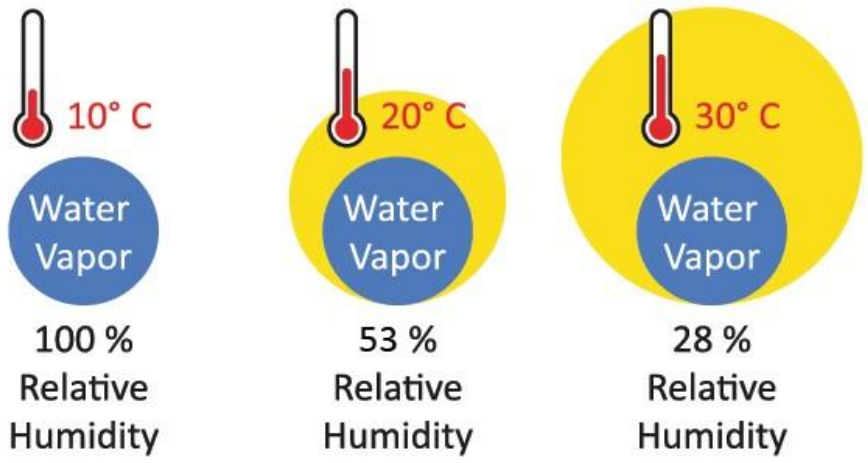

Figure 2.11 The relationship between RH and increasing air temperature

A concrete structure surrounded by low RH ambient air necessarily suffers more drying as a result of increasing the moisture evaporation from the surface of the concrete. Consequently, more water from the concrete will be removed; therefore, water withdrawal-induced stresses may cause shrinkage to the concrete.

Cheng and Johnson (1985) indicated that cracking tendency, particularly in fresh concrete, increases with a decrease in the RH surrounding the concrete structure. This is attributable to an increase in the rate of moisture evaporation from the

concrete surface which leads to an increase in the sensitivity of the concrete to plastic shrinkage cracking.

2.4.2 Air Temperature

The air temperature has a pronounced influence on the properties of concrete, especially with respect to shrinkage. A rise in air temperature can decrease the RH whereby an increase in concrete drying is expected. Furthermore, the rise may result in a thermal gradient with the concrete. Hence, the heat produced from cement hydration, as well as extreme weather conditions, considerably affects the properties of the concrete. As mentioned earlier, the appearance of effective differences in concrete temperatures, either with its surrounding atmosphere or within its profile depth, leads to the development of thermal stresses. Moreover, there are two types of temperature gradient: *external* and *internal*. The external temperature gradient occurs as a result of a difference in the rate of concrete cooling/heating and the rate of ambient air temperature change. Under conditions of very low temperatures, a high temperature gradient develops due to the hydration heat of the cement; thus, thermal shrinkage occurs as a result of the formation of thermal stress. Inversely, temperature variance occurs in very hot weather due to an increased/higher air temperature in comparison to the temperature of the concrete.

Schmitt and Darwin (1995) reported that construction time plays an important role in forming cracks in bridge deck concrete. The authors concluded that in either cold or hot weather conditions, the produced concrete is prone to cracking, particularly on the surface of overlays constructed on the deck slab. Moreover, the temperature variance between day and night also affects the properties of the produced concrete, especially in its durability aspects. Generally, placing concrete in an extreme temperature, whether high or low, leads to increased shrinkage. Consequently, an increase in the probability of cracking will occur. This may be attributed to a decrease in the RH, which is a key factor in providing more stresses inside the concrete as a result of drying (Figure 2.12). Undoubtedly, it is not recommended to cast concrete in these temperatures.

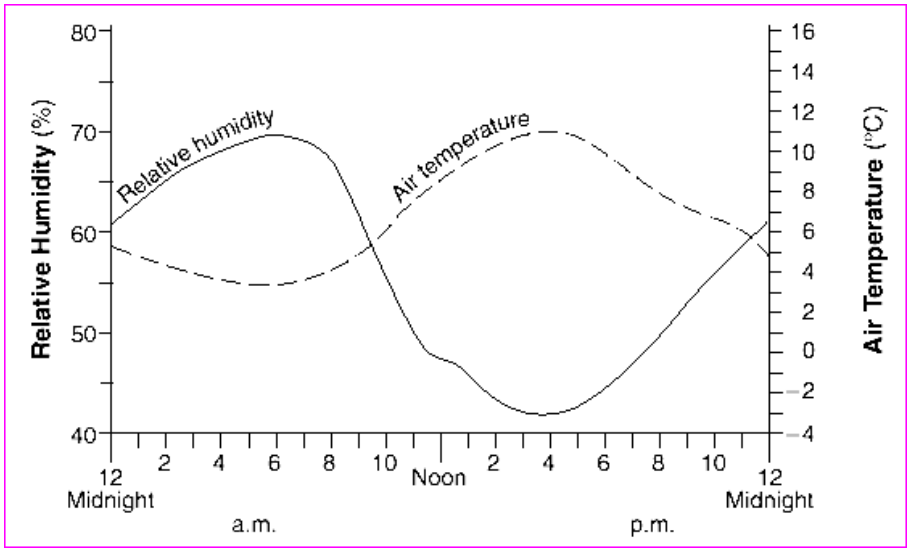

Figure 2.12 Variances of air temperature and RH during the day

2.4.3 The Effect of Wind Speed

Wind speeds, as well as other factors such as RH and concrete temperatures, are directly related to the evaporation rate of the mixing water. If the evaporation rate exceeds the water bleeding rate, shrinkage occurs in the concrete in both its fresh and hardened state. Water bleeding of concrete can be defined as the movement of water to the surface of the concrete. Hence, an increase in wind speeds and a decrease in RH may increase the rate of water evaporation; thus, the shrinkage of concrete also increases. With the respect to concrete structures, the rate of evaporation is a function of several factors such as air temperature, wind speed, RH and concrete temperature. In this regard, ACI (2001) proposed a nomograph (shown in Figure 2.13) to estimate the evaporation rate for concrete exposed to different environmental factors such as RH, wind speed and temperature.

ACI (2001) indicated that concrete bleeding is approximately 0.2 lb/ft^2/hr for normal concrete and 0.1 lb/ft^2/hr for high performance concrete made with low w/cm or concrete containing SF. Thus, many researchers have recommended a minimum evaporation rate by taking into account certain factors (e.g. windbreaker or fogging). The goal of decreasing evaporation is to keep it below the threshold of the concrete bleeding rate. Kochanski et al. (1990) recommended that the evaporation rate during concrete placement should be a maximum of 0.15 lb/ft^2/hr. VDOT (2016) recommended that, the maximum evaporation rate of high performance bridge deck concrete should not exceed 0.05 lb/ft^2/hr.

2.5 Construction Procedures and Curing

In the construction field, construction procedures such as sequences of concrete placing, rate of concrete pour and concrete finishing significantly affect the resistance of concrete to cracking. In this regard, Issa (1999) recommended special procedures to cast bridge deck spans. He recommends completing the concrete casting of the positive moment area of bridge deck spans before any negative areas in order to decrease the risk of cracking in the concrete. Kochanski et al. (1990) recommend 0.6 span length/hour as a minimum rate of concrete pour to avoid delays in concrete finishing. Moreover, Krauss and Rogalla (1996) reported that a delay in the start time of the concrete finishing leads to an increase in the cracking of the concrete.

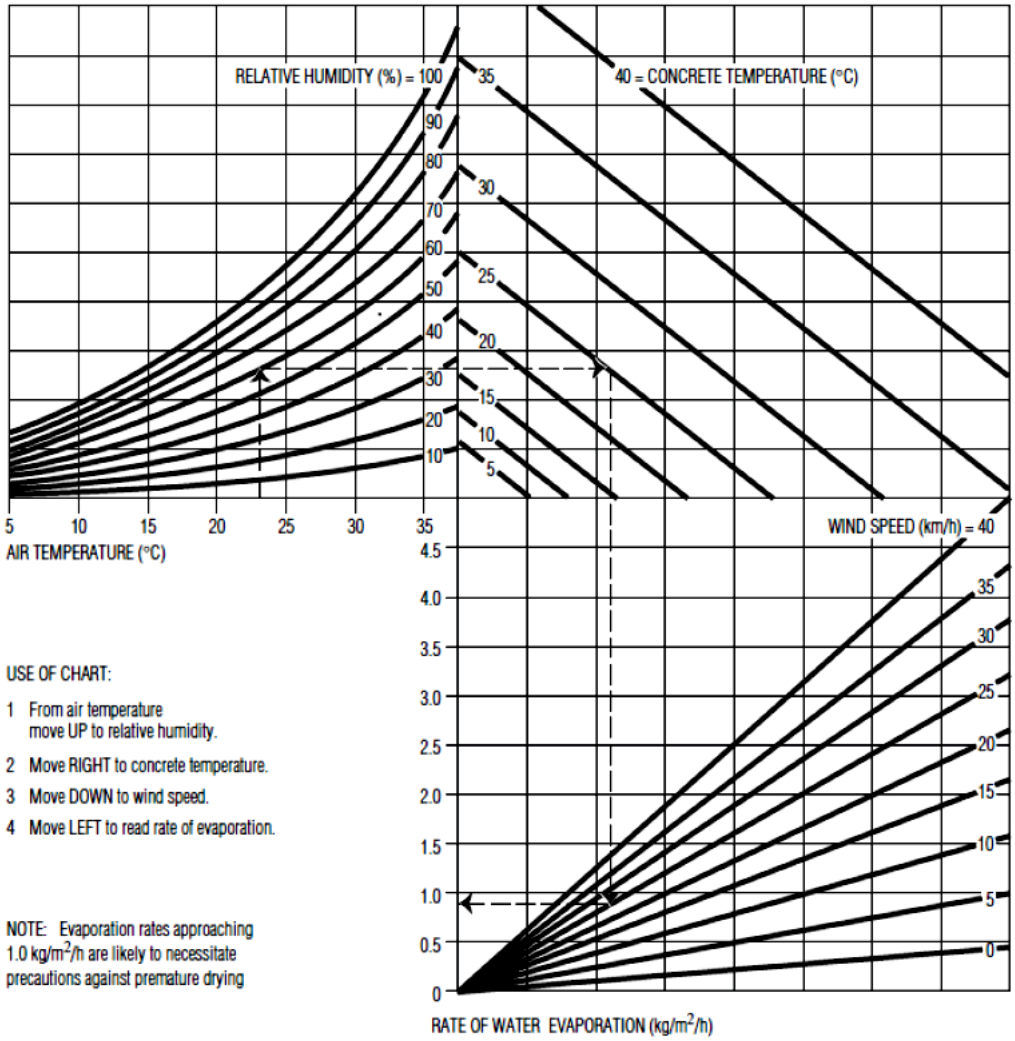

Figure 2.13 Nomograph to estimate the maximum rate of evaporation from concrete (ACI, 2001)

Curing is a preventive process the function of which is mainly aimed at keeping the concrete as saturated as possible. Two common methods of curing with different procedures are applied: *wet curing* and *membrane curing*. In general, the risk of cracking in concrete considerably decreases if adequate and timely curing procedures are followed. In concrete structures, whenever the area-to-volume ratio increases, the shrinkage and/or water drying also increases, particularly in thin structures such as bridge decks. Moreover, the delay or the exclusion curing process causes an increase in the tendency of concrete to crack due to shrinkage-induced stresses. Hence, proper curing should be conducted for concrete elements essentially after the cast of the concrete (Bentz and Jensen, 2004; Krauss and Rogalla, 1996; Schmitt and Darwin, 1995). Adequate curing not only decreases the risk of shrinkage cracks, it also enhances the strength of the concrete due to an available abundance of mixing water to complete the hydration process of the cement. In addition to mechanical properties, aspects of durability, such as permeability and sorptivity, are also enhanced by curing the concrete. Holt (2001) studied the effect of concrete curing on shrinkage properties by conducting three different types of curing. The author concluded that the highest values of shrinkage were recorded for dry air cured concrete. Moreover, the study results revealed that the best performance of shrinkage was observed for wet curing concrete (Figure 2.14).

2.6 The Design of Bridge Deck

2.6.1 Bridge Deck Type

In general, decks constructed using steel girders have a higher tendency to crack than those constructed with concrete girders (PCA, 1969; Cheng and Johnson, 1985; Krauss and Rogalla, 1996; Frosch et al., 2003). This behavior is attributed to the differences of thermal conductivity between the deck concrete and steel girder and the rate of temperature loss or gain between concrete and steel. However, Schmitt and Darwin (1995) investigated the effect of deck type on the crack density of bridge decks. The authors concluded that the deck types did not significantly affect the propagation of cracks in concrete.

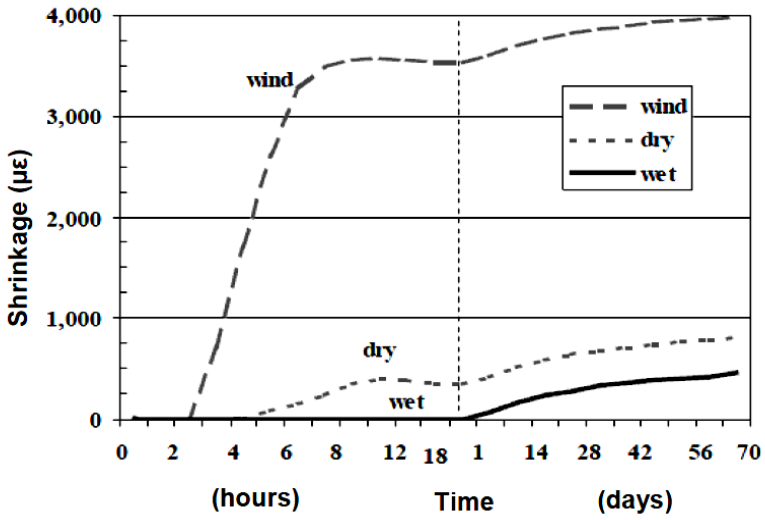

Figure 2.14 Effect of different type of curing on the shrinkage of concrete (Holt, 2001)

2.6.2 Deck Thickness

It can be argued that the increase in the thickness of a bridge deck directly leads to an increase in the resistance of concrete to cracking (Poppe, 1981; Kochanski, 1990; Ramey et al., 1997; French et al., 1999). When the deck thickness increases, the stress developed in the deck linearly decreases; thus, cracks created by shrinkage stresses decrease (Pease et al., 2006). However, Krauss and Rogalla (1996) reported that the decrease in the cracks for high thickness decks was attributable to non-uniform thermal and shrinkage stresses. Several studies recommend to increase the thickness of bridge decks in order to make the deck more resistant to cracking (Meyers, 1982). Hence, Kochanski et al., (1990) proposed a deck thickness of between 215 and 230 mm; while, French et al. (1999) suggested 160 mm as a typical thickness.

2.6.3 Top Cover of Concrete

The increase in the concrete cover may enhance the resistance of concrete to the potential of cracking and crack formation (Dakhil et al., 1975). Moreover, high thickness concrete covers lead to a decrease in crack width due to a decrease in reinforcing bar-induced stresses. Several previous studies proposed minimum limits for concrete covers in order to avoid cracks. Schmitt and Darwin (1995) suggested a concrete cover thickness ranging from 51 mm to 76 mm for monolithic decks.

Furthermore, Krauss and Rogalla (1996) reported that minimum cover thickness should be not less than 50 mm. However, for design considerations, AASHTO (2012) indicate a minimum top cover thickness of 63 mm.

2.6.4 Reinforcement

Reinforcement bar characteristics, such as size, type and spacing, significantly affect the presence of cracks in concrete structures (Dakhil et al., 1975; Kochanski et al., 1990). Several studies have proposed that a minimum bar size should be used in structural elements. Kochanski et al. (1990) and Ramey et al. (1997) suggested that the maximum reinforcing bar in concrete should not exceed size No. 5. Krauss and Rogalla (1996) recommended No.4 and 150 mm as a maximum bar size and maximum spacing, respectively. However, to decrease the tendency of cracking in concrete, the bar size and spaces between them should be reduced (French et al., 1999; Babaei and Hawkins, 1987; Schmitt and Darwin, 1999).

2.7 Restrained Shrinkage Test Methods

In general, free shrinkage studies are important for predicting the behavior of concrete with regard to the amount and volume change rates. Concrete with no external and/or internal restraints can freely shrink under a specific magnitude of strain. However, free shrinkage does not represent the actual tendency of concrete to crack because most structures have a degree of internal and/or external restraint.

The tensile stress in a concrete matrix forms and increases when; the structural concrete members are fully or partially restricted. Cracks form when the shrinkage-induced tensile stresses exceed the tensile strength of the concrete.

As mentioned earlier, cracks are deemed to be a negative factor in concrete because they provide an easy path for water, oxygen, moisture, chlorides and other harmful agents to ingress into the concrete. In addition, they reduce the ability of structural elements to carry and transform the applied loads. Therefore, crack formation decreases the durability and service life of the structural concrete. In general, the characteristics of cracks, such as their orientation, width, time-to-crack and crack density, are the essential expectations focused on in previous literature. Different methods have been proposed by several researchers to estimate the tendency of

concrete to crack. Tritsch et al. (2005) divided these tests into three main categories: linear, plate and ring tests. In the linear test, for example, uniaxial stress increases because concrete elements are restrained. Moreover, the test is often complicated because of the end condition of the bar used in the test (Weiss et al., 1998). However, several studies used flared ends in a closed loop apparatus to test the shrinkage of concrete specimens as a linear test (Paillere et al., 1989; Kovler, 1994; Bloom and Bentur, 1995). Moreover, this test is used to calculate the stresses induced in the concrete corresponding to any specified deformation. In the test, one of the specimen ends does not allow moving in order to develop a restraint in the specimen; the other side of the specimen is installed into a device loading to provide the required stress. However, the length of the specimen normally preserves its origin (i.e. stress control).

A plate specimen is used to simulate the structural elements or specimens which induce shrinkage stresses in two directions. The two directions of stress are normally called bi-axial stress. The plate tests are conducted to investigate the bi-axial restraint cracking of plastic shrinkage. In fact, when shrinkage stress develops as a bi-axil stress condition, the concrete will be affected by the structural (geometry of the specimen) and material properties. Thus, it is difficult to determine the effects of the material used to evaluate the tendency of concrete to crack (Grzybowski and Shah, 1990). Weiss and Shah (1997) reported that the structural elements can easily be correlated when using the bar and plate tests shapes because these tests simulate the behavior of the structural elements. In addition, Weiss et al. (1998) used the specimen geometry, similar to the plate shape, to simulate the restrained concrete in bridge decks and highway pavements. The authors used long and thin thickness specimens to prevent a variety of moisture between the concrete core and its surface and to provide sufficient tensile stress in the specimen, which can lead to the formation of cracks. Irrespective of the advantages in the bar and plate tests, they were deemed as eccentricities due to the difficulty of installing the ends of the specimen. Hence, researchers used cheap and easy tests (ring specimen tests) to estimate the tendency of concrete to shrink and crack as well as to estimate its cracking potential (time-to-cracking) and the behavior of the stresses in both the concrete and/or mortar.

The ring test is considered the easiest and most common test used by many researchers. In the test, concrete is cast around the steel ring of a specimen. The dimensions of a specimen vary depending on the restrained condition and the concrete material (e.g. aggregate size). Previous studies have revealed that ring diameter significantly affects the results for drying shrinkage. In a bridge deck, a 305-millimeter diameter steel ring was used to simulate the most critical case of restrained shrinkage (Morris, 2002). Moreover, a 305-millimeter diameter steel ring represents a condition of uniaxial stress which is applied to the restrained concrete specimen. In addition to stress, the test can evaluate the effect of various materials on the shrinkage tendency of concrete (Grzybowski and Shah, 1990; Shah et al., 1992; Weiss and Shah, 1997; Wiegrink et al., 1996).

2.8 Mechanism of Crack Formation in Fiber Reinforced Concrete

From a mechanical point of view, there are three phases present in concrete: the aggregate phase, the cement paste phase and the ITZ between the cement paste and the aggregate. In normal concrete, the ITZ layer is considered the weakest phase inside the concrete microstructures (Hearing, 1997; Nili and Ehsani, 2015). Due to this weakness of ITZ, micro-cracks form even without loads applied (Kwak and Filippou, 1992). As mentioned previously, micro-cracks form when the shrinkage or thermal stresses exceed the tensile strength of the concrete. Moreover, if the applied load exceeds low concrete tensile strength, cracks also appear. Hence, cracks are unavoidable inside the concrete matrix (Hameed et al., 2010).

In fiber reinforced concrete, the matrix transfers a part of the stress to the fibers before the onset of cracks (Døssland, 2008) by arresting any micro-cracks. Thus, fibers increase the strength of concrete because its elastic modulus is higher than the modulus of the concrete (Mo et al., 2014). As the load increases, the micro-cracks merge, grow wider and coalesce to form macro-cracks. In this case, if the fibers have sufficient length, a bridging will occur. This fiber bridging will control the crack propagation and an increase in toughness and ductility may result. The load transmission from the matrix due to the fiber is dependent on the properties of the fibers (e.g., physical, geometry, and mechanical), the matrix properties, and the matrix-fiber interface (e.g. the bond between the fiber and the surrounding matrix).

The fiber efficiency is the ability of the fiber to transfer the matrix stress by bridging. It ranges from 0% to 100%, depending on the fiber pullout behavior.

2.8.1 Cracking in Conventional Fiber Reinforced Concrete

In general, concrete that is prepared utilizing discontinuous fibers is known as Fiber Reinforced Concrete (FRC). Pozzolans and other admixtures might be added to this concrete to enhance its properties. In construction work, the aim of using FRC is to increase the toughness and load-carrying capacity of concrete. In FRC, there is no significant effect in the crack, post-crack stress and corresponding strain capacity of concrete because the volume fraction of fiber is low (approximately 1%). However, the initiation and/or propagation of cracks essentially decrease in FRC (Naaman and Reinhardt, 1995). In the same regard, the type of fiber used inside the concrete matrix play an essential role to indicate the response of concrete upon first cracking. Furthermore, another factor affecting concrete behavior is the fiber fraction volume. A critical fiber volume can be defined as the minimum amount of fiber required for hardening behavior after first crack occurrence. However, the volume fraction of the fiber used in concrete may be limited by the workability requirements of the concrete. Hence, utilizing the optimum amount of fiber leads to obtaining the hardening response in the concrete.

In conventional concrete, there is no load-carrying capacity after the first crack initiated because of the brittleness of the concrete. Conversely, in FRC, the load-carrying capacity continues to decrease with regard to the residual strength. The mechanism of the cracking in FRC mainly depends on the incorporated fiber characteristics, such as volume, physical properties, orientation and the interaction between the fibers and the concrete matrix. Upon the first crack in FRC, the load transfers across the crack via bridging fibers located in the ITZ of the concrete; therefore, a localized crack appears (Figure 2.15). Depending on the fiber characteristics and the interlocking with the concrete matrix, a crack of unlimited width results the strain-softening behavior in the concrete. This behavior is attributable to the pullout of the fibers due to an increase of the stress on the concrete. It was reported that the utilization of low fraction fiber leads to strain-softening behavior in FRC (Soroushian and Bayasi, 1991; Bayasi and Zeng, 1993; Shah et al., 1988). To obtain the desired application, different types of fiber, such as

steel, polypropylene and glass fiber, etc., could be used in concrete. Hence, it is important to accurately specify the proper type of fiber used in concrete to meet the required specifications.

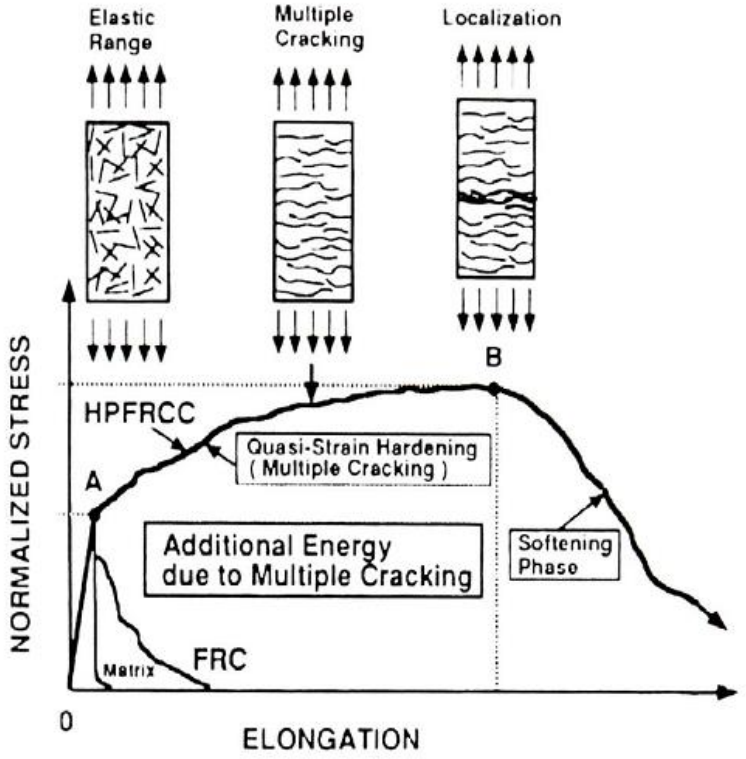

Figure 2.15 Multiple cracking mechanism and the effect of fibers on energy dissipation capacity (Naaman and Reinhardt, 1995)

2.8.2 Cracking in High-Performance Fiber Reinforced Concrete

In strain-softening, a single localized crack occurs when the load capacity of the concrete decreases and the crack width becomes unlimited. Conversely, multiple sub parallel fine cracks are formed after the formation of the first crack in a strain-hardening response system. Cracks form until the maximum post-crack stress is reached whereby load capacity rises as a result of creating new multiple micro-cracking somewhere else rather than a crack widening. Thus, more fracture energy absorption will occur.

Crack width is restricted due to the bridging formed by fibers which cause fiber pullout resistance. In fact, the limitation of crack width is known as crack control. Finally, after the maximum post-strength is reached, localized cracks form in the matrix at the weakest part. As a result, a reduction in fiber pullout resistance or fiber

fracture is expected whereby softening behavior similar to conventional FRC will occur.

High-Performance Fiber Reinforced Concrete (HPFRC) is a new type of concrete developed to describe the crack performance. It is concrete response as quasi-strain hardening behavior. Its behavior mostly appears as multiple cracks and energy absorption capacity. In Figure 2.15, the main point of a strain-hardening response system is that the post-cracking strength (point B) is greater than the first crack strength (point A). As previously mentioned, HPFRC can produce multiple cracks, mostly micro-cracks. As a result of the formation of multiple fine cracks (less than 100 micrometers in width), it helps to enhance the permeability of the concrete against harmful agents that penetrate into the concrete, thus enhancing the durability and service life of the concrete structures (Wang et al., 1997; Şahmaran et al., 2007; Mihashi et al., 2011). Moreover, when the produced concrete behaves as a strain/deflection hardening response, the stiffness of concrete structures also increases, so the excessive deflection due to applied loads decreases (Blunt and Ostertag, 2009).

2.8.3 Types of Fibers

Fibers can be divided according to their material, size and strength. Firstly, the material classification depends on the origin material from which the fiber is made, which may be polymeric, metallic, or natural. Indeed, the type of fiber material plays an important role in the bond between fibers and the concrete matrix. The bond may be classified into three main bonds: mechanical, physical or chemical bonds. For instance, steel fibers have a good mechanical anchor with the matrix, especially in the hooked end fiber type, whereas synthetic fibers have a chemical bond. Moreover, fiber bonds can be improved by adding admixtures according to the kind of fibers being used and the properties of the concrete.

The second classification of fibers is according to their size. Generally, they are divided into two types: micro-fibers and macro-fibers. Micro-fibers are defined by ACI (2016) as fibers with an equivalent diameter (d_e) of less than 0.3 mm. This type of fiber is usually used to enhance the concrete properties in a plastic state such that it increases crack resistance. On the other hand, macro-fibers are larger in size than

micro-fibers with an equivalent diameter greater than 0.3 mm. Moreover, they are used to increase post-cracking and toughness by bridging the crack zone, thus increasing the load which was transferred through the fibers.

The third and final classification of fibers is based on the fiber's strength or elastic modulus. They are grouped into either low or high elastic modulus in which low elastic modulus fibers refer to fibers that have a lower elastic modulus than that of concrete. Polypropylene, nylon and cellulose fibers are deemed examples of this type of fiber. Steel, glass and carbon fibers generally have elastic modulus greater than that of concrete (Yurtseven, 2004). The physical properties of some fibers are presented in Table 2.2.

Table 2.2 Physical properties of some fibers (Löfgren, 2005**)**

Type of Fiber	Diameter [μm]	Specific gravity [g/cm^3]	Tensile strength [MPa]	Elastic modulus [GPa]	Ultimate elongation [%]
Metallic					
Steel	5-1 000	7.85	200-2600	195-210	0.5-5
Glass					
E glass	8-15	2.54	2 000-4000	72	3.0-4.8
AR glass	8-20	2.70	1500-3700	80	2.5-3.6
Synthetic					
Acrylic (PAN)	5-17	1.18	200-1000	14.6-19.6	7.5-50.0
Aramid (e.g. Kevlar)	10-12	1.4-1.5	2000-3500	62-130	2.0-4.6
Carbon (low modulus)	7-18	1.6-1.7	800-1100	38-43	2.1-2-5
Carbon (high modulus)	7-18	1.7-1.9	1500-4000	200-800	1.3-1.8
Nylon (polyamide)	20-25	1.16	965	5.17	20.0
Polyester (e.g. PET)	10-8	1.34-1.39	280-1200	10-18	10-50
Polyethylene (PE)	25-1 000	0.96	80-600	5.0	12-100
Polyethylene (HPPE)	-	0.97	4100-3000	80-150	2.9-4.1
Polypropylene (PP)	10-200	0.90-0.91	310-760	3.5-4.9	6-15.0
Polyvinyl acetate	3-8	1.2-2.5	800-3600	20-80	4-12
Natural-organic					
Cellulose (wood)	15-125	1.50	300-2000	10-50	20
Coconut	100-400	1.12-1.15	120-200	19-25	10-25
Bamboo	50-400	1.50	350-50	33-40	-
Jute	100-200	1.02-1.04	250-350	25-32	1.5-1.9
Natural–inorganic					
Asbestos	0.02-25	2.55	200-1 800	164	2-3
Wollastonite	25-40	2.87-3.09	2700-4100	303-530	-

2.9 Hybrid FRC

In general, one of the most apparent disadvantages of concrete is its brittleness and low tensile strength, which leads to inferior resistance to cracks (Rashiddadash et al.,

2014; Yan et al., 1999; Kayali et al., 2003; Brandt, 2008). For this, fibers can be incorporated into concrete, thereby helping to overcome this defect of concrete by making the composite (matrix and fibers) exhibit higher tensile strength, toughness and durability than conventional concrete (Kuder and Shah, 2010; Balaguru et al., 1992; Lau and Anson, 2006; Vogel and Svecova, 2012; Ezeldin and Balaguru, 1989). Hence, the properties of thus-produced concrete significantly depend on the characteristics of the fibers being used, including the physical properties and the original material from which the fibers were made.

Concrete mainly has three phases, C-S-H gels which are measured at the micron scale, sand that is measured in millimeters, and gravel that is normally gauged in centimeters. Similarly, cracks which form in concrete are also measured at different scales. In fact, micro-cracks and macro-cracks are created at different ages in concrete even before uploading the concrete. During the application of a load on the concrete, a crack first appears at the weakest region, particularly in the ITZ, which surrounds the aggregate particles and fibers. Inside the concrete matrix, multiple numbers of fine micro-cracks gradually merge with each other, forming cracks larger in size (macro-cracks) (Van Mier, 1997). Hence, incorporating micro and/or macro fibers in the FRC has been investigated since the 1930s by studying the effect of adding hybrid fibers into concrete of different lengths and/or types (Naaman and Najm, 1991). Multi-Modal Fiber Reinforced Concrete (MMFRC) is the first type of hybrid fiber concrete that has been produced, first achieved by Rossi et al. (1987). Using two or more different types of fibers together in concrete is normally called hybridization. Indeed, based on the fiber function, this system may improve the problems in concrete at different scales or ages (Yazıcı et al., 2007; Banthia et al., 2014).

Furthermore, utilizing a single fiber system in concrete may improve such concrete properties. For example, micro-fibers have the ability to arrest micro-cracks thereby increasing its strength upon first crack. On the other hand, the macro-fibers can bridge the macro-cracks and control the propagation of crack width; thus, an increase in post-strength and toughness are expected. There is complete agreement that, fiber synergy can be achieved by using two or more fibers which have a difference in type or length; this synergy leads to each fiber carrying out its function at a different stage from the other fibers. Therefore, the concrete properties will be enhanced in more

than one direction. In this sense, the use of the hybrid fibers system is more effective than the use of the single (mono) fiber system with respect to concrete improvement (Yang, 2011; Yao et al., 2003; Dawood and Ramli, 2010; Mobasher and Li, 1996).

A number of previous studies have reported that using steel micro and macro-fibers at different lengths revealed better results in terms of post-peak strength (Stähli et al., 2007; Mihashi and Nishiwaki, 2014; Markovic et al., 2003). The effect of micro- and macro-fibers at different scale levels of cracking are shown in Figure 2.16.

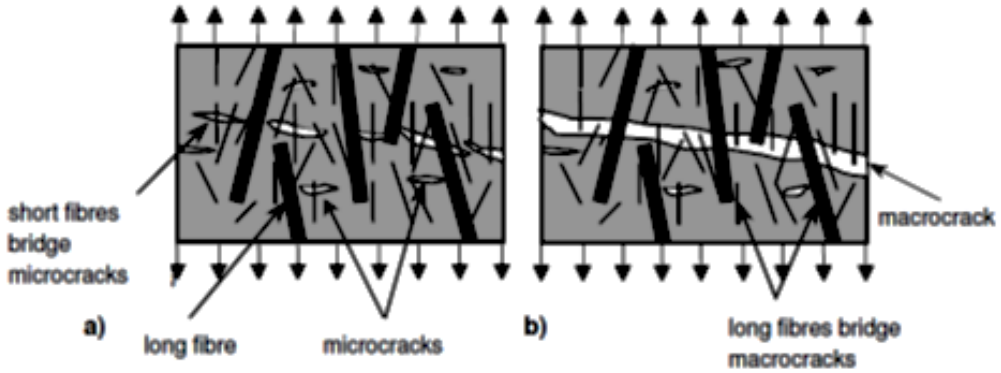

Figure 2.16 Effect of fiber size a) influence of short fibers on the bridging of micro-cracks b) influence of long fibers on the macro-cracks (Markovic, 2006)

The production of HPFRC is inversely affected by utilizing coarse aggregate because the risk of fiber balling increases in addition to an increase in the fracture toughness of the concrete; thus, it decreases the ductility (Li et al., 1995; Nallathambi et al., 1984). Irrespective of the fiber system (single or hybrid), HPFRC is generally produced by using a small aggregate size (Şahmaran et al., 2012; Ahmed and Maalej, 2009). However, limited literature has investigated the possibility of producing HPFRC by using a hybrid fiber system that overcomes the effect of coarse aggregate.

The effect of different types of fibers on the mechanical properties of concrete was investigated by Yao et al. (2003). For this, different types of fiber, such as carbon, steel and polypropylene fibers, are incorporated to examine the flexural strength and flexural toughness properties of concrete. The results showed that, even when using a single type of fiber, the fibers have positive effects on the toughness of concrete. Hence, optimum elastic-plastic response results were obtained by utilizing hybrid fibers (a combination of steel and carbon). Similarly, Yurtseven (2004) studied the effect of different types of fiber on the flexural strength and toughness of concrete.

The author used crushed limestone at maximum sizes of 12 mm and 5 mm as coarse and fine aggregate, respectively. Moreover, three types of fiber were used with a total fiber volume fraction of 1.5% as micro fibers. The results revealed that the inclusion of fibers leads to an increase of the flexural strength values. Furthermore, the increase in the aspect ratio of the fibers has a more obvious effect on the flexural strength property. The hybrid fiber system as a combination of macro steel fibers and micro steel fibers yielded optimum results. Blunt and Ostertag (2009) utilized a hybrid fiber system with a maximum aggregate size of 9.5 mm. The authors stated that the effect of this type of fiber system was more pruned than the single (mono) fiber system. As shown in Figure 2.17, the concrete produced by incorporating a 1.5% volume fraction of fiber revealed an increase in the value of its flexural strength in comparison with the single fiber system. Furthermore, the increase in flexural strength reached 196% when using the hybrid fiber system in comparison to plain concrete.

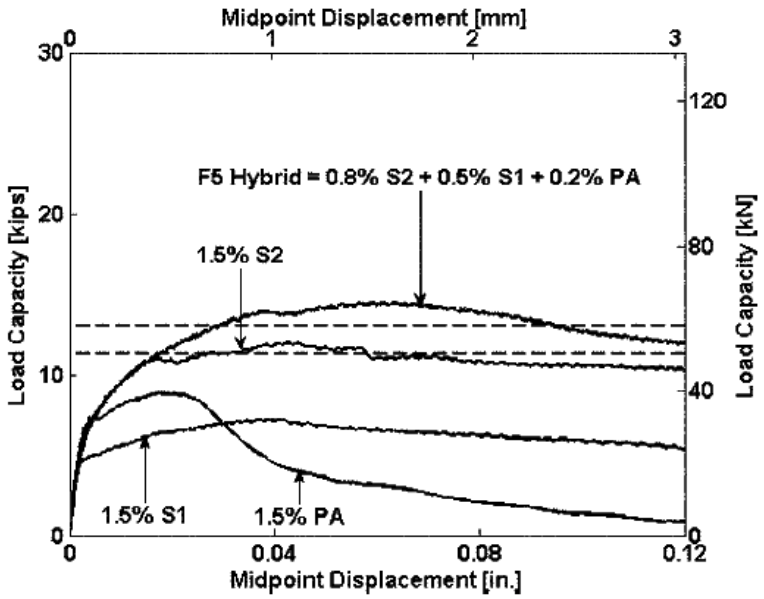

Figure 2.17 Typical flexural load-displacement curve of single and hybrid fiber proportion (Blunt and Ostertag, 2009)

2.9.1 Advantages of Hybrid Fiber

In terms of the type and/or geometry of the fibers, the incorporation of two or more different types of fiber in the concrete is called a hybrid fiber system. The main purpose of using a hybrid system in concrete is to combine each advantage of the fiber in a process called *synergy*; thus, the performance of a hybrid system would be

better than the use of a mono fiber system. According to Bentur and Mindess (2006), synergy can be classified into three main groups based on the cracking resistance mechanism:

- A hybrid system based on the strength and stiffness of fibers which can enhance the strength of concrete at different levels and/or ages of loading (pre-cracking and post-cracking). Fibers are more flexible and ductile than concrete; therefore, they are able to enhance the toughness of concrete and post-cracking behavior with regard to its hardening/softening response.

- A hybrid system based on the geometry of fibers where smaller sized fibers (micro-fibers) could arrest any micro-cracks, thereby delaying the merging of micro-cracks to form macro-cracks. Micro-fibers significantly affect the arresting of cracks due to their small diameter and due to the number of individual fibers (i.e. the least specific gravity and the greater numbers of fibers) which can be found in a cracked plane as compared to the same volume fraction of macro-fibers. The effect of fibers by delaying cracks leads to an increase of the tensile strength of the concrete. As shown in Figure 2.18, fibers also may restrict the propagation of opening cracks, thereby increasing the toughness of concrete and the composite strain (ductility of the fibers and matrix together).

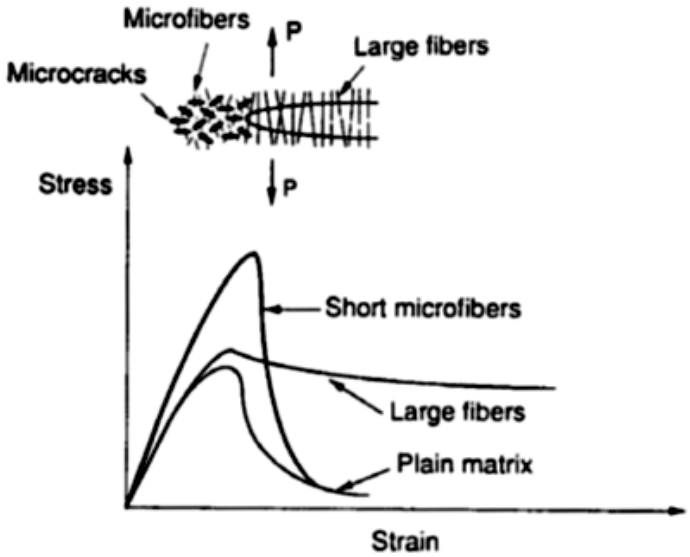

Figure 2.18 Effect of fiber size on crack bridging in concrete (Betterman et al., 1995)

- A hybrid system is based on the function of fibers; it improves the performance of concrete in the terms of its strength and toughness. Moreover, these fibers may enhance the resistance of concrete to cracking in the fresh stage. Incorporating low-modulus fibers enhances the shrinkage cracking resistance of concrete, whereas the toughness and ductility of concrete increase by adding high-modulus fibers. Similarly, using steel and synthetic fibers in concrete can increase the performance of the concrete in terms of toughness and cracking resistance, respectively (Cominoli et al., 2005).

The main purpose of fiber utilization in concrete, particularly the hybrid system, is to control the cracks that are formed in concrete at different sizes and at different loading ages. It can be argued that the increase in cracking width resistance leads to increases in the pre-cracking stress, toughness and post-cracking strength. Moreover, the increase in the post-cracking flexural strength makes the concrete prone to hardening behavior.

In the fresh state, using fibers significantly affects the workability of concrete, particularly in cases of casts in place (e.g. bridge deck slabs). Adding long fibers inversely affects the fresh properties of concrete, in particular at high dosages of fibers. A hybrid fiber system is deemed to be an alternative choice for preserving the consistency of concrete while keeping the mechanical properties at an acceptable level.

2.10 Factors Affecting Deflection/Strain Hardening Behavior

Hardening behavior is defined as applying load increases to concrete; in turn, the residual strength of the concrete correspondingly increases (i.e. the post-strength is higher than the first-crack strength). In FRC, this behavior mainly depends on the fiber efficiency to transfer the matrix load by fiber bridging. As mentioned earlier, the fiber efficiency is significantly affected by the matrix property, fiber and the matrix-fiber interface, which reflects, in turn, the fiber pullout behavior. In other words, the concrete's ingredient properties and their interaction with each other are intrinsic factors for identifying concrete behavior. The fiber pullout behavior (as a single fiber) and the volume fraction of the fiber added into the concrete dramatically affect concrete behavior as a hardening or softening response. As the subjected load

increases, the fiber pullout behavior goes through three major phases: de-bonding, full or partial chemical bond breaking and frictional resistance. At the final stage, the matrix-fiber interface may behave in a slip-hardening fashion, with constant friction, or with a slip-softening response (Figure 2.19).

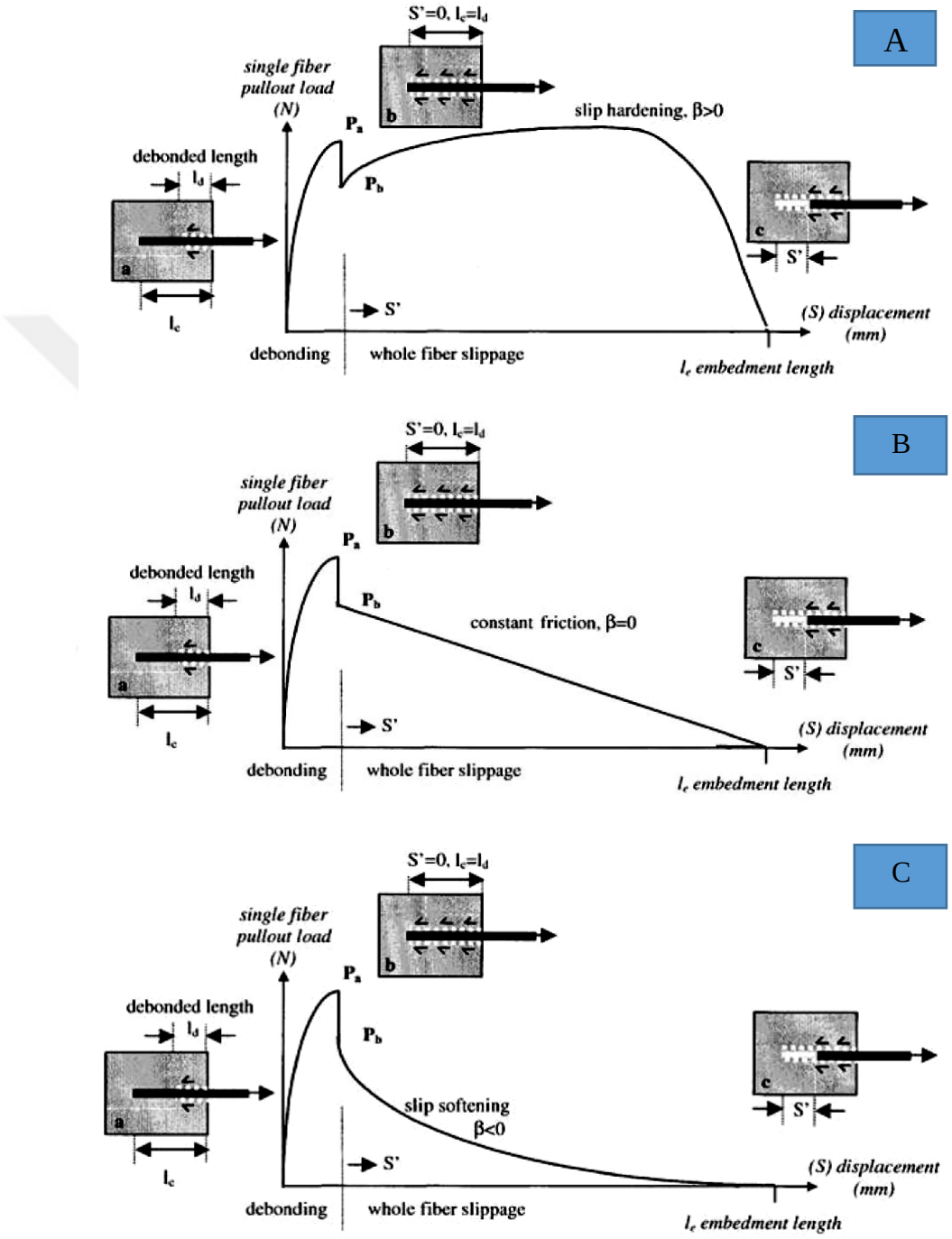

Figure 2.19 Pullout curve a) slip-hardening b) constant friction c) slip-softening (Redon et al., 2001)

The forming of multiple cracks in concrete mainly depends on the fiber, matrix and matrix-fiber interface properties. Finding equilibrium between these properties is essential. An increase in the bond between the fibers and the concrete matrix might increase strength accompanied by failure (rupture) due to a sudden break of the fiber itself and/or the aforementioned bond; thus, the composite (matrix and fibers) strength substantially depends only on the fiber strength. In terms of adhesive interfacial shear between the fiber and the concrete matrix, the fiber bridging may not be sufficient to transfer the load when the bond is not sufficiently strong. This phenomenon occurs due to the lack in the pullout resistance of the fibers; thus, the strength of the composite will indicate the level of strength in the concrete matrix. However, the fibers may fail to bridge the cracks even if the bond is strong. This behavior is attributable to the shortness of the embedment length inside the concrete matrix. Hence, to achieve adequate synergistic harmony between the strong-deformable fiber and the brittleness of concrete, a suitable ingredient should be selected regarding the fibers, matrix and the bonds between them.

2.10.1 Fiber parameters

Several properties of fibers, such as volume fraction, length and diameter, stiffness and strength, shape, and fiber material play important roles in fiber pullout behavior; thus, it will directly affect the behavior of the concrete. The distribution and orientation of fibers effectively contribute to increasing the tensile and flexural strength of concrete.

The inclusion of steel fibers at 2% in volume leads to an increase of the values of flexural strength as well as the modulus of the rupture of concrete (Song and Hwang, 2004). Moreover, hooked end steel fibers in concrete significantly increase toughness as compared with other types of fibers. Similarly, fiber content also plays an essential role in increasing the concrete's tendency to be more ductile. However, it was reported that the lengths of the hooked end steel fiber did not substantially affect the concrete's toughness (Balaguru et al., 1992).

The effects of fiber type on the flexural behavior of HPC were studied by Soroushian and Bayasi (1991). The authors reported that concrete at 2% hooked steel ends and aspect ratio ranged from 60 to 75 steel fibers revealed a higher flexural strength and

toughness than straight or crimped steel-fibered concrete. As previously mentioned, the aspect ratio of fibers has also a significant effect on the mechanical properties of the produced concrete. Yazıcı et al. (2007) reported that the incorporation of 45, 65 and 80 aspect ratio fibers could produce concrete with flexural strength values of 7.75, 9.33 and 10.76 MPa, respectively. However, Mehta and Monteiro (2014) reported that the inclusion of fibers has a greater effect on the toughness of concrete than the flexural strength. Indeed, the flexural strength and toughness values for fiber concrete increased by 2 and 20 times, respectively in comparison to plain concrete.

The material from which the fiber is made has a significant effect on the bond between the fiber and the surrounding matrix. This bond identifies the pattern of the failure during the pullout process. For example, steel fibers are considered to be hydrophobic fiber and the bond that develops during the pullout is a mechanical bond due to the anchoring at its ends. On the other hand, synthetic fibers, such as polyvinyl-alcohol (PVA) or nylon, have a hydrophilic characteristic which results in increasing the chemical and frictional bond. The fiber's hydrophilic nature allows water to ingress into the fiber surface leading to fiber swelling, which in turn causes an increase in fiber peeling followed by an increase in the pullout resistance after de-bonding (Geng and Leung, 1996). Some fibers have been treated with different types of material or their surface is deformed to enhance the bond. For instance, nylon fibers have been treated to enhance the surface bond and steel fibers are also coated or deformed for an improvement of the bond characteristic (Figure 2.20).

A good orientation and distribution of fibers positively affects the mechanical parameters of the concrete in terms of its post-cracking strength and ductility (Markovic et al., 2003; Stähli et al., 2007). It is believed that a sufficient orientation of fibers could decrease the fiber inclination angle with respect to the cracked tensile plane; thus, the effectiveness of the fiber to carry stress also increases via crack bridging. As depicted in Figure 2.21, the size and volume of the aggregate inside the concrete matrix inversely affect the orientation and distribution of the fiber as well as the consistency of the produced concrete. Hence, the utilization of coarse aggregate may increase the balling of the fiber; thus, there is a decrease in the distribution and orientation of the fiber. As a consequence, the numbers of fibers across the cracks would decrease in proportion to the increase in the inclination angle of the fibers (Johnston, 2004; De Koker and Van Zijl, 2004). The effectiveness of fibers to bridge

cracks increases or decreases according to the inclination angle of the fibers, especially when synthetic fibers are used, so that when the fibers are perpendicularly aligned to the cracked face, the fiber effectiveness becomes higher. Conversely, the effectiveness recorded a zero value when the fibers were parallel to the cracked face. Moreover, flexible fibers can be bent around aggregate particles sufficiently, thus significantly increasing the maximum fiber content at the cracked plane (Arısoy and Wu, 2008).

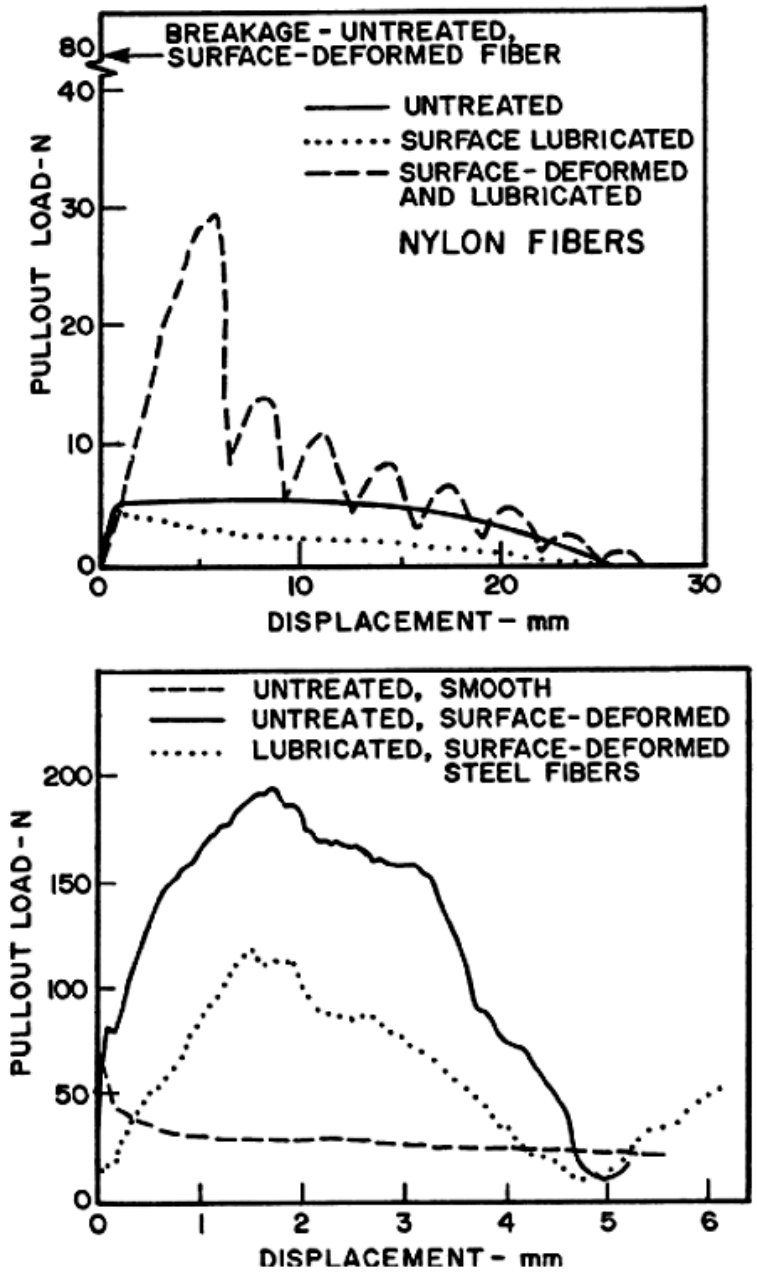

Figure 2.20 Comparative pullout resistance of smooth and surface-deformed nylon Fibers (upper) (Li et al., 1990) and steel fibers (lower) (Naaman and Najm, 1991)

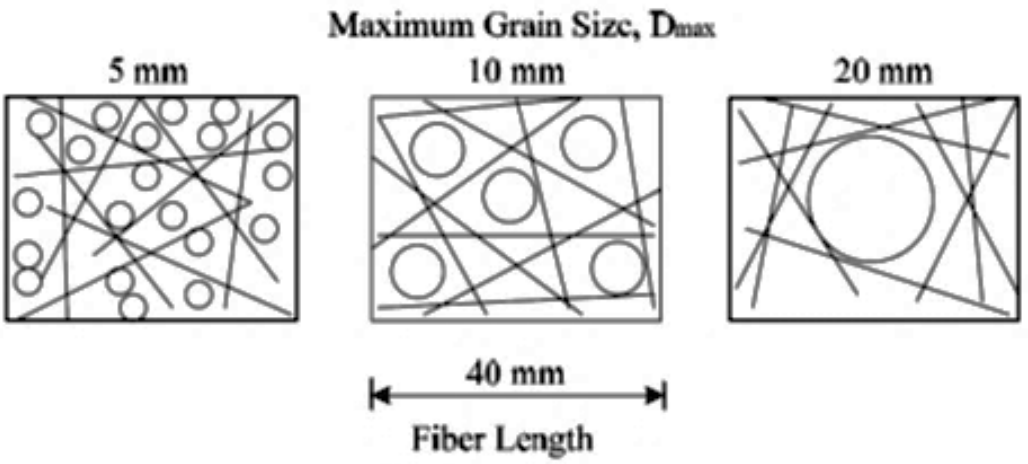

Figure 2.21 Effect of aggregate size on the fiber distribution (Johnston, 2004)

In the same regard, the tensile (pullout) strength of fibers deemed as the important factor affects the post-crack strength of concrete. Embedded large or long fibers lead to increase the surface area of fibers; thus, increasing the contact area between fibers and the surrounding matrix. On the other hand, some fibers ruptured before reaching to the full frictional resistance due to an increase in the surface strength of the fiber or lack in the fiber's tensile strength. Vandewalle (2002) recommended utilizing large fibers with lengths greater than the maximum aggregate size of the concrete mix. However, fibers with lengths greater than the maximum coarse aggregate size by a factor of 2-4 were also suggested in some of the literature, such as Grünewald and Walraven, (2002).

2.10.2 Concrete Matrix Parameters

As mentioned previously, the matrix properties play a significant role in identifying the fiber pullout behavior as a single fiber; thus, this behavior could reflect the behavior of concrete as a composite. In fact, the de-bonding of fibers as such does not occur at the surface between the fiber and the surrounding matrix; however, it is developed due to very fine cracks at a certain very small distance from the fiber (Bentur and Mindess, 2006). This distance is found in and through the ITZ (Figure 2.22). The figure shows that the pores size increases whenever the distance to the fiber is small. Therefore, improving the ITZ chemically or physically leads to enhancing the matrix-fiber interaction.

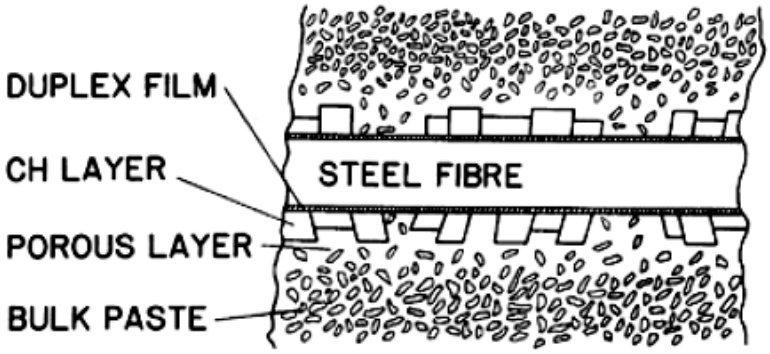

Figure 2.22 Schematic description of the ITZ around a fiber (Bentur and Mindess, 2006)

The inclusion of mineral admixtures, such as FA, SF and GGBFS, may increase the ITZ bond between the fiber and concrete matrix. The sizes of these materials are finer than cement particles; therefore, they are able to efficiently fill the empty voids between the cement particles and fibers. They are typical industrial by-products and thus they have two-fold benefits of being inexpensive and environmentally friendly. Table 2.3 illustrates some particle sizes of mineral materials. It should be noted that the particle sizes of these materials vary based on their manufacturing processes. In addition, Figure 2.23 shows some particle morphology of Portland cement, microsilica, fly ash and slag that are analyzed by a Scanning Electron Microscope (SEM).

Table 2.3 Typical particle sizes of common cementitious materials (Habeeb and Fayyadh, 2009)

Material	Typical particle size
Cement	10-40 µm
Fly Ash	0.5 µm to 100µm
Silica Fume	0.05 to 0.5 µm
Rice Husk Ash	20-60 µm
Slag	10- 50 µm

As shown in Figure 2.24, increasing the packing density of fine particles around the fiber also leads to an increase in the frictional bond. Guerrero and Naaman (2000) reported that an increase in the pullout strength of the fiber was enhanced when FA was incorporated into the concrete at 20% by volume. Furthermore, the packing density may be increased by optimizing the aggregate gradation used in concrete

mixtures. Silica fume exhibits a so-called pozzolanic reaction. During this reaction, the conventional calcium-hydroxide crystals are partly replaced with far stronger calcium silicate hydrate gel. This improves the overall strength and quality of the interfacial zone (Bentur et al., 1996). The shrinkage of concrete with a silica fume may also be 2 to 3 times higher compared to concrete without it. This means that the clamping pressure on the fiber due to the matrix shrinkage will also be higher if a silica fume is present in the concrete matrix (Li and Stang, 1997).

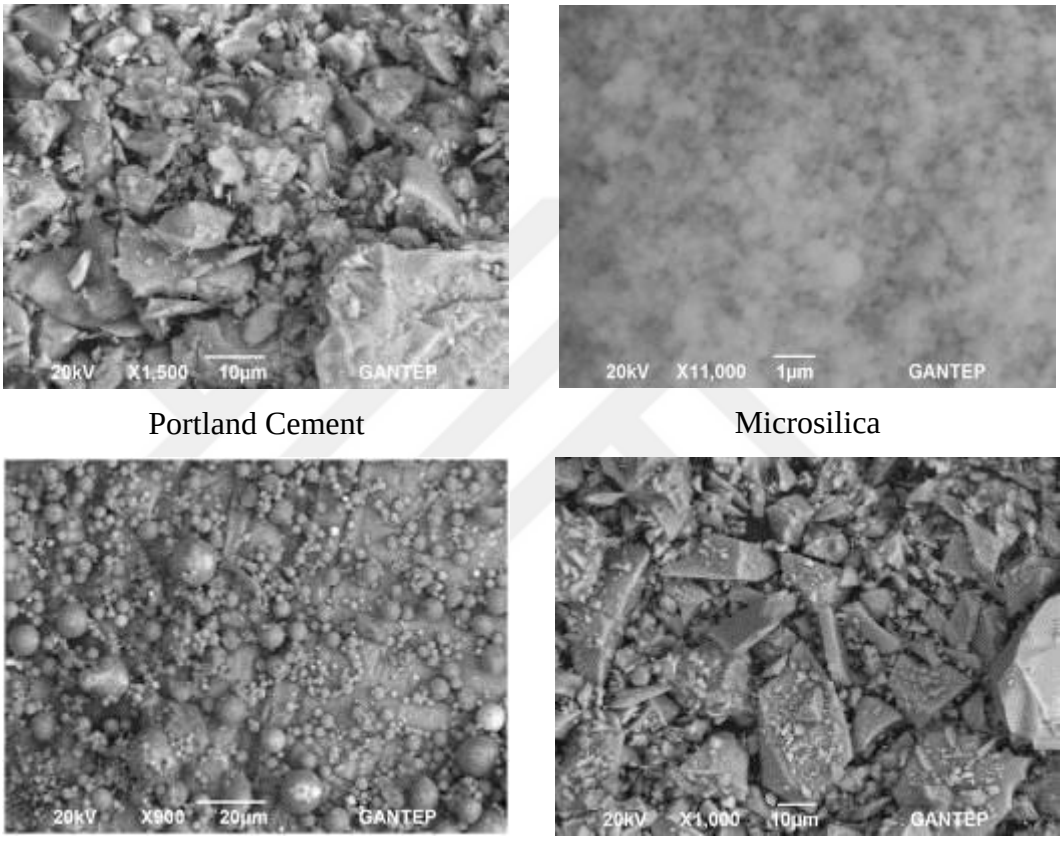

Figure 2.23 Particle morphology of Portland cement, microsilica, fly ash and slag analyzed by SEM (Yücel, 2013)

It is worth mentioning that a decrease in the w/cm ratio leads to an increase in the density of the micro-hardness layer surrounding the fibers (Wei et al., 1986) (as shown in Figure 2.25). Hence, a higher contact area between the fiber and the matrix is developed thereby contributing to an increase in the pullout capacity of the fibers (Van Gysel, 2000). The author also recorded an improvement in the pull-out force by 30-40% when the w/b ratio decreased from 0.45 to 0.29.

Increasing the quantity and/or aggregate size inside the concrete matrix may increase the fracture toughness; thus, it reduces the ductility of the produced concrete (Li et al., 1995; Nallathambi et al., 1984). However, utilizing industrial products as supplementary materials in concrete leads to a decrease in the concrete's fracture toughness (Şahmaran et al., 2012). Odendaal (2015) reported that an increase in aggregate size leads to a decrease in the values of the modulus of rupture. Furthermore, the energy absorbed decreased by 35% when the aggregate size increased from 6 mm to 19 mm.

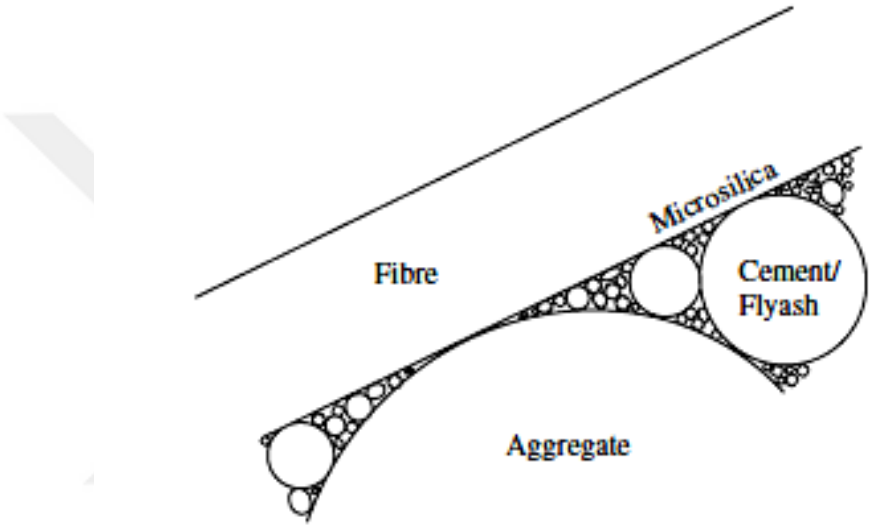

Figure 2.24 Dense packing of the concrete matrix close to a fiber (Stähli et al., 2007)

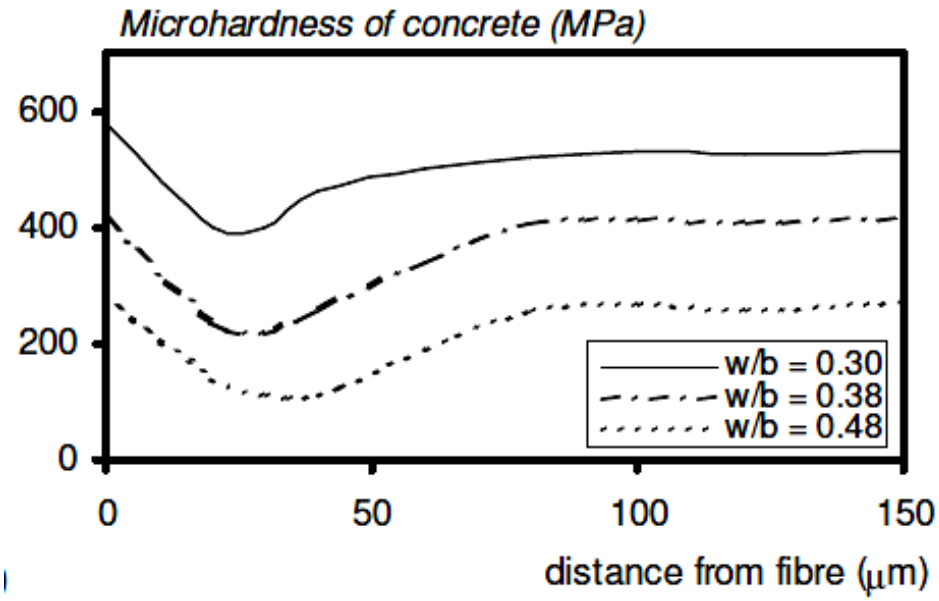

Figure 2.25 Effect of Water/Binder ratios on the micro-hardness around fiber (Wei et al., 1986)

2.10.3 Fiber-Matrix Interface

Cementitious composites are characterized by a transition zone in the vicinity of the reinforcing inclusion, in which the microstructure of the paste matrix is considerably different from that of the bulk paste away from the interface. The nature and size of this transition zone depends on the type of fiber and the production technology. In some instances, it can change considerably with time. These characteristics of the fiber-matrix interface exert several effects which should be taken into consideration, especially with respect to the fiber-matrix bond and the de-bonding process across the interface.

2.11 Evaluation of Concrete Performance Based on Slab Panel Specimen

The amount of energy absorbed while loading the structural elements, prior to and post fracture is named as toughness. The toughness and flexural performance of FRC can be calculated using several methods, two examples of which include beam and/or panel tests. The flexural and toughness of FRC is tested under uniaxial flexural circumstances using beam specimens. However, most structural applications, such as bridge decks, slabs and mine linings, mostly behave in a biaxial condition which may be investigated under a plate panel specimen (Preteseille et al., 2014). The measured flexural strength should be justified from a uniaxial stress condition to a biaxial stress condition. From a design point of view, the actual performance of structural design should be considered (Di Prisco et al., 2011; Minelli and Plizzari, 2007; Bernard, 2004; Destrée and Mandl, 2008). It is important to examine the flexural response of FRC under a biaxial condition to simulate the performance of the structural elements. Hence, panel tests are divided into two subcategories: square panels and round panels (Figure 2.26).

According to the European specification for sprayed concrete (EFNARC, 1996), the dimensions of the standard square panel specimen are 600×600×100 mm, whereas the round dimensions are 800 mm in diameter and 75 mm in height according to (ASTM- C1550, 2005). The toughness of concrete may be defined as the area under the load-deflection curve which is obtained from a bending panel test. Moreover, to calculate toughness, it is necessary to reach an ultimate value of deflection of 25 mm for square panel specimens and 40 mm for round panel specimens. Several studies

have reported that panel tests have less scatter (coefficient of variation) than beam tests (ASTM-C1609/C1609M, 2010; Bernard, 2004).

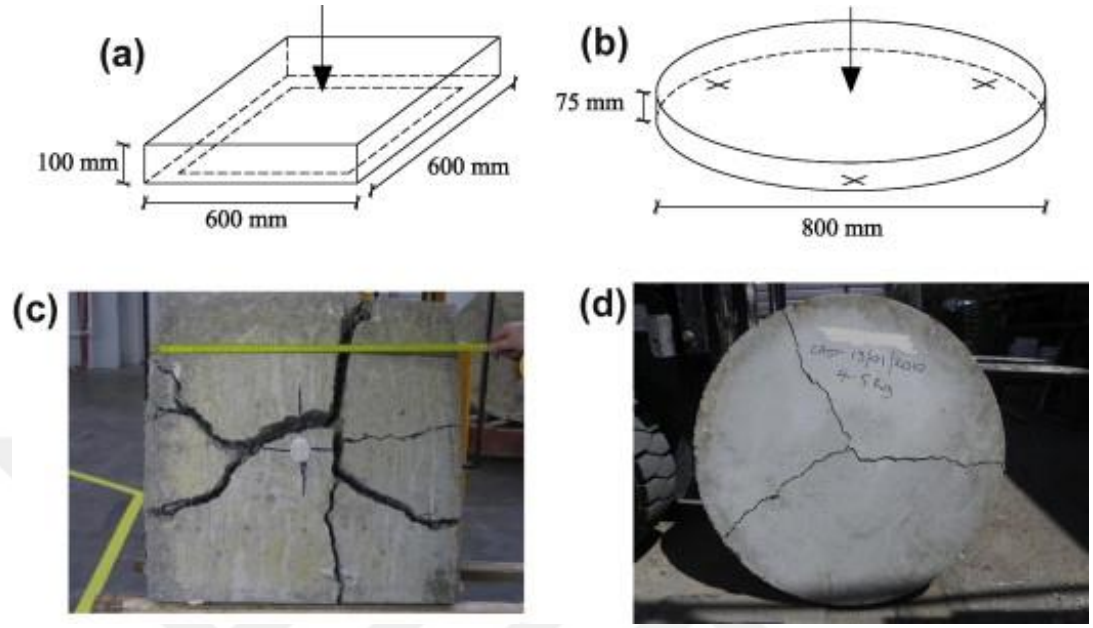

Figure 2.26 Round and square panel samples after testing (Ciancio et al., 2014)

Okuyucu et al. (2001) investigated two different types of fibers with a constant volume fraction of 1.5%. The fibers being used were hooked end steel fiber of length and diameter 30 mm and 0.55 mm respectively. The second type of fiber was polypropylene 50 mm in length and a 0.9 mm diameter. The authors conducted the panel test according to (EFNARC, 1996). The panel dimension was 600×600×100 mm. The results revealed that steel fiber showed higher ultimate loads than polypropylene fibers. Likewise, the energy absorption of 25 mm central deflection in polypropylene fibers concrete was higher than the other mixtures. Similarly, Cengiz and Turanli (2004) conducted experimental investigations on the effect of the incorporation of steel, steel mesh and High Performance Polypropylene Fiber (HPPF). The test was conducted using a panel in dimensions of 600×600×100 mm. The authors reported that HPPF enhanced the flexural ductility, toughness and load capacity of concrete. Moreover, the hybrid fiber made by mixing two types of fibers (steel and steel mesh fibers) showed encouraging performance in terms of mechanical properties in comparison to steel fiber and/or mono-steel concrete. Chao et al. (2011) also studied the effects of two different fiber contents (0.5% and 1.5 %) on the round panel. The hooked end steel fiber of length 39 mm and diameter 0.97

mm was adopted. The results showed that there was a deflection-hardening response under the round panel test, and a strain-softening behavior under a direct tensile test. The effect of both types of hybrid fibers on concrete was investigated by Rambo et al. (2014-a). The authors used straight steel fiber of length 12 mm and hooked end steel fibers of length and of fraction 35 mm and 1.0%, respectively, and 1.5% by volume. Furthermore, three different test methods were performed, namely direct tension, 4-point and round panel tests. Moreover, mineral admixtures were utilized in the concrete that was produced. The results revealed that the hybridized fiber system significantly restricted the initiation and propagation of cracks. Therefore, the appearance of a first-crack extended and increased the ultimate load on the concrete. Similarly, Rambo et al. (2014-b) studied the effect of hybrid fiber on the mechanical properties of maximum aggregate size 9.5-millimeter concrete. For this, two different types of fiber were used: straight fiber and hooked steel fiber. Their material and structural properties were tested with a 100×100×400-millimeter bending beam and a round panel 750 mm in diameter and 75 mm in thickness. The results showed that the hybridized fiber system was more significant in the panel test than in the bending beam test. The load to create the first crack as well as the ultimate load increased in the hybrid fiber concrete.

CHAPTER THREE

EXPERIMENTAL PROGRAM

3.1 Materials and Mixture Proportions

For the purpose of producing composite materials, CEM I 42.5R ordinary Portland cement (PC) which is similar to ASTM Type I cement, Class-F FA with a lime content of 9.78% and SF were used as the cementitious materials. The three different FA/PC ratios used throughout the present study were 0.20, 0.45 and 0.70. The total amount of SF utilized in the mixtures was kept constant at 7% of PC, by weight. Chemical and physical properties together with the particle size distributions of PC, FA and SF are shown in Table 3.1 and Figure 3.1, respectively. The used fine and coarse aggregates were river sand with a fineness modulus of 2.67 and crushed limestone with a maximum aggregate size (MAS) of 12 mm (Figure 3.2). As it can also be seen in Figure 3.1, fine and coarse aggregates were combined in order to obtain optimum gradation without sacrificing reasonable fresh concrete properties with the highest possible density. To find the well-graded aggregate combination, the 0.45 power chart method using the Fuller formula (Equation 3.1) was adopted. As a result, a combined aggregate gradation was formulated using 57% of fine and 43% of coarse aggregates by weight. During the production of the mixtures, three different total aggregates (coarse + fine aggregates) to binder (PC + FA + SF) ratios (A/B) were selected, as 1.0, 1.5 and 2.0.

$$PP_i = \left(\frac{d_i}{D}\right)^{0.45} \tag{3.1}$$

Where, PP_i is the cumulative percent passing from i^{th} sieve, d_i is the opening size of the i^{th} sieve and D is the maximum particle size (=12 mm).

Table 3.1 Chemical composition and physical properties of PC, FA and SF

Chemical Composition, %	**PC**	**FA**	**SF**
SiO_2	20.77	57.01	91.96
Al_2O_3	5.55	20.97	1.20
Fe_2O_3	3.35	4.15	0.84
MgO	2.49	1.76	1.02
CaO	61.4	9.78	0.62
Na_2O	0.19	2.23	0.67
K_2O	0.77	1.53	1.16
Loss on ignition	2.2	1.25	1.86
Physical Properties			
Specific gravity	3.06	2.02	0.60
Specific surface area (m^2/kg)	325	290	19080

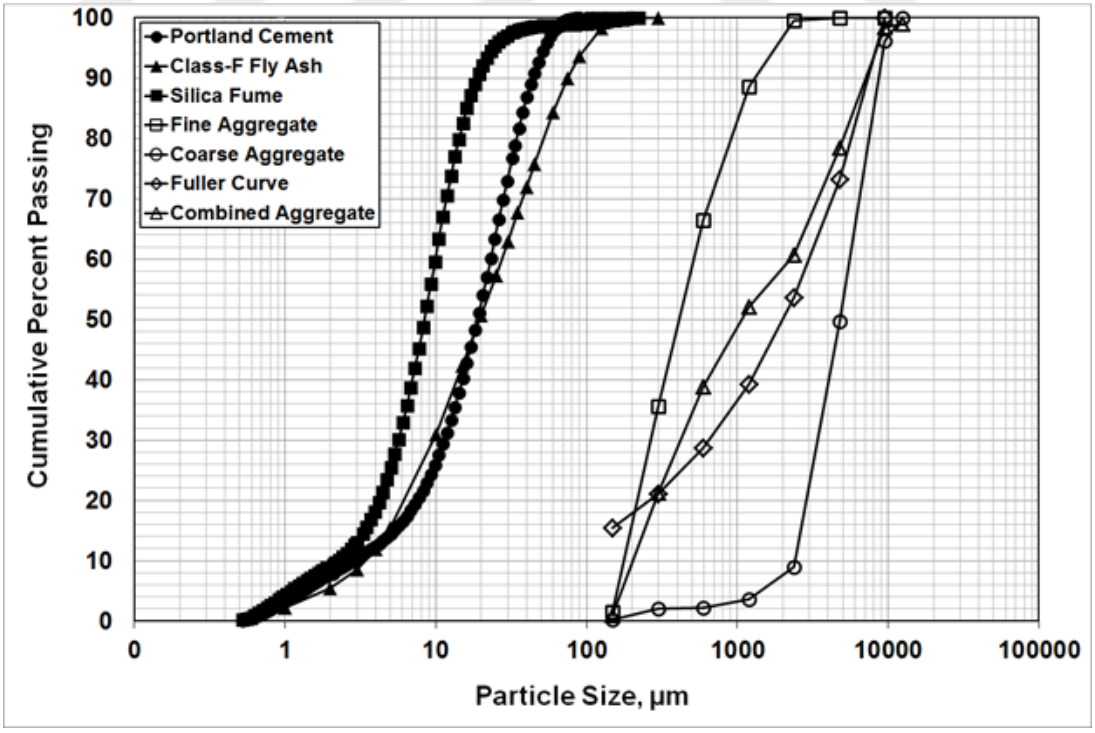

Figure 3.1 Particle size distributions of PC, FA, SF and aggregates used in the study

In addition to the materials mentioned above, water and a polycarboxylate-ether-based High Range Water-Reducing Admixture (HRWRA) master Glenium 51 were used, as shown in Figure 3.3. HRWRA contents were not kept constant in the mixtures and special attention was paid to obtain uniform distribution of fibers and adequate workability characteristics (all of the mixtures were almost self-compacting and no further compaction was required).

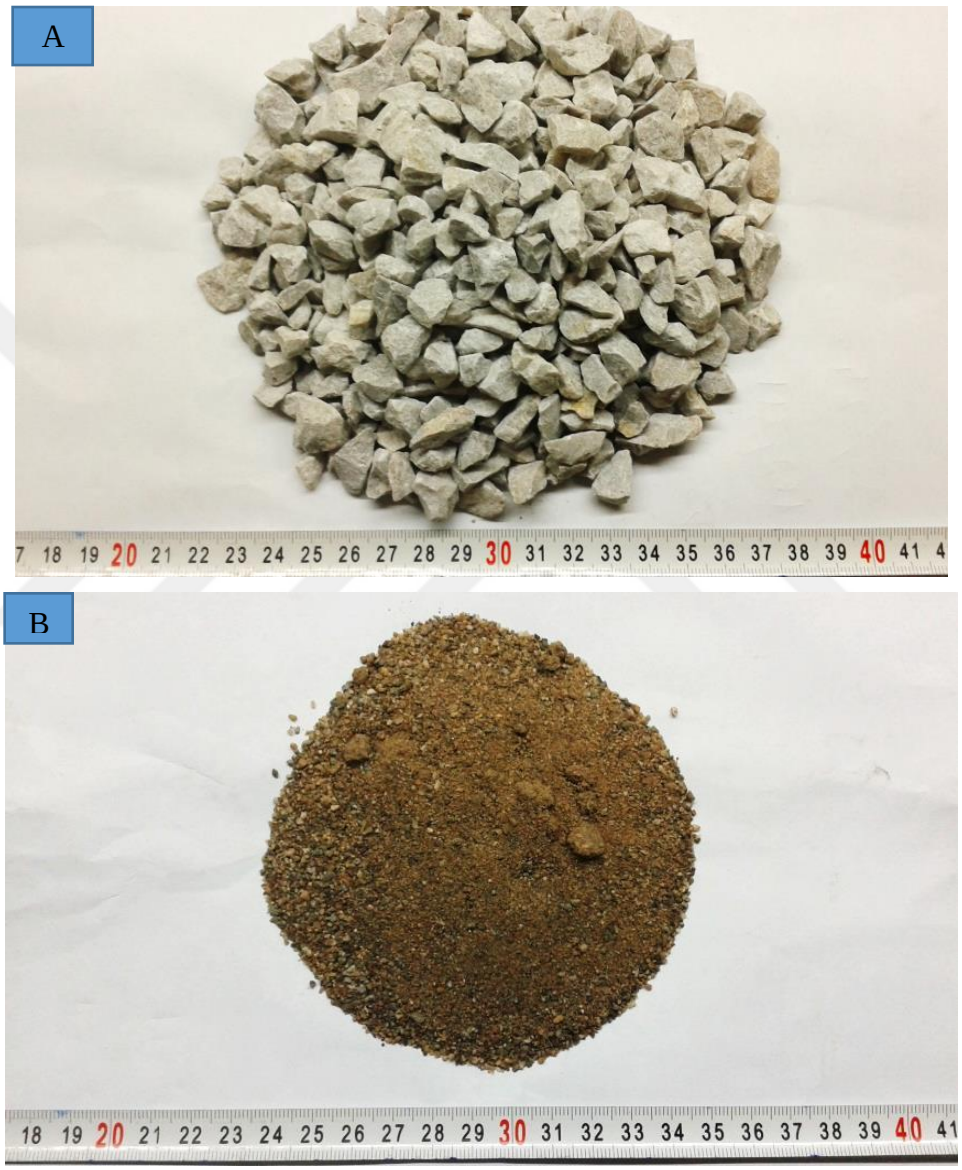

Figure 3.2 Aggregate used A) Crashed limestone as coarse aggregate B) River sand as fine aggregate

Figure 3.3 High range water-reducing admixtures

As mentioned previously, the main purpose of the present study is to achieve a deflection-hardening response under bending loading via using cementitious composites hybridized with different types of fibers by incorporating the maximum amount and size of coarse aggregates possible. Three different fibers at moderate volume (≤2%) in total were used herein, namely: polyvinyl-alcohol (P), hooked-end steel (S), and nylo-mono (N) fibers. The properties of different fibers are shown individually in Table 3.2 and Figure 3.4.

Table 3.2 Properties of different fibers

Fiber type	Length (mm)	Diameter (mm)	Tensile strength (MPa)	Elastic modulus (GPa)	Specific gravity
Polyvinyl-alcohol (P)	18	0.20	1000	29	1.30
Hooked-end steel (S)	30	0.75	1100	200	7.80
Nylo-mono (N)	19	0.05	966	25	1.14

After a preliminary investigation, 24 HPFRC mixtures were developed with water to binder ratio (W/B) of 0.40. Table 3.3 presents the composition and labeling of the HPFRCs that were prepared. As it can be seen in that table, the mixtures are labeled such that the ingredients are identifiable from their IDs. For example, in the case of the 16th mixture that was labeled P0.5S1N0.5_0.20_1.0, polyvinyl-alcohol (P), hooked-end steel (S) and nylon (N) fibers represent 0.5%, 1.0% and 0.5% of total mixture volume, respectively. For the same mixture, 0.20 and 1.0 stand for FA/PC ratio and A/B ratio, respectively.

Polyvinyl-alcohol (P)

Hooked-end steel (S)

Nylo-mono (N)

Figure 3.4 Fibers used in the this study

3.2 Mixing

In this study, all of the mixtures were prepared by using a pan type concrete mixer having a 40-L capacity. The same mixing procedure was followed for all of the proposed mixtures. During preparation, fine and coarse aggregates were mixed first in a dry state for 3 minutes. After inclusion of PC and FA to the dry aggregate blend, mixing is continued for an additional 5 minutes. SF, HRWRA and water were first mixed separately and then were added into the previously prepared PC-FA-aggregate blend and mixing had continued for 5 minutes. Fibers were added to the fresh concrete mixture as the final step and mixed for 5 more minutes. Figure 3.5 shows the mixing procedure for all of produced HPFRC mixtures.

Table 3.3 Ingredients used during the production of mixtures (units are in kg/m^3)

Mix. No	Mix. ID	PC	FA	SF	Fine Agg.	Coarse Agg.	Water	HRWRA	Fibers		
									P	S	N
1	P0S0N0_0.20_1.0	690	138	48	495	380	351	-	-	-	-
2	P0S0N0_0.45_1.0	567	255	40	488	375	345	-	-	-	-
3	P0S0N0_0.70_1.0	481	337	34	483	372	341	-	-	-	-
4	P0S1N0_0.20_1.0	683	137	48	490	376	347	0.6	-	78	-
5	P0S1N0_0.45_1.0	562	253	39	482	370	342	0.5	-	78	-
6	P0S1N0_0.70_1.0	477	334	33	477	367	338	0.4	-	78	-
7	P1S1N0_0.20_1.0	675	135	47	486	374	343	0.9	13	78	-
8	P1S1N0_0.45_1.0	555	250	39	479	368	337	0.8	13	78	-
9	P1S1N0_0.70_1.0	472	330	33	472	363	334	0.5	13	78	-
10	P1S1N0_0.20_1.5	579	116	41	622	478	294	1.8	13	78	-
11	P1S1N0_0.45_1.5	477	215	33	614	472	290	1.5	13	78	-
12	P1S1N0_0.70_1.5	405	284	28	610	469	287	1.2	13	78	-
13	P1S1N0_0.20_2.0	505	101	35	726	559	257	1.9	13	78	-
14	P1S1N0_0.45_2.0	417	188	29	718	552	254	1.8	13	78	-
15	P1S1N0_0.70_2.0	356	249	25	711	547	252	1.6	13	78	-
16	P0.5S1N0.5_0.20_1.0	675	135	47	486	374	343	1.0	6.5	78	5.7
17	P0.5S1N0.5_0.45_1.0	555	250	39	479	368	337	0.8	6.5	78	5.7
18	P0.5S1N0.5_0.70_1.0	472	330	33	472	363	334	0.7	6.5	78	5.7
19	P0.5S1N0.5_0.20_1.5	578	116	40	623	479	294	3.5	6.5	78	5.7
20	P0.5S1N0.5_0.45_1.5	477	215	33	614	472	290	3.3	6.5	78	5.7
21	P0.5S1N0.5_0.70_1.5	405	284	28	610	469	287	3.0	6.5	78	5.7
22	P0.5S1N0.5_0.20_2.0	505	101	35	726	559	257	5.0	6.5	78	5.7
23	P0.5S1N0.5_0.45_2.0	417	188	29	718	552	254	4.9	6.5	78	5.7
24	P0.5S1N0.5_0.70_2.0	355	249	25	712	548	251	4.8	6.5	78	5.7

Solid Ingredients

Mixing FA,SP and water

Adding mixing water to blended material

Inclusion (S) fibers into concrete

Inclusion (P) fibers into concrete

Final mixing of all materials

Figure 3.5 Mixing procedures for production of HPFRC mixtures

3.3 Sample Preparing and Test

3.3.1 Flexural and Compressive Tests

In line with the main purpose of this investigation, prism specimens measuring 80×75×400 mm were cast and then tested under four-point bending/loading to determine the flexural parameters: flexural strength based on Modulus of Rupture (MOR) and mid-span beam deflection. Furthermore, cubic specimens with dimensions of 100 mm were also prepared for the evaluation of compressive strength. After casting the specimens, the molds were covered with plastic sheets and subjected to an initial curing for 24 hours under laboratory conditions at 50±5% RH

and 23±2 ^{o}C. After 24 hours, both prismatic and cubic specimens were moved into isolated plastic bags having a controlled environment set at 95±5% RH and 23±2 ^{o}C to be further cured until the end of 7, 28 and 90 days. For each initial curing age and test type, six separate specimens were produced, tested, and the obtained results were averaged. During the four-point bending tests, prism specimens were placed on support points 350 mm away from each other and loading was applied from a central span length of 116 mm at a rate of 0.1 mm/sec. Bending tests were performed by using closed-loop material testing equipment and data was recorded with the help of a computerized data recording system. In addition, to more accurately record the mid-span beam deflection results directly from the specimens, two Linear Variable Differential Transducers (LVDT) were brought into contact with the tensile region of the prism specimens. The process of preparing and testing the flexural and compression specimen is shown in Figure 3.6 and Figure 3.7, respectively.

a) Oiling the molds before casting

b) Casting the concrete into mold

c) Curing of specimens in the plastic bags at control room

Figure 3.6 Specimens preparing for flexural and compressive tests

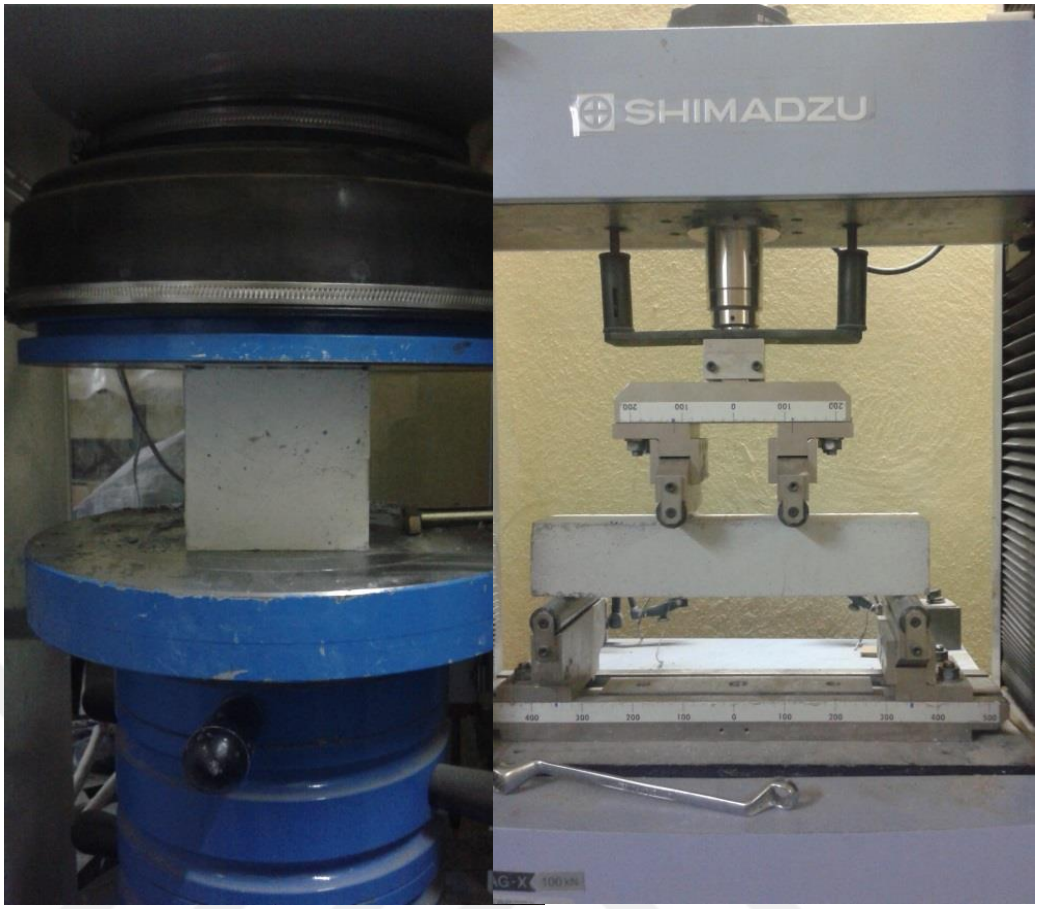

Cubic specimen under compression test

Prism specimen under bending test

Figure 3.7 Specimens tested under flexural and compressive tests

3.3.2 Flexural Impact Test

Beam specimens with the dimensions of 50×50×750 mm were produced without any continuous steel reinforcement to characterize the impact behavior of HPFRCC mixtures**.** After casting of the specimens, molds were covered with plastic sheets and initial curing under laboratory conditions at 50±5% RH and 23±2 ^{o}C was applied for one day. With the completion of one day, beam specimens were moved into isolated plastic bags having controlled environment set at 95±5% RH and 23±2 ^{o}C to be further cured until the age of 28 days.

Impact loads were applied via test set-up, details of which are provided in Figure 3.8. The test setup itself allows weights of varying magnitudes to be dropped from a maximum height of 2500 mm onto test specimens of varying dimensions. The weight and drop height of the hammer were kept constant during the experiment; a 9 kg

hammer was dropped from a height of 600 mm to create impact loading from the same contact point for different beam specimens. High-strength 50×50×4 mm steel plate was placed on the contact point to prevent local fractures from the point of contact and achieve distributed loading. The steel plate to which loading was applied was fixed to specimens with a mechanical anchor. A piece of rubber was placed between the plate and specimens to prevent stress localization due to rough surface properties.

Hammer weight, drop height and impact energy level were selected to best trace damage occurrence. The capacity of dynamic accelerometers and load cell were also considered during hammer weight and drop height selection. Special attention was paid to these two parameters during decision making to avoid very high energy impact, which can lead to sensor limits being exceeded and sudden, substantial damage to test specimens. To avoid these problems, impact loads levels were limited to 600×9.81×9.0=52.97 Joule. Accelerations from two symmetrical points were measured to observe the effects of impact loading. Accelerometers were placed symmetrically 150 mm away from the point of impact loading and fixed with brass connection apparatus through using mechanical anchors. Displacements were measured by using two LVDTs that were placed symmetrically 50 mm away from the point of impact loading (Figure 3.8).

Figure 3.9 shows a beam specimen ready for impact resistance testing. A dynamic data collection system with specifically designed software was used to properly save impact testing data. The loading created by the drop hammer was measured via using a dynamic load cell. Impact velocity of the drop hammer was calculated by a speedometer placed on top of the hammer, and average measured impact velocities of beam specimens were 3.5 m/s. These values, measured from different specimens, were very close to each other. Identical impact loading was applied to all specimens. The accelerometers and LVDTs were connected to the data logger with computerized software to record acceleration time, displacement time and impact load time graphs after applying the impact load. Figure 3.9 shows the layout of the tested beam specimen used in the impact test.

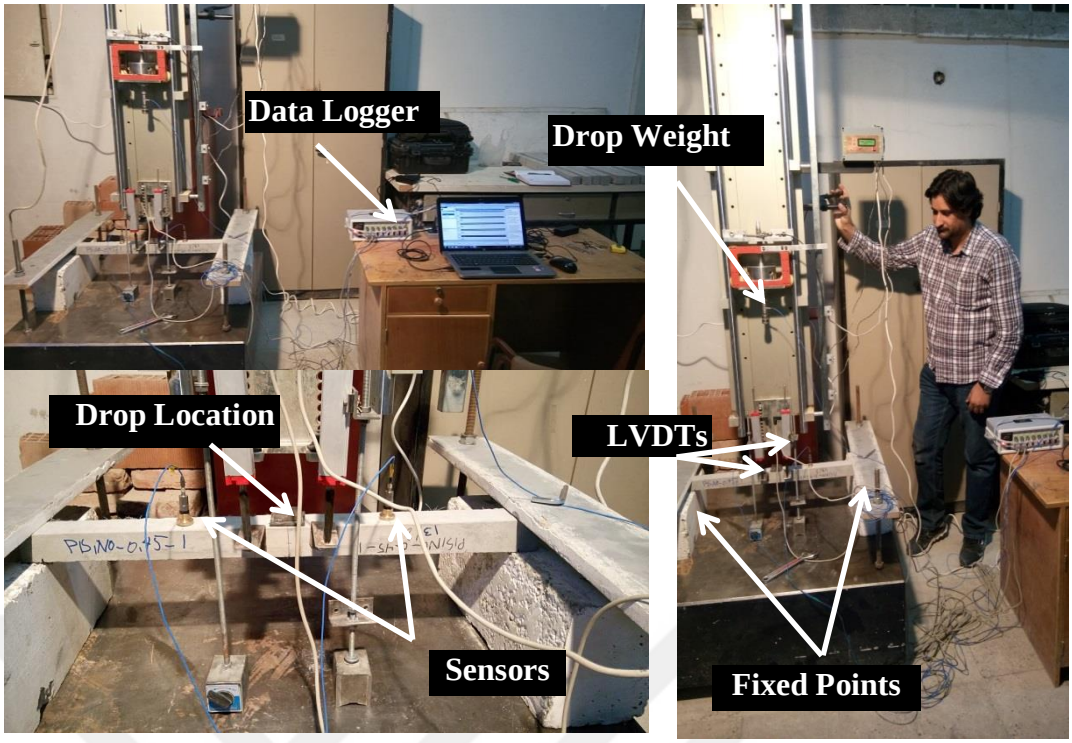

Figure 3.8 Free fall drop-weight test set-up and view of beam specimen

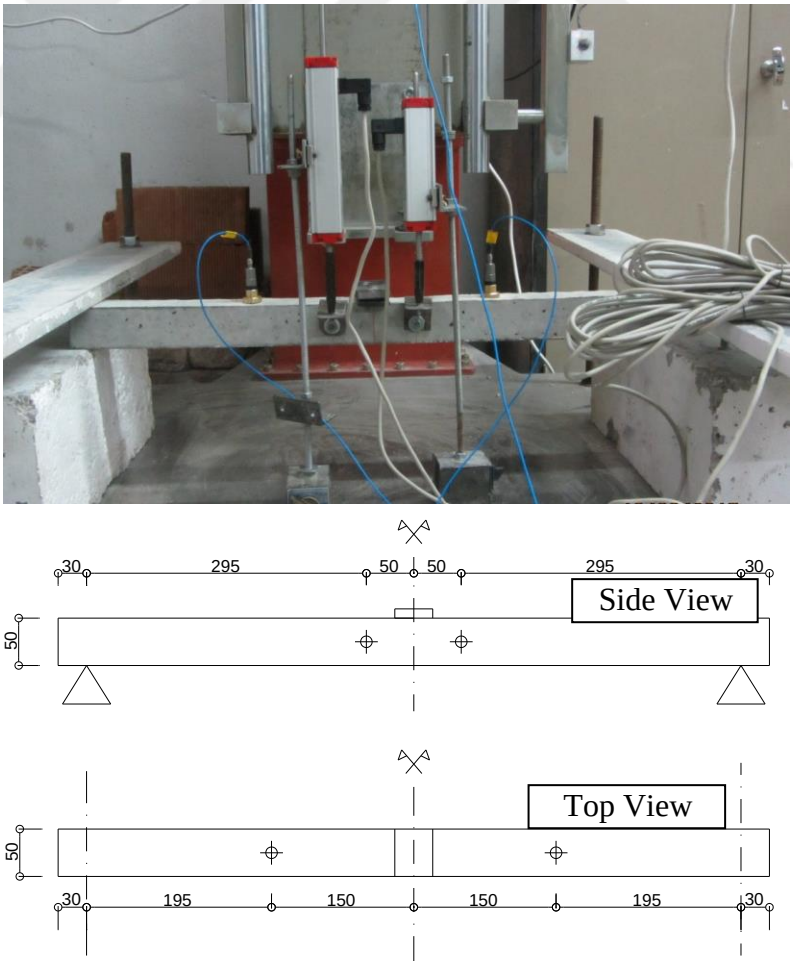

Figure 3.9 Free fall drop-weight test layouts for test set-up (All dimensions are in mm)

3.3.3 Shrinkage Tests

3.3.3.1 Drying Shrinkage Test

In accordance with (ASTM-C157/C157M, 2008) (the standard test method for length change of hardened hydraulic-cement mortar and concrete), three square (50×50×200 mm) specimens for each mixture were prepared and tested to calculate the free drying shrinkage strain. After twenty four hours of casting, the specimens were demolded, then kept in control environmental room at (50%+5 RH and 23+2 ^{o}C). The initial reading was immediately taken on the specimens after remolding. In this study, the length changes of concrete bar specimens were read up to 150 days, the weights were also calculated to monitor the mass loss due to drying. To achieve reliable results, it was important to place the reference bar and the specimens in the same orientation. Marks were made on the reference bar (comparator) and specimens to indicate the top and bottom. Measurements for both length change and mass loss of the specimens were taken at 1, 2, 3, 4, 5, 6, 7, 14, 21, 28, 56, 84, and 150 days after they were stored in the dry air condition. Figure 3.10 shows a digital dial gage length comparator and bar specimen preparing and testing.

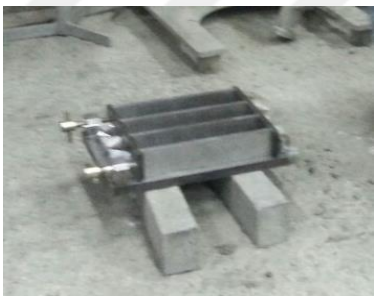

Free drying shrinkage molds

Samples under drying

Length comparator

sample under test

Figure 3.10 Prepartion and testing for free drying shrinkage bar specimen

3.3.3.2 Restrained Shrinkage Test

Restrained shrinkage cracking is a critical problem in concrete construction. Free shrinkage tests alone could not offer sufficient information with respect to the behavior of concrete structures because virtually every concrete structure is restrained in some manner, either by reinforcement or the boundary condition of the structure.

In according to (AASHTO, 1999) restrained shrinkage test was investigated. This test was used to identify the tendency of restrained concrete to shrinkage cracking. The ring molds were oiled and then 30 mm thickness of ring concrete with (152 mm in height) was cast around outer steel ring that has 280 and 305 mm inner and outer diameters, respectively. After twenty four hours of casting, the exterior mold was removed and silicone-based sealant was used to seal the top surface of the concrete ring to prevent the evaporation from the top. The drying was allowed from the outer circumferential surface of concrete. The concrete rings were kept in control environmental room at (50%+5 RH and 23+2 ^{o}C).Time to cracking, numbers and crack width were monitored every day for 28 days. For each crack, three locations were marked to take a reading and then the average value was recorded. Digital microscope connected to computerized software was used to measure the crack width that resulted from restrained shrinkage. Figure 3.11 shows a restrained shrinkage sample prepared to crack width reading.

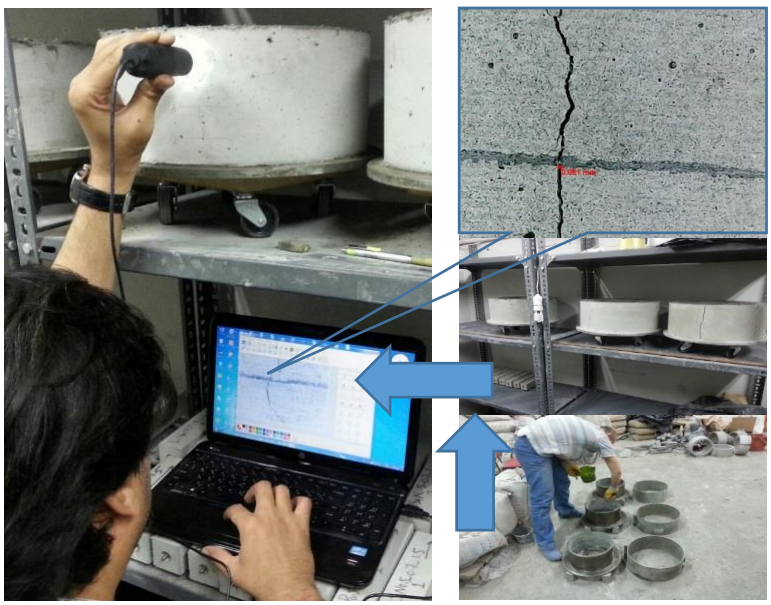

Figure 3.11 Restrained shrinkage specimens prepartion and crack width reading

3.3.4 Panel Test

The square panel tests (Bending test) according to European specification for sprayed concrete (EFNARC, 1996) were performed with specimens' dimensions of (400mm×400mm×50 mm of thickness) which are smaller than the dimensions recommended by the above standard. This dimensions were adopted due to the limitation of loading machine and it is easy to be carried as compared to the standard specimen' weight of 90 kg. After casting of the specimens, molds were covered with plastic sheets and initial curing under laboratory conditions at 50±5% RH and 23±2 ^{o}C was applied for one day. With the completion of one day, panel specimens were moved into isolated plastic bags having controlled environment set at 95±5% RH and 23±2 ^{o}C to be further cured until 28 days. Bending tests were performed by using a closed-loop material testing equipment and data was recorded with the help of a computerized data recording system. The load was applied to the panels via using a rigid steel cylinder (50 mm of diameter) in the top surface at displacement rate of 0.3 mm/min. The deflection and load were recorded to calculate the absorbed energy which is the area under the line of load-deflection curve. The deflection was recorded until 10 mm instead of 25 mm as recommended in standard method because of the thinness and large-aspect-ratio of the plate specimens used (Kim and Weiss, 2003). The panels were sitting on four simply supported edges steel frame. Panel specimen dimensions and its setup are shown in Figure 3.12.

3.3.5 Freezing- and Thawing Test

Freeze-thaw cycle could be deleterious porous and fragile cement composite such as concrete. Therefore, frost action represented by freezing-thawing durability of cement composite has considerable effect on the service life of concrete structure, especially at cold weather. The frost resistance of concrete can be estimated by different properties depending on loss of strength, weight change, dilation and fundamental frequency transmission time.

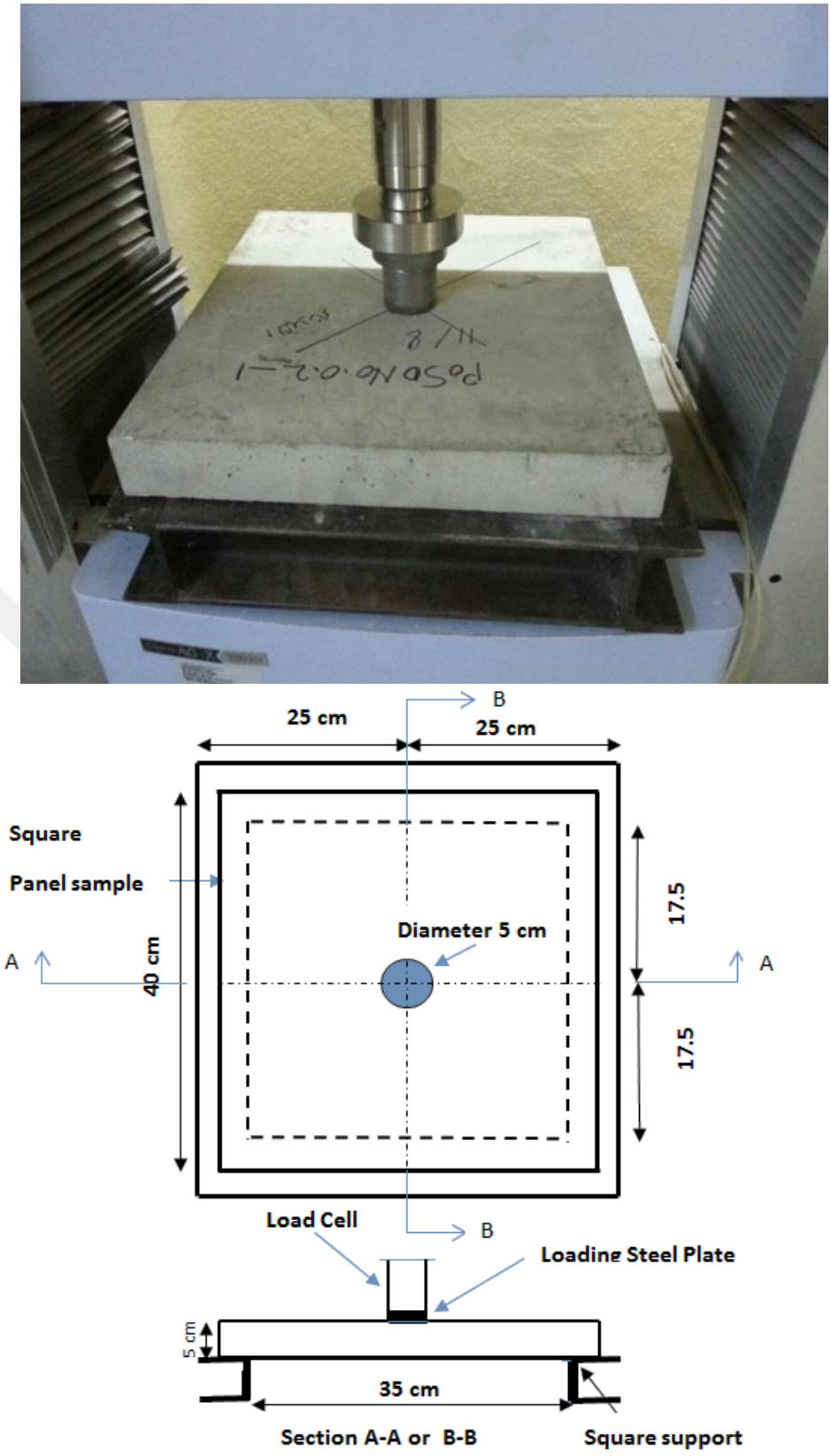

Figure 3.12 Panel test layout for test set-up (All dimensions are in cm)

In the current study, the ASTM standard (ASTM-C666/C666M, 2003) is adopted to evaluate the produced mixtures exposed to freeze and thawing condition. Concrete was cast into a mold of (80mm×75×400mm). After 24 hours, the mold was opened and the specimens were cured in plastic packages with (100% RH and 23 ^{o}C) for 28 days. The specimens were stored in saturated lime water for 2 days before freezing-and-thawing tests started. The apparatus temperatures exposed to the samples for freezing-thawing cycles were ranged within (+4 to -18 ^{o}C) and subjected to between five and six freeze-thaw cycles per day period. After every 30 cycles, the transverse frequency and mass loss of concrete specimens were monitored.

The test provides a failure criterion using the Durability Factor (DF) which is calculated according to Equation 3.2.

$$DF= (RDME)N/300 \quad (3.2)$$

where, N is the number of Freeze-Thawing (F/T) cycles necessary to reach a proposed critical value of the Relative Dynamic Modulus of Elasticity (RDME); threshold, e.g., 60%. If the RDME remains higher than this critical value after ending the 300 F/T cycles, then N can be set to 300. The fundamental transverse resonance of concrete under accelerated freezing and thawing cycles was conducted by following (ASTM-C215, 2002) impact method. Computing of RDME is shown in Equation 3.3.

$$RDME=(n_1^2/n^2)100 \quad (3.3)$$

where:

RDME is the relative dynamic elasticity modulus
n is the fundamental transverse frequency at 0 cycles of freezing and thawing, and
n_1 is the fundamental transverse frequency after c cycles of freezing and thawing.

The procedure of freeze-thaw testing and the instrument for measurement the transverse frequency are shown in Figure 3.13. Transvers resonance frequency testing setup is stated in Figure 3.14.

Samples in freeze-thaw mechine

Sample Weight

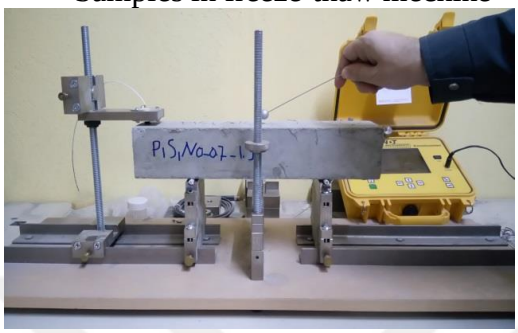

Sample under transvers resonance frequency

Rresonance frequency instrument

Figure 3.13 Frost resistance durability test procedures

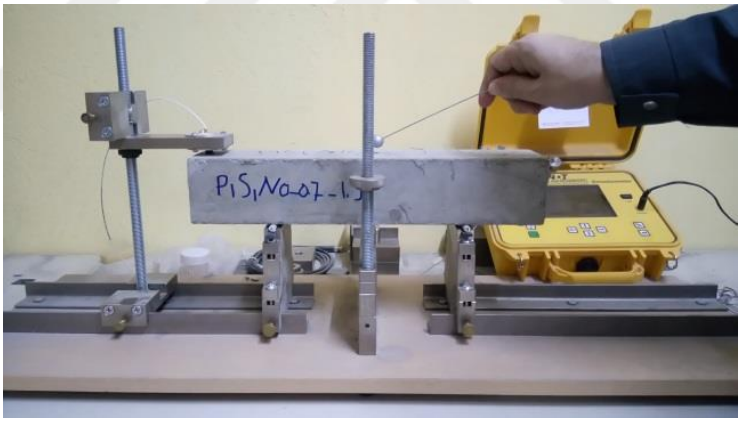

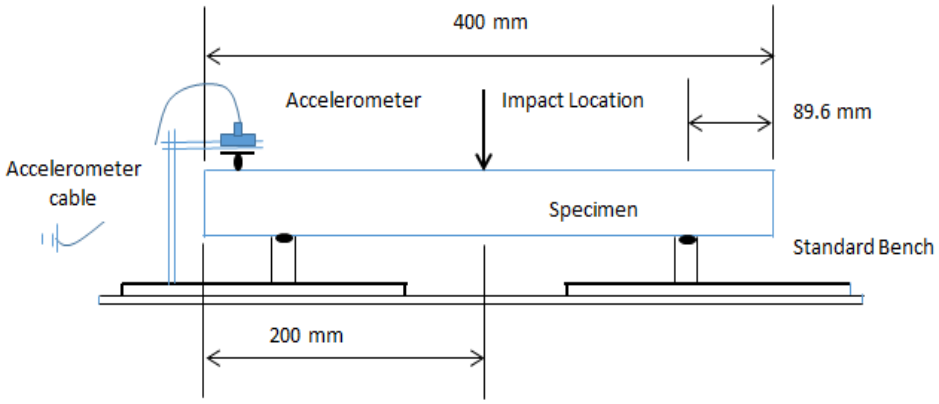

Figure 3.14 Transvers resonance frequency test layout for testing set-up

CHAPTER FOUR

RESULTS AND DISCUSSION

4.1 Mechanical Properties

4.1.1 Compressive strength

The average of compressive strength test results at 7-, 28- and 90-day ages of different mixtures are shown in Table 4.1. For all of the proposed mixtures, there were stable increments in the compressive strength test results with prolonged curing ages, although this was more pronounced between the ages of 7 to 28 days as compared to 28 to 90 days, in general. This is due to the influence of ongoing hydration reactions densifying the matrices of composite materials. Regardless of the different initial curing ages and mixture types, the obtained compressive strength results from mixtures with the same A/B ratio and fiber type/dosages dropped considerably when higher amounts of FA were utilized in the mixtures. Taking the P0S0N0_0.20_1.0 mixture as an example, when the FA/PC ratio was increased from 0.20 to 0.45 and to 0.70, there were reductions of 28% and 49% in the average 7-day compressive strength results, respectively. This was also true for 28- and 90-day specimens with varying rates. However, it is notable that even the lowest average compressive strength value recorded at the end of 28 days from the P0S0N0_0.70_1.0 mixture with the value of 31.3 MPa, which is higher than that of normal strength concrete (30 MPa) and it is adequate for most conventional construction practices.

Comparing the mixtures numbered from 1 to 3 with those numbered from 4 to 6, the effect of hooked-end steel fiber additions on the compressive strength results of the composite mixtures with the same A/B ratio can be seen in Table 4.1. For further clarification, Figure 4.1 illustrates the effect of steel fiber utilization on the compressive strength results of composite specimens with different FA/PC ratios and a constant A/B ratio (1.0). As it can be seen from Table 4.1 and Figure 4.1, after

reinforcing the fibreless control mixtures with only 1% of hooked-end steel fibers, there were improvements in the compressive strength results up to 9.9 MPa, although this behavior was found to be dependent on the initial curing age and selected FA/PC ratio (Gao et al., 1997). Improvements in the compressive strength results with the incorporation of steel fibers can be ascribed to the ability of fibers to delay crack formation (Şahmaran and Yaman, 2007). Looking at mixtures with FA/PC ratio of 0.20 (numbered 1 and 4 for this case), the addition of steel fibers to the control specimens reduced the compressive strength results for samples cured for 7 and 28 days, although the results were almost similar for 90-day specimens. When the FA/PC ratio was increased to 0.45, greater improvements in the compressive strength results were found as compared to the control mixtures, especially at later ages (34.4-29.1=5.3, 48.5-40.2=8.2 and 57.5-47.6=9.9 MPa for 7-, 28- and 90-day specimens, respectively). Although the incremental trend was also valid for specimens with FA/PC ratio of 0.70, the extent was limited so that differences in the results as compared to control mixtures were lower (22.3-20.6=1.8, 35.6-31.3=4.3 and 47.3-42.4=4.9 MPa for 7-, 28- and 90-day specimens). These findings reveal that, for a low utilization rate (1%, by volume) of hooked-end steel fibers, there seems to be an optimal level of Class-F fly ash replacement (FA/PC ratio of 0.45 for this study). Lower levels can interfere with uniform dispersibility of the steel fibers, resulting in lower compressive strength results as compared to associated control mixtures. Considerably higher amounts of fly ash inclusion can have an adverse effect on further improvement in the values.

For the same A/B ratio (1.0), the addition of P and N fibers to cementitious mixtures incorporating hooked-end steel fibers affects the compressive strength results for different FA/PC ratios which can be seen in Table 4.1 (mixtures numbered from 4 to 6, 7 to 9, and 16 to 18). For a clearer picture of the effects of different fibers on compressive strength results of composite specimens, Figure 4.1 is also informative. With the addition of macro-size fibers into the mixtures incorporating only steel fibers, the expected flaws at micro levels will not be accounted for and no improvement in the compressive strength results will appear. As expected, Table 4.1 and Figure 4.1show that, the addition of different macro fibers to the mixtures with only steel fibers (4 to 6) did not make improvement on compressive strength results.

Table 4.1 Average compressive strength, flexural strength and mid-span beam deflection results of different mixtures after 7, 28 and 90 days

Mix. No	Mix. ID	Compressive strength (MPa)			Flexural strength (MPa)			Mid-span beam deflection (mm)		
		7 d.	28 d.	90 d.	7 d.	28 d.	90 d.	7 d.	28 d.	90 d.
1	P0S0N0_0.20_1.0	40.5	50.6	57.2	3.83	3.20	4.90	0.34	0.22	0.21
2	P0S0N0_0.45_1.0	29.1	40.2	47.6	2.60	3.50	4.15	0.28	0.20	0.19
3	P0S0N0_0.70_1.0	20.6	31.3	42.4	1.68	3.00	3.93	0.38	0.20	0.11
4	P0S1N0_0.20_1.0	34.0	47.9	57.4	6.00	6.00	6.95	1.75	1.60	1.80
5	P0S1N0_0.45_1.0	34.4	48.5	57.5	4.98	5.48	6.03	1.81	1.49	1.25
6	P0S1N0_0.70_1.0	22.3	35.6	47.3	4.33	4.68	3.70	1.65	1.43	1.00
7	P1S1N0_0.20_1.0	40.5	52.9	60.5	7.98	5.88	8.78	2.25	1.93	2.05
8	P1S1N0_0.45_1.0	32.7	44.6	53.0	6.28	7.95	8.70	2.40	1.75	1.53
9	P1S1N0_0.70_1.0	23.3	38.1	47.3	5.85	7.58	7.75	2.15	1.58	1.53
10	P1S1N0_0.20_1.5	39.3	55.0	65.6	7.58	8.83	8.78	1.60	1.13	1.90
11	P1S1N0_0.45_1.5	26.9	44.6	50.7	6.35	8.03	8.80	2.13	1.38	1.70
12	P1S1N0_0.70_1.5	21.2	38.0	47.6	6.75	8.40	9.25	2.70	1.52	1.55
13	P1S1N0_0.20_2.0	40.0	56.8	67.4	9.03	7.05	8.50	1.63	1.33	1.58
14	P1S1N0_0.45_2.0	33.0	48.6	56.4	7.28	8.55	9.40	1.88	1.63	1.65
15	P1S1N0_0.70_2.0	30.6	43.6	55.0	7.18	7.48	8.03	1.93	1.23	1.10
16	P0.5S1N0.5_0.20_1.0	40.5	51.9	56.6	6.68	6.27	7.73	2.05	1.47	1.68
17	P0.5S1N0.5_0.45_1.0	33.0	45.4	51.3	6.93	7.20	7.20	1.70	1.70	1.23
18	P0.5S1N0.5_0.70_1.0	26.5	40.9	48.9	5.55	6.60	6.03	2.18	1.77	1.40
19	P0.5S1N0.5_0.20_1.5	44.1	60.2	65.6	7.43	6.98	8.95	1.63	1.30	1.78
20	P0.5S1N0.5_0.45_1.5	40.3	54.5	63.6	7.15	8.45	6.47	2.40	1.78	1.43
21	P0.5S1N0.5_0.70_1.5	30.7	46.9	57.4	6.75	7.03	7.43	2.15	1.83	1.58
22	P0.5S1N0.5_0.20_2.0	46.1	60.4	72.2	9.17	8.30	8.47	1.87	1.43	1.53
23	P0.5S1N0.5_0.45_2.0	39.5	56.3	65.0	7.90	7.13	6.28	1.83	1.27	1.43
24	P0.5S1N0.5_0.70_2.0	26.5	51.0	64.5	6.15	7.78	5.70	2.30	1.68	1.18

In the case of specimens with S and P fibers (7 to 9) which are belong to mixture ID P1S1N0 and mixtures having S, P and N fibers with mixture ID P0.5S1N0.5 as numbered (16 to 18), there were both increments and decrements in the values. With regard to compressive strength development in the presence of different fiber types in varying amounts, overall results of control mixtures do not change appreciably, although fibers (especially hooked-end steel fibers for this study) do have limited effectiveness in increasing the compressive strength results through delaying and bridging of cracks (Figure 4.1). It seems that the paste and matrix properties are better predictors of the compressive strength results of cementitious composite mixtures (Alhozaimy et al., 1996).

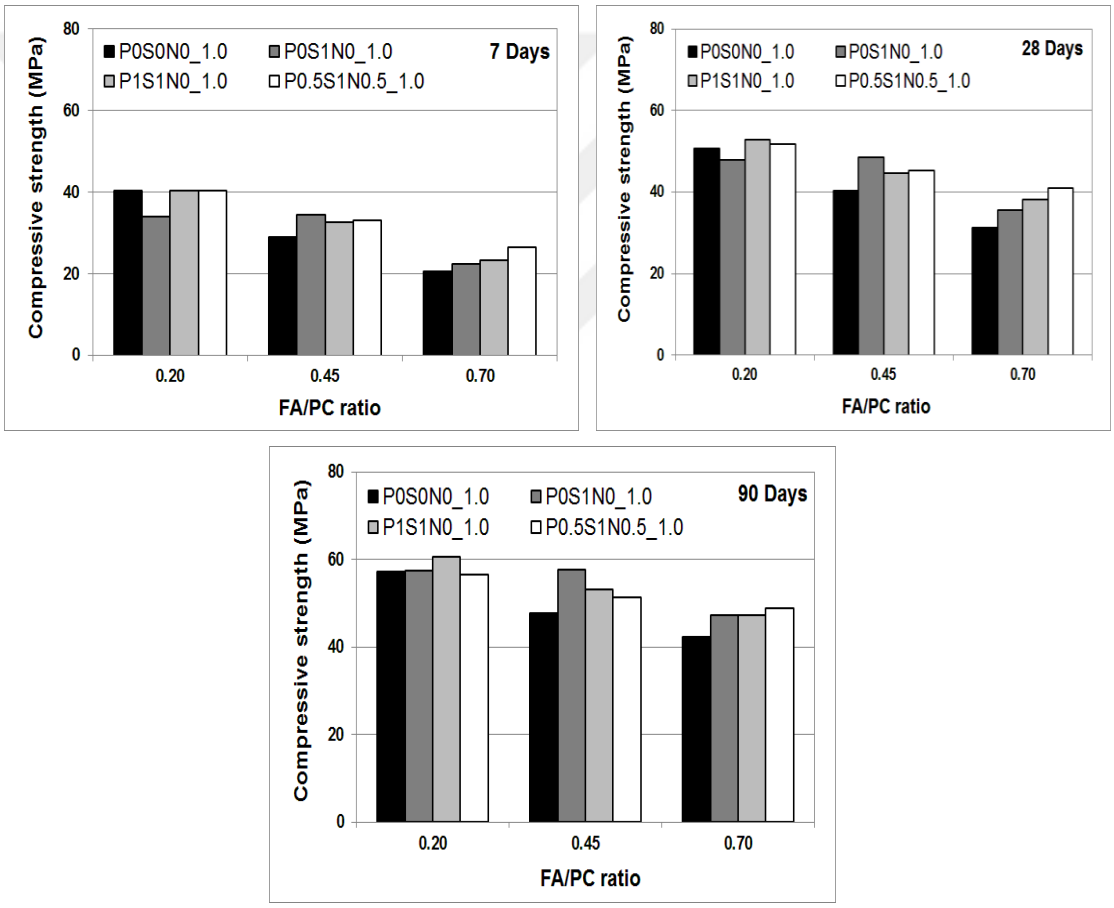

Figure 4.1 Effects of fiber utilization on the compressive strength results at a constant A/B ratio (1.0) and different FA/PC ratios

Another parameter studied herein that could be effective on compressive strength results is the A/B ratio. The influence of the A/B ratio on the compressive strength of cementitious composites can be understood by checking the mixtures numbered from 7 to 15 and 16 to 24. As shown in Table 4.1, when the A/B ratio is increased from

1.0 to 2.0, compressive strength results increased in general, although this behavior was more apparent in the case of specimens incorporating all three different fiber types (numbered from 16 to 24). When P0.5S1N0.5_0.20_1.0, P0.5S1N0.5_0.20_1.5 and P0.5S1N0.5_0.20_2.0 mixtures are carefully evaluated, it can be seen that 7-day compressive strength results were 40.5, 44.1 and 46.1 MPa, respectively. Results were even higher in the case of higher A/B ratios at later ages. For example, the values for 28- and 90-day specimens from the same mixtures cited above were 51.9, 60.2, 60.4 and 56.6, 65.6, 72.2 MPa, respectively. Although increasing A/B ratios brought about lower binder amounts and expectedly lower compressive strength results, the incremental trend in the values when targeting higher A/B ratios could be related to the tortuosity of the cracking path. It is well known that under loading, cracks prefer to propagate along the weaker interfacial zone or larger pores in the matrix (De Larrard and Belloc, 1997). As the crack meets an aggregate particle, it is forced to propagate either through the aggregate or to deflect and travel around the aggregate-mortar interface. The path that a crack will follow is dependent on the strength of both aggregate and cement paste. Given a more tortuous crack path, the ultimate energy absorption capacity reached at the point of failure and the final compressive strength results increased. It appears that this situation was observed herein. Figure 4.2 shows the cross section of a failed cubic specimen from the P0S0N0_0.20.1.0 mixture. Even at the lowest A/B ratio of 1.0, there were empty spaces left by popped-out coarse aggregates and protruded coarse aggregates that were not affected by the cracking matrix. Moreover, the behavior observed in Figure 4.2 is more likely to happen when higher A/B ratios are selected. This implies that, although some of the aggregates were crushed during internal cracking due to compressive loading, cracking in the matrix followed a more tortuous path around the coarse aggregate particles rather than failing the coarse aggregate phase entirely, which is reflected in higher compressive strength results. It should be noted that despite the selection of different A/B ratios, HPFRCs produced in this study are already binder-rich mixtures. Changing the amount of binder does not make a significant impact on the compressive strength development after a certain level since hydration reactions reached a limit due to the availability of empty spaces in cementitious systems, especially over extended periods. Under such conditions, changes in the coarse aggregate phase may overtake the changes observed in compressive strength results and it seems to confirm the situation here. Overall, these

findings are also in line with the literature which states that, at least in the strength range of structural concrete (conventional concrete), increased aggregate content (reduced paste content) increases compressive strength concordantly (De Larrard and Belloc, 1997; Stock et al., 1979).

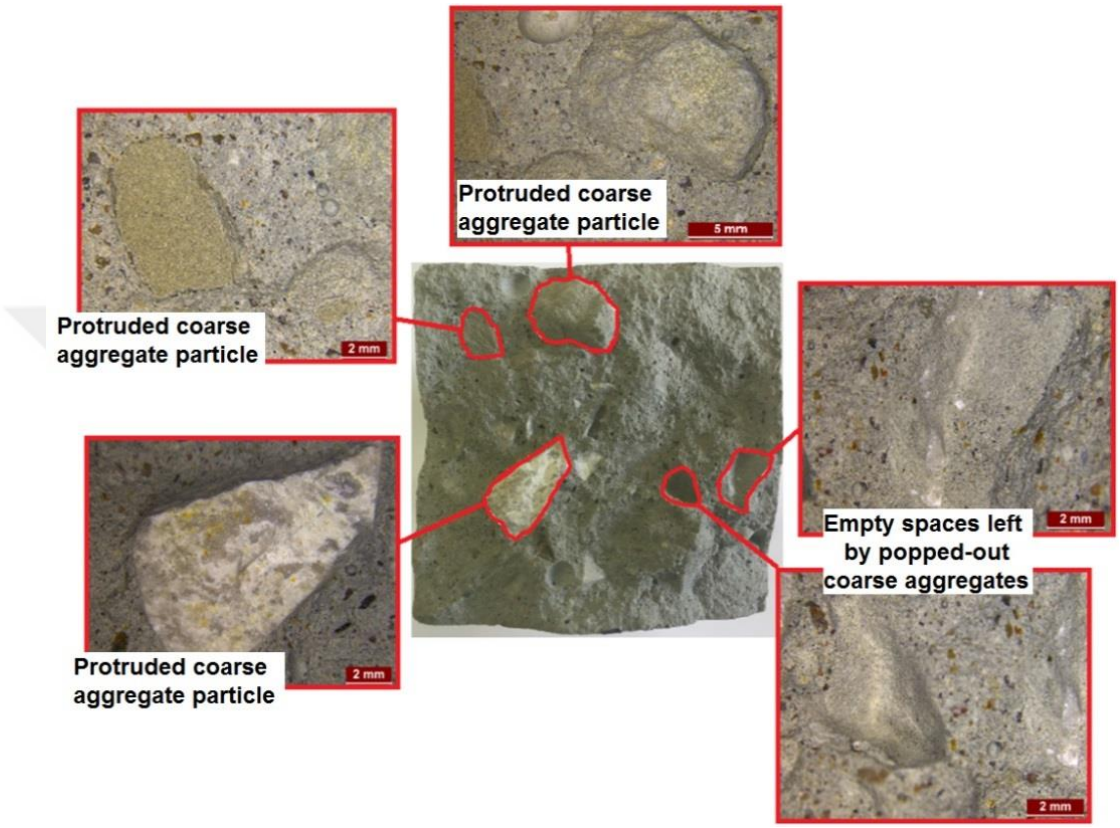

Figure 4.2 Cross-sectional view of P0S0N0_0.20_1.0 cubic specimen after testing for compressive strength

As previously stated and can be seen from Table 4.1, the incremental trend in compressive strength results with increasing A/B ratios was less evident when composite mixtures were hybridized with two different types of fiber (P and S) as compared to mixtures with three different types of fiber (P, S and N). For example, the 90-day average compressive strength results of P1S1N0_0.45_1.0 and P1S1N0_0.45_2.0 mixtures were 53.0 and 56.4 MPa, respectively. On the other hand, similar values of the same age for P0.5S1N0.5_0.45_1.0 and P0.5S1N0.5_0.45_2.0 mixtures were 51.3 and 65.0 MPa, respectively. It appears that replacing half of the volume of P fibers with N fibers contributed to higher compressive strength results. The fiber parameter that is generally responsible for the

changes in the compressive strength of a composite material is tensile strength. Fibers having higher tensile strength values are capable of transferring larger tensile stresses from a cracked matrix to the fibers (Song et al., 2005). Although P fibers have higher tensile strength (1000 MPa) as compared to N fibers (966 MPa), higher compressive strength results obtained in the case of specimens with increased N fibers can be associated with the amide chains (–CO–NH–) of N fibers and their reactions with water. With the absorption of moisture and its bonding to the polymer backbone, nylon swells (Giles Jr et al., 2005). This improves stiffness and allows a greater capacity for tensile stress (Yap et al., 2013). Given their lower cost in comparison to P fibers, N fibers can be regarded as an alternative reinforcing material and are likely to replace P fibers in terms of compressive strength performance. However, to be precise about completely replacing the P fibers with N fibers, tensile properties must be comprehensively evaluated as well (see next section).

4.1.2 Flexural parameters

4.1.2.1 Flexural strength- modulus of rupture (MOR)

Flexural strength or modulus of rupture (MOR) results found by averaging the values from six different specimens are presented in Table 4.1 for each mixture. For most of the mixtures in this table, MOR results showed an increasing trend with further curing, although there were deviations from this behavior depending on the mixture type and further curing ages. This was an expected outcome since flexural strength results were also influenced by the parameters affecting compressive strength results. Thus with extended initial curing ages, matrix properties are likely to improve, resulting in higher strength values. As Compared to compressive strength results however, the rate of increment in MOR values was not that high. For instance, between the ages of 7 and 90 days, average compressive strength results of the P1S1N0_0.20_1.5 mixture changed from 39.3 to 65.6 MPa while flexural strength changed from 7.58 to 8.78 MPa. Complex parameters of the used materials (such as tensile first cracking strength, ultimate tensile strength and tensile strain capacity) could be responsible for the behavior of strength measurements under compression and bending.

For almost all of the mixtures with the same A/B ratio, MOR results declined considerably when the FA/PC ratio was increased regardless of the different initial curing ages; the reduction became more evident at higher FA/PC ratios. For example, the percentage reductions in the average 7-day MOR results of P0.5S1N0.5_0.20_2.0 specimens were 14% (from 9.17 MPa to 7.90 MPa) and 33% (from 9.17 to 6.15 MPa) when the FA/PC ratio was increased from 0.20 to 0.45 and 0.70, respectively. As discussed in the previous section, the relatively high amounts of Class-F fly ash utilized in different mixtures reduced the compressive strength results markedly. Reduced compressive strength results are likely to be associated with the reduced strength in flexure as well (Yoo et al., 2015). Another matrix parameter that influenced the MOR results of various mixtures was the A/B ratio. According to Table 4.1, for the same FA/PC ratio and type/amount of fiber utilization there was a generally increasing trend in the MOR values with increasing A/B ratios regardless of initial curing ages. Seven-day MOR results were 6.68, 7.43 and 9.17 MPa, respectively, for the 16^{th}, 19^{th}, and 22^{nd} mixtures (shown in Table 4.1), and could be considered likely explanations for this situation. A suggestion was made by (Snyder and Lankard, 1972) that the addition of coarse aggregate to the mortars incorporating steel fibers causes reduced ultimate flexural strength results and that it is possible to keep those losses under 20%, as long as the MAS of coarse aggregate is restricted to 9.5 mm and the coarse aggregate amount does not exceed 25%, by weight. Unlike the abovementioned study, the experimental results presented in Table 4.1 clearly demonstrate that it is possible to obtain reasonably high MOR results even in the presence of a moderate volume of hybrid fibers and increased amounts of coarse aggregate (or a higher A/B ratio) with a MAS of 12 mm by modifying the paste properties even when the amount of coarse aggregate reaches 25% by weight (Table 3.3). It seems that the addition of Class-F fly ash particles improved the workability of mixtures, enhanced fiber distribution, and by the remaining intact (to be further hydrated at later ages), helped improve MOR results in the case of increasing A/B ratios. The expected negative effects on MOR results were due to the significantly reduced paste content. The use of coarse aggregates (with increased MAS) in greater amounts was compensated for by the use of Class-F fly ash with its beneficial effects on fiber dispersion and hydration characteristics. A general incremental trend in MOR results with increasing A/B ratios was also in line with the behavior observed

in the case of compressive strength results and could also be attributable to the development in the tortuosity of crack path under loading as previously discussed.

The effect of additional S fibers on the flexural strength results of control mixtures with no fiber reinforcement can be seen in Table 4.1. To more easily compare the effect of various additional fibers on the MOR results of different mixtures, Figure 4.3 can also be reviewed. When a comparison is made between the results of mixtures numbered from 1 to 3 and 4 to 6, it can be noted that average MOR results significantly improved at the end of all various initial curing ages after reinforcement with S fibers. For example, average MOR results after 28 days were 3.20, 3.50 and 3.00 MPa for P0S0N0_0.20_1.0, P0S0N0_0.45_1.0 and P0S0N0_0.70_1.0, respectively, while the values were 6.00, 5.48 and 4.68 MPa for P0S1N0_0.20_1.0, P0S1N0_0.45_1.0 and P0S1N0_0.70_1.0 mixtures, respectively (Figure 4.3). Incremental rates in the MOR values of given mixtures after 28 days of curing were 47, 36 and 36%, respectively. As it is evident from Figure 4.3, the same modality held true for 7- and 90-day specimens. A valid increasing trend in MOR values was also observed when other fiber types (P and/or N) were incorporated in mixtures with S fibers. For example, the average 7-day MOR results of P0S1N0_0.20_1.0, P0S1N0_0.45_1.0 and P0S1N0_0.70_1.0 mixtures numbered from 4 to 6 were 6.00, 4.98 and 4.33 MPa. When mixtures incorporating only S fibers were amended with P fibers, these values increased to 7.98, 6.28 and 5.85 MPa for P1S1N0_0.20_1.0, P1S1N0_0.45_1.0 and P1S1N0_0.70_1.0 mixtures, respectively (Table 4.1). When three different fiber types were used in the mixtures, MOR values were also found to be higher than that of mixtures with only S fibers. Hence, average of MOR results recorded from P0.5S1N0.5_0.20_1.0, P0.5S1N0.5_0.45_1.0 and P0.5S1N0.5_0.70_1.0 mixtures were 6.68, 6.93 and 5.55 MPa, respectively. Based on these findings, it can generally be stated that S fibers were the most influential in enhancing MOR results followed by P and N fibers (Figure 4.3). The more pronounced effect of S fibers on MOR results is attributable to the significantly higher elastic modulus of S fibers (Table 3.2) (Ahmed et al., 2007). Although P fibers are more influential in further increasing the MOR results of mixtures with only S fibers, the values obtained for mixtures with S and P fibers were very close to those with S, P and N fibers for the same fiber volume (2%) (Table 4.1, Figure 4.3). Given the lower cost of N fibers as compared to P fibers and the beneficial effects of

using N fibers as shown in the compressive strength measurements discussed above, the amount of P fibers can be reduced by half when used with N fibers without substantially sacrificing flexural strength.

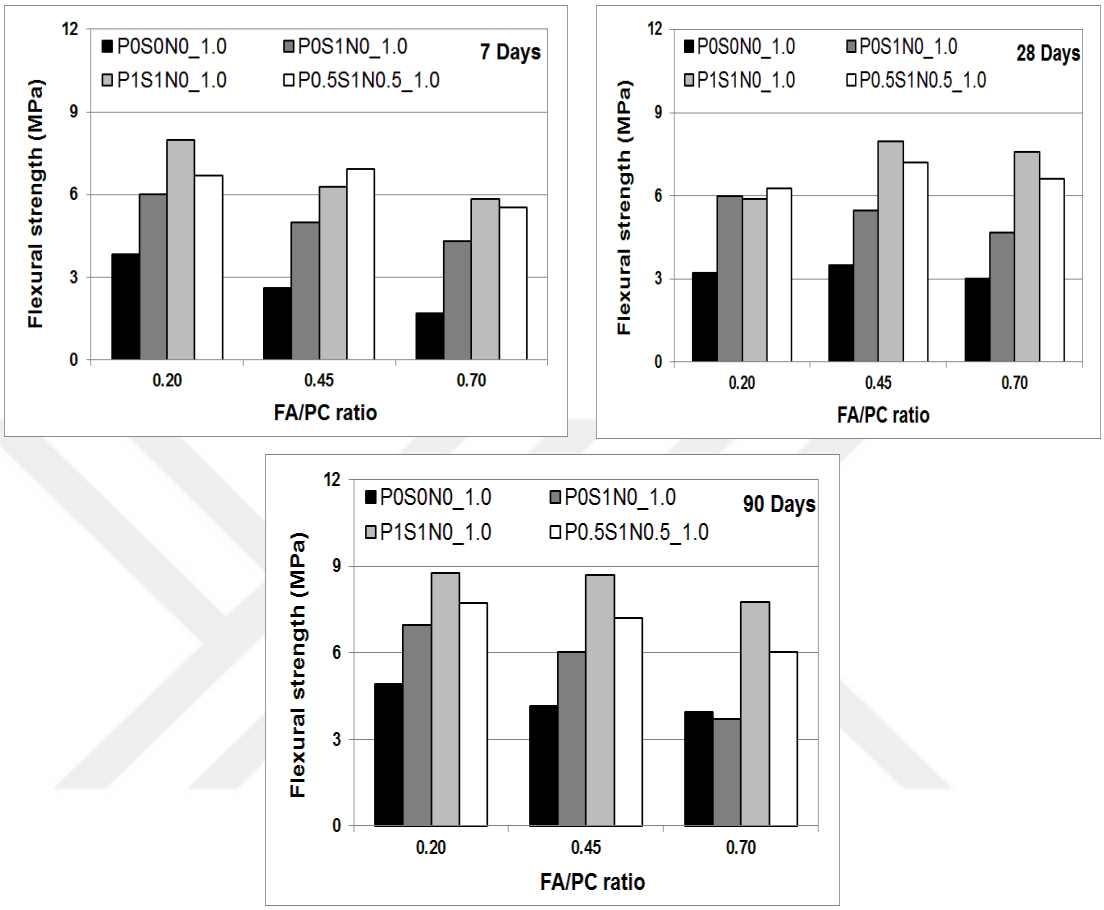

Figure 4.3 Effects of fiber utilization on the MOR results at a constant A/B ratio (1.0) and different FA/PC ratios

4.1.2.2 Mid-span beam deflection

The Average of mid-span beam deflection results which can be regarded as the indicator of overall ductility of mixtures, is included in Table 4.1. The values shown in this table were found by taking average results obtained from six different specimens; they corresponded to the maximum flexural strength values.

The initial curing period was one of the parameters influencing the mid-span beam deflection results of different mixtures as can be seen in Table 4.1. For almost all of the mixtures studied, there were continuous drops in the values when the initial curing time of specimens was extended; this was attributed to the fiber-to-matrix interface properties that were continuously improving with time (Şahmaran et al.,

2013). Moreover, when the FA/PC ratio was increased for mixtures with the same A/B ratios, differences between mid-span beam deflection results of specimens cured for short and long terms increased in most cases. For example, between the ages of 7 and 90 days, the differences in the average mid-span beam deflection results of P0S0N0_0.20_1.0 and P0S0N0_0.70_1.0 were 0.13 mm (=0.34-0.21) and 0.27 mm (=0.38-0.11), respectively. This might be due to the relatively high amounts of hydrated FA particles staying in the matrices without any reaction at early ages and hydrating later on. When FA is further hydrated, matrix and related strength properties improved, but this led to relatively brittle cementitious systems with low ductility.

Although there were natural variations in the results, increasing FA/PC ratios resulted in higher mid-span beam deflection results for a given mixture and A/B ratio. This was also evident for specimens with fiber reinforcement. In particular, the behavior observed for fiber reinforced specimens can be attributed to the tendency of FA particles to reduce chemical bonding between the synthetic fibers and the matrix (and reduce matrix fracture toughness itself) while enhancing frictional bonding in the interface to further favor high ductility (Sherir et al., 2015). In addition, spherical morphology of FA particles favoring the uniform distribution of individual fibers in mono and/or hybrid systems can be partly responsible for the higher deflection results obtained in the case of higher FA/PC ratios (Qian and Stoeven, 2000).

The A/B ratio is another variable parameter to be taken into consideration during the production of different mixtures, and was expected to have a significant impact on the mid-span beam deflection results. Almost half of the weight of the total aggregate combination (43%) was composed of coarse aggregates, which can cause the interruption of smaller fibers (P and N) mixing. However, it can also be seen from Table 4.1, even at the highest A/B ratio selected for the present study, mid-span beam deflection results of specimens initially cured for different ages were not necessarily decreased as compared to specimens with lower A/B ratios. There were several occasions where the anticipated reductions in the mid-span beam deflection values with increasing A/B ratios were compensated by the use of a reasonable amount of FA. Thus, A/B ratio did not affect the overall ductility of the mixtures as

long as the FA amount was optimized. This finding was also in line with results stated in the study of (Şahmaran et al., 2012).

As stated previously, one of the main objectives of this study is to manufacture cementitious composite mixtures incorporating the maximal amount of coarse aggregates to favor cost and dimensional stability without compromising the deflection-hardening behavior under bending loads. In this sense, the addition of single and/or multiple fibers into the cementitious systems of control mixtures is of primary importance. For a better visualization of the effect of fiber addition in composite materials, Figure 4.4 was drawn for mixtures with a constant A/B ratio of 1.0 and different FA/PC ratios. Similar to the case observed in the MOR results, inclusion of S fibers in control mixtures caused increments in the mid-span beam deflection results, although the increment rates were more dramatic (Figure 4.4, Table 4.1). For example, 28-day average MOR results of the P0S0N0_0.20_1.0 mixture increased almost two-fold (from 3.20 to 6.00 MPa) when 1% of S fibers were included in the cementitious system, although the rate of increment was more than seven-fold (from 0.22 to 1.60 mm) considering the average mid-span beam deflection results of similar mixtures of the same age. As observed in the case of S fiber inclusion, this behavior was also valid for 7- and 90-day specimens. Therefore, the value of adding fibers into control mixtures relates not so much to the improvement of strength but the capability of crack control and deformation. To better illustrate the effect of S fiber addition to the control mixtures, some of the selected flexural stress vs. mid-span beam deflection graphs of 28-day specimens belonging to P0S0N0 and P0S1N0 mixtures with an A/B ratio of 1.0 are shown as examples in Figure 4.5-a and Figure 4.5-b, respectively. As it can easily be seen in these figures, significant improvements in both MOR and mid-span beam deflection results were also confirmed by these plots. Thus, deflection-hardening behavior can be verified when the peak load reached during a certain bending test is higher than the first cracking load. Additionally, if the mid-span beam deflection at the peak load is higher than that corresponding to its first cracking load, deflection-hardening behavior is further enhanced. It can therefore be stated that deflection-hardening behavior is confirmed if the peak load and its corresponding mid-span beam deflection is greater than the first cracking load and its corresponding mid-span deflection at first cracking load, respectively. By further increasing the gap between

the first cracking load / peak load and deflection at the first cracking load / deflection at the peak load, deflection-hardening behavior can be improved (Shaikh, 2013). Based on the abovementioned statement and the representative plots presented in Figure 4.5-b, it can thus be stated that even the composite mixtures incorporated with S fibers only (1%, by volume) exhibit deflection-hardening behavior. Although all of the specimens from the P0S1N0 mixture were not displayed in Figure 4.5-b, deflection-hardening behavior was valid regardless of different ages and FA/PC ratios.

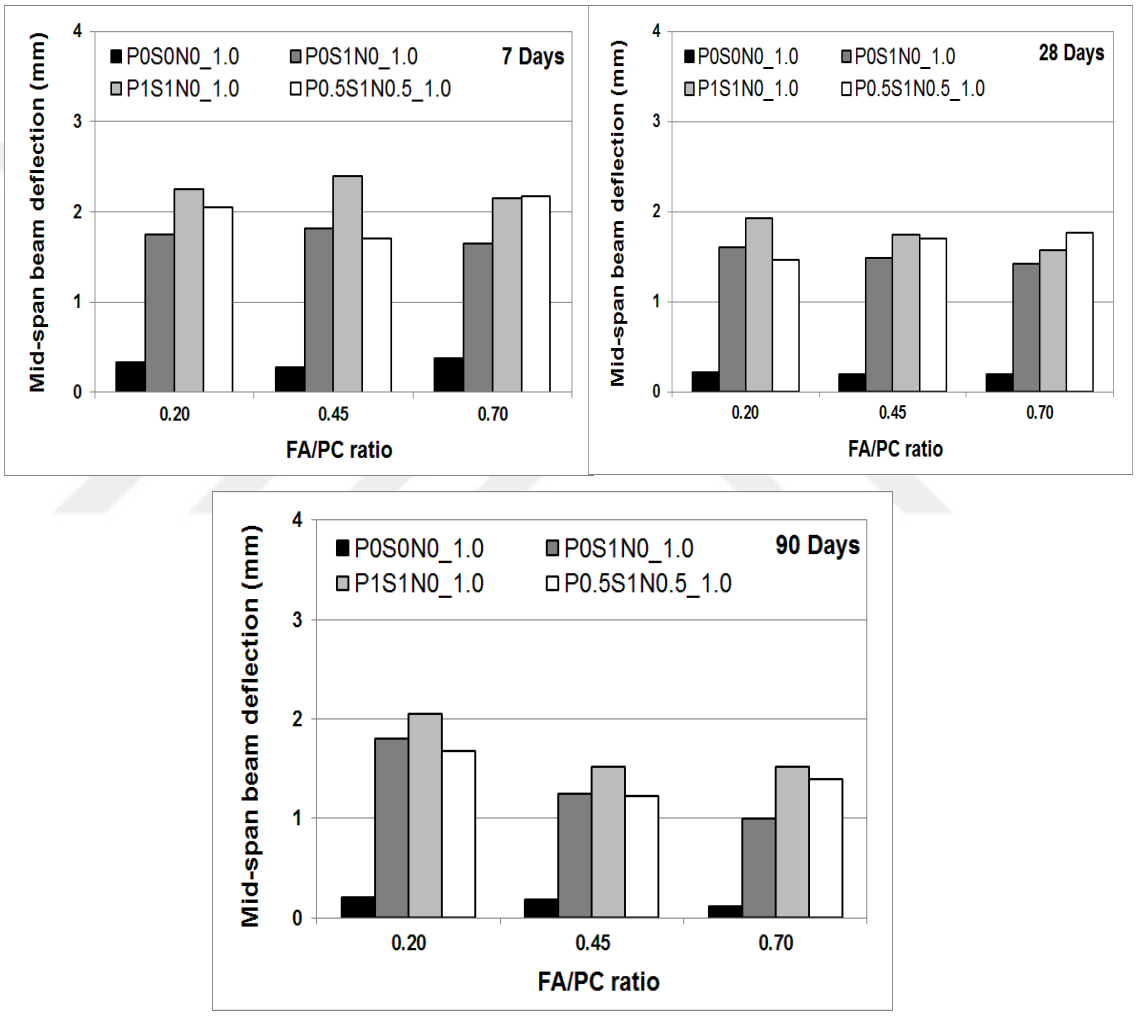

Figure 4.4 Effects of fiber utilization on the mid-span beam deflection results at a constant A/B ratio (1.0) and different FA/PC ratios

Marked improvements were also seen in the MOR and mid-span deflection results of composite mixtures (P1S1N0 and P0.5S1N0.5) as compared to control mixtures. Figure 4.5-c and Figure 4.5-d clearly demonstrate that deflection hardening behavior was further improved when cementitious systems were hybridized with P, S and/or

P, S and N fibers. In accordance with the plots shown in these figures, one can easily see that the gaps between first cracking stress and peak stress are greater as compared to composite mixtures with only S fibers; the same is true for deflection at the first cracking stress and deflection at the ultimate (peak) stress. It seems that the addition of P and N fibers further enhanced the deflection-hardening behavior. Further enhancement in deflection-hardening behavior (ductility) with the addition of P or P, N fibers to composite mixtures incorporating only S fibers was observable in terms of crack characteristics as well. As Figure 4.6 reveals, cracks smaller in width and higher in number (6 to 7 cracks with widths around 100 μm and less) were observed on the surfaces of failed specimens belonging to P1S1N0 and P0.5S1N0.5 mixtures, which suggests improved ductile behavior. (Multiple micro-size cracking behavior—four to five cracks with the widths around 200 μm—was also valid for P0S1N0 specimens.) Similarly, the deflection-hardening behavior of specimens from P1S1N0 and P0.5S1N0.5 mixtures was also apparent for different initial curing ages and A/B ratios. Comparing the representative flexural stress vs. mid-span beam deflection plots of P1S1N0 and P0.5S1N0.5 mixtures, it can be seen that both MOR and deflection results along with general behavior under flexural loads were very similar. Therefore, N fibers can be replaced with P fibers by up to 50% for the sake of reduced material cost without compromising flexural strength and deflection characteristics. This conclusion was also in line with the compressive strength results.

In order to see the effect of A/B ratios on the flexural behavior of composite mixtures manufactured with P, S and P, S, N fiber combinations, Figure 4.5-e and Figure 4.5-f were drawn. When these figures are checked against Figure 4.5-c and Figure 4.5-d, one can clearly observe that an increase in aggregate content was not a restrictive parameter on both MOR and mid-span beam deflection results, and plots that are relatively similar to each other were obtained (thus confirming the deflection-hardening behavior). The plots also correspond to the individual bulk data presented in Table 4.1 and are valid for specimens with an A/B ratio of 1.5 and subjected to 7 or 90 days of initial curing. It seems that proper optimization of the matrix properties with reasonable amounts of FA can compensate for the possible negative effects of high amounts of coarse aggregate usage on fiber clumping and related (but less pronounced) flexural parameters.

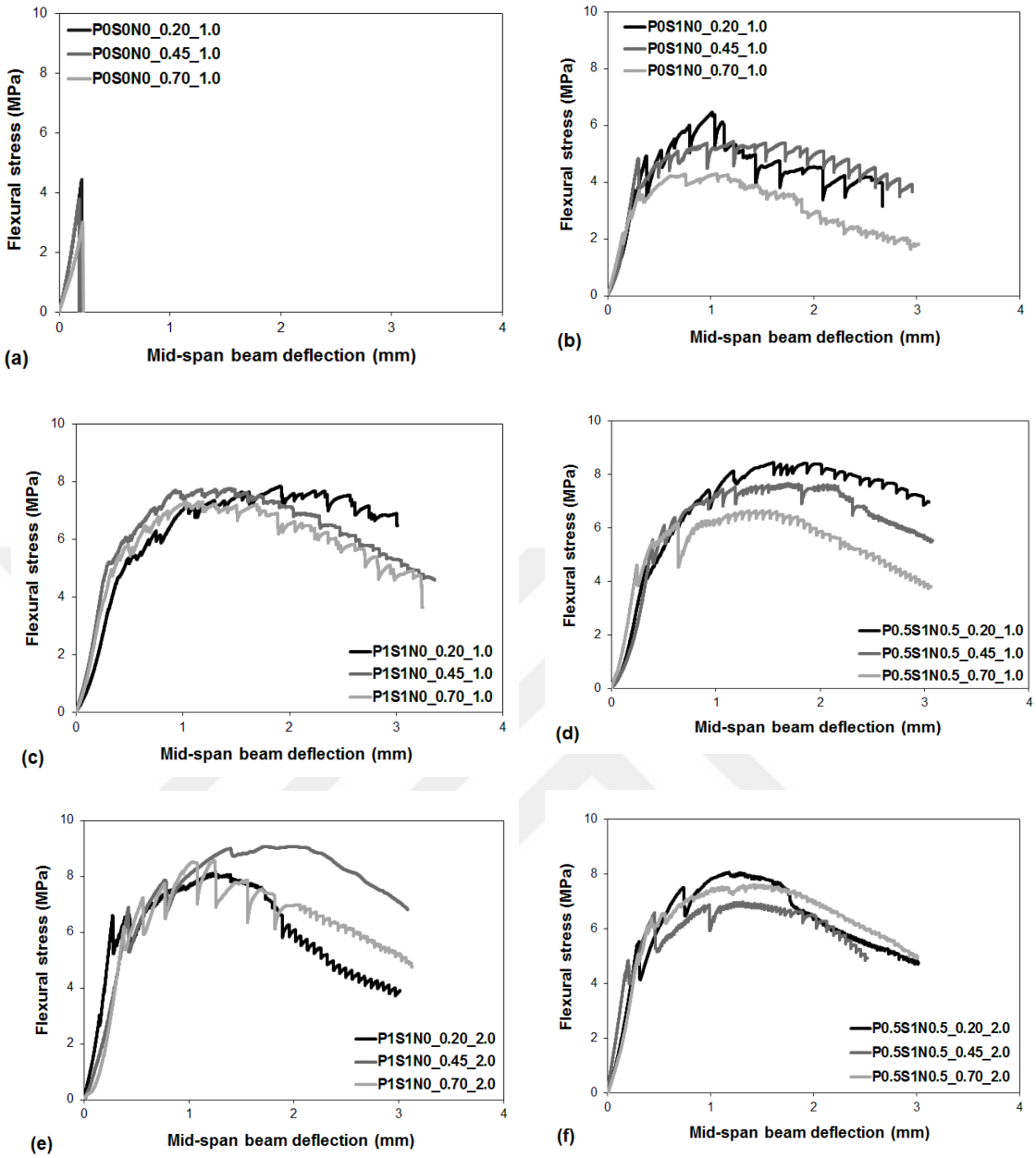

Figure 4.5 Representative 28-day-old flexural strength – mid-span beam deflection plots of mixtures based on the effects of utilization of fibers with different types/amounts (a-d) and A/B ratios (c-f)

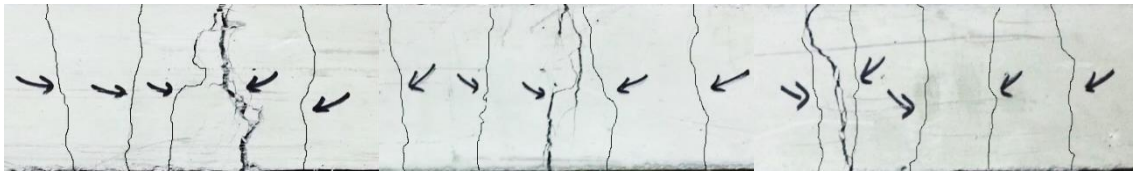

P0S1N0 mixture

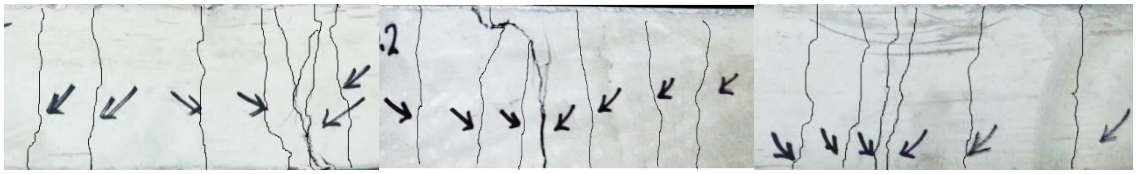

P1S1N0 mixture

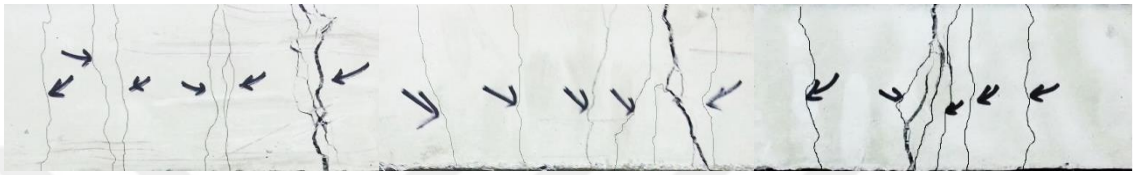

P0.5S1N0.5 mixture

Figure 4.6 General multiple microcracking behavior observed on the tensile faces of several specimens from different mixtures

4.2 Free Fall Drop-Weight Impact Test

4.2.1 Results of Experimental Part

To assess the impact performance of beam specimens produced with different HPFRC mixtures, specimens were subjected to constant-energy (52.97 Joule) impact loading by dropping the impact hammer freely by using the proposed test setup. The performance was analyzed by commenting on the data related to graphs showing impact load vs. time, acceleration vs. time (from 2 different points) and displacement vs. time (from 2 different points). Examples of acceleration vs. time, displacement vs. time and impact load vs. time graphs are shown in Figures 4.7, 4.8 and 4.9, respectively. Maximum acceleration (for left and right points), displacement (for left and right points) and impact load results are summarized in Table 4.2.

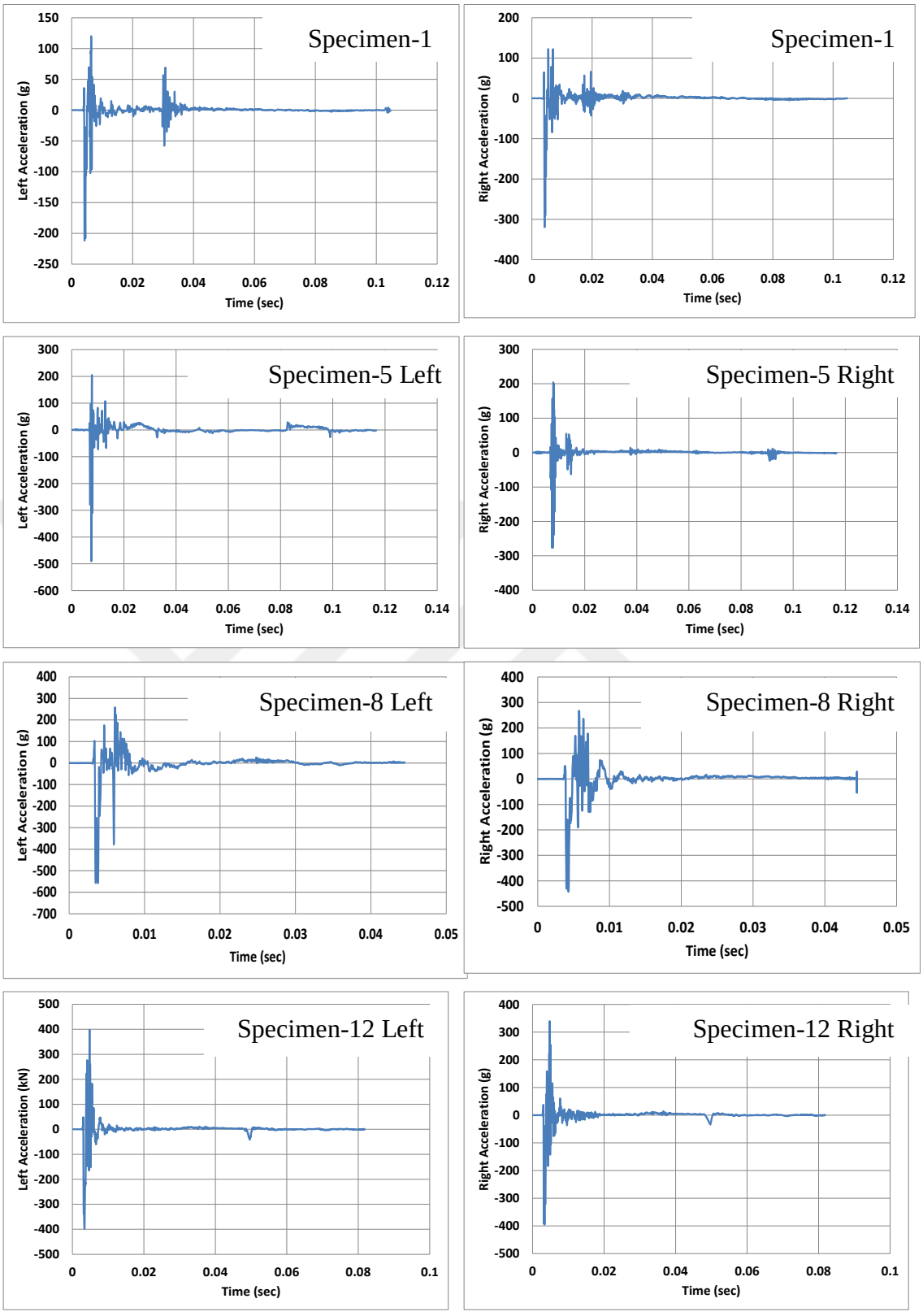

Figure 4.7 Typical acceleration vs. time graphs for selected specimens

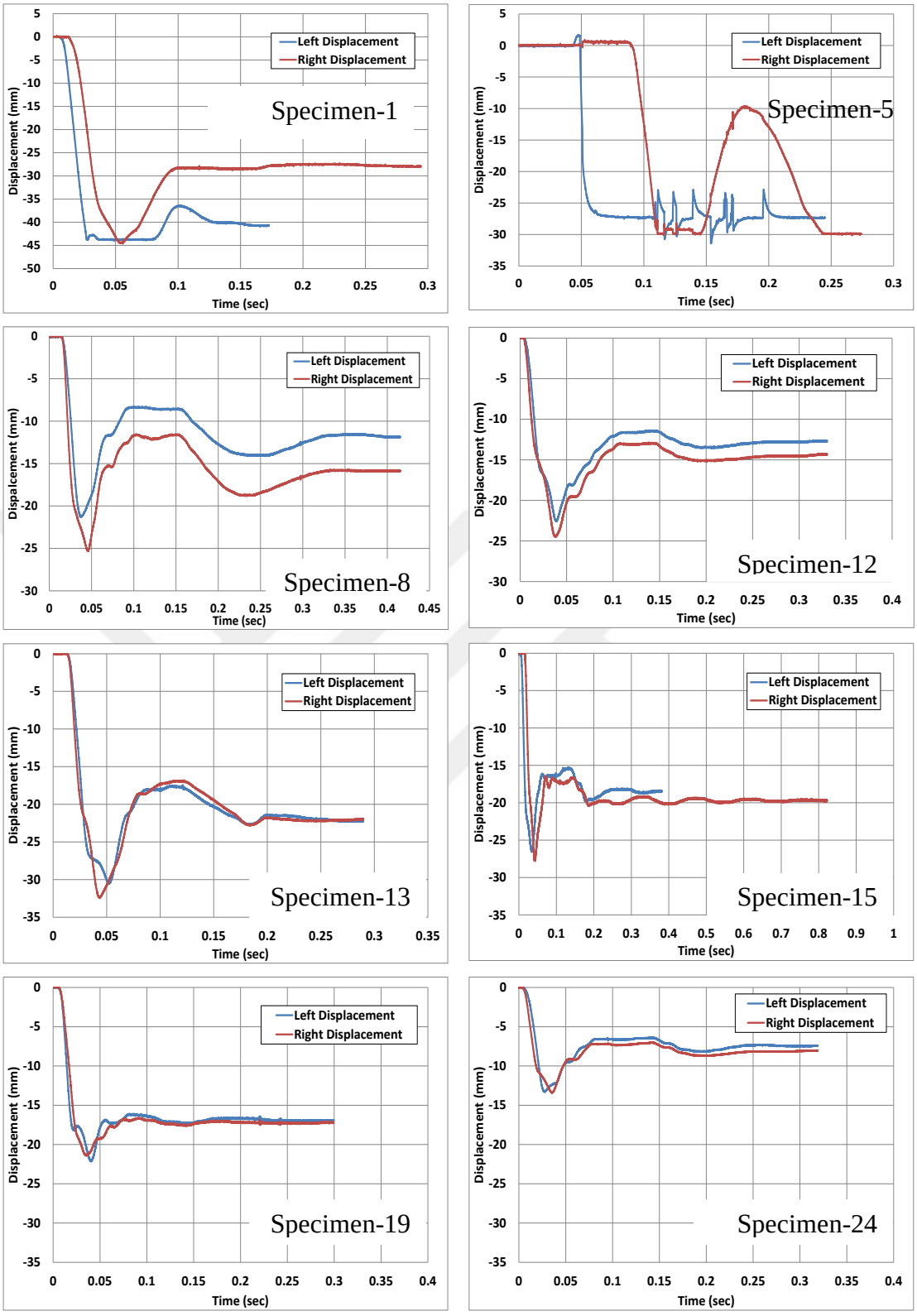

Figure 4.8 Typical displacement vs. time graphs for selected specimens

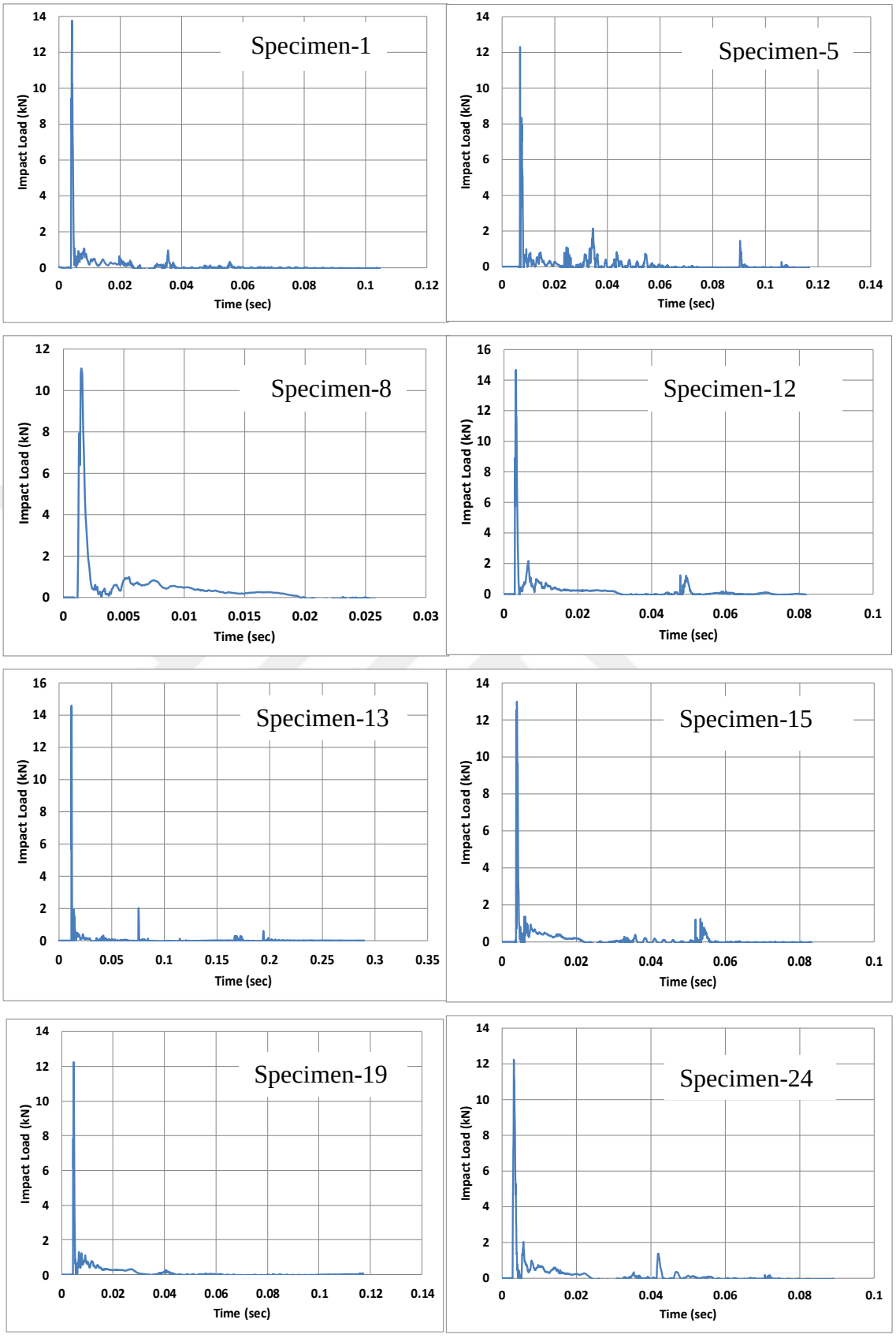

Figure 4.9 Typical impact load-time graphs for selected specimens

Table 4.2 Free fall drop-weight test results

Mix. No	Mix. ID	Acceleration (g)				Displacement (mm)		Impact Load (kN)	Residual Displacement (mm)
		Left		Right					
		Max.	Min.	Max.	Min.	Left	Right		
1	P0S0N0_0.20_1.0	120.00	-211.64	122.37	-319.50	-44.05	-44.65	13.78	28.51
2	P0S0N0_0.45_1.0	132.03	-118.18	140.01	-139.85	-40.77	-39.14	12.32	30.13
3	P0S0N0_0.70_1.0	152.28	-533.06	155.94	-418.31	-36.81	-36.79	12.32	24.90
4	P0S1N0_0.20_1.0	188.05	-303.22	187.33	-331.66	-34.79	-33.21	12.04	27.12
5	P0S1N0_0.45_1.0	205.08	-490.27	204.08	-276.38	-31.42	-30.15	12.31	27.25
6	P0S1N0_0.70_1.0	227.18	-284.04	225.26	-377.47	-29.59	-27.93	12.32	27.79
7	P1S1N0_0.20_1.0	216.11	-334.17	223.38	-265.52	-25.91	-27.62	12.24	19.78
8	P1S1N0_0.45_1.0	258.70	-556.95	267.38	-442.21	-21.32	-25.33	11.07	11.79
9	P1S1N0_0.70_1.0	319.51	-372.02	327.10	-552.77	-20.34	-22.80	12.39	11.82
10	P1S1N0_0.20_1.5	262.95	-262.88	261.20	-260.91	-29.12	-31.44	14.45	13.43
11	P1S1N0_0.45_1.5	323.12	-323.03	320.96	-289.25	-26.47	-28.08	12.47	14.00
12	P1S1N0_0.70_1.5	398.05	-397.94	339.73	-394.93	-22.60	-24.51	14.67	12.87
13	P1S1N0_0.20_2.0	293.19	-556.95	300.39	-485.11	-30.57	-32.44	14.60	16.78
14	P1S1N0_0.45_2.0	356.70	-445.56	334.80	-531.03	-28.78	-30.40	12.08	15.63
15	P1S1N0_0.70_2.0	423.40	-423.28	431.55	-540.64	-26.58	-27.81	12.98	20.08
16	P0.5S1N0.5_0.20_1.0	300.90	-512.39	315.35	-342.72	-19.36	-17.09	12.24	14.26
17	P0.5S1N0.5_0.45_1.0	349.52	-902.25	350.04	-491.38	-12.76	-12.13	12.50	5.49
18	P0.5S1N0.5_0.70_1.0	471.91	-556.95	473.67	-552.77	-10.32	-10.94	12.18	4.89
19	P0.5S1N0.5_0.20_1.5	376.41	-556.95	388.94	-545.97	-22.15	-21.42	12.24	16.63
20	P0.5S1N0.5_0.45_1.5	429.12	-662.77	432.38	-417.42	-14.80	-15.57	12.18	9.26
21	P0.5S1N0.5_0.70_1.5	572.29	-983.00	571.78	-1232.67	-12.13	-11.43	12.68	8.07
22	P0.5S1N0.5_0.20_2.0	421.73	-421.61	423.30	-818.10	-24.35	-24.82	12.26	19.15
23	P0.5S1N0.5_0.45_2.0	475.93	-1175.16	466.01	-1166.34	-16.21	-16.22	12.77	10.07
24	P0.5S1N0.5_0.70_2.0	618.91	-1164.02	619.79	619.10	-13.32	-13.40	12.24	8.17

The experimental program investigated the effects of three variables on the impact resistance of HPFRC beam specimens. The first variable is the type of fiber reinforcement (S, P and N). As indicated by the denominations listed in Table 4.2, specimens 1 to 3 had no fiber reinforcement (reference specimens). In specimens 4 to 6, only S fiber (1%, by volume) was used, and in specimens 7 to 15, S (1%) and P (1%) (total of 2%, by volume) were used. In specimens 16 to 24, S (1%), P (0.5%) and N (0.5%) fibers (total of 2%, by volume) were used simultaneously. Addition of fiber reinforcement into the HPFRC beam specimens was very effective on measured acceleration and displacement results, leading to significant increments in acceleration results and decrements in displacement results. For specimens with an A/B ratio of 1.0, the average of left and right acceleration results for specimens with only S fibers was 33% higher than that of reference specimens with no fibers, while the average of displacement results was 23% lower. For specimens with S and P fibers at the same A/B ratio, the average of left and right acceleration results was 23% higher, and the average displacement was 23% lower as compared to reference specimens. In the mixtures incorporating all three fiber types, the average of acceleration and displacement results were 29% higher and 42% lower than in the reference specimens, respectively. Based on these results, the best impact performance for specimens with A/B ratio of 1.0 was obtained from specimens incorporating three types of fibers simultaneously. Increments in the acceleration results imply that these specimens exhibit more rigid performance and have potential to withstand higher impact levels. Likewise, the maximum reduction in average displacement results (42%) was obtained when the reference specimens were reinforced with three different fibers. This finding also confirms that these specimens show a more rigid behavior, have a high residual impact capacity and can endure higher impact loads.

The second variable of the experimental program was A/B ratio; the three selected A/B ratios were 1.0, 1.5 and 2.0. The effect of A/B ratio on impact performance was evaluated for specimens with S, P and S, P, N fibers. For the A/B ratio of 1.5, the average of left and right side acceleration results and displacement results of specimens with S and P fibers were 31% lower and 40% higher, respectively, than in specimens with S, P and N fibers. When A/B ratio was increased to 2.0, the results were 29% lower and 39% higher. In general, increments in A/B ratio caused

increased acceleration and decreased displacement results. Using higher amounts of aggregates in test specimens had a positive effect on confronting impact loads and strengthened their skeleton for transferring the loads. Further, it increased the rigidity of concrete and caused displacement results to drop. Based on the aforementioned results, increasing the weight of aggregates in beam specimens also increased their resistance to higher acceleration levels and heavier weights, and contributed to lower displacement. A possible explanation for improved impact resistance with higher amounts of aggregates (A/B ratios) could be related to increased energy levels (due to a more tortuous cracking path) causing final fracturing of beam specimens. The area under the load-displacement curve represents the fracture energy (toughness). As reported in literature, concrete mixtures outperform paste mixtures in terms of impact resistance, given their higher energy needs, to cause final fracture (Banthia, 1987). In line with this finding, increasing the amount of aggregates in HPFRC mixtures is likely to increase the fracture energy, leading to higher impact resistance. Moreover, increasing amounts of aggregates necessitate lower amounts of binder, which is the phase confronting the accumulation of stresses. Therefore, reducing paste content may result in a more stable concrete mixture and increased impact resistance.

The third investigated variable was FA/PC ratio; the FA/PC selected ratios were 0.20, 0.45 and 0.70. As the amount of FA increased, acceleration results increased while displacement results decreased. This finding was observed in all proposed HPFRC mixtures, with and without different fiber combinations. In the reference HPFRC beam specimens, when FA/PC ratio was increased from 0.20 to 0.45, the average acceleration obtained from the left and right sides of the specimens increased by 11%, while displacement was reduced by 10%. When FA/PC ratio was increased from 0.45 to 0.70 for the same specimens, the average acceleration results increased by 12% and displacement results was decreased by 8%, respectively. In HPFRC beam specimens reinforced only with S fibers, when the FA/PC ratio was increased from 0.20 to 0.45, average acceleration and displacement results increased by 8% and decreased by 9%, respectively. When FA/PC ratio was increased from 0.45 to 0.70, average acceleration and displacement results for the same specimens increased by 10% and decreased by 7%, respectively. When the ratio was increased from 0.20 to 0.45 for specimens with S and P fibers, average acceleration results increased by

16% and displacement results was decreased by 10%. When the ratio was increased from 0.45 to 0.70, average acceleration increased by 17% while displacement decreased by 10%. Finally, in the specimens produced with three different fibers, increasing FA/PC ratio from 0.20 to 0.45 caused average acceleration results to increase by 11% and displacement results to decrease by 32%. By increasing FA/PC ratio for the same specimens from 0.45 to 0.70, average acceleration results increased by 25% and displacement results decreased by 18%. Therefore, incorporating higher amounts of FA improved the rigidity, acceleration capacity and impact resistance of HPFRC mixtures under sudden loading. It also reduced displacement with impact loading and enhanced resistance to higher rates of acceleration and impact energy. This outcome was valid even for reference specimens not reinforced with fiber. To be more precise, increasing FA was most effective in increasing acceleration and decreasing displacement for specimens reinforced with three different fibers. The possible explanation for the more pronounced impact performance in HPFRC specimens with fibers with increased FA may be the influence of FA particles in more uniformly distributing individual fibers due to their spherical surface characteristics and ability to lower matrix fracture toughness results in favor of increased ductility (flexural displacement) (Table 4.1).

Figure 4.10 shows examples of cracking behavior of beam specimens after application of impact load, Figure 4.8 shows examples of displacement vs. time graphs obtained from left- and right-hand-side LVDTs, and maximum displacement values are illustrated in Table 4.2. In addition to maximum displacement values measured in the first moment of drop hammer impact, the residual displacement values remained on the beam specimens after the impact tests were measured for all specimens, as shown in the displacement-time graphs. Residual displacement values remaining on beam specimens after completion of impact loading are listed in the last column of Table 4.2. Based on the residual displacement results and typical cracking behavior after impact loading (Figure 4.10), maximum damage occurred in reference specimens with no fibers, with an average residual displacement of 27.85 mm for the specimen series with no fibers. Average residual displacement of specimens with only S fibers was very close to that of reference specimens at 27.39 mm. For those incorporating S and P fibers, the value was 15.13 mm, which is 45% smaller than that obtained from specimens without fibers and with only S fibers.

Average residual displacement in specimens with three different fibers was 10.67 mm, which is 30% smaller than the values of specimens with S and P fibers. Maximum and residual displacement values were comparably lower in specimens reinforced with P, S and N fibers. This finding demonstrates that these beam specimens were the least affected by the impact load.

4.2.2 Results of Numerical Part

In the numerical part of the study, an explicit module of the ABAQUS finite element analysis software was used to investigate the behavior of structural members underperformed dynamic effects for non-linear analysis. Test setup and specimens were modeled in the software, and element types, material properties, mesh sizes, time steps and boundary were defined. Specimen sizes and support conditions were noted, as in the test program. No external forces were applied to the system, excluding gravitational force. As in the experimental program, the drop height and mass of the steel drop hammer were 600 mm and 9 kg in the analysis, respectively. The element type selected was C3D10M (10-node modified tetrahedron), which gives the best results under dynamic effects. A steel plate was located on the mid-point of specimen to prevent local crushing from the point of impact loading. Finite element models were created after completing the node and element numbers of the test specimen, hammer and steel plate. Since specimen sizes were the same, the same node and element numbers were defined in the software.

Material properties were assigned to the related geometries in the software. The software's concrete damage plasticity model was used to define non-linear behavior of concrete material. Linear elastic material models were defined for the steel hammer and plate, as presented in Table 5. Properties of HPFRC mixtures changed, since the material properties and fractions of ingredients in the mixtures were relatively different. As a result of tests performed on HPFRC mixtures used in producing beam specimens, compressive stress-strain and uniaxial tensile stress-strain graphs of each mixture were obtained experimentally. In the finite element analysis, material models obtained separately for each beam specimen in both compression and uniaxial tensile stress-strain were used and entered into the ABAQUS software as raw data. Examples selected from material models used in the

analysis of test specimens are shown in Figures 4.11 and 4.12 for compressive and uniaxial tensile stresses, respectively.

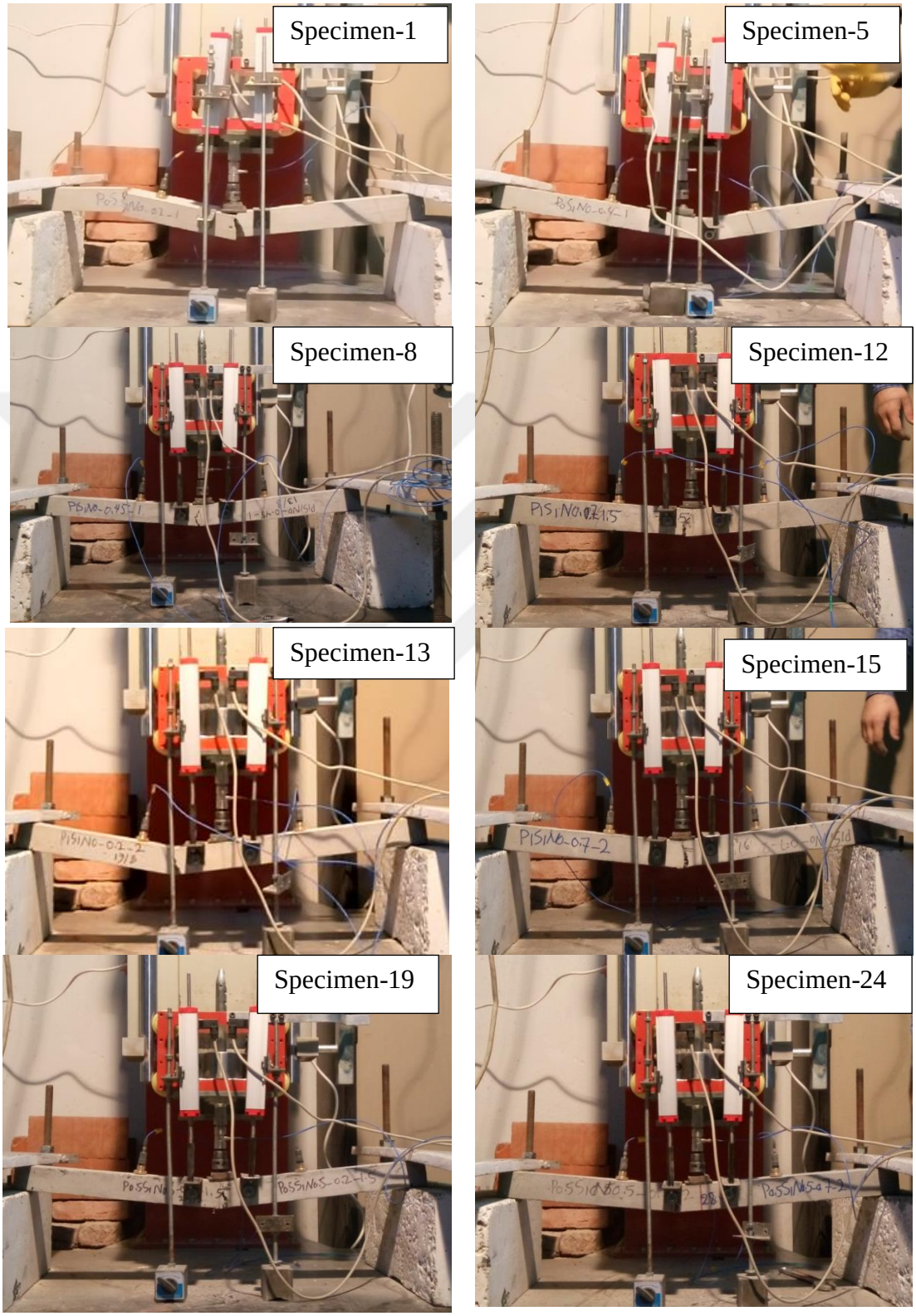

Figure 4.10 Typical view of the final failure of specimens

Table 4.3 Material properties of steel hammer and plate used for finite element analysis model

Property	Steel hammer and plate
Weight per unit of volume (kg/m^3)	7850
Modulus of elasticity (MPa)	200000
Poisson's ratio	0.30
Shear modulus(MPa)	76923
Bulk modulus(MPa)	166670

After material properties were assigned to the related geometries, support conditions were provided for each test specimen. The geometries were then divided into small pieces to properly investigate the effect of impact. For this purpose, mesh design operation was performed to reach correct results. Finally, based on a comparative analysis of results between 10 and 30 mm mesh sizes, 15 mm mesh was chosen. Figure 4.13 shows a finite element model of a test specimen before and after mesh design.

Connection between the surfaces was provided by defining contact surfaces. For this purpose, surface to surface contact was selected between the steel hammer and the test specimen. The surface of the hammer applying the impact load was chosen as master, and the corresponding part of the specimen was chosen as slave. Behavior of the contact surfaces was tangential in the software. Since friction effects occurred during the experimental program, the coefficient of friction for contact surfaces was taken as 0.2. Before starting analysis, time steps and time spans were defined in the software, and time increments were assigned for each drop movement of the hammer. As the analysis was an incremental dynamic problem, it was performed for short time intervals to reach the proper results. Time increments were very short values as the hammer started to apply loading on the test specimen.

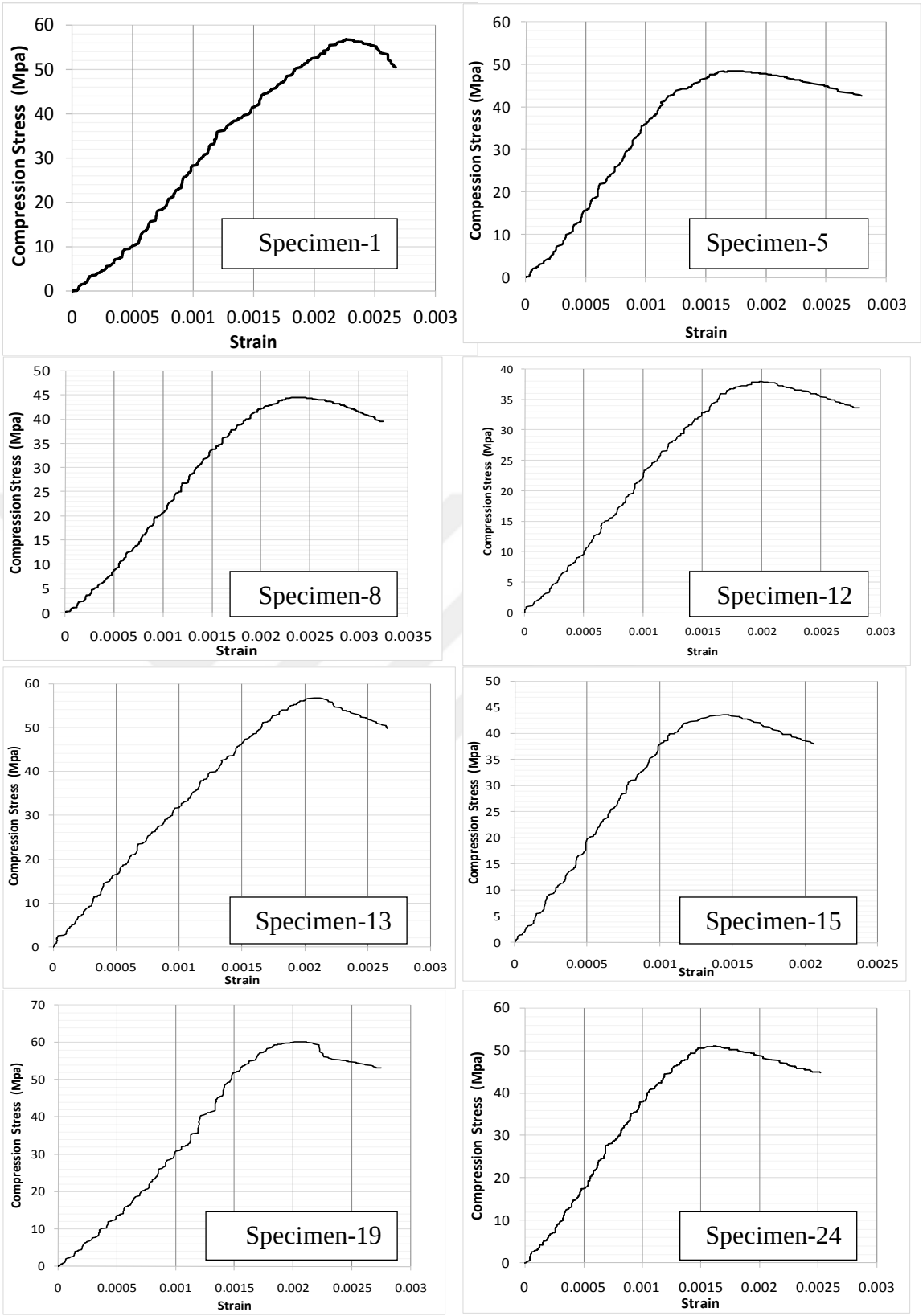

Figure 4.11 Typical compressive stress vs. strain models for finite element analysis model

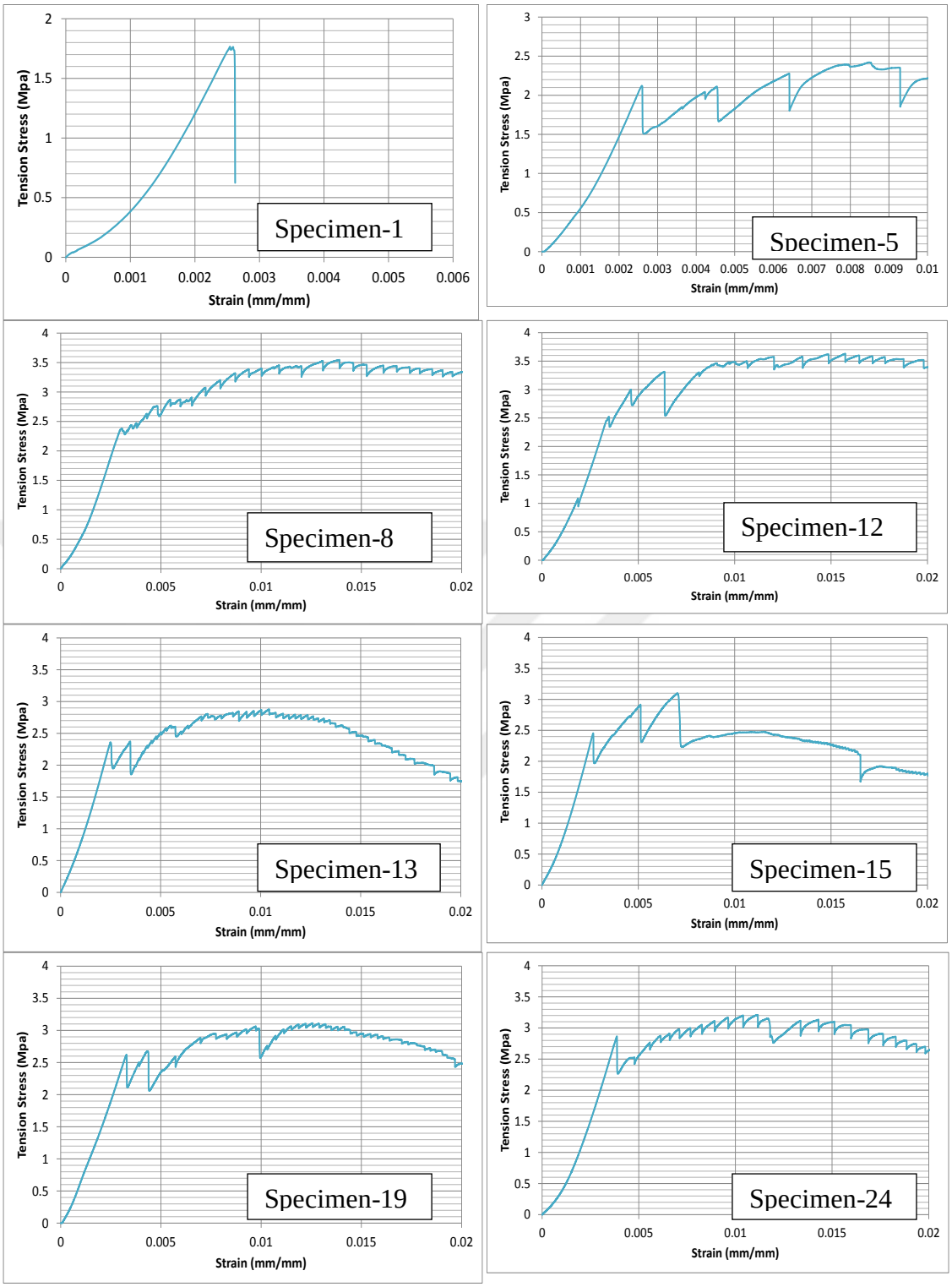

Figure 4.12 Typical uniaxial tensile stress vs. strain models for finite element analysis model

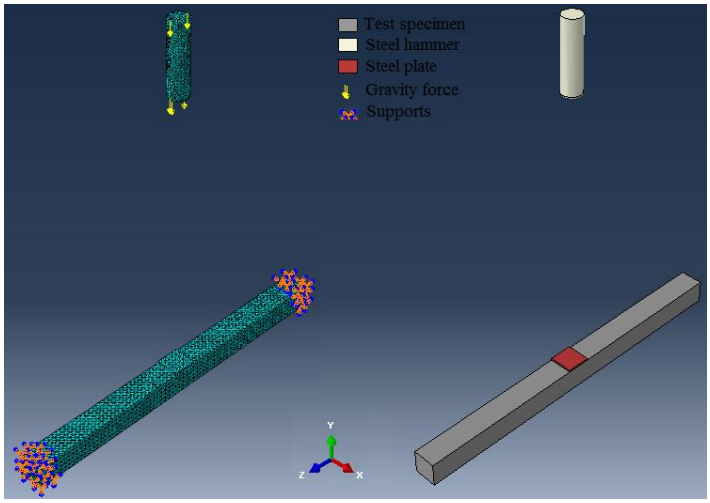

Figure 4.13 Typical finite element model meshes

4.2.3 Comparison of Experimental and Numerical Results

A finite elements analysis was performed for each test specimen. Acceleration, displacement, impact load and residual displacements were obtained after completing non-linear analysis. A high-performance computer was used to obtain realistic results in a shorter time span. Using this process, finite element analysis can be used as an option for investigating the behavior of test specimens under impact loading. Figure 4.14 shows maximum acceleration vs. time, displacement vs. time and impact load vs. time graphs after analysis for specimen number 8. Graphs were acquired for a single drop of the steel hammer so results from the analysis could be compared with the test results. Maximum results obtained from the analysis are summarized in Table 4.4.

When the results presented in Table 4.4 are evaluated, it is evident that maximum acceleration rates that obtained from actual experiments and finite element analysis range between 0.80 and 1.10. Maximum displacement rates obtained from the experiments and finite element analysis range between 0.84 and 1.13. The rates of residual displacements obtained from the experiments and finite element analysis range between 0.86 and 1.25. These findings show that results of ABAQUS analysis are in good agreement with the experimental results.

After completing the application of loading, Von-Misses stress distributions were determined. Cracks and damage were observed due to the development of stress distributions; stress distributions on three test specimens are shown in Figure 4.15 to

present the behavior under impact loading. Finally, maximum stress values occurred around impact point for all test specimens. Deformed specimen shapes were also determined after performing non-linear finite elements analysis; examples are presented in Figure 4.16. Cracks and distributed damage monitored after the actual experiments were in line with figures acquired as a result of the analysis. Maximum displacement and stresses were observed close to the mid-point where the impact loading was applied, which is similar to that observed in laboratory experiments.

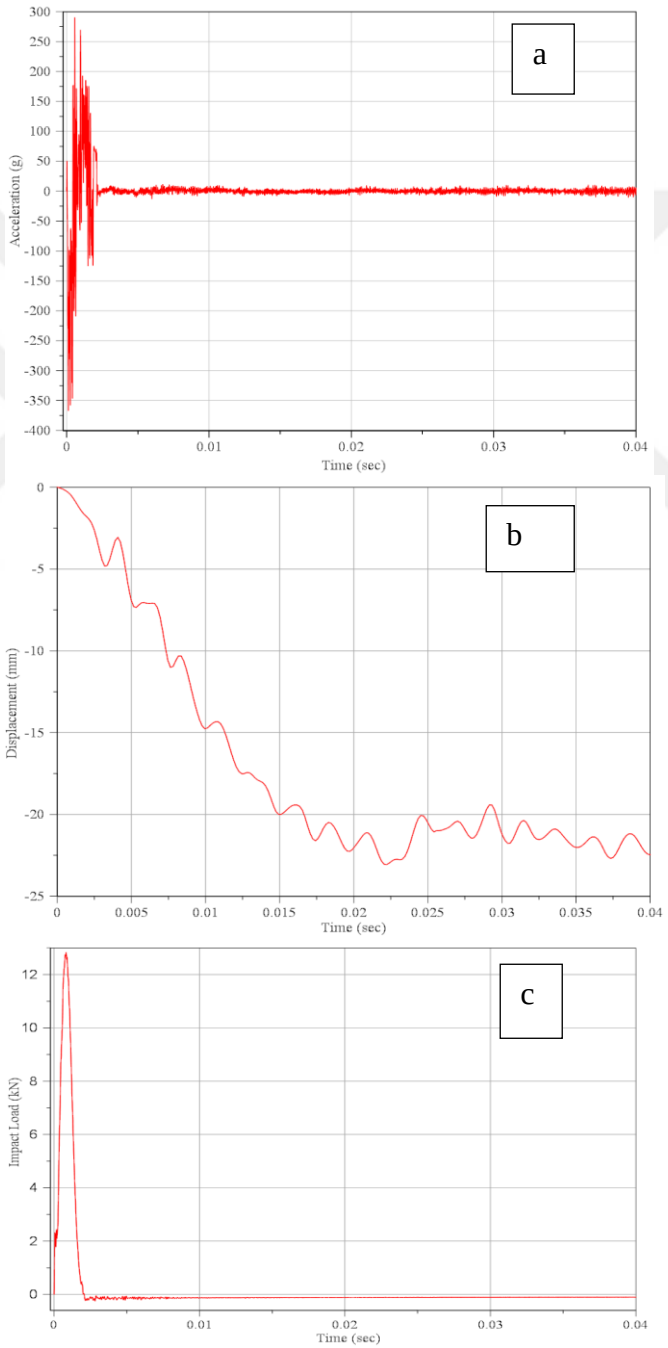

Figure 4.14 a) Acceleration vs. time b) Displacement vs. time and c) Impact load vs. time graphs of Specimen 8 obtained by finite element analysis

Table 4.4 Comparison of experimental and numerical results

Mix. No	Left Acceleration (g)					Left Displacement (mm)			Impact Load (kN)			Residual Displacement (mm)		
	Exper.		ABAQUS		Ratio*									
	Max	Min	Max	Min		Exper.	ABAQUS	Ratio**	Exper.	ABAQUS	Ratio***	Exper.	ABAQUS	Ratio****
1	120.00	-211.64	122.13	-181.47	0.98	-44.05	-48.24	0.91	13.78	15.61	0.88	28.51	24.22	1.18
2	132.03	-118.18	131.53	-148.29	1.00	-40.77	-43.33	0.94	12.32	14.62	0.84	30.13	27.26	1.11
3	152.28	-533.06	174.61	-203.41	0.87	-36.81	-40.02	0.92	12.32	15.03	0.82	24.90	21.53	1.16
4	188.05	-303.22	235.16	-197.47	0.80	-34.79	-37.21	0.93	12.04	13.86	0.87	27.12	25.01	1.08
5	205.08	-490.27	254.86	-301.38	0.80	-31.42	-34.24	0.92	12.31	14.38	0.86	27.25	24.68	1.10
6	227.18	-284.04	266.81	-227.51	0.85	-29.59	-33.17	0.89	12.32	13.96	0.88	27.79	22.22	1.25
7	216.11	-334.17	224.76	-277.61	0.96	-25.91	-28.53	0.91	12.24	13.29	0.92	19.78	16.23	1.22
8	258.70	-556.95	297.65	-366.43	0.87	-21.32	-23.07	0.92	11.07	12.63	0.88	11.79	13.77	0.86
9	319.51	-372.02	304.57	-351.73	1.05	-20.34	-23.45	0.87	12.39	12.51	0.99	11.82	12.36	0.96
10	262.95	-262.88	286.23	241.55	0.92	-29.12	-27.63	1.05	14.45	13.92	1.04	13.43	12.89	1.04
11	323.12	-323.03	293.84	-277.16	1.10	-26.47	-26.59	1.00	12.47	13.75	0.91	14.00	13.27	1.06
12	398.05	-397.94	371.65	-344.28	1.07	-22.60	-25.83	0.87	14.67	14.61	1.00	12.87	12.17	1.06
13	293.19	-556.95	327.73	-389.24	0.89	-30.57	-28.77	1.06	14.60	14.88	0.98	16.78	13.63	1.23
14	356.70	-445.56	344.57	-373.54	1.04	-28.78	-30.29	0.95	12.08	13.52	0.89	15.63	13.47	1.16
15	423.40	-423.28	413.54	-379.51	1.02	-26.58	-28.42	0.94	12.98	13.24	0.98	20.08	17.57	1.14
16	300.90	-512.39	354.38	-378.27	0.85	-19.36	-20.34	0.95	12.24	13.16	0.93	14.26	12.19	1.17
17	349.52	-902.25	366.07	-443.18	0.95	-12.76	-14.24	0.90	12.50	13.09	0.95	5.49	5.73	0.96
18	471.91	-556.95	475.62	-403.24	0.99	-10.32	-10.04	1.03	12.18	12.66	0.96	4.89	4.55	1.07
19	376.41	-556.95	381.44	-438.51	0.99	-22.15	-19.68	1.13	12.24	12.97	0.94	16.63	13.88	1.20
20	429.12	-662.77	398.73	-442.54	1.08	-14.80	-17.36	0.85	12.18	12.87	0.95	9.26	10.63	0.87
21	572.29	-983.00	525.91	-418.44	1.09	-12.13	-13.48	0.90	12.68	14.01	0.91	8.07	9.35	0.86
22	421.73	-421.61	419.56	-441.83	1.01	-24.35	-21.47	1.13	12.26	13.21	0.93	19.15	16.77	1.14
23	475.93	-1175.16	433.88	-479.56	1.10	-16.21	-17.53	0.92	12.77	14.03	0.91	10.07	9.86	1.02
24	618.91	-1164.02	601.32	-473.51	1.03	-13.32	-15.84	0.84	12.24	13.11	0.93	8.17	9.55	0.86

* Ratio of left experimental maximum acceleration to numerical maximum acceleration values
** Ratio of left experimental displacement to numerical maximum displacement values
*** Ratio of experimental impact load to numerical impact load values
**** Ratio of experimental residual displacement to numerical residual displacement values

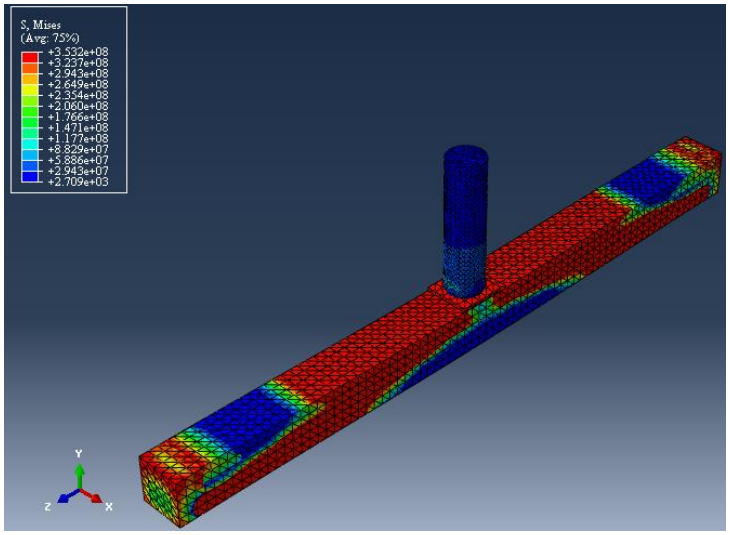

a) Specimen 1

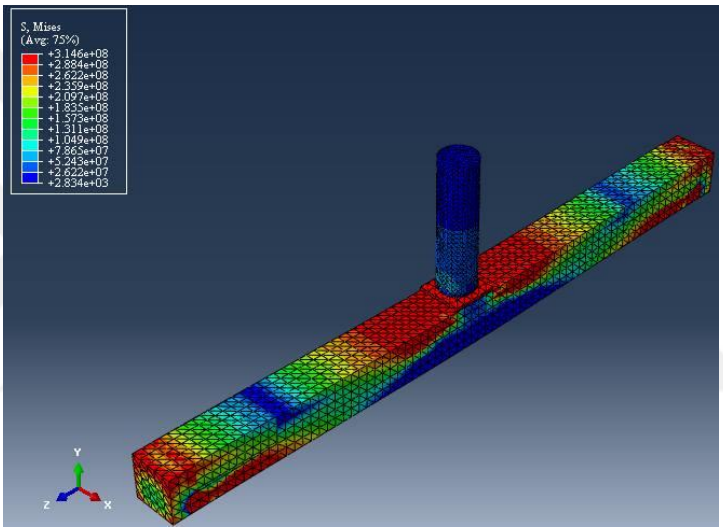

b) Specimen 4

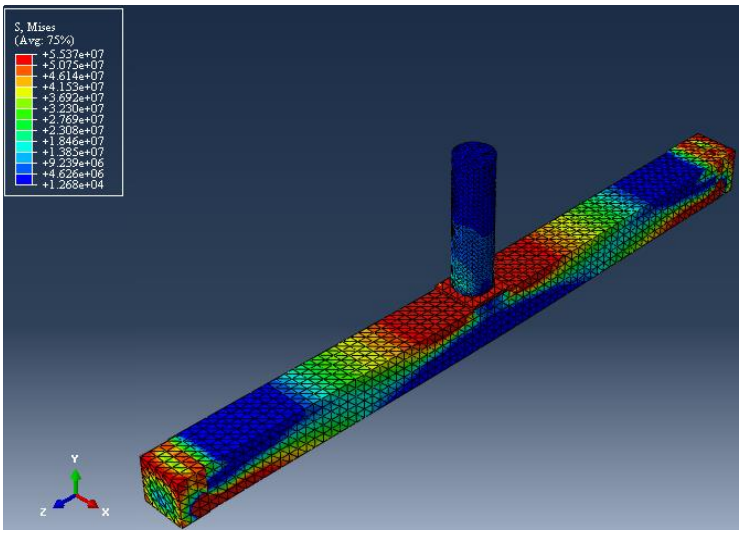

c) Specimen 8

Figure 4.15 Typical stress distributions during impact loading

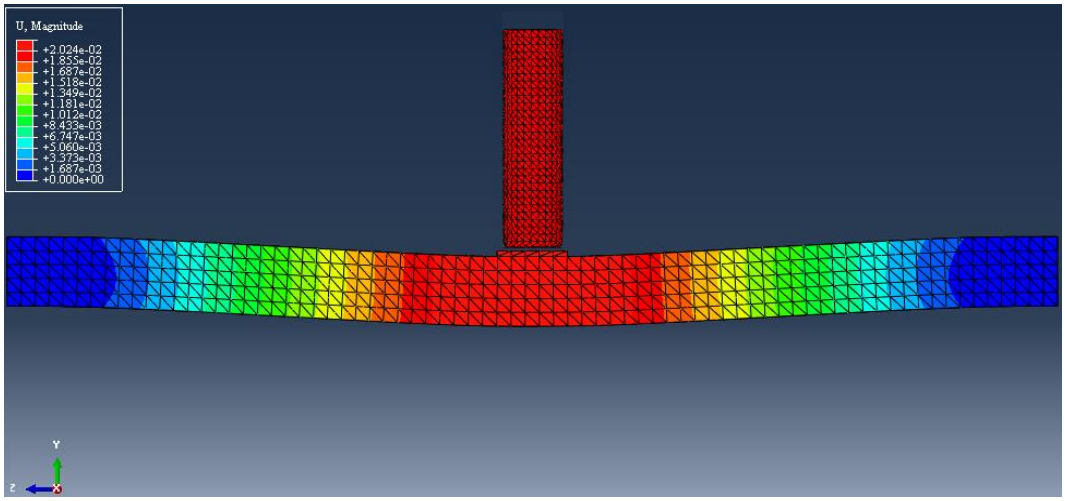

a) Specimen 1

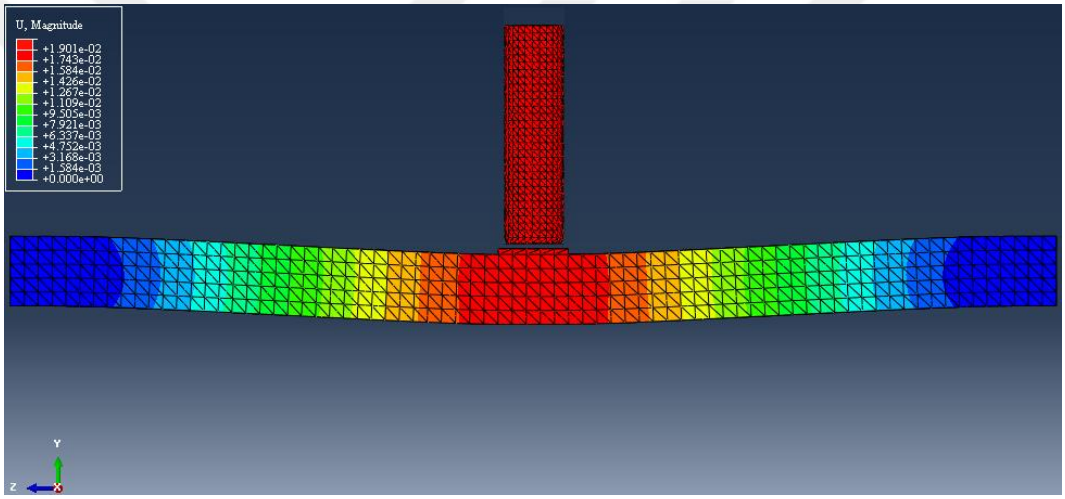

b) Specimen 4

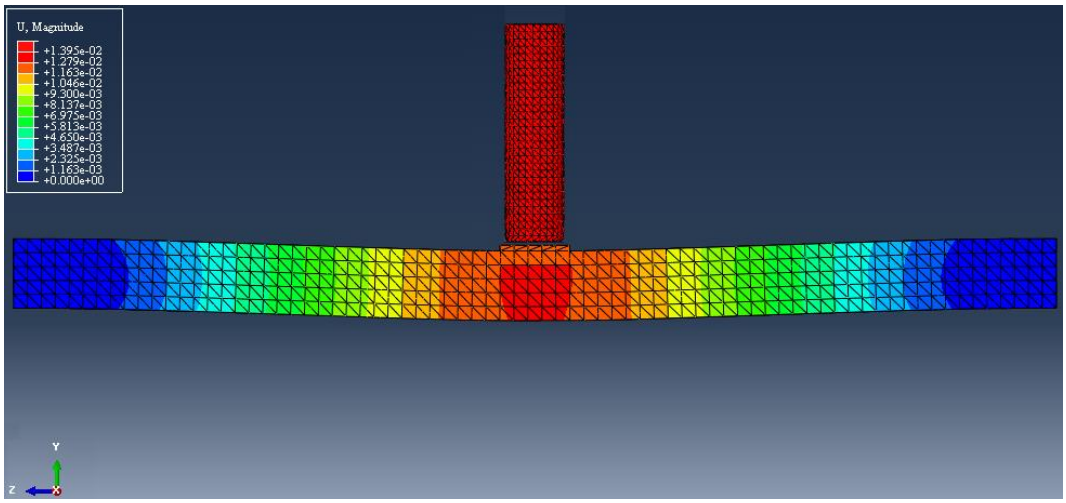

c) Specimen 8

Figure 4.16 Typical deformed shapes during impact loading

4.3 Drying Shrinkage Tests

4.3.1 Free Drying Shrinkage

The experimental program in the current study investigates the effects of three parameters on the free drying shrinkage strain of developed HPFRC mixtures. Figures 4.17 to 4.20 reveal the results of free drying shrinkage strain for the control and fiber reinforced mixtures up to a drying duration of 150 days. Furthermore, the drying shrinkage strain and mass loss of all mixtures at ages 28 days and 150 days are also illustrated in Table 4.5.

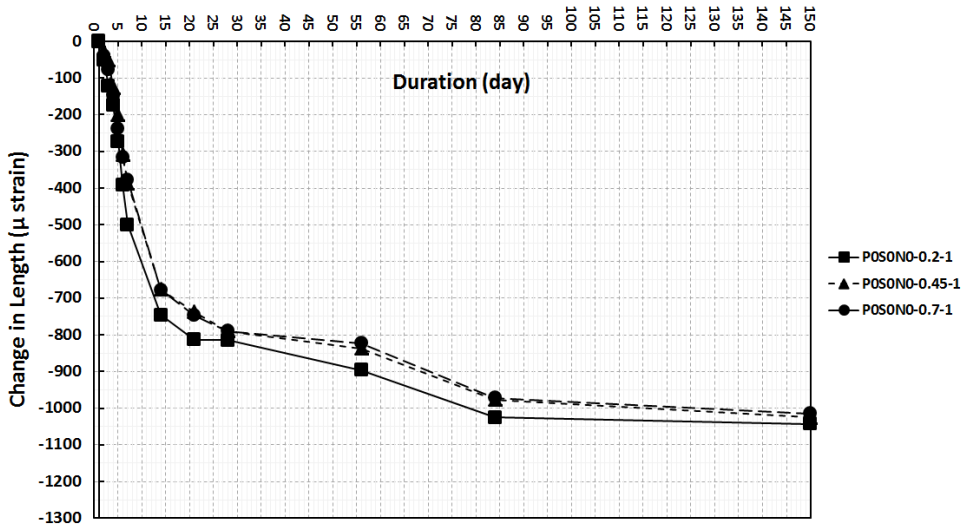

Figure 4.17 Free drying shrinkage strain for control mixtures without fibers

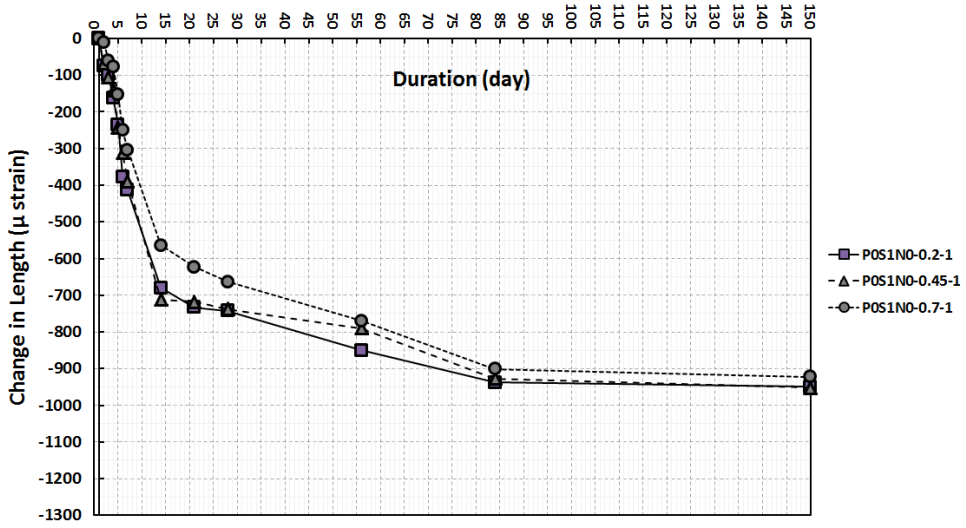

Figure 4.18 Free drying shrinkage strain for mixtures with S fibers

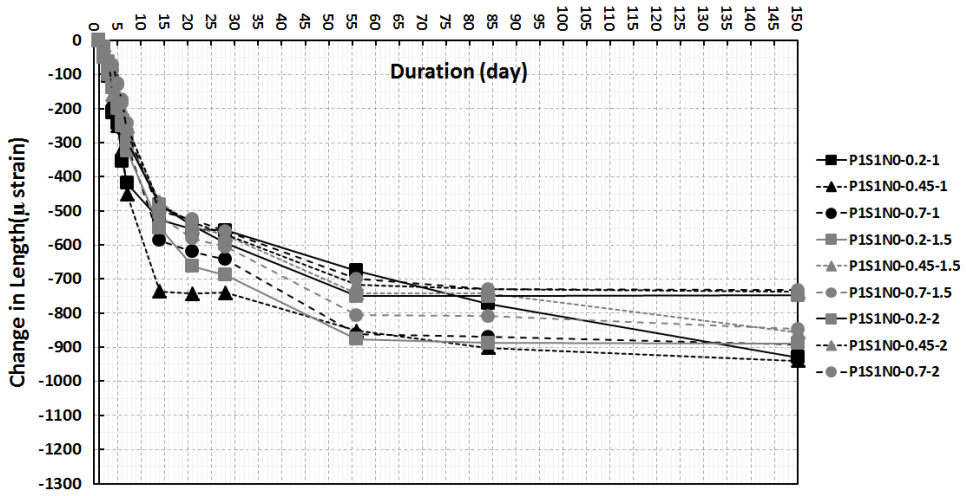

Figure 4.19 Free drying shrinkage strain for mixtures containing P and S fibers

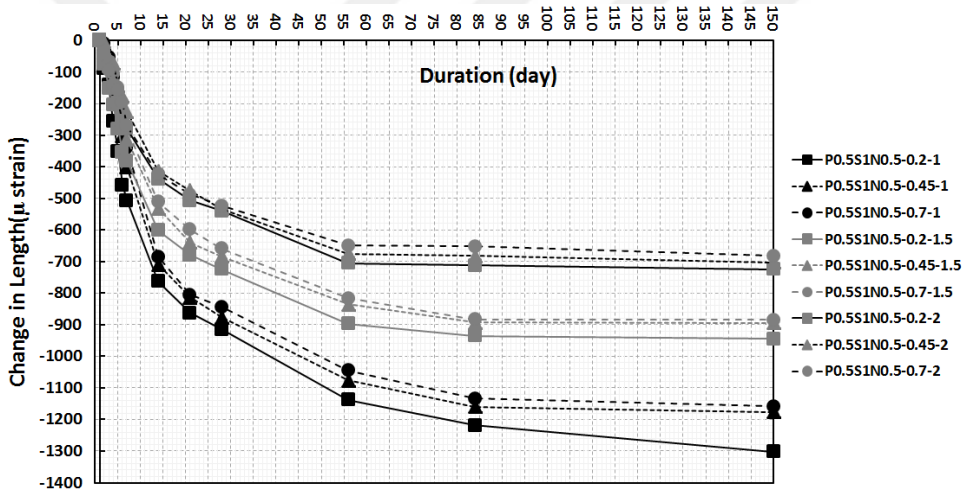

Figure 4. 20 Free drying shrinkage strain for mixtures having P, S, and N fibers

The influence of the inclusion of fibers in the concrete and its effects on the drying shrinkage strain are shown in Figure 4.21. It can be seen that, for an A/B ratio of 1.0, the results of the drying shrinkage strain show a decrease in its values due to addition of single fibers (only S fibers), as presented in mixtures No. 4 to 6, which belong to the mixtures ID of P0S1N0. As a result, the reductions in shrinkage strain were 8.9, 10 and 9.1% for FA/PC ratios of 0.2, 0.45 and 0.7, respectively. This reduction may be ascribed to the fact that, as the matrix shrinks, a shear stress along the fiber and matrix interface would develop, imposing a compressive stress on the reinforcing fibers and a tensile stress on the cement matrix itself (Zhang and Li, 2001). Thus, increasing the elastic modules of fibers is an effective way to compensate for matrix shrinkage in fiber reinforced cementitious composites.

Table 4.5 Free drying shrinkage and mass loss values for all of the produced mixtures

		28 Days		150 Days	
Mix. No.	**Mix ID**	**Change in Length micro strain**	**Change in Mass %**	**Change in Length micro strain**	**Change in Mass %**
1	P0S0N0-0.2-1	-815	-6.41	-1043	-6.42
2	P0S0N0-0.45-1	-790	-7.33	-1025	-7.39
3	P0S0N0-0.7-1	-790	-6.52	-1015	-6.65
4	P0S1N0-0.2-1	-742	-6.09	-950	-6.10
5	P0S1N0-0.45-1	-738	-4.88	-951	-5.00
6	P0S1N0-0.7-1	-663	-7.32	-922	-7.27
7	P1S1N0-0.2-1	-557	-4.54	-940	-4.56
8	P1S1N0-0.45-1	-740	-4.86	-910	-5.05
9	P1S1N0-0.7-1	-642	-6.07	-891	-6.17
10	P1S1N0-0.2-1.5	-688	-3.80	-888	-3.99
11	P1S1N0-0.45-1.5	-572	-5.79	-856	-5.84
12	P1S1N0-0.7-1.5	-605	-6.28	-847	-6.33
13	P1S1N0-0.2-2	-595	-3.89	-747	-3.99
14	P1S1N0-0.45-2	-570	-4.04	-737	-4.17
15	P1S1N0-0.7-2	-560	-4.71	-732	-4.81
16	P0.5S1N0.5-0.2-1	-915	-3.97	-1301	-4.21
17	P0.5S1N0.5-0.45-1	-877	-4.84	-1176	-5.11
18	P0.5S1N0.5-0.7-1	-843	-5.742	-1158	-5.93
19	P0.5S1N0.5-0.2-1.5	-725	-3.58	-945	-3.710
20	P0.5S1N0.5-0.45-1.5	-683	-4.48	-895	-4.55
21	P0.5S1N0.5-0.7-1.5	-530	-6.82	-885	-6.85
22	P0.5S1N0.5-0.2-2	-540	-3.55	-725	-3.67
23	P0.5S1N0.5-0.45-2	-533	-4.09	-703	-4.17
24	P0.5S1N0.5-0.7-2	-523	-4.81	-681	-4.85

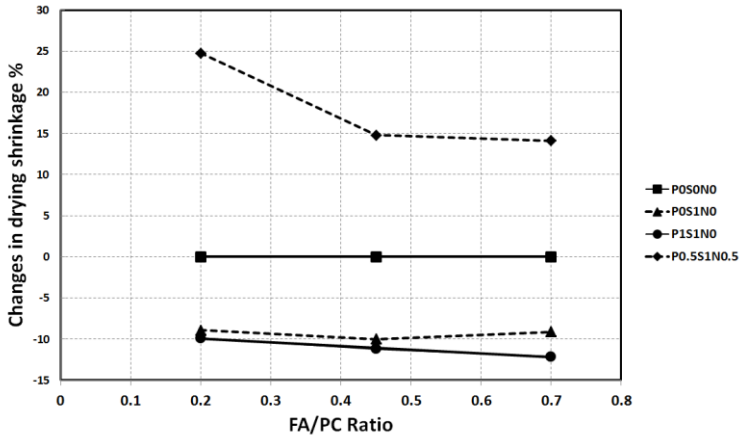

Figure 4. 21 Effect of adding fibers on drying shrinkage strain compared with control mixture at an A/B ratio of 1.0

Furthermore, it can be seen in Table 4.5 and Figure 4.21that the reduction in shrinkage strain slightly increased with the inclusion of S and P fibers into the concrete as shown in mixtures No. 7to 9, which are represented as hybrid fiber mixtures. The mitigations in the obtained shrinkage strain values were 9.9, 11.2 and 12.1% for the same value of fly ash replacements of 0.2, 0.45 and 0.7, respectively. On the other hand, when compared with control mixtures, the results revealed a negative effect when increasing the shrinkage strain as a result of replacing P fibers by 50% N fiber, as shown in 16^{th} to 18^{th} mixtures belonging to mixtures ID P0.5S1N0.5. The values of the increase in the shrinkage strain were 24.7, 14.8 and 14.12% for FA/PC ratios of 0.2, 0.45 and 0.7, respectively. This increase in drying shrinkage strain values is most likely due to the N fiber's surface texture in which the hydrophilic nature of N fibers can absorb water during the fresh state of the concrete and release this absorbed water whenever the concrete hardens (Noushini et al., 2014). To investigate the effect of fiber addition on the shrinkage strain values at a higher A/B ratio, two different values of A/B of 1.5 and 2.0 were evaluated. For example, at an A/B ratio of 1.5, replacing half of the P fiber with N fiber revealed an increment in the shrinkage strain values in comparison to mixtures with only P and S fibers. The increases were 6.38, 4.56, and 4.49% for FA/PC ratios of 0.2, 0.45 and 0.7 respectively. On the other hand, at an A/B ratio of 2.0, an adverse trend was observed such that the shrinkage strain values reduced due to the replacement of the 50% of the P fiber with N fiber. The mitigations were 3.01, 4.63, and 6.93% for the same FA replacement ratios. Thus, the effect of adding N fiber becomes greater by increasing the A/B ratio.

The second parameter that was tested in the present study is the effect of increasing the aggregate content on the shrinkage strain values. The results plotted in Figure 4.22 show the effect of the A/B ratio increment on the shrinkage strain of hybrid fiber reinforced mixtures. For mixtures with P and S fibers (represented in mixtures ID P1S1N0), the results reveled that these mixtures exhibited less shrinkage strain when the A/B ratio was increased from 1.0 to 2.0. As a result, the alleviations in shrinkage were 20.4, 18.9 and 17.8% for FA replacement 0.2, 0.45 and 0.7, respectively. Furthermore, mixtures reinforced with three fibers S, P, and N had further decrement in shrinkage strain values in which the results revealed a clear decrease in shrinkage strain through increasing A/B ratio from 1.0 to 2.0. Therefore, these findings reinforce the fact that increasing the aggregate amount could enhance the concrete performance with regard to the drying shrinkage strain (Almudaiheem and Hansen, 1987).

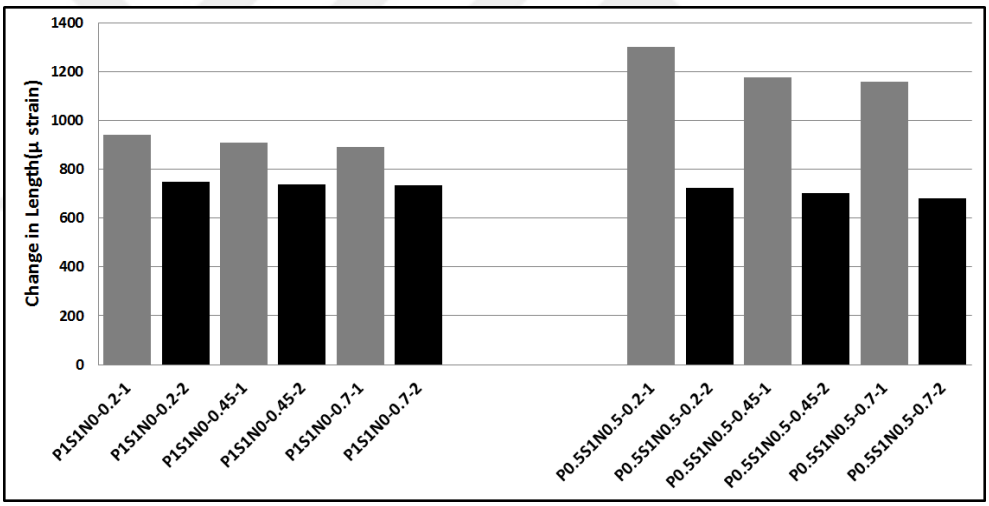

Figure 4.22 Effect of increasing the A/B ratio from 1.0 to 2.0 on the drying shrinkage strain values

The third parameter that was evaluated in this work is the effect of fly ash replacement on the behavior of developed mixtures with regard to the shrinkage strain. As seen in Table 4.5, the results of the control mixtures made without fibers and the mixtures with S fibers show a slight decrease in drying shrinkage strain when FA/PC ratio was increased from 0.2 to 0.7. The alleviations in drying shrinkage strain were 2.7 and 2.9% for the control mixtures and mixtures with S fibers, respectively. This mitigation in shrinkage resulting from an increase of the FA amount may be attributed to the influence of the anhydrated FA particles which act

as aggregates, thereby providing a restraint to shrink the cement paste, and the coarser pore structure, which results in decreased surface tension when a meniscus is formed and, thus lowering the shrinkage forces exerted on the surrounding cement paste (Zhang, 1995; Şahmaran et al., 2007). Moreover, the decrease in the shrinkage strain value, by increasing the FA amount, appears considerably in mixtures with a hybrid fiber system. For instance, the results of the P1S1N0 mixtures revealed a reduction in shrinkage strain due to an increasing FA from 0.2 to 0.7 replacements by weight of cement. As a result, the mitigations were 5.14, 4.65 and 2.0% for A/B ratios of 1.0, 1.5 and 2.0, respectively. Furthermore, the reductions in shrinkage strain values were observed to be higher in P0.5S1N0.5 mixtures, mixtures which were reinforced with three types of fibers. The decrements were 11.0, 6.34 and 5.96% respectively, for the same above A/B ratios.

A total mitigated shrinkage strain value as a result of the inclusion fibers, cement replacement by FA, and increasing A/B ratio from 1.0 to 2.0 ratios were calculated. The shrinkage strain was mitigated by average values of 28.07 and 31.5 % for the P1S1N0 and P0.5S1N0.5 mixtures, respectively. This implies that utilizing N fiber instead of P fiber leads to a greater reduction of the shrinkage strain value. Moreover, N fiber can be replaced with P fiber by up to 50% in order to reduce material costs without compromising any mechanical properties. This conclusion was also in line with the mechanical results regarding compressive and flexural strengths.

As a result of drying, the specimens undergo water loss in addition to the water consumed by hydration. From the data in Table 4.5, the effect of the fibers and the matrix composition (i.e. aggregate and FA) on the final mass loss due to drying can be drawn. It can be seen that the tendency of the concrete to lose more mass was clear with an increase of the FA/PC ratio from 0.2 to 0.7. For example, the mass loss value of the control mixture increased from 6.42 to 6.65% as a result of an increase in the FA amount. In addition, the mass loss of the mixtures that were reinforced with the S fibers increased from 6.1 to 7.2%. Furthermore, hybrid fiber mixtures with two types of fiber (S and P) or three types of fiber (S, P, and N) revealed the same trend to lose mass due to increasing the FA replacement. This may be ascribed to the fact that an increase occurs in the unhydrated water (unconsumed water) with cementitious material. It is well known that FA is a pozzolanic material in which

reacts with hydrated cement products and not with water directly; thus, there is an increase in the amount of unhydrated water. Therefore, the water will be subjected to drying freely. Furthermore, the rate of water loss shows a pronounced increase up to the range of the free shrinkage strain approximately 100-200 µstrain and followed by an increasing rate of water loss that gradually decreases (Figure 4.23). This is most likely due to the sequential removal of the water found in the saturated cements particles (Mehta and Monteiro, 2006).

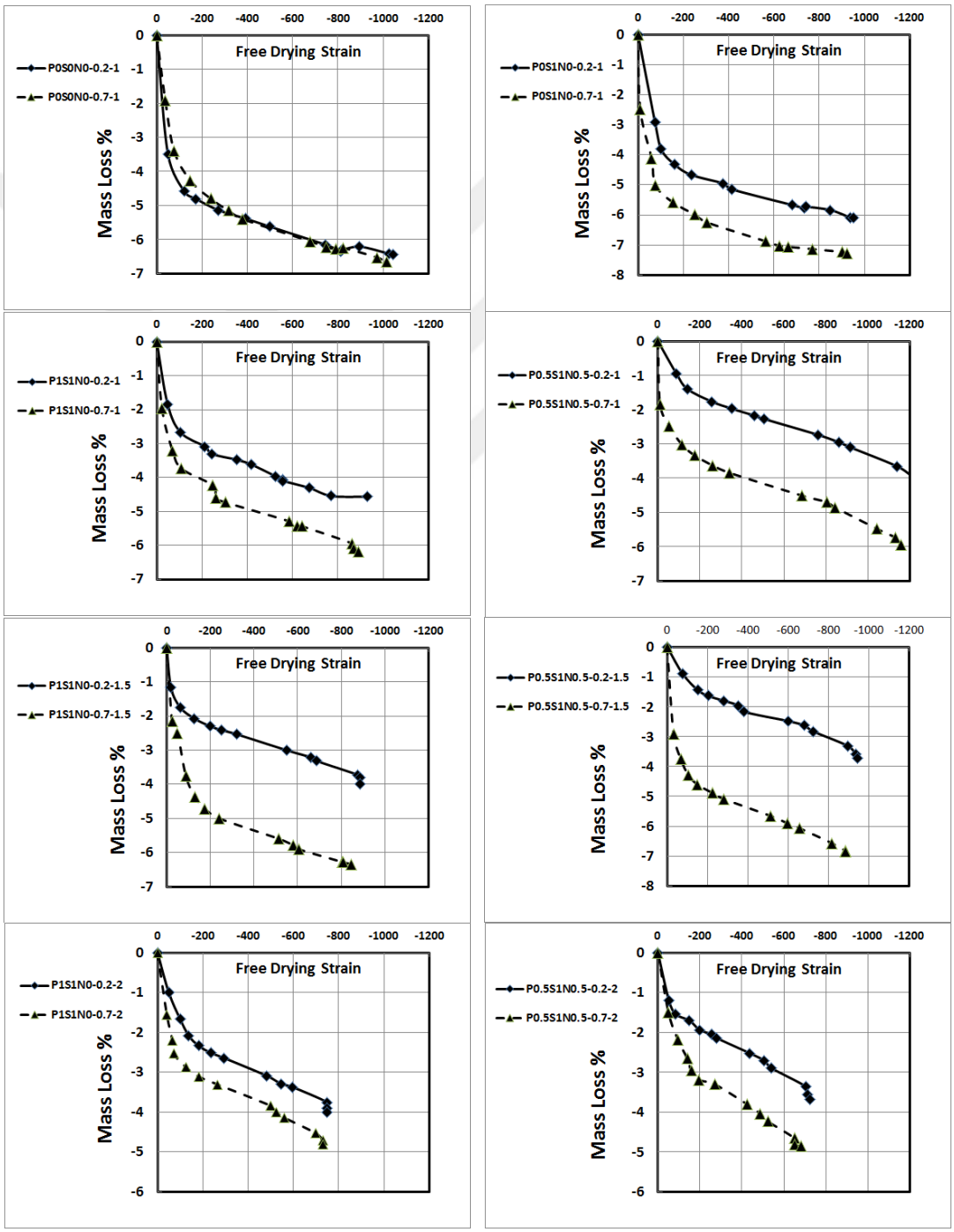

Figure 4.23 Relationship between the free drying strain and the mass loss

The sequence of the water removal in saturated cement particles is such that the free water found in capillary pores would be removed without causing shrinkage as this type of water has no chemical-physical bond with the cement particles. Then, the capillary water found in pores less than 0.05 micrometer and the adsorbed water held with cement particles through hydrogen bonding may be removed; therefore, removal of these kinds of water due to drying would leads to volume changes and shrinkage of the cement.

On the other hand, increasing the aggregate content is an adverse factor leading to decreasing the water loss. For a better visualization of the effect of increasing the A/B ratio on the water loss, Figure 4.24 was drawn for all tested mixtures. The results revealed that an increase in the A/B ratio from 1.0 to 2.0 leads a reduction of the mass loss regardless of the FA replacement or the used fibers.

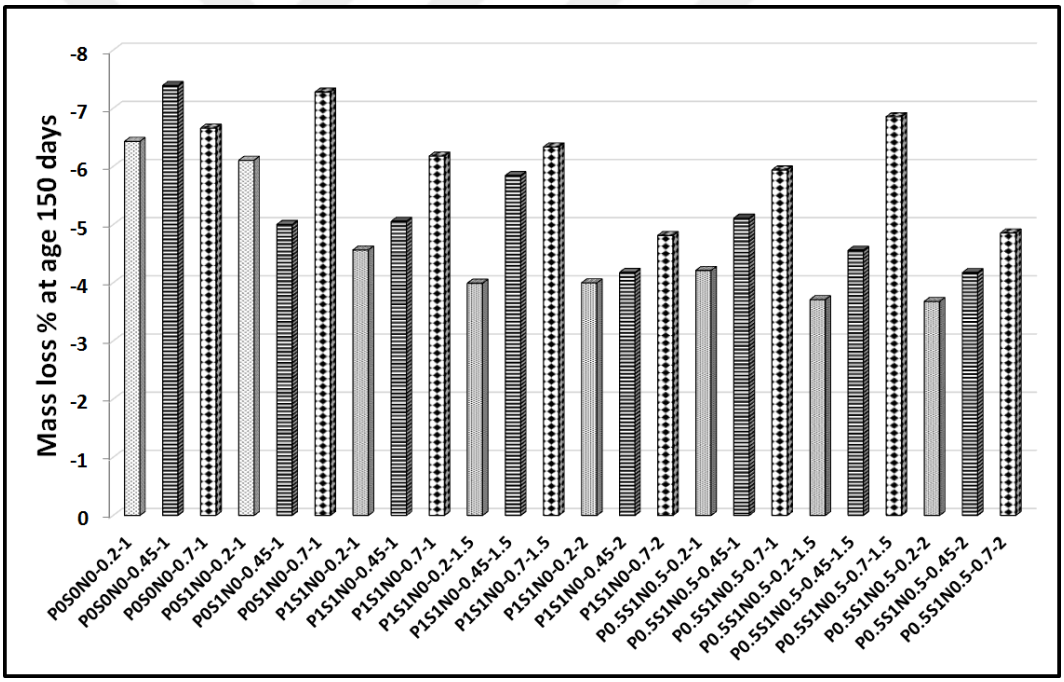

Figure 4.24 Effect of the A/B ratio on mass loss of concrete mixtures

4.3.2 Restrained Drying Shrinkage

In the present study, a restrained shrinkage test is carried out to evaluate three different parameters: fiber type, aggregate amount, and FA replacement ratios on the performances of the developed HPFRC mixtures with regard to cracking resistance and crack width. In this line, the results of the restrained shrinkage of the ring test are

shown in Table 4.6 with a summary of crack width values of the ring specimens tested at age 28 days. In Table 4.6, the shrinkage strain values of the restrained specimens are computed by dividing the total shrinkage values (summation of all crack widths) by the concrete specimen circumference (1052 mm).

4.3.2.1 Total and Maximum Crack Widths

In this study, three variables were studied to evaluate their influences on the cracking resistance for all of the produced HPFRC mixtures. These variables are the effects of the inclusion of fibers into the concrete, the A/B ratio, and the FA replacement ratio.

As can be seen in Table 4.6, reinforcing the fibreless control mixtures revealed a considerable improvement in the reduction of the crack width values resulting from a restrained shrinkage. For mixtures with an A/B ratio of 1.0, the results show significant reductions in both total and maximum crack width values, as recorded for mixtures reinforced with S fibers represented by the ID of the P0S1N0 mixtures. The results of the decrements were 84.6, 85.6 and 79.1% for total crack width and 94.9, 93.3 and 92.7% for the maximum crack width for FA/PC 0.2, 0.45 and 0.7, respectively. Although increasing the fiber reinforcement in concrete mixtures with S and P fibers revealed an improvement in total crack width, it showed that the maximum crack width values did not change or even slightly decreased. The percentage reductions in the total crack width were 91.7, 92.1 and 89.1% for FA/PC 0.2, 0.45 and 0.7, respectively, whilst the percentage rate of reductions in maximum crack widths were 96.6, 96.5 and 94.5% for the same above FA/PC ratios. It appears that replacing half of the volume of the P fiber with N fiber had an adverse effect on reducing the total crack width values. These mixtures are represented in the No. 16^{th} to 18^{th} mixtures with three fibers S, P and N. The reductions in total crack width were 86.9, 86.2 and 84.7%. Regarding the maximum crack width, the decreasing trend in the maximum crack width was dropped slightly; the values were 94.6, 93.9 and 94.5% for the same FA replacements ratios. These findings were also in agreement with results stated in the present study with regard to the free drying shrinkage strain values, the results of which revealed the adverse effect of replacing 50% of the P fibers with N fibers for an A/B ratio of 1.0. Finally, for further clarification, Figure 4.25 shows the average improvements in the reduction of the

total and maximum crack width values for every of fiber reinforced mixture at an A/B ratio of 1.0.

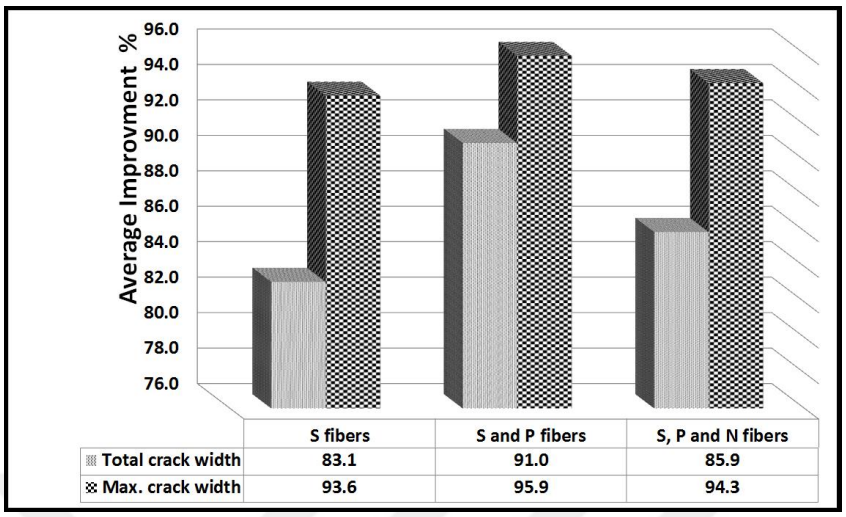

Figure 4.25 Average improvements in total and maximum crack width values at an A/B ratio of 1.0

Obviously, the numbers of cracks increased when the control mixtures were reinforced by fibers. For an A/B ratio of 1.0, the number of cracks increased from 1 crack for control mixtures regardless of the FA/PC ratios to 4, 3 and 3 cracks for concrete with S fibers for FA/PC 0.2, 0.45 and 0.7, respectively. The same trend was observed when increasing the reinforcement of fibers, in which the numbers of cracks increased in the hybrid fiber mixtures containing P and S fibers. The readings were 3, 3 and 2 cracks for the same above FA replacement ratios. Furthermore, it appears that replacing half of the volume of the P fiber with N fiber did not change the number of cracks. It recorded an average reading of 3 cracks.

These behaviors of the reduction in the total and maximum crack widths, in addition to an increase in the numbers of cracks due to the addition of fibers into the concrete may be ascribed to the mechanism of deflection hardening response. In other words, due to the crack bridging by fibers and fiber-pull out resistance, the crack opening width would be limited and other cracks would appear in other places (Li et al., 2008). As mentioned previously in Section 4.1, every concrete mixture that was developed in this study was investigated by applying the four-point bending test; the results were that every mixture behaved as a deflecting-hardening response (Table 4.1); thus, this type of concrete behavior may enhance the increase of the cracking resistance.

Table 4.6 Summary of restrained shrinkage ring test results at age 28 days

Mix. No.	Mixture ID	No. of Cracks	Time to Cracking (days)	Crack Width (micro meter)				Total Crack Width (micro meter)	Max. Crack Width (micro meter)	Total Shrinkage Strain (micro strain)
1	P0S0N0-0.2-1	1	4	3417				3417	3417	3248
2	P0S0N0-0.45-1	1	5	2833				2833	2833	2693
3	P0S0N0-0.7-1	1	6	1833				1833	1833	1743
4	P0S1N0-0.2-1	4	6	175	150	100	100	525	175	499
5	P0S1N0-0.45-1	3	6	191	141	75		407	191	387
6	P0S1N0-0.7-1	3	7	125	133	125		383	133	364
7	P1S1N0-0.2-1	3	7	116	91	75		282	116	268
8	P1S1N0-0.45-1	3	8	75	50	100		225	100	214
9	P1S1N0-0.7-1	2	10	100	100			200	100	190
10	P1S1N0-0.2-1.5	2	8	100	50			150	100	143
11	P1S1N0-0.45-1.5	2	9	75	60			135	75	128
12	P1S1N0-0.7-1.5	2	14	50	50			100	50	95
13	P1S1N0-0.2-2	2	10	86	85			171	86	163
14	P1S1N0-0.45-2	2	11	59	73			132	73	125
15	P1S1N0-0.7-2	2	14	60	60			120	60	114
16	P0.5S1N0.5-0.2-1	3	6	155	186	106		447	186	425
17	P0.5S1N0.5-0.45-1	3	7	173	118	98		390	173	371
18	P0.5S1N0.5-0.7-1	3	9	81	100	100		281	100	267
19	P0.5S1N0.5-0.2-1.5	2	11	221	81			302	221	287
20	P0.5S1N0.5-0.45-1.5	1	15	173				173	173	164
21	P0.5S1N0.5-0.7-1.5	0	30	-	-	-	-	0	0	0
22	P0.5S1N0.5-0.2-2	0	30	-	-	-	-	0	0	0
23	P0.5S1N0.5-0.45-2	0	30	-	-	-	-	0	0	0
24	P0.5S1N0.5-0.7-2	0	30	-	-	-	-	0	0	0

The fibers in the concrete had different mechanisms regarding the reduction of the shrinkage strain when the tested prism is unrestrained or when it is fully or partially restrained. As previously mentioned, the total shrinkage strain values in the restrained shrinkage specimens were measured. The results of the restrained shrinkage values were compared to the results obtained from the free drying shrinkage strain values at 28 days of drying duration. The comparison revealed that, for the same mixtures, the results of the restrained shrinkage test values were lower than the values from the free shrinkage test. For further clarification, Figure 4.26 and Table 4.7 illustrate the differences between the restrained and free shrinkage strain values. This outcome may be attributed to the fact that the fibers are designed to be active in cementitious composites as tension components, more so than in compression usages. In Figure 4.26, the values show that every mixture containing three fibers (S, P, and N), regardless of the A/B and FA replacement ratios, had a higher trend in the differences between the restrained and free shrinkage strain values. These findings encourage the use of N fibers by replacing 50% of the P fibers by volume.

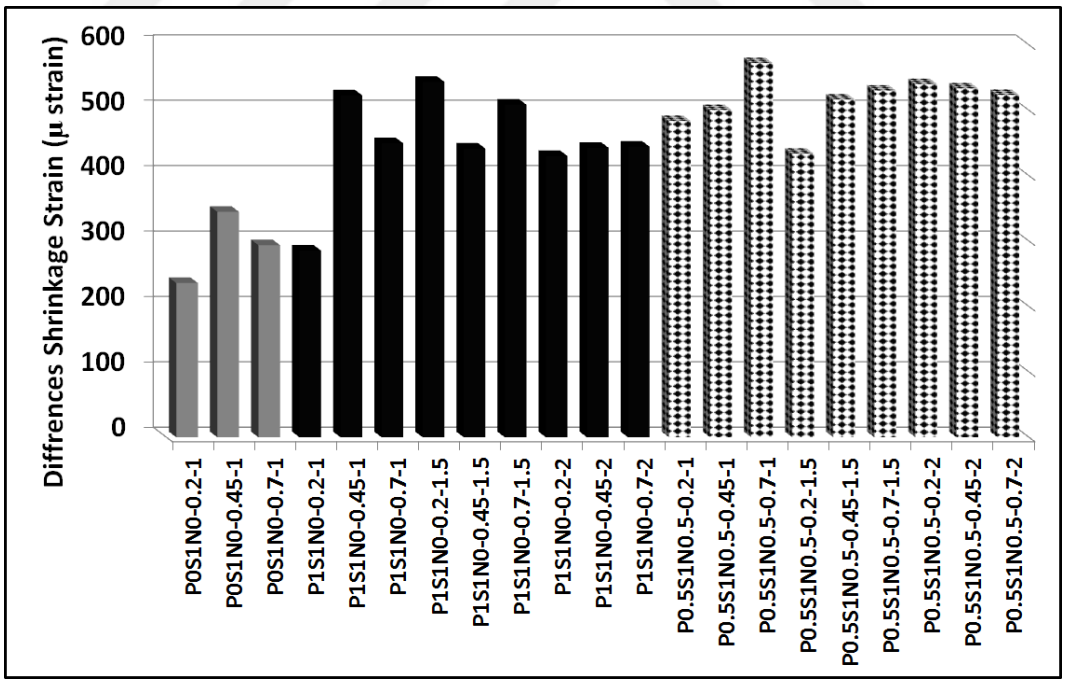

Figure 4.26 Differences of shrinkage strain between restrained and free drying tests

Table 4.7 Differences between free drying shrinkage strain and restrained drying shrinkage at age 28 days for fibered reinforced mixtures

Mix. No. (1)	Mixture ID (2)	Total Restrained Shrinkage Strain (micro strain) (3)	Free drying Shrinkage (micro strain) (4)	(4-3) (micro strain)
1	P0S0N0-0.2-1	3248	815	
2	P0S0N0-0.45-1	2693	790	
3	P0S0N0-0.7-1	1743	790	
4	P0S1N0-0.2-1	499	742	243
5	P0S1N0-0.45-1	387	738	351
6	P0S1N0-0.7-1	364	663	299
7	P1S1N0-0.2-1	268	557	289
8	P1S1N0-0.45-1	214	740	526
9	P1S1N0-0.7-1	190	642	452
10	P1S1N0-0.2-1.5	143	688	546
11	P1S1N0-0.45-1.5	128	572	443
12	P1S1N0-0.7-1.5	95	605	510
13	P1S1N0-0.2-2	163	595	432
14	P1S1N0-0.45-2	125	570	445
15	P1S1N0-0.7-2	114	560	446
16	P0.5S1N0.5-0.2-1	425	915	490
17	P0.5S1N0.5-0.45-1	371	877	506
18	P0.5S1N0.5-0.7-1	267	843	576
19	P0.5S1N0.5-0.2-1.5	287	725	438
20	P0.5S1N0.5-0.45-1.5	164	683	519
21	P0.5S1N0.5-0.7-1.5	0	530	530
22	P0.5S1N0.5-0.2-2	0	540	540
23	P0.5S1N0.5-0.45-2	0	533	533
24	P0.5S1N0.5-0.7-2	0	523	523

The second investigated parameter is the A/B ratio. As mentioned previously, the selected A/B ratios were 1.0, 1.5 and 2.0. Figure 4.27 shows the influence of increasing the A/B ratio from 1.0 to 1.5 and 2.0 by reducing the total and maximum crack width. It can be seen that the drops in the total and maximum crack widths were appreciably higher in the concrete reinforced with a hybrid fiber system,

especially so with concrete mixtures with three types of fiber, namely P, S and N. As can be seen in Figure 4.27, the reduction reached 100%, particularly with mixtures reinforced with S, P and N fibers for an A/B ratio of 2.0. This implies that, no cracks appeared. In other words, the effectiveness of using N fibers by replacing with 50% of the P fibers in addition to increasing the aggregate content was clearly better. This may be attributed to the fiber rigidity wherein the less rigid fibers (therefore with more flexibility) can easily bend-around the aggregates for greater alignment in order to arrest or bridge any cracks. It is notable that the fibers used in this study are S fiber (with high rigidity), P fiber (semi rigid) and N fiber (flexible). Replacing a part of the P fiber with N fiber (50% by volume) may reduce the effect of increasing the aggregate amount on the fiber orientation. Thus, a decrease in the negative aggregate influence may lead to an increase in the fibers effectiveness, thereby limiting the crack width by means of fiber bridging.

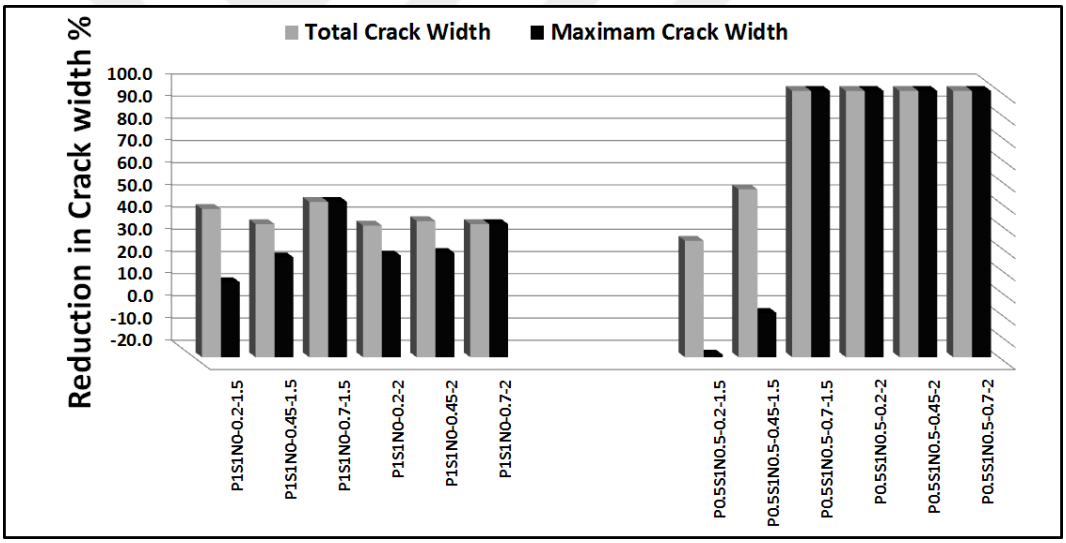

Figure 4.27 The effect of increasing the A/B ratio on the total and maximum crack width for fibre reinforced mixtures

The third variable of the experimental program with regard to the total and maximum crack widths was the FA replacement ratios. The effect of increasing the FA/PC ratio from 0.2 to 0.7 presented a positive impact with respect to the reduction in the total and maximum crack widths. For an A/B ratio of 1.0, the total crack width was minimized from 3417 to 1833 μm for the control concrete due to increasing the FA replacement ratio from 0.2 to 0.7. The same trend was observed for mixtures reinforced with S fibers, in which the reductions in the total and maximum crack widths as a result of increasing the FA/PC ratio from 0.2 to 0.7 were 525 to 383 μm

and 175 to 133 μm, respectively. To evaluate the increase of the FA replacement ratio from 0.2 to 0.7 in hybrid fiber reinforced mixtures, mixtures having two and three fibers were evaluated. The drops in maximum crack width with regard to hybrid fiber mixtures with (P and S fibers) were 116 to 100 μm, 100 to 50 μm and 86 to 60 μm for A/B ratios of 1.0, 1.5 and 2.0, respectively. Furthermore, for mixtures containing three types of fiber, marked improvements in minimizing the crack width were evident by increasing the FA content, as shown in Table 4.6. The value of the maximum crack width dropped due to increasing the FA replacement ratio from 0.2 to 0.7, in which the values become 100 μm instead of 186 μm for an A/B ratio of 1.0, and no cracks appeared when the FA/PC ratio was increased to 0.7 for an A/B ratio of 1.5. In addition, no cracks occurred in any of the mixtures at an A/B ratio of 2.0, regardless of the FA/PC ratios.

The strong cracking resistance that is shown in the mixtures with S, P and N fibers at an A/B ratio of 2.0 may be ascribed to the increase in the amount of micro-fibers. The diameter of the N fiber is less than the diameter of the P fiber (Table 3.2); thus, it has more micro properties thereby increasing the cracking resistance and reducing crack width (Qi et al., 2003; Passuello et al., 2009).

The combined effect of the inclusion of fibers in concrete, the increase of the FA replacement, and an increase of the A/B ratio on reducing the total and maximum crack widths of the produced HPFRC mixtures are presented in Figure 4.28. The average reductions were 92 and 96.3% for the total and maximum crack widths, respectively. This improvement enhanced the average maximum crack width of fibreless concrete mixtures through the reduction in crack width from 2694 to 100 μm for reinforced fiber mixtures. Thus, some of the concrete mixtures behave as crack-free concrete. For fiber reinforced mixtures, Figure 4.28 shows a better visualization of the total and maximum crack widths recorded for control mixtures without fibers and mixtures having different types of fiber.

Moreover, the correlations between the maximum crack width with free and restrained shrinkage strain values at an age of 28 days were measured, as shown in Figures 4.29 and 4.30, respectively. These figures show correlation coefficients R^2 equal to 0.5735 and 0.7701 for free and restrained shrinkage, respectively.

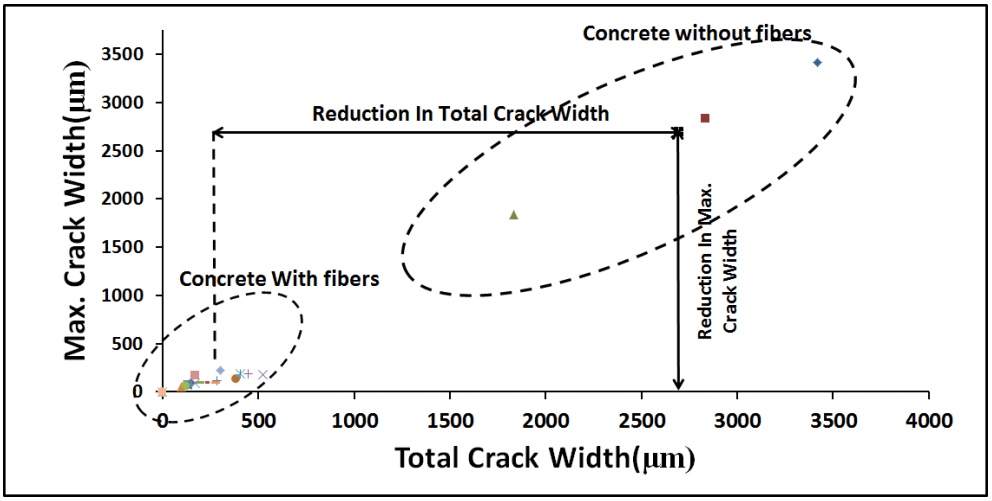

Figure 4.28 Maximum crack widths for fiber reinforced mixtures

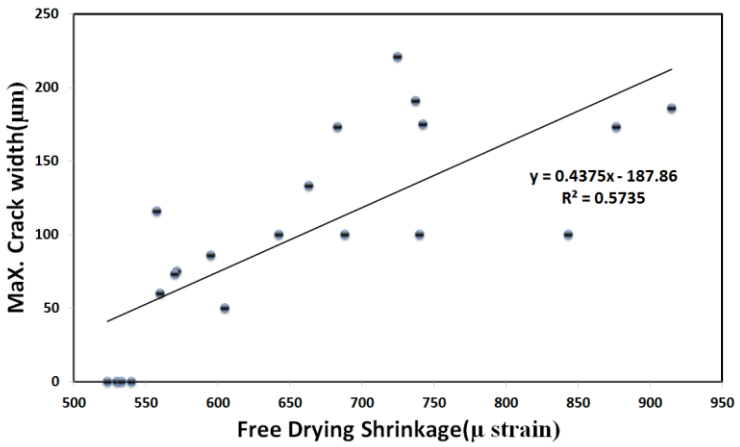

Figure 4.29 Relationship of the free drying shrinkage strain and the maximum crack width for fiber reinforced mixtures

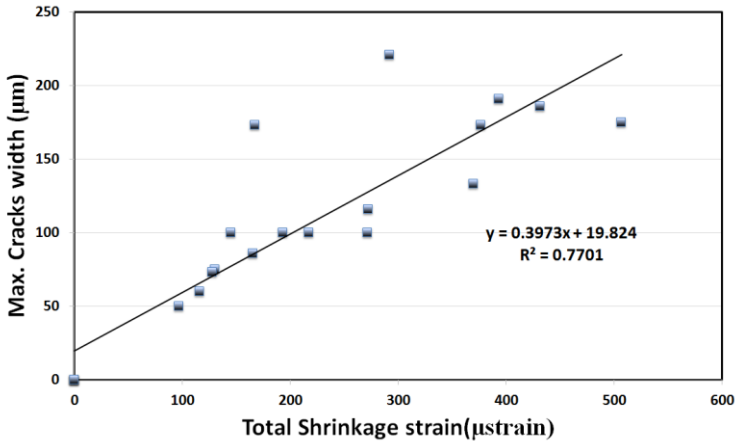

Figure 4.30 Relationship of the restrained drying shrinkage strain and the maximum crack width for fiber reinforced mixtures

4.3.2.2 Cracking Resistance and Cracking Potential Classification

A restrained ring test may provide a comprehensive estimation of the cracking potential of concrete materials. ASTM-C1581/C1581M (2009) and Attiogbe et al. (2004) classified the cracking potential of concrete depending either on the stress rate at the time to cracking or on the time to cracking individually. In the present study, the cracking potential was calculated based on time to cracking. Time to cracking is the difference between the age at cracking and the age at which drying is initiated. It can be used to assess the relative cracking performance of specimens that were cracked during the test.

For an A/B ratio of 1.0, the average time to cracking for the control concrete mixture without fibers was 5 days. Reinforcing the concrete mixtures with S fibers showed a slight improvement in terms of increasing the time to cracking. This improvement was an average value of 6.33 days. The cracking resistance increased when more fibers were added in the concrete mixtures. As shown in Table 4.6, when the mixtures were reinforced with S and P fibers, the time to cracking increased to 8.33 days. As expected, and depending on the results obtained from the free and restrained shrinkage strain values, replacing 50% of the P fiber with N fiber leads to decreasing the time to cracking, thus increasing the cracking potential value for mixtures with an A/B ratio of 1.0.

Another parameter studied herein that may be effective on the cracking resistance is the A/B ratio. In general, as the A/B ratio increases, the cracking potential decreases. For example, the time to cracking for mixtures reinforced with S and P fibers were improved when the A/B ratio increased. This improvement clearly increased with increasing FA/PC ratios. As shown in Table 4.6, the results revealed that by increasing the A/B ratio to 1.5, the time to cracking value increased to 8, 9 and 14 days for FA replacement ratios of 0.2, 0.45, and 0.7, respectively. For the same mixture reinforced with (S and P fibers), the time to cracking slightly increased by increasing the A/B ratio to 2.0. These values were 10, 11 and 14 days for the same above FA/PC ratios. Furthermore, a further improvement when increasing the time to cracking appeared in mixtures containing three types of fiber, namely S, P, and N. This implies that by replacing 50% of the P fiber with N fiber, the produced HPFRC mixtures were guaranteed to be completely without cracks, particularly with an A/B

ratio of 2.0. The results revealed that no cracks appeared even when the drying time exceeded 30 days. These findings are consistent with most previous studies, including Şahmaran et al. (2012). They indicate that the first crack is significantly delayed when using FA and increasing the aggregate content.

Figure 4.31 illustrates and further clarifies the cracking potential for all of mixtures based on (ASTM-C1581/C1581M, 2009; Attiogbe et al., 2004) classifications. The results indicated that mixtures without fibers presented in mixtures ID P0S0N0, and mixtures that are reinforced with S fibers can be classified as high potential cracking mixtures. Conversely, mixtures reinforced with S, P and N fibers, particularly at an A/B ratio of 2.0 can be classified as low cracking potential. This improved performance may be ascribed to the N fibers having a micro property related to their diameter. Therefore, increasing the micro fiber content shows an improvement in concrete cracking resistance (Qi et al., 2003; Passuello et al., 2009). And as stated previously, the utilization of N fibers as a replacement of up to 50% of the P fiber shows better performance in terms of cracking potential.

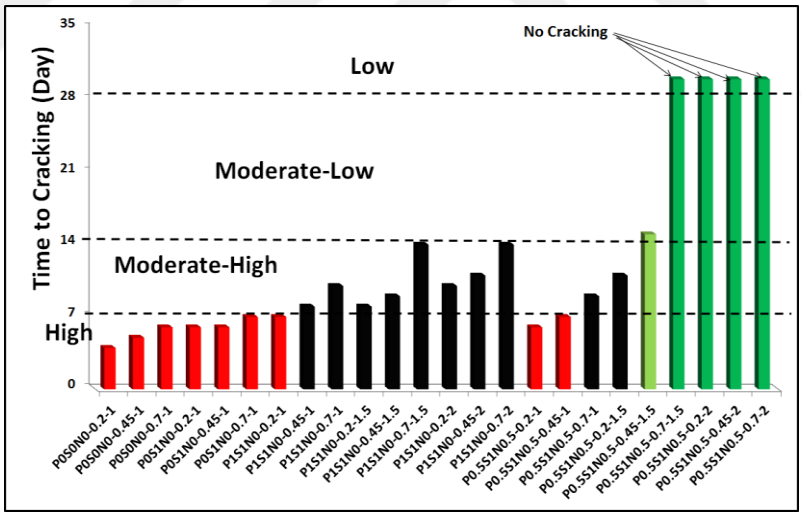

Figure 4.31 Cracking potential classification based on time to cracking

4.4 Slab Panel Test Results

As mentioned earlier, most of the structural applications such as bridge decks, slabs and mines lining have mostly behaved as biaxial condition which it could be investigated under plate tests (Preteseille et al., 2014). In this regard, the measured flexural strength should be justified from uniaxial to biaxial stress condition. In this aspect, the load–deflection curves of square panel specimens were measured for all

of the developed HPFRC mixtures, with and without fibers. Typical load-deflection curves are shown in Figures 4.32 to 4.34. According to the data in these figures, the energy absorption values (EA) were calculated by integrating the area under the load-deflection curves. In addition to the EA, First load (FL), Ultimate load (UL) and deflections corresponding to these loads were also measured, as presented in Table 4.8. The FL refers to the load capacity of the concrete at the first crack that happens during the loading. Furthermore, the EA values of the fiber reinforced mixtures were calculated at different deflection levels of 2.5, 5, 7.5, and 10 mm, as shown in Table 4.9. For making a correlation between the flexural strength obtaining from beam specimen and the flexural strength of the slab panel specimen, the values of UL obtaining from panel test were transformed by using a certain formula to get on their corresponding strength values.

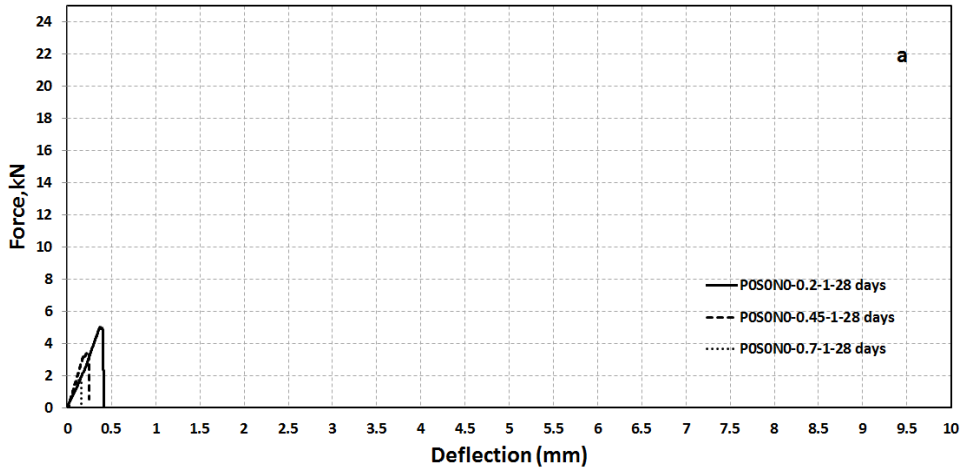

a) Mixtures without fibers

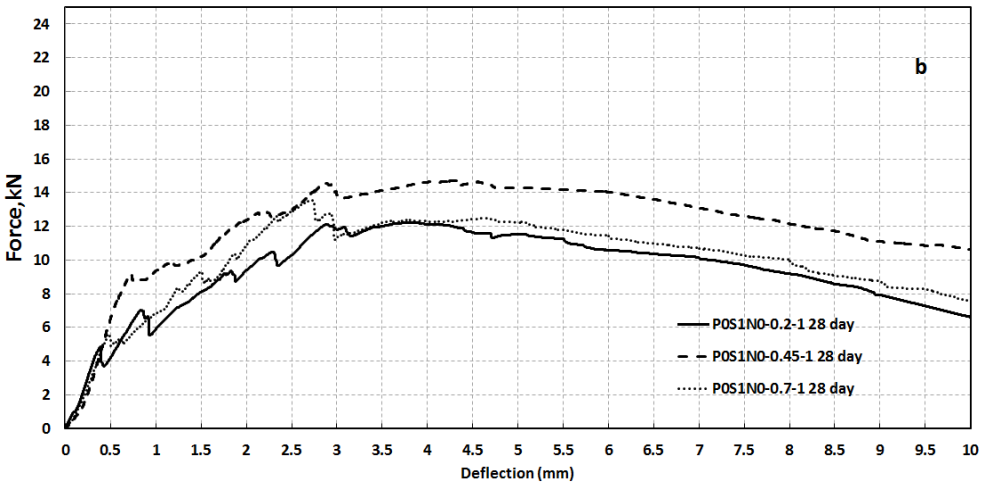

b) Mixtures with S fibers

Figure 4.32 Load-deflection curve of panel test

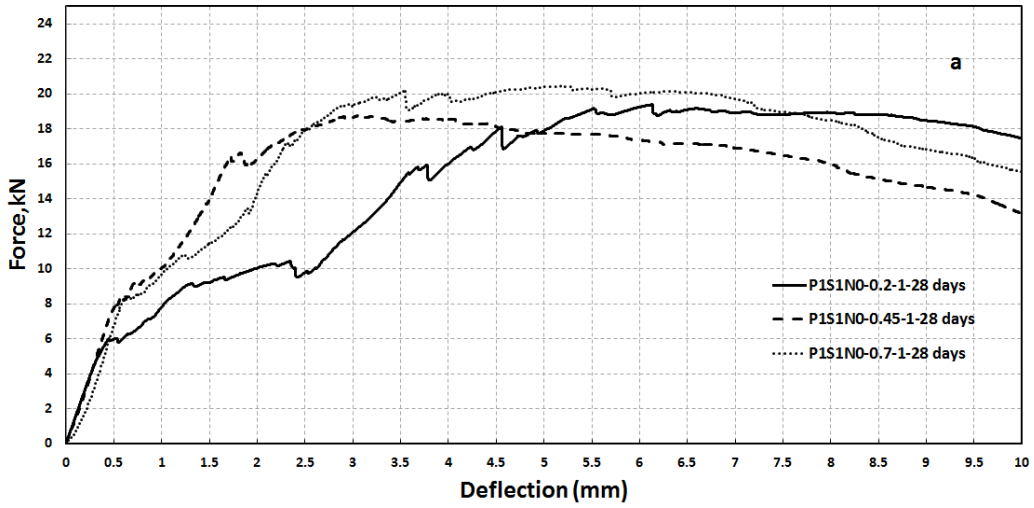

a) A/B=1.0

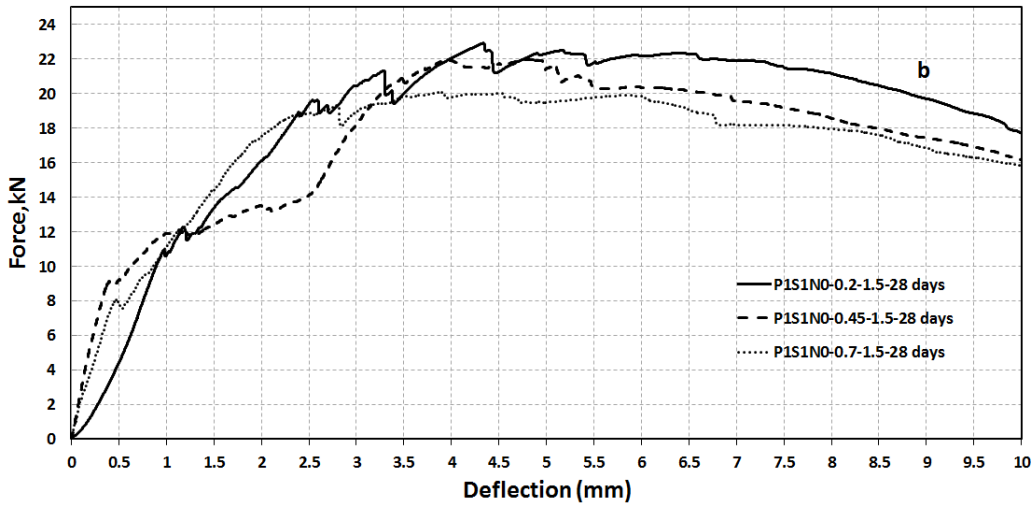

b) A/B=1.5

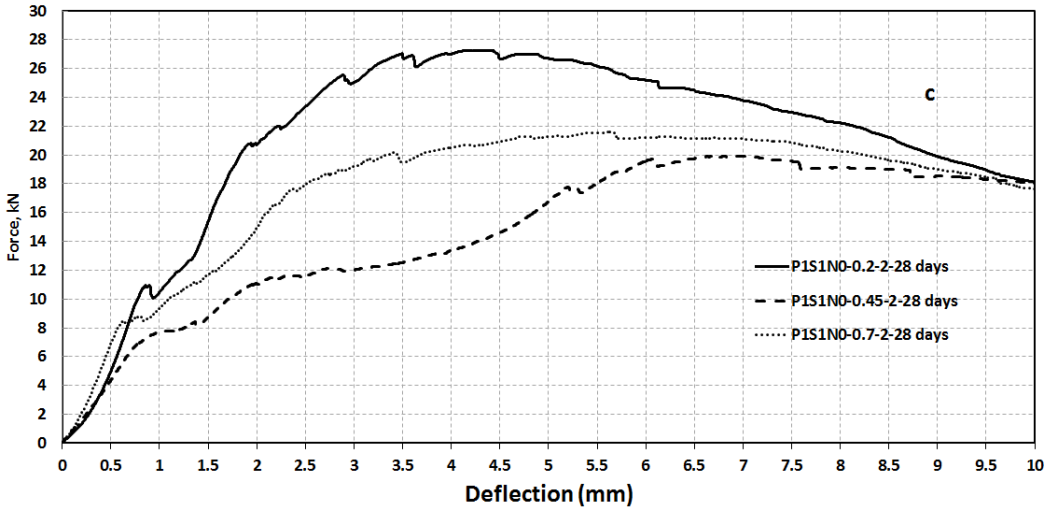

c) A/B=2.0

Figure 4.33 Load-deflection curve of panel test for mixtures having P and S fibers

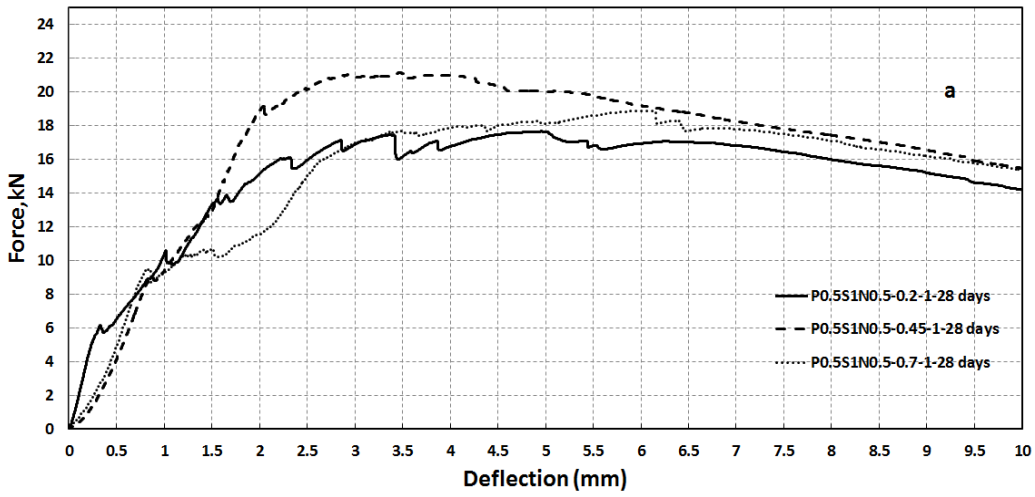

a) A/B=1.0

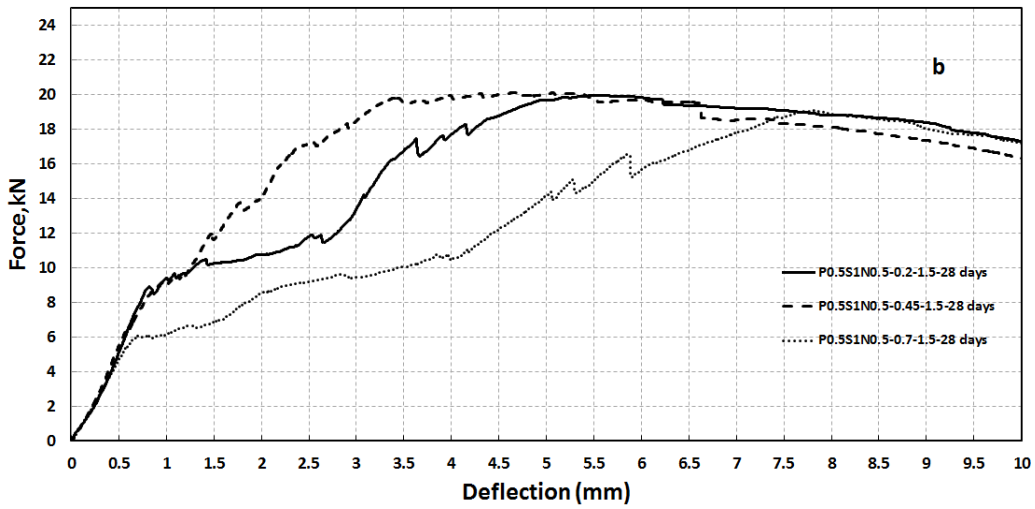

b) A/B=1.5

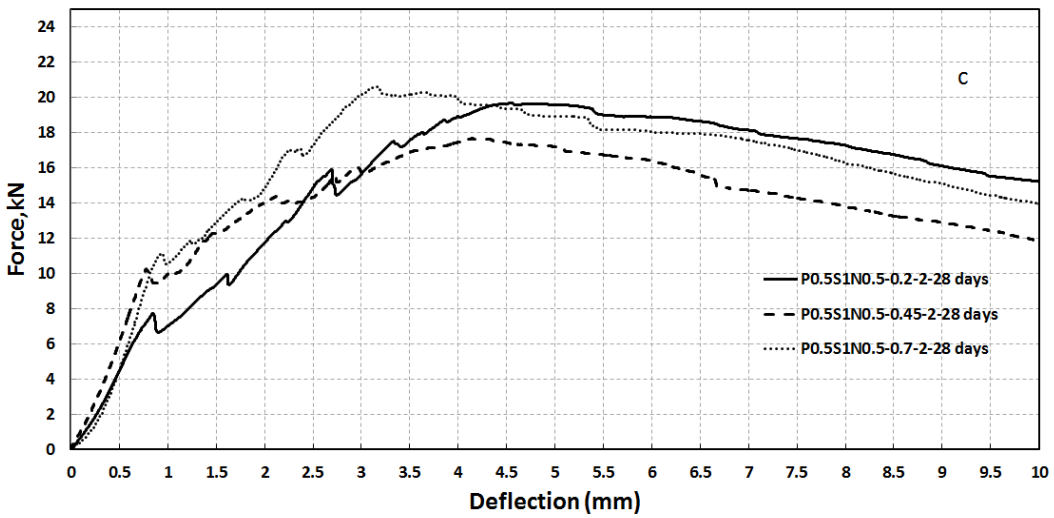

c) A/B=2.0

Figure 4.34 Load-deflection curve of panel test for mixtures having P, S and N fibers

4.4.1 First and Ultimate Loads

As explained previously, the main purpose of the present study is to develop HPFRC mixtures with deflecting-hardening response. After adoption of certain mixtures, evaluating of the performances of the produced mixtures with regard to the different properties of the concrete was performed. Toward achieving this goal, the experimental program investigates the effects of three variable parameters on the behavior of the HPFRC slab panel specimen under bending.

The first investigated parameter is the effect of the inclusion of fiber in the concrete. As can be seen in Table 4.8, at an A/B ratio of 1.0, the UL of the control mixtures are 5, 3.5 and 2.0 kN for FA/PC ratios of 0.2, 0.45 and 0.7, respectively. The inclusion of fibers into the concrete has significant effects by enhancing the strength of the concrete in terms of the ultimate load. The results revealed that reinforcing the fibreless mixtures with S fiber, as presented in the mixtures 4 to 6 showed an increase in the UL values. The incremental trend increases when the FA replacement ratio increases. The percentages of the increase were 1.44 %, 3.2% and 5.74% for FA/PC ratios of 0.2, 0.45, and 0.7, respectively. Moreover, an increase in the volume of fibers by adding the P fibers in addition to the S fibers into the concrete leading to improve this increasing trend. The improvement of the UL values when inclusion of two fibers S and P were 2.86, 4.33 and 9.21% for the same above FA/PC ratios. However, replacing about 50% P fiber with N fiber did not show significant changes in increasing the ultimate load as shown in the 16^{th} to 18^{th} mixtures. The percentages of the increase were 2.52, 2.99 and 8.42% for the same FA/PC ratios. To investigate the effect of the adding fibers on the UL values at a higher level of A/B ratio, two different values of A/B ratios of 1.5 and 2.0 were evaluated. For example, at an A/B ratio of 1.5, replacing half of the P fiber with N fiber revealed a decrement in the UL values as comparing to the mixtures containing only P and S fibers. The rates of decrease were 12.45, 8.61, and 4.64% for FA/PC ratios 0.2, 0.45, and 0.7 respectively. Similarly, this decreasing trend is valid for an A/B ratio of 2.0. The percentages of the decrease were 29.03, 10.96, and 4.50% for the same FA replacement ratios.

The second parameter is the A/B ratio. The three selected A/B ratios were 1.0, 1.5, and 2.0. As can be shown in Table 4.8, when the A/B ratio was increased from 1.0 to

2.0, the UL values increase. However, the increasing trend of UL values showed a decrease in their values when the FA replacement ratios increases. For example, when the A/B ratio was increased to 2.0, the increment percentages in the UL values of the mixtures reinforced with the S and P fibers were 41.19 and 5.48% for FA/PC 0.2 and 0.7, respectively. Furthermore, regarding with the mixtures containing three fibers S, P, and N, the trend in increase of the UL values was presented due to increasing the A/B ratios. As a result of increasing the A/B ratio to 2.0, the increasing rates in the UL values were 9.88 and 9.12% for the same above FA replacement ratios.

The third variable parameter is increasing the FA replacement ratio. As can be seen in Table 4.8, at an A/B ratio of 1.0 and as a result of an increase of the FA/PC ratio, there were both increments and decrements in the values of UL. For instance, the UL values of the control mixtures decreased when the FA/PC ratio was increased from 0.2 to 0.7. The decrement percentage was 60%, as shown in the mixture No. 4. In contrast, the UL values were increased by 10.5% when the FA/PC ratio was increased from 0.2 to 0.7 for the mixtures containing S fibers. Furthermore, the trend of increment is valid for the mixtures with S and P fibers. The increase in the UL as a result of increasing the FA content was 5.8%. Also, it appears that when replacing 50% of the P fiber with N fiber, the trend continues increasing due to increase the FA content with the rate of 7.1%. Moreover, at a higher level of A/B ratio, the change in UL value are different, regarding with the mixtures with a hybrid fiber system. For example, at an A/B ratio of 2.0 and as a result of increasing the FA/PC ratio from 0.2 to 0.7, the UL value decreased 20.9% in the mixtures containing the S and P fibers, while the UL value increased in the mixtures reinforced with three type of fiber, namely S, P, and N. The increase in the UL value was 6.35%.

Regarding the FL values, the effect of increasing FA/PC ratios was taken into consideration as an affective factor. In general, the results of the slab panel test values revealed an incremental trend in the FL values for all of the fiber reinforced concrete mixtures. On the other hand, increasing FA led to drop in the FL values with the mixtures without fiber. For further clarification, Figure 4.35 illustrates the effect of increasing the FA replacement ratios on the FL values. It seems that addition of the Class-F fly ash particles improved the workability of the mixtures

thereby more uniformly distributing of the individual fibers is created as a result of spherical surface characteristics of the FA particles.

Furthermore, as a result of increasing the aggregate amount, the trend of the change in FL value is similar to the trend of UL values. As can be seen in Table 4.8, as a result of increasing the A/B ratio from 1.0 to 2.0 and for the mixtures with S and P fibers, although there was an evident improvement in increasing the FL value reached 83.3% at FA/PC ratio 0.2, the FL value did not change at FA/PC ratio of 0.7. Regarding the hybrid fiber mixtures, the mixtures reinforced with S, P, and N fibers had improvements in FL in both FA/PC ratios. The percentages of the increase were 33.33 and 15.78% for FA replacement ratios of 0.2 and 0.7 respectively.

Table 4.8 Summary of Load-deflection data under panel test

	First crack parameters		Ultimate parameters		
Mixture ID	**Load , kN**	**Deflection (mm)**	**Load , kN**	**Deflection (mm)**	**UL/FL***
P0S0N0-0.2-1	5.0	0.40	5.00	0.40	1.00
P0S0N0-0.45-1	3.5	0.25	3.50	0.25	1.00
P0S0N0-0.7-1	2.0	0.15	2.00	0.15	1.00
P0S1N0-0.2-1	5.0	0.40	12.20	3.75	2.44
P0S1N0-0.45-1	9.0	0.70	14.70	4.40	1.63
P0S1N0-0.7-1	5.5	0.45	13.49	2.70	2.45
P1S1N0-0.2-1	6.0	0.40	19.30	6.10	3.21
P1S1N0-0.45-1	8.0	0.50	18.68	3.10	2.33
P1S1N0-0.7-1	8.5	0.60	20.42	5.50	2.40
P1S1N0-0.2-1.5	11.0	1.00	22.90	4.30	2.08
P1S1N0-0.45-1.5	9.0	0.40	21.94	4.70	2.43
P1S1N0-0.7-1.5	8.0	0.45	19.82	5.60	2.47
P1S1N0-0.2-2	11.0	0.8	27.25	4.40	2.47
P1S1N0-0.45-2	7.0	1.00	19.80	7.00	2.82
P1S1N0-0.7-2	8.5	0.60	21.54	5.60	2.53
P0.5S1N0.5-0.2-1	6.0	0.30	17.60	3.40	2.93
P0.5S1N0.5-0.45-1	9.0	0.80	20.99	4.00	2.33
P0.5S1N0.5-0.7-1	9.5	0.70	18.85	6.15	1.98
P0.5S1N0.5-0.2-1.5	9.0	0.70	20.05	5.40	2.22
P0.5S1N0.5-0.45-1.5	9.0	0.90	20.05	5.40	2.22
P0.5S1N0.5-0.7-1.5	6.0	0.70	18.90	7.60	3.15
P0.5S1N0.5-0.2-2	8.0	0.80	19.34	4.50	2.41
P0.5S1N0.5-0.45-2	10.0	0.75	17.63	4.20	1.76
P0.5S1N0.5-0.7-2	11.0	0.90	20.57	3.20	1.87

*** > 1 deflection-hardening response**

In order to evaluate the performance of the developed mixture with regard to the deflection-hardening responses, the ratios of the ultimate load to the first load values (UL/FL) were calculated, as shown in Table 4.8. This ratio is an indicator to the performance of the mixture as stiff material. As UL/FL value increases, the hardening behavior index increases. As evident in Table 4.8, every developed mixture has an UL/FL ratio greater than 1.0. This implies that the behavior of every mixture exhibits as a deflection-hardening response.

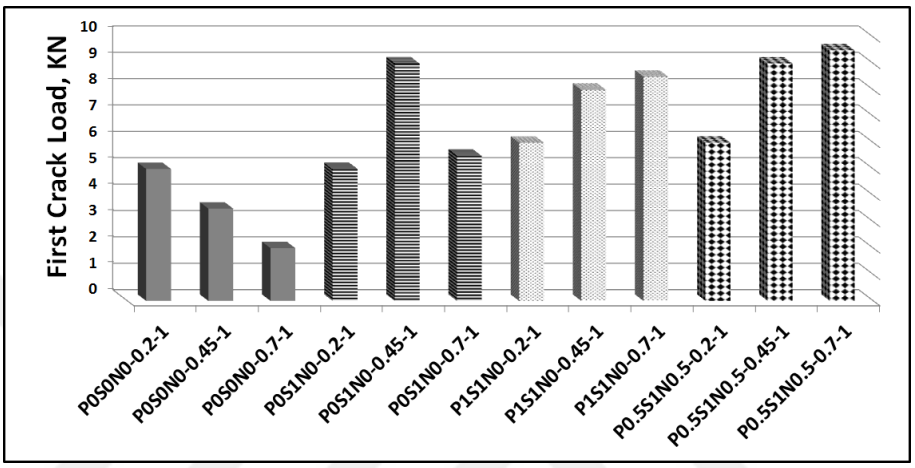

Figure 4.35 The effect of increasing the FA ratio on the first crack load for an A/B ratio of 1.0

4.4.2 Energy Absorption

In this study, three variables were studied to evaluate their effects on the EA values for all of the HPFRC mixtures produced in the present study. These variables are; effect of inclusion of the fiber in the concrete, increasing the A/B ratio, and effect of the FA replacement ratio.

The first variable is the type of fiber reinforcement. As can be seen in Figure 4.36 and Table 4.9, the results revealed that inclusion of the fiber in the concrete had an appreciable effect through an increase in the toughness of the evaluated mixtures. For example, addition of the S fibers with only 1% by volume in the fibreless mixtures led to increase the EA values to 93.67, 120.9, and 100.1 joule for FA/PC ratios of 0.2, 0.45, and 0.7, respectively. Furthermore, adding more fibers into the concrete show a higher improvement in the EA values, as shown in the mixtures containing S and P fibers. The EA values were 149.98, 155.28, and 167.64 joule for the same FA replacement ratios. On the other hand, replacement 50% of the P fiber with N fiber

appeared a different trend, in which there are no variations in EA at FA/PC ratio of 0.2 while the EA values increased by 8.8% at FA/PC ratio of 0.45, and at FA/PC ratio of 0.7 there is a drop in the EA values reached 9.2%.

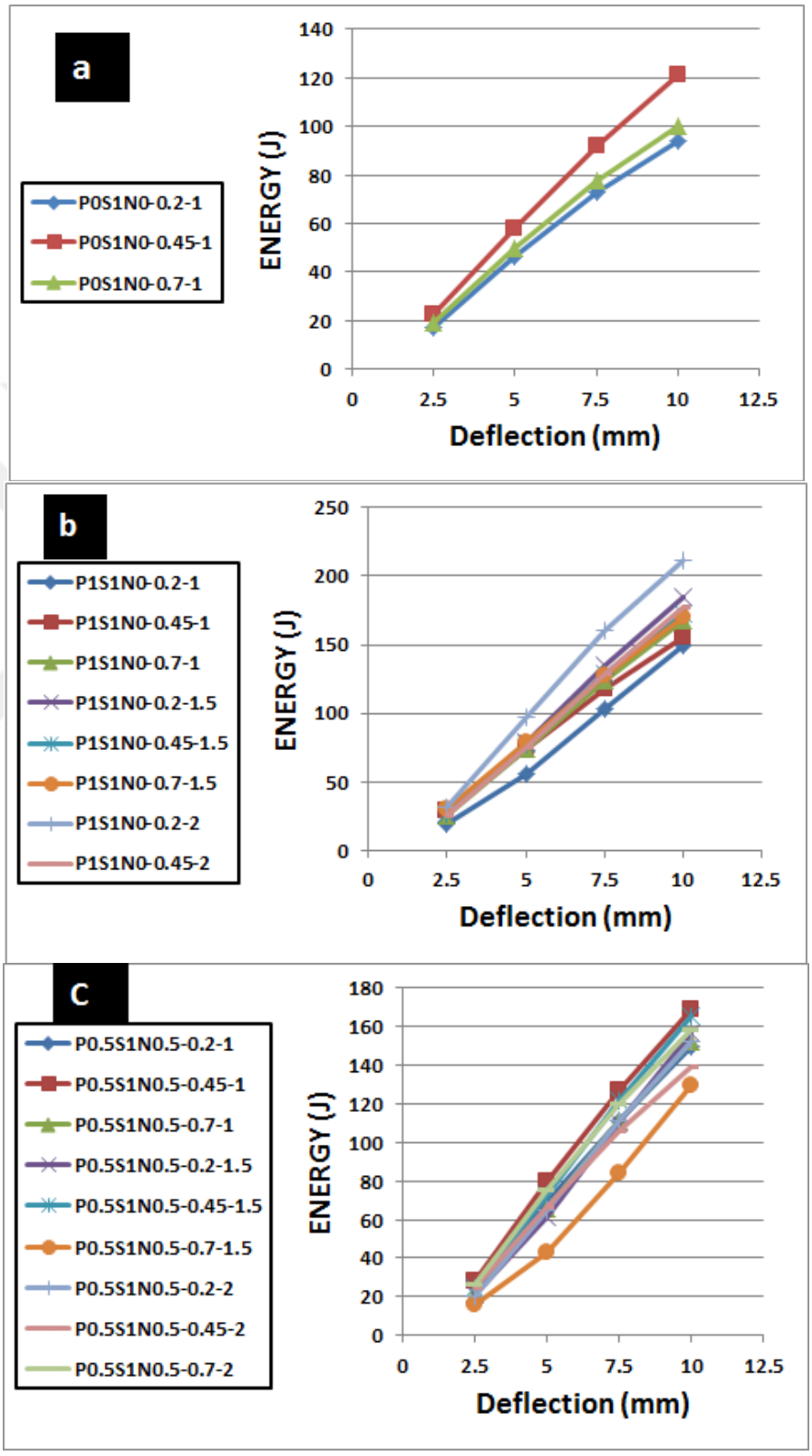

Figure 4.36 Energy absorption of the fiber reinforced mixtures at different deflection a) S fibers b) P and S fibers c) P, S and N fibers mixtures

Table 4.9 Energy absorption (J) corresponding to different deflection

	Deflection (mm)			
MIX. ID	**2.5**	**5**	**7.5**	**10**
P0S0N0-0.2-1	0	0	0	0
P0S0N0-0.45-1	0	0	0	0
P0S0N0-0.7-1	0	0	0	0
P0S1N0-0.2-1	17.26	46.67	73.08	93.67
P0S1N0-0.45-1	22.49	58.07	92.25	120.97
P0S1N0-0.7-1	19.01	49.80	77.81	100.17
P1S1N0-0.2-1	19.37	56.48	103.73	149.98
P1S1N0-0.45-1	28.91	74.74	117.88	155.28
P1S1N0-0.7-1	25.48	74.58	124.44	167.64
P1S1N0-0.2-1.5	27.09	79.76	134.92	184.82
P1S1N0-0.45-1.5	27.58	77.96	128.42	172.68
P1S1N0-0.7-1.5	30.58	79.41	127.20	170.02
P1S1N0-0.2-2	32.08	97.91	160.10	211.47
P1S1N0-0.45-2	19.09	52.46	100.20	146.98
P1S1N0-0.7-2	25.97	76.15	129.19	177.49
P0.5S1N0.5-0.2-1	26.75	69.29	111.54	149.95
P0.5S1N0.5-0.45-1	27.97	79.67	127.11	168.91
P0.5S1N0.5-0.7-1	22.11	65.73	111.19	152.22
P0.5S1N0.5-0.2-1.5	20.77	61.79	110.65	156.57
P0.5S1N0.5-0.45-1.5	24.80	73.12	121.40	165.11
P0.5S1N0.5-0.7-1.5	15.60	42.61	83.70	129.36
P0.5S1N0.5-0.2-2	20.08	64.71	111.38	152.43
P0.5S1N0.5-0.45-2	25.00	66.78	106.30	139.04
P0.5S1N0.5-0.7-2	26.18	75.13	120.09	158.57

The second investigated parameter is the FA replacement ratios. The results showed that the effect of increasing the FA amount on the EA values is affected by the amount of aggregate content. For further clarification, Figure 4.37 illustrates the effect of increasing the FA on the EA values. The values in this figure show a difference in the EA values when the FA was increased from 0.2 to 0.7. The results

revealed that increasing the FA content has a positive effect at low level of an A/B ratio of 1.0 whilst it has an adverse role at a higher level of aggregate amount as shown in A/B ratios of 1.5 and 2.0. However, there is an increase in the EA value for the mixtures reinforced with three fibers S, P, and N at an A/B of 2.0.

As can be seen in Table 4.9, the hybrid fiber reinforced mixtures showed that increasing the A/B ratio led to increase the energy absorption. At the same time, the EA decreased with increasing FA content. For example, the mixtures containing P and S fibers with FA/PC ratio of 0.2 showed that the EA increased 23.23% and 41.00% when the A/B was increased to 1.5 and 2, respectively. The increase in the value of EA reduced to 1.49% and 5.8% when FA/PC ratio was increased to 0.7. In case of the mixtures with three fibers (P, S and N), the EA values are less than the values of the mixtures with two fibers (P and S). As a result, at FA/PC ratio of 0.2, the EA increased by 4.41% and 1.65 when the A/B was increased to 1.5 and 2, respectively.

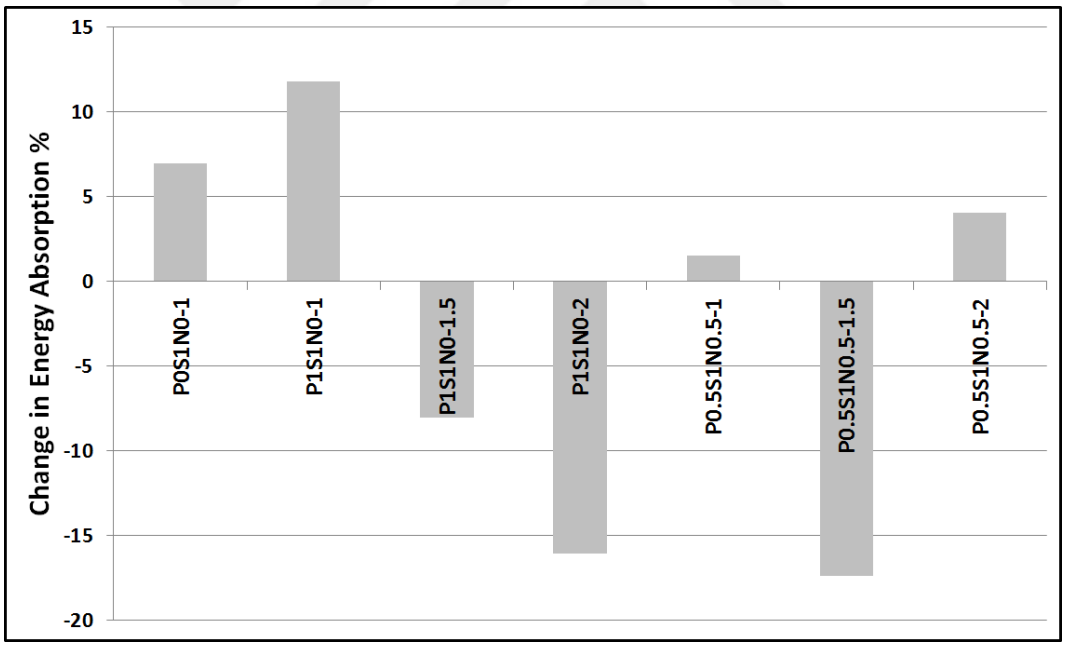

Figure 4.37 Effect of increasing the FA ratio from 0.2 to 0.7 on the energy absorption value

4.4.3 Cracking Pattern

Due to the continuous support of the panel specimen with frame base, there are no predictable failure lines showing cracks. The number of cracks and their locations depend on the mixtures properties. In fact, the cracks generally propagate at the

weakest path. There are two commonly failure patterns in the bending square panel specimen: upper bound and conservative (Uotinen, 2011). The upper bound crack pattern does not consider as a fan mechanism at the panel corners and it has no possibility to uplift the corners. On the other hand, the second type of crack pattern happens due to the possibility of uplifting the panel corners of the square specimens. In this study, with loading process, the contacted area of the panel specimen which is supported on the steel frame decreased and, closed toward the mid of the panel edges. In addition, the panel corners continue uplifting simultaneously, as illustrated in Figure 4.38. This mechanism can be described such that at the beginning of loading, multi cracks start appearing with uniformly radial form and then, with increasing the loads, these cracks will be limited toward the mid edges of the panel as a result of decreasing the contacted area.

Figure 4.38 a) Panel under test b) Zoom in at uplift coroner

For further clarification, Figure 4.39 shows the cracks pattern of the every tested mixture. The results appeared that most the panel's specimens cracked with main of 5-8 localized cracks accompanying with multi-micro cracks. Besides that, the cracking pattern of every tested specimen was tacked place with regard to the second form of failure (conservative) as mentioned above. The cracks appeared by radial cracks that starting from the corner to the mid edge of panel specimens. This pattern of cracks may be attributed to the deflection-hardening behavior of the developed mixtures which may cause a fan mechanism that result in losing the contact area when the applied load was increased thereby developing new cracked surfaces (multi cracks).

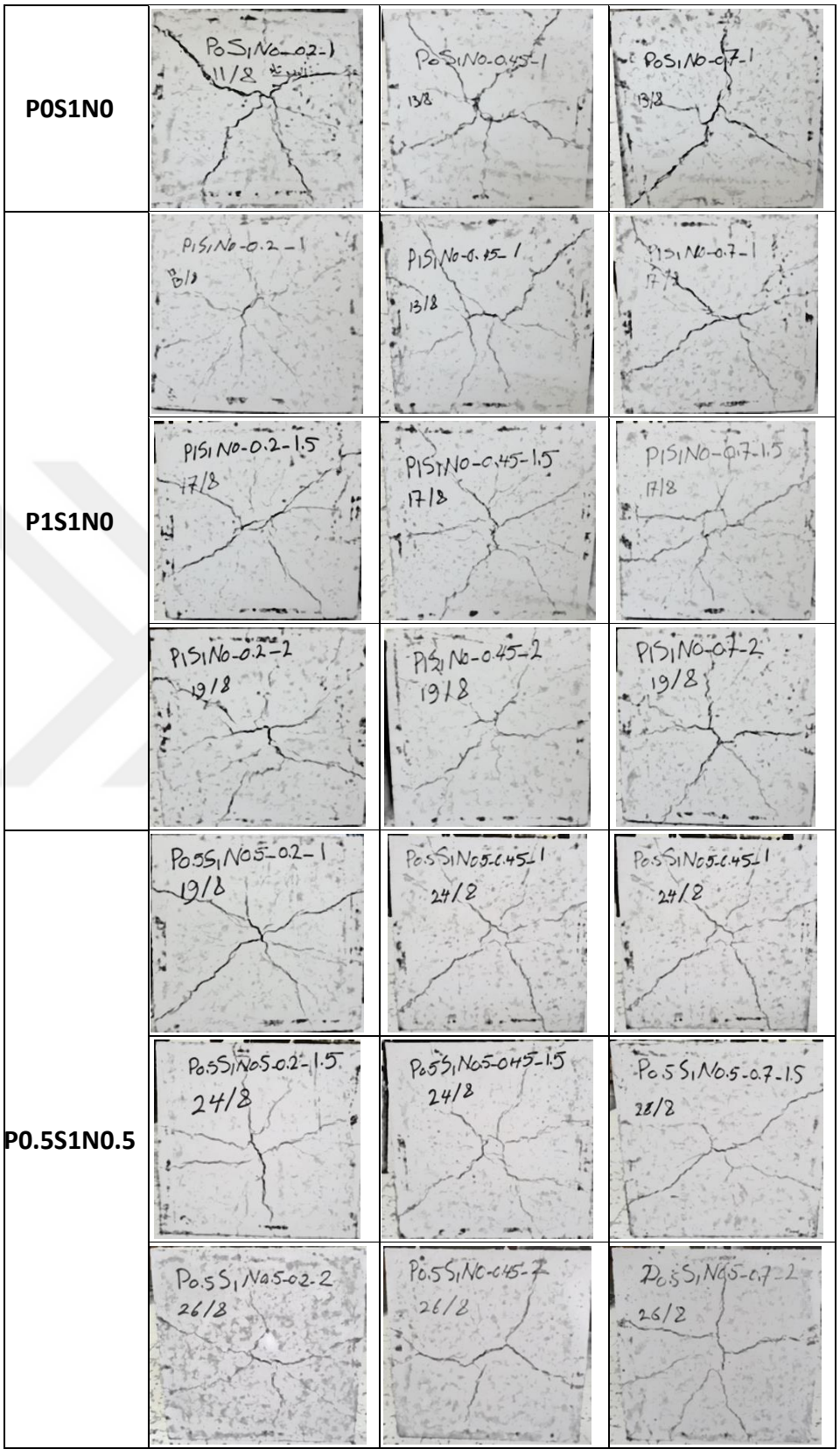

Figure 4.39 Cracks patterns of fiber reinforced mixtures after testing

4.4.4 Flexural Strength of the Panel Test

In this study, flexural strength under biaxial condition represented by the panel test was calculated depending on yield-line theory. The yield line theory is commonly used method to determine the capacity of the reinforced concrete panels (Holmgren, 1993). Depending on this theory, the ultimate load which is recorded from the load-deflection curve was transformed to the flexural strength by using the below Equation (Uotinen, 2011). All results of the flexural strength of the developed mixtures are shown in Table 4.10.

$$\sigma = 0.75\frac{UL}{h^2} \tag{4.1}$$

where, σ is the flexural tensile strength (MPa),
UL is the ultimate load recorded (N), and
h is the thickness of panel (mm)

Table 4.10 Flexural strength under Beam and panel tests at age 28 days

Mixture ID	Flexural strength (MPa) Panel test	Flexural strength (MPa) Beam test
P0S0N0-0.2-1	1.50	3.20
P0S0N0-0.45-1	1.05	3.50
P0S0N0-0.7-1	0.60	3.00
P0S1N0-0.2-1	3.66	6.00
P0S1N0-0.45-1	4.41	5.48
P0S1N0-0.7-1	4.047	4.68
P1S1N0-0.2-1	5.79	5.88
P1S1N0-0.45-1	5.60	7.95
P1S1N0-0.7-1	6.12	7.58
P1S1N0-0.2-1.5	6.87	8.83
P1S1N0-0.45-1.5	6.58	8.03
P1S1N0-0.7-1.5	5.94	8.40
P1S1N0-0.2-2	8.17	7.05
P1S1N0-0.45-2	5.94	8.55
P1S1N0-0.7-2	6.462	7.48
P0.5S1N0.5-0.2-1	5.28	6.27
P0.5S1N0.5-0.45-1	6.29	7.20
P0.5S1N0.5-0.7-1	5.65	6.60
P0.5S1N0.5-0.2-1.5	6.01	6.98
P0.5S1N0.5-0.45-1.5	6.01	8.45
P0.5S1N0.5-0.7-1.5	5.67	7.03
P0.5S1N0.5-0.2-2	5.80	8.3
P0.5S1N0.5-0.45-2	5.28	7.13
P0.5S1N0.5-0.7-2	6.17	7.78

Furthermore, the flexural strength calculated under square panel specimen and the flexural strength measured under four points bending test (Table 4.1) were correlated. The correlation between the above tests is shown in Figure 4.40. The positive correlation with coefficient of correlation R^2=0.75 was found between the strength values of the beam and panel tests. Moreover, as shown in Table 4.10, the flexural strength values of the panel test are less than the flexural strength values resulting from the beam test. The correlation between the flexural strength under panel test and the energy absorption at 10 mm deflection is shown in Figure 4.41. The results show a very high correlation coefficient R^2 =0.97.

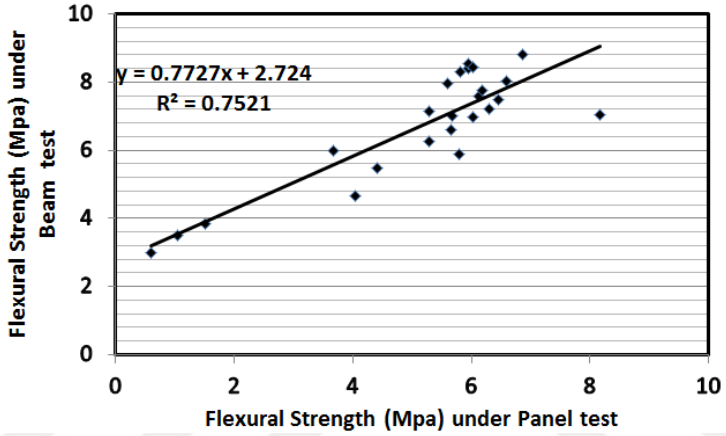

Figure 4.40 Correlation between flexural strength between beam and panel tests

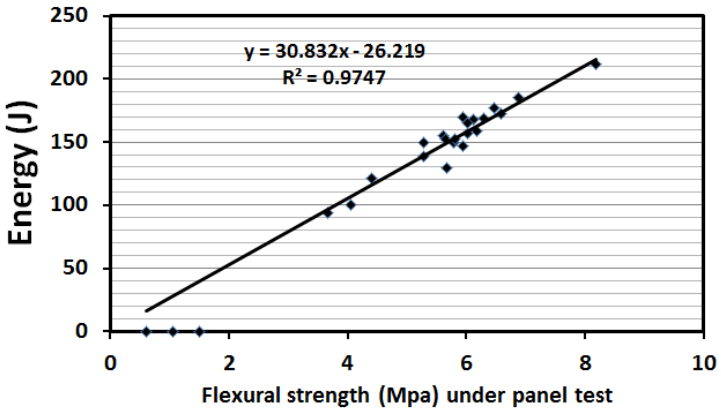

Figure 4.41 Correlation between flexural strength under panel tests and energy absorption at 10 mm deflection

4.5 Freezing and Thawing (F/T) Test Results

The Relative Dynamic Modulus of Elasticity (RDME) values for every produced HPFRC mixture was calculated as a ratio of the fundamental transverse frequency at

a certain number of F/T cycles to the initial value of fundamental transverse frequency before subjecting to the freezing and thawing condition. It is notable that every mixture was failed before reaching to 300 cycles; therefore, a 60% of the RDME values were selected for the comparison between the performances of the developed mixtures. For a better visualization of the effect of freezing and thawing on the developed HPFRC mixtures, Figures 4.42 to 4.45 were drawn for all of the mixtures. Through the plots in these figures, the numbers of F/T cycles that cause the mixture failed at 60% of the RDME were found. Based on the numbers of F/T cycles that found for every mixture, the durability factor (DF) of each mixture was calculated according to the Equation 3.3.

In order to see the effect of inclusion of the fiber on the frost resistance, different types of fiber were used. For an A/B ratio of 1.0, it is easily seen in Table 4.11 that addition of S fibers in the control mixtures led to evident deterioration in the DF. The percentages of the decrement were 55.0, 81.52, and 53.19% for FA replacement ratios of 0.2, 0.45, and 0.7, respectively. However, the decreasing trend in the DF was improved by adding more fibers. For example, the mixtures reinforced with S and P fibers declined the reduction in the DF values. The reduction in the DF values became 28.33, 71.73, and 36.17% for the same FA replacement ratios. Moreover, the replacement of 50% of the P fiber with N fiber showed more decrease in the DF values compared to the mixtures with S and P fibers. The reductions in the DF were 38.33, 61.95, and 40.42%. The reduction in the DF values as a result of addition of the S fibers may be attributed to the reduction in the void space as a result of occupation of the fiber to these spaces. Therefore, an increase in the micro-cracks found around these fibers resulting from volumetric changes-induced stresses of the water in the concrete. As mentioned earlier, the steel fiber can be considered as a rigid fiber. Due to this rigidity, the steel fiber has a lower ability to absorb the stresses resulting from the expansion of water which found around the fiber itself. On the contrary, the rest of the used fibers such as P and N fibers are more flexible than S fiber. For further clarification, Figure 4.46 describes the cross section of water exposed to freezing around rigid and flexible fibers. To investigate the effect of the type of fiber on the frost resistance at higher level of A/B ratios, a comparison between the mixtures containing two and three types of fiber was performed. For example, at an A/B ratio of 1.5 the DF values of the mixtures reinforced with S and P

fibers were 6.2, 7.2, and 5.4 for FA/PC ratios of 0.2, 0.45 and 0.7, respectively. These values of the DF were improved by replacing half of the P fiber with N fiber where the percentages of the improvement were 87.09, 83.33, and 88.88%. The incremental trend of the improvement is valid for an A/B ratio of 2.0.The increase of the DF values were appreciable as a result of replacing 50% of the P fiber with N fiber, particularly at FA/PC ratios of 0.2 and 0.45. It is found that the improvements were 151.11, 105.12, and 49.97% for FA/PC ratios of 0.2, 0.45, and 0.7, respectively. And as stated previously, the utilization of the N fiber instead of 50% of the P fiber has greater effect, especially at a higher level of A/B ratio.

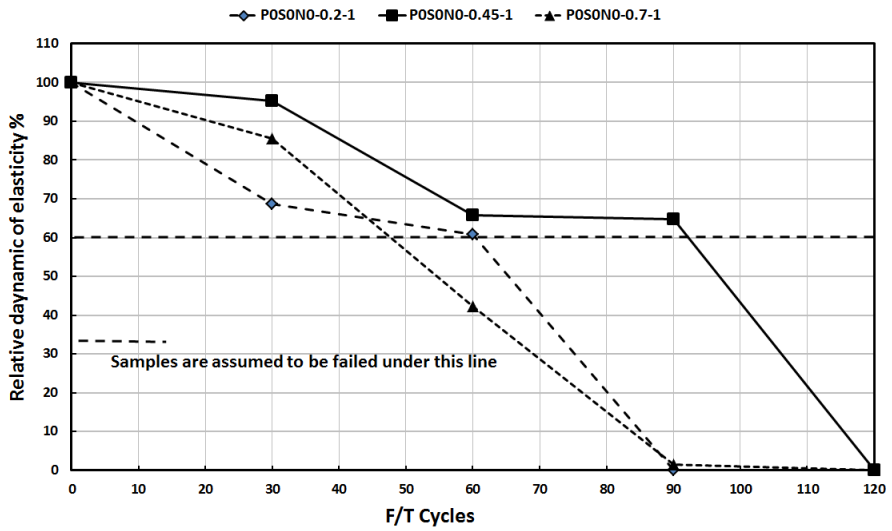

Figure 4.42 Relative dynamic modulus of concrete mixtures without fibers

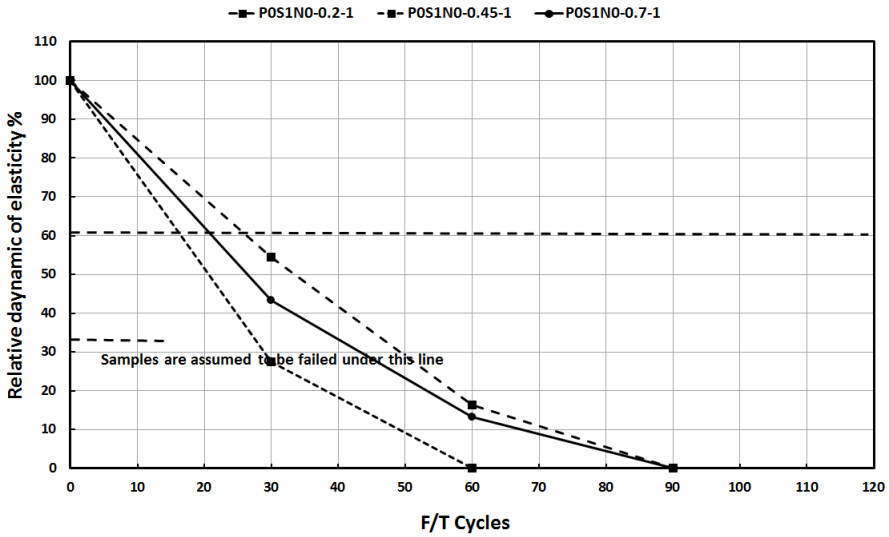

Figure 4.43 Relative dynamic modulus of concrete mixtures with S fibers

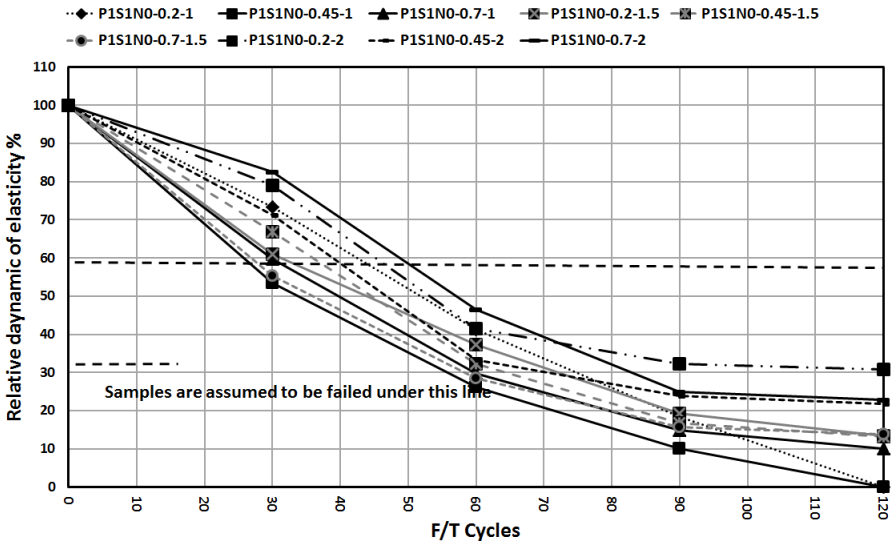

Figure 4.44 Relative dynamic modulus of concrete mixtures with S and P fibers

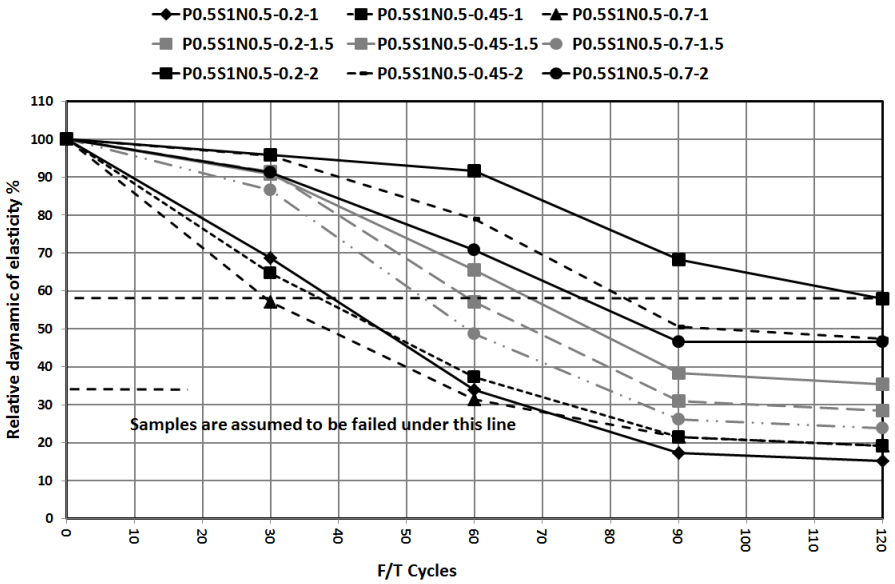

Figure 4.45 Relative dynamic modulus of concrete mixtures with S, P, and N fibers

The second investigated parameter to evaluate the frost resistance is increasing the aggregate amount. In general, the results revealed an incremental trend in increasing the DF values when the A/B ratio was increased from 1.0 to 2.0. For example, the value of the DF increases when the A/B ratio increases for the mixtures with S and P fibers. The percentages of increase were 4.65, 50, and 63.33% for FA replacement ratios of 0.2, 0.45, and 0.7, respectively. The incremental trend in the DF values is valid for the mixtures reinforced with three fibers, namely S, P and N. The increments were higher where the DF values increased by 205, 128, and 160% for the same above FA replacements ratios.

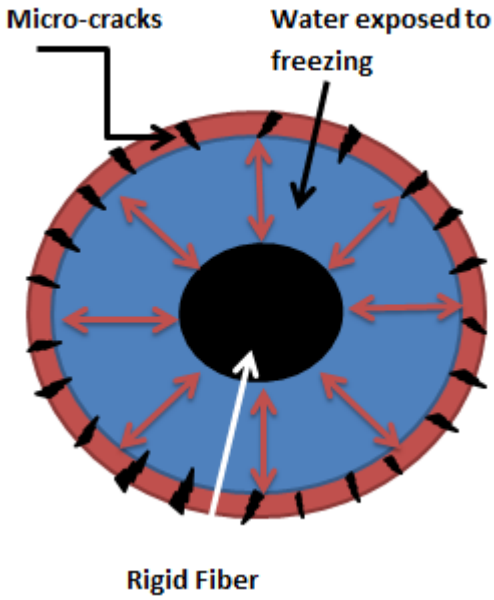

a) Rigid fiber

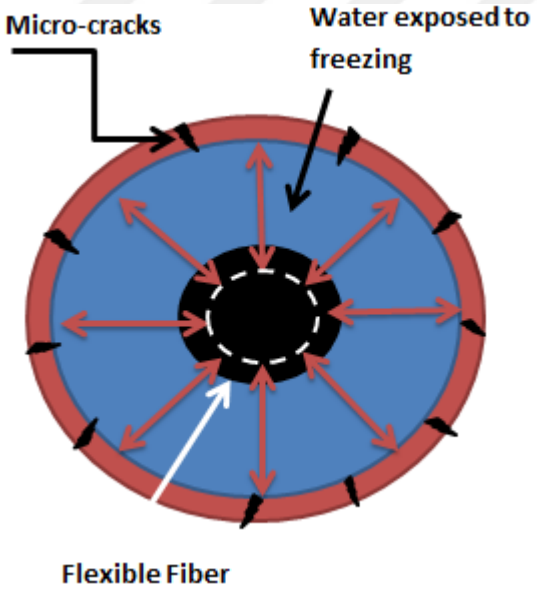

b) Flexible fiber

Figure 4.46 Schematic description for water exposed to freezing around fiber

The reason of an increase of the DF values when increasing the aggregate amount in the concrete mixtures may be ascribed to the fact that an increase in the voids thereby can accommodate the volumetric changes resulting from exposing the water in the concrete to freezing; thus, reducing the stresses-induced micro cracks.

Table 4.11 Number of cycles of 60% RDME and corresponding mixtures' durability factor (DF)

Mix. No.	Mix. ID	No. of cycles	DF
1	P0S0N0-0.2-1	60	12.0
2	P0S0N0-0.45-1	92	18.4
3	P0S0N0-0.7-1	47	9.4
4	P0S1N0-0.2-1	27	5.4
5	P0S1N0-0.45-1	17	3.4
6	P0S1N0-0.7-1	22	4.4
7	P1S1N0-0.2-1	43	8.6
8	P1S1N0-0.45-1	26	5.2
9	P1S1N0-0.7-1	30	6.0
10	P1S1N0-0.2-1.5	31	6.2
11	P1S1N0-0.45-1.5	36	7.2
12	P1S1N0-0.7-1.5	27	5.4
13	P1S1N0-0.2-2	45	9.0
14	P1S1N0-0.45-2	39	7.8
15	P1S1N0-0.7-2	49	9.8
16	P0.5S1N0.5-0.2-1	37	7.4
17	P0.5S1N0.5-0.45-1	35	7.0
18	P0.5S1N0.5-0.7-1	28	5.6
19	P0.5S1N0.5-0.2-1.5	58	11.6
20	P0.5S1N0.5-0.45-1.5	66	13.2
21	P0.5S1N0.5-0.7-1.5	51	10.2
22	P0.5S1N0.5-0.2-2	113	22.6
23	P0.5S1N0.5-0.45-2	80	16.0
24	P0.5S1N0.5-0.7-2	73	14.6

The Third parameter was evaluated to assess the frost resistance is the replacement of cement by FA. In general, the results showed a decrease in the DF when the FA/PC ratio was increased. For the control mixtures the DF values dropped by 21.66% as a result of increasing FA/PC from 0.2 to 0.7. Similarly, the trend in decrease of the DF values due to increasing FA are exist even the fibreless mixtures reinforced with fibers. For example, the reduction in the DF of the mixtures reinforced with S fiber was 18.5%. Same trend is clear in the mixtures reinforced with two or three types of fiber. For example at an A/B ratio of 1.5, the reduction in the DF value was 12.90% for the mixtures reinforced with S and P fibers. Furthermore, the decreasing trend in reducing the DF values for mixtures containing S, P, and N fibers was observed where the percentages of the reduction were 12.06 and 35.39% for A/B ratios 1.5 and 2.0, respectively. It seems that the addition of Class-F fly ash particles reduced the strength of the mixtures to resist the internal stresses inducing from expansion of the water to freezing. For a better visualization of the effect of increasing the FA in composite materials, Figure 4.47 was drawn for all of the evaluated mixtures.

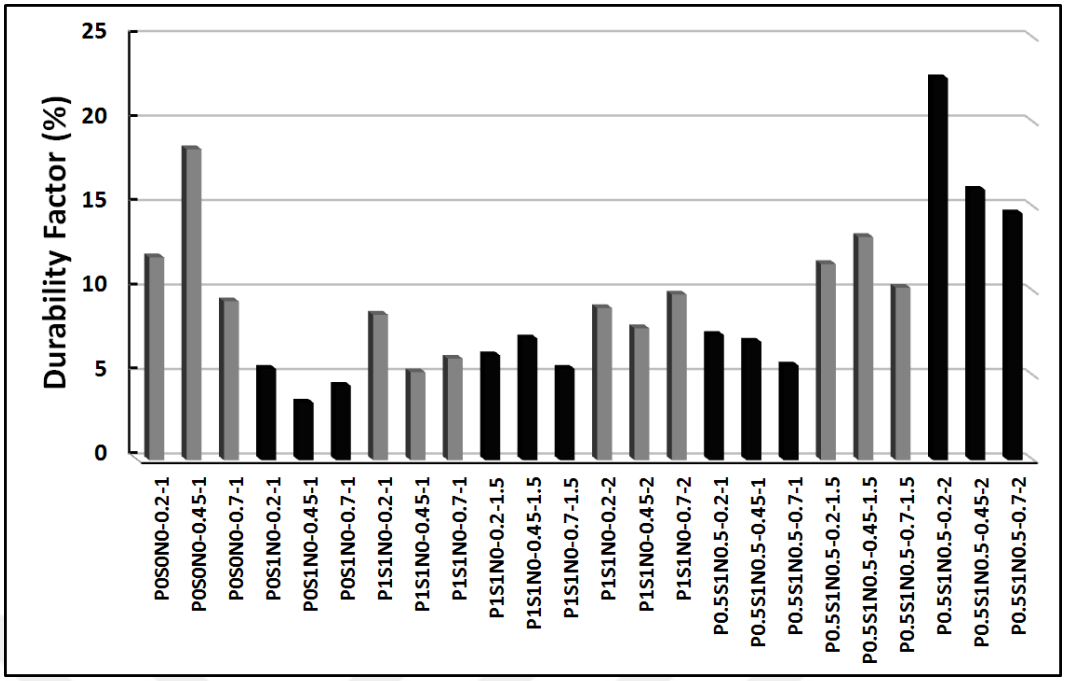

Figure 4.47 Effect of increasing the FA/PC ratio on the DF

4.6 Normalization of Tests Results and Selection of Optimal Mixtures

Based on the results obtained from the above tests, every investigated mixture was ranked upon the performance rank analysis. In addition to the performance ranking of the mixtures, the effect of the cement content was also included, where it consider as a negative factor during the production of the cement in terms of air pollution (CO_2 emission). Table 4.12 shows the parameters adopted for each test and its related reference. The performance of the every mixture was normalized according to the Equation below.

$$Normalized\ Performance = \frac{P_i - P_{min}}{P_{max} - P_{min}} \tag{4.3}$$

Where P_i is the performance of the tested mixtures, for a given property, P_{min} and P_{max} are the minimum and maximum performances among the tested mixtures. In addition to the each performance, the overall performances of every mixture were calculated and then normalized to find the rank of every mixture. Table 4.13 summarizes the normalized performances of the tested mixtures. Finally, ranking the mixtures depending on overall normalized performances was performed, as shown in Table 4.14.

Table 4.12 Test parameters adopted to normalize the mixtures performance

Test	Parameters	Reference
CO_2	Cement content (kg/m^3)	Table 3.3
Compression	Compressive Strength (MPa)	Table 4.1
Bending	Flexural Strength (MPa)	
	Deflection (mm)	
Impact	Residual Displacement (mm)	Table 4.2
Drying Shrinkage	Free drying shrinkage strain (µstrain)	Table 4.7
	Restrained drying shrinkage strain (µstrain)	
Slab panel	Ultimate load (kN)	Table 4.8
	Energy absorption (j)	Table 4.9
Freeze and thawing	Durability factor (%)	Table 4.11

As can be easily seen in Table 4.14, the overall performance of the mixtures was clearly increased when the mixtures containing three types of fiber, as presented in the mixtures ID of P0.5S1N0.5. The increase in performance of the mixtures was improved by increasing the A/B ratios, especially at an A/B ratio of 2.0. The improvement in the performance of the mixtures was followed by the mixtures having two types of fiber, as shown in hybrid fiber reinforced mixtures containing P and S fibers. The bottom of ranking with regard to the overall performance of the mixtures appeared in the mixtures with single fiber system (only steel fiber), in which they showed the low overall performance. Furthermore, the concrete mixtures without fibers have the lowest rank respect to the overall performance. Finally, inclusion of the fibers in concrete, especially hybrid fibers, and increasing the A/B ratios enhanced the overall performance of the mixtures developed in the present study. In addition to performances of the mixtures, the lower cost of the N fiber as compared to the P fiber encourages the usage of the N fiber instead of the P fiber. As the results revealed in the present study, the mixtures having three types of fiber (S, P, and N) with an A/B ratio of 2.0, and FA/PC ratios ranged between 0.2 to 0.7 replacements can be ranked as optimal mixtures.

Table 4.13 Summarize of normalized overall performances of tested mixtures*

	Compression Test	Bending Test		Impact Test	Drying Shrinkage Test		Slab Panel Test		Freeze and Thawing Test	CO_2	
Mix. ID	**Compressive Strength**	**Flexural Strength**	**Deflection**	**Residual Displacement**	**Restrained shrinkage**	**Free drying shrinkage**	**UL**	**EA**	**DF**	**Cement Content**	**Overall Performance**
P0S0N0-0.2-1	66	3	1	6	0	26	12	0	45	0	16
P0S0N0-0.45-1	31	9	0	0	17	32	6	0	78	37	21
P0S0N0-0.7-1	0	0	0	21	46	32	0	0	31	62	19
P0S1N0-0.2-1	57	51	81	12	85	44	40	44	10	2	43
P0S1N0-0.45-1	59	43	75	11	88	45	50	57	0	38	47
P0S1N0-0.7-1	15	29	71	9	89	64	46	47	5	64	44
P1S1N0-0.2-1	74	49	100	41	92	91	69	71	27	4	62
P1S1N0-0.45-1	46	85	90	73	93	45	66	73	9	40	62
P1S1N0-0.7-1	23	79	80	73	94	70	73	79	14	65	65
P1S1N0-0.2-1.5	81	100	54	66	96	58	83	87	15	33	67
P1S1N0-0.45-1.5	46	86	68	64	96	88	79	82	20	64	69
P1S1N0-0.7-1.5	23	93	76	68	97	79	71	80	10	85	68
P1S1N0-0.2-2	88	69	65	53	95	82	100	100	29	55	74
P1S1N0-0.45-2	59	95	83	57	96	88	70	70	23	81	72
P1S1N0-0.7-2	42	77	60	40	96	91	77	84	33	100	70
P0.5S1N0.5-0.2-1	71	56	73	63	87	0	62	71	21	4	51
P0.5S1N0.5-0.45-1	48	72	87	98	89	10	75	80	19	40	62
P0.5S1N0.5-0.7-1	33	62	91	100	92	18	67	72	11	65	61
P0.5S1N0.5-0.2-1.5	99	68	64	53	91	48	71	74	43	33	65
P0.5S1N0.5-0.45-1.5	80	93	91	83	95	59	71	78	51	64	77
P0.5S1N0.5-0.7-1.5	54	69	94	87	100	98	67	61	35	85	75
P0.5S1N0.5-0.2-2	100	91	71	44	100	96	69	72	100	55	80
P0.5S1N0.5-0.45-2	86	71	62	79	100	97	62	66	66	81	77
P0.5S1N0.5-0.7-2	68	82	86	87	100	100	74	75	58	100	83

***All values are in (%)**

Table 4.14 Ranking the tested mixtures depending on overall performance

Mix no.	Mixture ID	Normalized overall performances (%)	Ranking
24	P0.5S1N0.5-0.7-2	100	1
22	P0.5S1N0.5-0.2-2	95	2
23	P0.5S1N0.5-0.45-2	91	3
20	P0.5S1N0.5-0.45-1.5	91	4
21	P0.5S1N0.5-0.7-1.5	88	5
19	P0.5S1N0.5-0.2-1.5	86	6
13	P1S1N0-0.2-2	84	7
14	P1S1N0-0.45-2	81	8
15	P1S1N0-0.7-2	79	9
11	P1S1N0-0.45-1.5	78	10
12	P1S1N0-0.7-1.5	77	11
10	P1S1N0-0.2-1.5	73	12
9	P1S1N0-0.7-1	73	13
8	P1S1N0-0.45-1	69	14
7	P1S1N0-0.2-1	69	15
17	P0.5S1N0.5-0.45-1	68	16
18	P0.5S1N0.5-0.7-1	67	17
16	P0.5S1N0.5-0.2-1	52	18
5	P0S1N0-0.45-1	46	19
6	P0S1N0-0.7-1	42	20
4	P0S1N0-0.2-1	40	21
2	P0S0N0-0.45-1	7	22
3	P0S0N0-0.7-1	5	23
1	P0S0N0-0.2-1	0	24

CHPTER FIVE

CONCLUSIONS AND RECOMMENDATIONS

5.1 Conclusions

In the present study, efforts were made to develop deflection-hardening concrete mixtures with a maximal amount of coarse aggregates. Mixtures incorporating 43% coarse aggregate (with a maximum size of 12 mm) of total aggregate combination, and having different A/B ratios of (1.0, 1.5 and 2.0) and FA/PC (0.20, 0.45 and 0.70) ratios were produced with different combinations of P, S and N fibers. In addition, the produced mixtures were evaluated in different concrete properties to assess their performances. In the light of the current work, the following conclusions can be drawn:

5.1.1 Mechanical Tests

Based on the compositions of different mixtures and initial curing ages, compressive strength results changed. As expected, with further aging, there were constant increments in compressive strength. Increased FA/PC ratios caused relatively low results; however, even the lowest average compressive strength result was more than 30 MPa. Although higher A/B ratios were expected to lower compressive strength, this did not happen and it was attributed to the tortuosity and higher energy absorption capacity associated with increasing of A/B ratios. In general, adding fiber to control mixtures had no even slight influence on results.

For a given A/B ratio, increasing FA/PC ratios led to a decline in the MOR results of all mixtures and became more pronounced when higher ratios were used. This behavior was similar to that obtained in the case of compressive strength results and was associated with parameters affecting compressive strength. Although increasing A/B ratios was expected to reduce MOR results, the selection of a proper FA/PC ratio and fiber type/amount produced an opposite behavior. Fiber addition was

effective in improving MOR results; S fibers were the most influential due to their significantly higher elastic modulus. Although P fibers were more effective in enhancing the MOR results as compared to N fibers, results for mixtures incorporating both P and N fibers were very close to each other, this means that as in compressive strength, P fibers can be replaced with N fibers (by up to half of the volume of P fibers) without compromising flexural strength. Despite the variations in the MOR results of mixtures with different FA/PC ratios, A/B ratios, and fiber type/dosage, the lowest 28-day average flexural strength value recorded from the fiber reinforced cementitious composites herein was 5.48 MPa for P0S1N0_0.45_1.0 mixture.

In mixtures of a given A/B ratio, increasing FA/PC ratios resulted in higher mid-span beam deflection values in general. Even at the highest A/B ratio of 2.0, the deflection results of specimens were not necessarily decreased. For the specimens produced herein, the A/B ratio should not be regarded as a determinant of overall deflection capacity as long as the amount of FA particles is optimized. Fiber addition made substantial increments in the deflection results regardless of the type and/or dosage of fibers. The deflection-hardening response under four-point bending or loading was confirmed even from mixtures incorporating 1% S fibers, by volume, irrespective of FA/PC and A/B ratios. However, deflection-hardening behavior was further enhanced when S fibers were combined with P or P, N fibers.

HPFRC mixtures can incorporate coarse aggregates similar to those most frequently used in actual field applications (with a MAS of 12 mm) and industrial by-products such as fly ash in large proportions without compromising deflection-hardening (ductile) behavior. The final composite material will exhibit superior mechanical and durability characteristics, enhanced greenness, and result in materials that are easy to apply in practice at a lower cost.

5.1.2 Impact Test

In the present study, impact resistance of beam specimens produced by deflection-hardening HPFRC mixtures was evaluated after implementing free fall drop-weight tests. Because of its nature, impact loading is not very well known as the static and dynamic loading types. Primary importance was given to observe the effects of three

main variables (type of fiber reinforcement, A/B ratio and FA/PC ratio) on the impact behavior of HPFRC beams. To see the effects of these variables on the impact behavior of HPFRC beam specimens, acceleration vs. time, displacement vs. time, and impact load vs. time graphs were obtained and analyzed. Moreover, tested beam specimens were modelled in finite element program (ABAQUS) and incremental nonlinear dynamic analysis were performed. As a final step, the results obtained experimentally in the laboratory were compared with the ones obtained from numerical study.

Results obtained from the experimental and numerical studies showed that for the similar fiber reinforcement, increasing the amount of fly ash and coarse aggregate in the mixtures significantly improved the impact resistance of HPFRC beam specimens. Additionally, fiber hybridization was found to be very effective in enhancing the resistance to impact loading. The best performance in terms of impact resistance was achieved from the specimens produced with FA/PC ratio of 0.7, A/B ratio of 2.0 and three different fiber combinations (S, P and N).

ABAQUS finite element software used for the purposes of numerical analysis was found to be successful in modeling the impact behavior of HPFRC beam specimens so that acceleration, displacement and residual displacement results obtained from both experimental and numerical studies were in good agreement. This finding, therefore, suggests that ABAQUS program can be used in the design process before implementing the actual tests.

To sum up, HPFRC mixtures with deflection-hardening capability are believed to be benefited from absorbing blasting effects, to produce anti-ballistic shielding and/or as protective barriers to prevent vehicle crushes near bridge pears and so on given their superior resistance to sudden impact loads.

5.1.3 Shrinkage Tests

The results obtained from the free drying shrinkage test revealed that addition the fibers in the concrete led to decrease the free shrinkage strain values. However, replacing 50% of the P fiber with N fiber at an A/B ratio of 1.0 states an adverse trend. The increase in drying shrinkage strain values is most likely due to the N fiber's surface texture in which the hydrophilic nature of N fibers can absorb water

during the fresh state of the concrete and release this absorbed water whenever the concrete hardens. However, the results were in contrary as a result of replacing half of P fiber with N fibers at a higher A/B ratio, where the results revealed a decrease in free shrinkage strain values through increasing the aggregate content at A/B ratios of 1.5 and 2.0. Furthermore, increasing the aggregate amount mitigated markedly the free drying shrinkage strain values. Similarly, increasing the FA replacement ratios alleviated the shrinkage strain regardless of the produced mixtures that reinforced with fibers or not. In generally, a total mitigated shrinkage strain values as a result of inclusion of fibers, cement replacement by FA, and increasing A/B ratio from 1.0 to 2.0 ratios were calculated. The shrinkage strain values were mitigated by average value 28.07 and 31.5 % for the mixtures ID of P1S1N0 and P0.5S1N0.5, respectively. This implies that utilization of the N fiber instead of the P fiber leads to greater decrease in the shrinkage strain value.

In the present study, the restrained shrinkage test is carried out to evaluate three different parameters on the performances of the produced HPFRC mixtures: fiber type, aggregate amount, and FA replacement ratios. The results showed that reinforcing the fibreless control mixtures revealed a considerably improvement in the reduction of both total and maximum crack width values resulting from the restrained shrinkage conditions. Furthermore, the numbers of cracks increased when the control mixtures were reinforced by fibers. Due to increasing the A/B ratios from 1.0 to 2.0, it is found that the drops in the total and maximum crack widths were appreciably higher in the concrete reinforced with a hybrid fiber system, especially with three fibers, namely P, S, and N. As a result of increasing FA content, the effect of increasing FA/PC ratio from 0.2 to 0.7 presented a positive impact with respect to the reduction in the total and maximum crack widths. Marked improvements in minimizing the crack width were evident by replacing half of the volume of the P fiber with N fiber where the results revealed that mixtures with three type of fiber (S, P, and N) at an A/B ratio of 2.0 showed no cracks as a result of restrained drying shrinkage conditions. Finally, the combined effect of: inclusion of fibers in concrete, FA replacement increases, and increasing A/B ratio on reducing the total and maximum crack width of the produced HPFRC mixtures were 92 and 96.3% for the total and maximum crack width, respectively. This improvement decreased the

average maximum crack width of the fibreless concrete mixtures through a reduction in crack width from 2694 to 100 μm for the reinforced fiber mixtures.

In this study, cracking potential was calculated based on the time to cracking. Time to cracking is the difference between the age at cracking and the age at which drying is initiated. The results stated that reinforcing the concrete mixtures with S fibers showed a slight improvement in terms of increasing the time to cracking. Moreover, when the control mixtures reinforced with (S and P) fibers, the time to cracking shows more increasing. In general, as the A/B ratio increases, the cracking potential decreases. Marked improvement appeared in the mixtures containing three types of fiber S, P, and N. This implies that by replacing 50% of the P fiber with N fiber, the produced HPFRC mixtures were guaranteed to be completely without cracks, particularly with an A/B ratio of 2.0. Finally, the results indicated that the mixtures without fibers, which presented in mixtures ID P0S0N0 and mixtures that reinforced with S fibers can be classified as high potential cracking mixtures. Conversely, mixtures reinforced with S, P, and N fibers particularly with an A/B ratio of 2.0 are classified as mixtures with a low cracking potential.

5.1.4 Slab Panel Test

The main purpose of the present study is to develop HPFRC mixtures with deflecting-hardening responses. After the adoption of certain mixtures, evaluating the performances of the mixtures with regard to the different properties was performed. In this line, the experimental program investigates the effects of three variables parameters on the HPFRC slab panel specimens under bending. Inclusion of fibers in concrete had significant effects by enhancing the strength of the concrete in terms of the ultimate load (UL). The results revealed that reinforcing the fibreless mixtures with S fibers showed an increase in the UL values. Moreover, an increase in the volume of fibers by adding P and S fibers in the concrete led to improve this increasing trend. To investigate the effect of fiber on the UL values at a higher level of A/B ratio, two different values of A/B of 1.5 and 2.0 were evaluated. For example, at A/B ratios of 1.5and 2.0, by replacing half of the P fiber with N fiber revealed a decrement in the UL values as compared to mixtures containing P and S fibers. Whilst, increasing A/B ratio from 1.0 to 2.0 showed an increase in the UL values. In order to evaluate the performances of the mixture with regard to the deflection-

hardening responses, the ratio of ultimate load to the first load values (UL/FL) was calculated. This ratio is an indicator to the performance of mixture as a stiff material. As UL/FL value increases, the hardening behavior index increases. As evident in the test results, all of the fiber reinforced mixtures which are developed have UL/FL ratio greater than 1.0. This implies that all of the produced mixtures exhibited as a deflection-hardening response under panel test condition.

The results revealed that inclusion of the fibers in concrete has an appreciable effect through increasing the toughness (energy absorption (EA)) of all of the evaluated mixtures under panel test. Furthermore, by adding more fibers in concrete, the results show a higher improvement in the energy absorption values. Moreover, at hybrid fiber reinforced mixtures, the increasing A/B led to increase the energy absorption. The results stated that the effect of increasing FA amount on the EA values was affected by the amount of aggregate.

The results appeared that most the panel's specimens cracked with main of 5-8 localized cracks accompanying with multi-micro cracks. Besides that, the pattern of cracking of all tested specimens was tacked place similar to the second form of failure (conservative). The cracks appeared by radial cracks starting from the corner to the mid edge of panel specimens. This pattern of cracks may be attributed to the deflection-hardening behavior of the mixtures which may cause a fan mechanism resulting in losing the contact area with increasing loads thereby developing new cracked surfaces (multi cracks).

In the current study, flexural strength under biaxial condition represented by panel test was calculated depending on yield-line theory. The yield line theory is a common used method to determine the capacity of reinforced concrete panels (Holmgren, 1993). Depending on this theory, the ultimate load recorded from the load-deflection curve was transformed to the flexural strength. The positive correlation with coefficient of correlation R^2=0.75 was found between the strength of the beam and panel values. Furthermore, correlation between flexural strength under panel test and the energy absorption at 10 mm deflection showed a very high correlation coefficient of R^2 =0.97.

5.1.5 Freezing and Thawing Test

The relative dynamic modulus of elasticity (RDME) values for every produced HPFRC mixture was calculated as a ratio of the fundamental transverse frequency at a certain number of F/T cycles to the initial value of fundamental transverse frequency before subjecting to freezing and thawing condition. It is notable that every mixture was failed before reaching to 300 cycles. Therefore, a 60% of the RDME values were selected for a comparison between the performances of the developed HPFRC mixtures. Based on the numbers of F/T cycles, durability factor (DF) value of each mixture was calculated. For an A/B ratio of 1.0, it can easily be seen that adding S fibers in the control mixtures leads to evident deterioration in the DF. However, the decreasing trend in the DF was improved by adding more fibers. To investigate the effect of type of fiber on the frost resistance at a higher level of A/B ratio, a comparison between mixtures containing two and three types of fiber was performed. For example, at A/B ratios of 1.5 and 2.0 the DF values for the mixtures reinforced with S and P fibers were improved by replacing half of the P fibers with N fibers. In general, the results revealed an incremental trend in increasing the DF values due to increasing the A/B ratio from 1.0 to 2.0. Conversely, the results showed a decrease in the DF when the FA/PC ratio increases.

5.1.6 Optimal Mixtures Selection

Based on the obtained results from the above tests, every investigated mixture was ranked upon the performances rank analysis. In addition, the performance ranking of mixtures included the cement content effects which considers as a negative factor during the production of the cement in terms of the air pollution (CO_2 emission). The overall performance of the mixtures was clearly increased with mixtures containing three types of fiber, as presented in the mixtures ID P0.5S1N0.5. The increase in performance of the mixtures was improved throughout increasing the A/B ratios, especially at an A/B=2.0. The improvement in performance of the mixtures was followed by the mixtures with two types of fiber, as shown in hybrid fiber mixtures containing P and S fibers. The bottom of ranking with regard to the overall of mixtures was appeared in the mixtures with single fiber system (only steel fibers) in which they showed the low performance values. Furthermore, the concrete mixtures without fibers have the lowest rank respect to the overall performance of mixtures.

Finally, inclusion of fibers in concrete, especially hybrid fibers, and increasing A/B ratios enhanced the overall performance for the mixtures produced in present study. In addition to mixtures performances, the lower cost of N fiber as compared to P fiber encourages the usage of the N fiber instead of the P fiber. The results revealed in the following study, the mixtures that having three types of fiber S, P, and N at an A/B ratio of 2.0, and with FA/PC ratios ranged between of 0.2 to 0.7 replacements can be ranked as optimal mixtures.

5.2 Recommendations for Future Studies

In accordance with the current work and its results, the upcoming points can be recommended for future studies.

- Evaluating the performance of the mixtures produced in the present study under fatigue cyclic loading to simulate the mixtures behavior for a structural element exposing to the heavy vehicle loading range.
- Studying the behavior of the developed material as over layer material paved on the cracked Portland concrete pavement to evaluate their performance in terms of reflecting cracking.
- Studying the behavior of the mixtures with regard to the their permeability and investigating their durability performance by adding nano-mineral material and/or using a higher type of cement in strength.
- Investigating the behavior of the produced material in large scale beam specimen with different steel bar reinforcement ratios under monotonic and cyclic flexural loading.

REFRENCES

AASHTO. American Association of State Highway and Transportation Officials. (1999). Standard Practice for Estimating the Cracking Tendency of Concrete. 99th Edition. USA.

AASHTO. American Association of State Highway and Transportation Officials. (2012). LRFD Bridge Design Specifications. 6th Edition. USA.

ACI. American Concrete Institute. (2001). 308R-01: Guide to curing concrete. USA, Farmington Hills, MI.

ACI. American Concrete Institute. (2010). 231R-10: Report on early-age cracking: causes, measurement and mitigation. USA, Farmington Hills, MI.

ACI. American Concrete Institute. (2016). ACI Concrete terminology - An ACI standard. USA, **CT-16:** 1-74.

Ahmed, S., Maalej, M. (2009). Tensile strain hardening behaviour of hybrid steel-polyethylene fibre reinforced cementitious composites, *Construction and Building Materials*, **23**(1), 96-106.

Ahmed, S. F. U., Maalej, M., Paramasivam, P. (2007). Flexural responses of hybrid steel–polyethylene fiber reinforced cement composites containing high volume fly ash, *Construction and Building Materials*, **21**(5), 1088-1097.

Aitcin, P. C. (1998). Autogenous shrinkage measurement. *Autoshrink 98, Proceedings of the International Workshop on Autogenous Shrinkage of Concrete*, Hiroshima, Japan, ed. E. Tazawa, 245-256.

Al-Attar, T. S. (2008). Effect of coarse aggregate characteristics on drying shrinkage of concrete, *Journal of Engineering and Technology*, **26**(2).

Alhozaimy, A., Soroushian, P., Mirza, F. (1996). Mechanical properties of polypropylene fiber reinforced concrete and the effects of pozzolanic materials, *Cement and Concrete Composites*, **18**(2), 85-92.

Almudaiheem, J. A., Hansen, W. (1987). Effect of specimen size and shape on drying shrinkage of concrete, *Materials Journal*, **84**(2), 130-135.

Arisoy, B., Wu, H.-C. (2008). Material characteristics of high performance lightweight concrete reinforced with PVA, *Construction and Building Materials*, **22**(4), 635-645.

ASTM. American Society for Testing and Materials. (2008). Standard test method for length change of hardened hydraulic-cement mortar and concrete. C157/C157M. Annual Book of ASTM Standards**:** 7.

ASTM. American Society for Testing and Materials. (2002). Standard test method for fundamental transverse, longitudinal, and torsional frequencies of concrete specimens. C215. Annual Book of ASTM Standards**:** 7.

ASTM. American Society for Testing and Materials. (2003). Standard test method for resistance of concrete to rapid freezing and thawing. C666/C666M. Annual book of ASTM standards**:** 6.

ASTM. American Society for Testing and Materials. (2005). Standard test method for flexural toughness of fiber reinforced concrete (using centrally loaded round panel). C1550. Annual Book of ASTM Standards**:** 13.

ASTM. American Society for Testing and Materials. (2009). Standard test method for determining age at cracking and induced tensile stress characteristics of mortar and concrete under restrained shrinkage. C1581/C1581M. Annual book of ASTM standards**:** 7.

ASTM. American Society for Testing and Materials. (2010). Standard test method for flexural performance of fiber-reinforced concrete (using beam with third-point loading). C1609/C1609M. Annual Book of ASTM Standards**:** 9.

Attiogbe, E. K., See, H. T., Miltenberger, M. A. (2004). Potential for restrained shrinkage cracking of concrete and mortar, *Cement, concrete and aggregates*, **26**(2), 1-8.

Babaei, K., Hawkins, N. (1987). Evaluation of bridge deck protective strategies. NCHRP Report 297. Washington, D.C., Transportation Research Record.

Babaei, K., Purvis, R. L. (1995). Prevention of cracks in concrete bridge decks: Report on laboratory investigations of concrete shrinkage. Wilbur Smith Associates Report, Pennsylvania Department of Transportation. Project No. 89-01.

Balaguru, P., Narahari, R., Patel, M. (1992). Flexural toughness of steel fiber reinforced concrete, *ACI Materials Journal*, **89**(6), 541-546.

Banthia, N. P. (1987). Impact resistance of concrete. Ph.D. thesis. University of British Columbia,

Banthia, N. P. (2000). Crack growth resistance of high performance hybrid fiber reinforced cement composites. *Proceedings of the International Symposium: High Performance Concrete–Workability, Strength and Durability, Editors: Leugn, C., Li, Z. and Ding, J.T.*, Hong Kong.

Banthia, N. P., Gupta, R. (2006). Influence of polypropylene fiber geometry on plastic shrinkage cracking in concrete, *Cement and Concrete Research*, **36**(7), 1263-1267.

Banthia, N. P., Majdzadeh, F., Wu, J., Bindiganavile, V. (2014). Fiber synergy in Hybrid Fiber Reinforced Concrete (HyFRC) in flexure and direct shear, *Cement and Concrete Composites*, **48**, 91-97.

Banthia, N. P., Yan, C., Mindess, S. (1996). Restrained shrinkage cracking in fiber reinforced concrete: a novel test technique, *Cement and Concrete Research*, **26**(1), 9-14.

Bayasi, Z., Zeng, J. (1993). Properties of polypropylene fiber reinforced concrete, *ACI Materials Journal*, **90**(6), 605-610.

Bentur, A., Mindess, S. (2006). Fibre reinforced cementitious composites. 2nd edition: CRC Press.

Bentur, A., Wu, S., Banthia, N., Baggott, R., Hansen, W., Katz, A., Leung, C., Li, V., Mobasher, B., Naaman, A. (1996). Fiber-matrix interfaces, *Proceedings of the Second International Workshop on High Performance Fiber Reinforced Cement Composites. Edited by A.E. Naaman and H. W. Reinhardt*, 149-192.

Bentz, D. P., Jensen, O. M. (2004). Mitigation strategies for autogenous shrinkage cracking, *Cement and Concrete Composites*, **26**(6), 677-685.

Bernard, E. S. (2004). Design performance requirements for fibre reinforced shotcrete using ASTM C-1550. *Shotcrete: More Engineering Developments: Proceedings of the Second International Conference on Engineering Developments in Shotcrete, October 2004, Cairns, Queensland, Australia.*, Taylor & Francis.

Betterman, L., Ouyang, C., Shah, S. (1995). Fiber-matrix interaction in microfiber-reinforced mortar, *Advanced Cement Based Materials*, **2**(2), 53-61.

Bissonnette, B., Pierre, P., Pigeon, M. (1999). Influence of key parameters on drying shrinkage of cementitious materials, *Cement and Concrete Research*, **29**(10), 1655-1662.

Bloom, R., Bentur, A. (1995). Free and restrained shrinkage of normal and high-strength concretes, *ACI Materials Journal*, **92**(2), 211-217.

Blunt, J. D., Ostertag, C. P. (2009). Deflection hardening and workability of hybrid fiber composites, *ACI Materials Journal*, **106**(3), 265-272.

Boulfiza, M., Sakai, K., Banthia, N., Yoshida, H. (2003). Prediction of chloride ions ingress in uncracked and cracked concrete, *ACI Materials Journal*, **100**(1), 38-48.

Brandt, A. M. (2008). Fibre reinforced cement-based (FRC) composites after over 40 years of development in building and civil engineering, *Composite structures*, **86**(1), 3-9.

Brown, M., Sellers, G., Folliard, K., Fowler, D. (2001). Restrained shrinkage cracking of concrete bridge decks: State-of-the-art review (No. FHWA/TX-0-4098-1).

Cengiz, O., Turanli, L. (2004). Comparative evaluation of steel mesh, steel fibre and high-performance polypropylene fibre reinforced shotcrete in panel test, *Cement and Concrete Research*, **34**(8), 1357-1364.

Chao, S.-H., Cho, J.-S., Karki, N. B., Sahoo, D. R., Yazdani, N. (2011). FRC performance comparison: uniaxial direct tensile test, third-point bending test and round panel test, *SP-276. Durability Enhancements in Concrete with Fiber Reinforcement*, **276**, 1-20.

Cheng, T. T., Johnson, D. W. (1985). Incident assessment of transverse cracking in bridge decks: construction and material consideration, Report No. FHWA/NC/85-002, Federal Highway Administration, Washington, DC. **Vol. 1**.

Ciancio, D., Mazzotti, C., Buratti, N. (2014). Evaluation of fibre-reinforced concrete fracture energy through tests on notched round determinate panels with different diameters, *Construction and Building Materials*, **52**, 86-95.

Cohen, M. D., Olek, J., Dolch, W. L. (1990). Mechanism of plastic shrinkage cracking in portland cement and portland cement-silica fume paste and mortar, *Cement and Concrete Research*, **20**(1), 103-119.

Cominoli, L., Meda, A., Plizzari, G. (2005). Hybrid fibers to enhance fracture properties of concrete pavements. *Proc. of the Third Int. Conf. on Construction Materials, Vancouver, Canada*.

Dakhil, F. H., Cady, P. D., Carrier, R. E. (1975). Cracking of fresh concrete as related to reinforcement, *Journal Proceedings*, **72**(8), 421-428.

Darwin, D., Browning, J., Deshpande, S. (2007a). Evaluating free shrinkage of concrete for control of cracking in bridge decks. The university of Kansas center for research, *Structural Engineering and Engineering Materials. SM Report*, **89**, 90-95.

Darwin, D., Browning, J., Lindquist, W., McLeod, H., Yuan, J., Toledo, M., Reynolds, D. (2010). Low-cracking, high-performance concrete bridge decks: case studies over first 6 years, *Transportation Research Record: Journal of the Transportation Research Board*(2202), 61-69.

Darwin, D., Browning, J., Lindquist, W. D. (2004). Control of cracking in bridge decks: observations from the field, *Cement, concrete and aggregates*, **26**(2), 1-7.

Darwin, D., Lindquist, W., McLeod, H., Browning, J. (2007b). Mineral admixtures, curing, and concrete shrinkage. *Ninth Cement/ACI International Conference on Fly Ash, Silica Fume, Slag and Natural Pozzolans in Concrete, Warsaw, Poland*.

Dawood, E. T., Ramli, M. (2010). Development of high strength flowable mortar with hybrid fiber, *Construction and Building Materials*, **24**(6), 1043-1050.

De Koker, D., Van Zijl, G. (2004). Extrusion of engineered cement-based composite material. *Proceedings of the 6th RILEM Symposium on Fiber-Reinforced Concretes (FRC)*, Citeseer, 20-22.

De Larrard, F., Belloc, A. (1997). The influence of aggregate on the compressive strength of normal and high-strength concrete, *ACI Materials Journal*, **94**(5), 417-426.

De Larrard, F., Buil, M. (1987). Particle size and compactness in civil engineering materials, *Materials and Structures*, **20**, 117-126.

Delatte, N., Crowl, D. (2012). Case studies of internal curing of bridge decks in the greater cleveland area, *Special Publication*, **290**, 1-12.

Destrée, X., Mandl, J. (2008). Steel fibre only reinforced concrete in free suspended elevated slabs: case studies, design assisted by testing route, comparison to the latest SFRC standard documents. *Proceedings of the fib symposium on tailor made concrete structures. Taylor & Francis Group, Amsterdam*.

Di Prisco, M., Dozio, D., Colombo, M., Toledo Filho, R., Silva, F., Koenders, E., Fairbairn, E. (2011). On the bearing capacity of FRC structures is the material characteristic value the right choice, *2nd International RILEM Conference on Strain Hardening Cementitious Composites (SHCC2-Rio), Rio de Janeiro, RILEM Proceedings*, **8**, 279-287.

Døssland, Å. L. (2008). Fibre reinforcement in load carrying concrete structures, *Norwegian University of Science and Technology, Printed by NTNU Trykk*.

EFNARC. European Federation of National Associations of Specialist Contractors and Material Suppliers for the Construction Industry. (1996). European Specification for Sprayed Concrete. UK, **EN 934-5**.

Ezeldin, A., Balaguru, P. (1989). Bond behavior of normal and high-strength fiber reinforced concrete, *ACI Materials Journal*, **86**(5), 515-524.

Feldman, R., Sereda, P. (1970). A new model for hydrated Portland cement and its practical implications, *Engineering Journal*, **53**(8/9), 53-59.

Folliard, K., Smith, C., Sellers, G., Brown, M., Breen, J. (2003). Evaluation of alternative materials to control drying-shrinkage cracking in concrete bridge decks, No. FHWA/TX-04/0-4098-4.

French, C., Eppers, L., Le, Q., Hajjar, J. (1999). Transverse cracking in concrete bridge decks, *Transportation Research Record: Journal of the Transportation Research Board*(1688), 21-29.

Frosch, R. J., Blackman, D. T., Radabaugh, R. D. (2003). Investigation of bridge deck cracking in various bridge superstructure systems, Publication FHWA/IN/JTRP-2002/25. Joint Transportation Research Program, Indiana Department of Transportation and Purdue University, West Lafayette, Indiana.

Fu, T., Deboodt, T., Ideker, J. H. (2016). Development of shrinkage limit specification for high performance concrete used in bridge decks, *Cement and Concrete Composites*, **72**, 17-26.

Fuller, W. B., Thompson, S. E. (1907). The laws of proportioning concrete, *Asian Journal of Civil Engineering Transport*, **59**, 67-143.

Gao, J., Sun, W., Morino, K. (1997). Mechanical properties of steel fiber-reinforced, high-strength, lightweight concrete, *Cement and Concrete Composites*, **19**(4), 307-313.

Geng, Y., Leung, C. K. (1996). A microstructural study of fibre/mortar interfaces during fibre debonding and pull-out, *Journal of materials science*, **31**(5), 1285-1294.

Giles Jr, H. F., Mount III, E. M., Wagner Jr, J. R. (2005). Extrusion: the definitive processing guide and handbook. USA: William Andrew, Inc.

Grünewald, S., Walraven, J. (2002). Self-compacting fibre reinforced concrete-orientation and distribution of steel fibres in beams, Report 24.5-02-3 2002. Delft University of Technology, The Netherlands.

Grzybowski, M., Shah, S. P. (1990). Shrinkage cracking of fiber reinforced concrete, *ACI Materials Journal*, **87**(2), 138-148.

Guerrero, P., Naaman, A. E. (2000). Effect of mortar fineness and adhesive agents on pullout response of steel fibers, *ACI Materials Journal*, **97**(1), 12-20.

Habeeb, G., Fayyadh, M. (2009). Rice husk ash concrete: the effect of RHA average particle size on mechanical properties and drying shrinkage, *Australian Journal of Basic and Applied Sciences*, **3**(3), 1616-1622.

Hadidi, R., Saadeghvaziri, M. A. (2005). Transverse cracking of concrete bridge decks: state-of-the-art, *Journal of Bridge Engineering*, **10**(5), 503-510.

Hameed, R., Turatsinze, A., Duprat, F., Sellier, A. (2010). A study on the reinforced fibrous concrete elements subjected to uniaxial tensile loading, *KSCE Journal of Civil Engineering*, **14**(4), 547-556.

Hearing, B. P. (1997). Fracture behavior of mortar-aggregate interfaces in concrete. M.Sc. thesis. Massachusetts Institute of Technology, USA.

Hindy, E., Miao, B., Chaallal, O., Aitcin, P.-C. (1994). Drying shrinkage of ready-mixed high-performance concrete, *ACI Materials Journal*, **91**(3), 300-305.

Holmgren, J. (1993). The use of yield-line theory in the design of steel-fibre reinforced concrete slabs, *Shotcrete for underground support VI, ASCE*, 91-98.

Holt, E. E. (2001). Early age autogenous shrinkage of concrete. Technical Research Centre of Finland.

Hooton, R. D., Stanish, K., Angel, J., Prusinski, J. (2009). The effect of ground granulated blast furnace slag (sag cement) on the drying shrinkage of concrete–A critical review of the literature, *ACI Special Publication*, **263**, 79-85.

Hwang, S.-D., Khayat, K. H. (2008). Effect of mixture composition on restrained shrinkage cracking of self-consolidating concrete used in repair, *ACI Materials Journal*, **105**(5), 498-508.

Issa, M. A. (1999). Investigation of cracking in concrete bridge decks at early ages, *Journal of Bridge Engineering*, **4**(2), 116-124.

Jansen, D. C., Shah, S. P., Rossow, E. C. (1995). Stress-strain results of concrete from circumferential strain feedback control testing, *ACI Materials Journal*, **92**(4), 419-428.

Jensen, O. M., Hansen, P. F. (2001). Water-entrained cement-based materials: I. Principles and theoretical background, *Cement and Concrete Research*, **31**(4), 647-654.

Johnston, C. (2004). 14 Proportioning, mixing and placement of fibre-reinforced cements and concretes, *Production Methods and Workability of Concrete*, **32**, 155.

Kawashima, S., Shah, S. P. (2011). Early-age autogenous and drying shrinkage behavior of cellulose fiber-reinforced cementitious materials, *Cement and Concrete Composites*, **33**(2), 201-208.

Kayali, O., Haque, M., Zhu, B. (2003). Some characteristics of high strength fiber reinforced lightweight aggregate concrete, *Cement and Concrete Composites*, **25**(2), 207-213.

Kim, B., Weiss, W. J. (2003). Using acoustic emission to quantify damage in restrained fiber-reinforced cement mortars, *Cement and Concrete Research*, **33**(2), 207-214.

Kochanski, T., Parry, J., Pruess, D., Schuchardt, L., Ziehr, J. (1990). Premature cracking of concrete bridge decks study, *Final Report. Wisconsin Department of Transportation, Madison, WI*.

Krauss, P. D., Rogalla, E. A. (1996). Transverse cracking in newly constructed bridge decks, NCHRP Report No. 380, Project 12-37 FY'92. USA: Transportation Research Board.

Kovler, K. (1994). Testing system for determining the mechanical behaviour of early age concrete under restrained and free uniaxial shrinkage, *Materials and Structures*, **27**(6), 324-330.

Kuder, K. G., Shah, S. P. (2010). Processing of high-performance fiber-reinforced cement-based composites, *Construction and Building Materials*, **24**(2), 181-186.

Kwak, H., Filippou, F. (1992). Finite element analysis of reinforced concrete structures under monotonic and cyclic loads, *10th World Conference in Earthquake Engineering, Madrid, Spain*, 4227-4232.

Lange, D. A., Roesler, J. R., Dambrosia, M. D., Grasley, Z. C., Lee, C. J. (2003). High performance concrete for transportation structures (No.UILU-ENG-2006-2006).

Lau, A., Anson, M. (2006). Effect of high temperatures on high performance steel fibre reinforced concrete, *Cement and Concrete Research*, **36**(9), 1698-1707.

Lawler, J. S. (2007). Guidelines for concrete mixtures containing supplementary cementitious materials to enhance durability of bridge decks, NCHRP Report 566. USA: Transportation Research Board.

Lee, K., Lee, H., Lee, S., Kim, G. (2006). Autogenous shrinkage of concrete containing granulated blast-furnace slag, *Cement and Concrete Research*, **36**(7), 1279-1285.

Li, V. C., Yang, E. H., Li, M. (2008). Field demonstration of durable link slabs for jointless bridge decks based on strain-hardening cementitious composites-phase 3: shrinkage control. Michigan Department of Transportation.

Li, J., Yao, Y. (2001). A study on creep and drying shrinkage of high performance concrete, *Cement and Concrete Research*, **31**(8), 1203-1206.

Li, V. C., Mishra, D. K., Wu, H.-C. (1995). Matrix design for pseudo-strain-hardening fibre reinforced cementitious composites, *Materials and Structures*, **28**(10), 586-595.

Li, V. C., Stang, H. (1997). Interface property characterization and strengthening mechanisms in fiber reinforced cement based composites, *Advanced Cement Based Materials*, **6**(1), 1-20.

Li, V. C., Wang, Y., Backer, S. (1990). Effect of inclining angle, bundling and surface treatment on synthetic fibre pull-out from a cement matrix, *Composites*, **21**(2), 132-140.

Li, Z. (2011). Advanced concrete technology. 1st edition. USA & Canada: John Wiley & Sons.

Li, Z., Qi, M., Li, Z., Ma, B. (1999). Crack width of high-performance concrete due to restrained shrinkage, *Journal of materials in civil engineering*, **11**(3), 214-223.

Lindquist, W. D. (2008). Development and construction of low-cracking high-performance concrete (LC-HPC) bridge decks: Free shrinkage, mixture optimization, and concrete production. Ph.D. thesis. University of Kansas, USA.

Löfgren, I. (2005). Fibre-reinforced Concrete for Industrial Construction-a fracture mechanics approach to material testing and structural analysis. Ph.D. thesis. Chalmers University of Technology, Göteborg, Sweden.

Lura, P., Pease, B., Mazzotta, G. B., Rajabipour, F., Weiss, J. (2007). Influence of shrinkage-reducing admixtures on development of plastic shrinkage cracks, *ACI Materials Journal*, **104**(2), 187-194.

Markovic, I. (2006). High-performance hybrid-fibre concrete: development and utilisation. Ph.D. thesis. TU Delft, Delft University of Technology, Netherlands.

Markovic, I., Walraven, J., Van, M. (2003). Self compacting hybrid fiber concrete-mix design, workability and mechanical properties, *Proceedings of third international symposium on self-compacting concrete*, 763-775.

McKeel Jr, W. (1985). Evaluation of deck durability on continuous beam highway bridges, FHWA/VA-85/32, VHTRC 85-R32**:** 28.

McLeod, H. A. K. (2009). Development and construction of low-cracking high-performance concrete (LC-HPC) bridge decks: Construction methods, specifications, and resistance to chloride ion penetration. Ph.D. thesis. University of Kansas, USA.

Mehta, P. K., Monteiro, P. J. M. (2006). Concrete: Microstructure, properties and materials. 3rd edition. USA: McGraw-Hill.

Mehta, P. K., Monteiro, P. J. M. (2014). Concrete: Microstructure, properties and materials. 4th edition. New York: McGraw-Hill Education.

Meyers, C. (1982). Survey of cracking on underside of classes B-1 and B-2 concrete bridge decks in district 4, *Investigation No. 82-2*,(Division of Material and Research, Missouri Highway and Transportation Department. Jefferson City. MO).

Mihashi, H., Ahmed, S. F. U., Kobayakawa, A. (2011). Corrosion of reinforcing steel in fiber reinforced cementitious composites, *Journal of Advanced Concrete Technology*, **9**(2), 159-167.

Mihashi, H., Nishiwaki, T. (2014). Tailoring Hybrid Strain-Hardening Cementitious Composites, *ACI Materials Journal*, **111**(2), 220-230.

Mindess, S., Young, J. F., Darwin, D. (2003). Concrete. 2nd edition. Upper Saddle River, NJ: Prentice Hall.

Minelli, F., Plizzari, G. (2010). Fiber reinforced concrete characterization through round panel test–Part II: Analytical and numerical study. *Proceedings of 7th international conference on fracture mechanics of concrete and concrete structures FRaMCoS*.

Mo, K. H., Yap, K. K. Q., Alengaram, U. J., Jumaat, M. Z. (2014). The effect of steel fibres on the enhancement of flexural and compressive toughness and fracture characteristics of oil palm shell concrete, *Construction and Building Materials*, **55**, 20-28.

Mobasher, B., Li, C. Y. (1996). Mechanical properties of hybrid cement-based composites, *ACI Materials Journal*, **93**, 284-292.

Morris, J. (2002). A comparative study of shrinkage and cracking of high performance concrete mixtures for bridge decks. Ph.D. thesis. West Virginia University,

Naaman, A. E., Najm, H. (1991). Bond-slip mechanisms of steel fibers in concrete, *ACI Materials Journal*, **88**(2), 135-145.

Naaman, A.E., Reinhardt, H. W., (1995), High Performance Fiber Reinforced Cement Composites, *Pre-Proceeding: 2nd International Workshop*, June **2**, 11-14.

Nallathambi, P., Karihaloo, B., Heaton, B. (1984). Effect of specimen and crack sizes, water/cement ratio and coarse aggregate texture upon fracture toughness of concrete, *Magazine of Concrete Research*, **36**(129), 227-236.

Nassif, H., Aktas, K., Najm, H. (2007). Concrete shrinkage analysis for bridge deck concrete, Technical Report FHWA-NJ-2007-007. USA, New Jersey Department of Transportation**:** 1-115.

Neville, A. M. (1995). Properties of concrete. 4th edition. UK: Pearson Education Limited.

Nili, M., Ehsani, A. (2015). Investigating the effect of the cement paste and transition zone on strength development of concrete containing nanosilica and silica fume, *Materials & Design*, **75**, 174-183.

Nmai, C., Tomita, R., Hondo, F., Buffenbarger, J. (1998). Shrinkage-reducing admixtures, *Concrete International*, **20**(4), 31-37.

Noushini, A., Vessalas, K., Arabian, G., Samali, B. (2014). Drying shrinkage behaviour of fibre reinforced concrete incorporating polyvinyl alcohol fibres and fly ash, *Advances in Civil Engineering*, **2014**, 1-10.

Odendaal, C. M. (2015). Establishment of performance-based specifications for the structural use of locally available macro-synthetic fibres. M.Sc. thesis. Stellenbosch: Stellenbosch University,

Okuyucu, D., Turanlı, L., Uzal, B., Tankut, T. (2011). Some characteristics of fibre-reinforced semi-lightweight concrete with unexpanded perlite, *Magazine of Concrete Research*, **63**(11), 837-846.

Ostertag, C. P., Blunt, J. (2008). Use of fiber reinforced concrete in bridge approach slabs, Report No. CA09-0632**:** 79.

Paillere, A. M., Buil, M., Serrano, J. (1989). Effect of fiber addition on the autogenous shrinkage of silica fume, *ACI Materials Journal*, **86**(2), 139-144.

Passuello, A., Moriconi, G., Shah, S. P. (2009). Cracking behavior of concrete with shrinkage reducing admixtures and PVA fibers, *Cement and Concrete Composites*, **31**(10), 699-704.

Paulsson-Tralla, J., Silfwerbrand, J. (2002). Estimation of chloride ingress in uncracked and cracked concrete using measured surface concentrations, *ACI Materials Journal*, **99**(1), 27-36.

PCA. The Portland Cement Association. (1969). Durability of concrete bridge decks: A cooperative study.

Pease, B., Rajabipour, F., Moon, J.-H., Weiss, J. (2006). Quantifying the influence of specimen geometry on the results of the restrained ring test, *Journal of ASTM international*, **3**(8), 1-14.

Pickett, G. (1956). Effect of aggregate on shrinkage of concrete and a hypothesis concerning shrinkage, *Journal Proceedings*, **52**(1), 581-590.

Pidwirny, M. 2006. Atmospheric humidity. Fundamentals of physical geography. 2nd edition.Available at:http://www.physicalgeography.net/fundamentals/8c.html. Accessed by 05/10/2016.

Poppe, J. (1981). Factors affecting the durability of concrete bridge decks, *Rep. No. FHWA/CA/SD-81/2, Division of Transportation Facility, California Department of Transportation, Sacramento, Calif*.

Preteseille, M., Lenoir, T., Gennesseaux, E., Hornych, P. (2014). Structural test at the laboratory scale for the utilization of stabilized fine-grained soils in the subgrades of High Speed Rail infrastructures: Analytical and numerical aspects, *Construction and Building Materials*, **61**, 164-171.

Qi, C., Weiss, J., Olek, J. (2003). Characterization of plastic shrinkage cracking in fiber reinforced concrete using image analysis and a modified Weibull function, *Materials and Structures*, **36**(6), 386-395.

Qian, C., Stroeven, P. (2000). Development of hybrid polypropylene-steel fibre-reinforced concrete, *Cement and Concrete Research*, **30**(1), 63-69.

Qiao, P., McLean, D. I., Zhuang, J. (2010). Mitigation strategies for early-age shrinkage cracking in bridge decks, Report No. WA-RD 747.1**:** 10.

Quangphu, N., Linhua, J., Jiaping, L., Qian, T., Tienquan, D. (2008). Influence of shrinkage-reducing admixture on drying shrinkage and mechanical properties of high-performance concrete, *Water Science and Engineering*, **1**(4), 67-74.

Quiroga, P. N., Fowler, D. W. (2004). The effects of aggregates characteristics on the performance of Portland cement concrete, International Center for Aggregates Research, University of Texas at Austin.

Radlinska, A., Pease, B., Weiss, J. (2007). A preliminary numerical investigation on the influence of material variability in the early-age cracking behavior of restrained concrete, *Materials and Structures*, **40**(4), 375-386.

Radlinska, A., Rajabipour, F., Bucher, B., Henkensiefken, R., Sant, G., Weiss, J. (2008). Shrinkage mitigation strategies in cementitious systems: A closer look at differences in sealed and unsealed behavior, *Transportation Research Record: Journal of the Transportation Research Board*(2070), 59-67.

Radocea, A. (1992). A study on the mechanism of plastic shrinkage of cement-based materials. Göteborg, Sweden: Chalmers University of Technology.

Rajabipour, F., Sant, G., Weiss, J. (2008). Interactions between shrinkage reducing admixtures (SRA) and cement paste's pore solution, *Cement and Concrete Research*, **38**(5), 606-615.

Rajabipour, F., Wright, J., Laman, J., Radlińska, A., Morian, D., Jahangirnejad, S., Cartwright, C. (2012). Longitudinal cracking in concrete at bridge deck dams on structural rehabilitation projects, Report No. FHWA-PA-2012-006-100303, Citeseer**:** 220.

Rambo, D. A. S., de Andrade Silva, F., Toledo Filho, R. D. (2014a). Mechanical behavior of hybrid steel-fiber self-consolidating concrete: materials and structural aspects, *Materials & Design*, **54**, 32-42.

Rambo, D. A. S., Silva, F. d. A., Toledo Filho, R. D. (2014b). Flexural behavior of hybrid steel fiber reinforced self-consolidating concretes, *Rem: Revista Escola de Minas*, **67**(1), 27-32.

Ramey, G. E., Wolff, A. R., Wright, R. L. (1997). Structural design actions to mitigate bridge deck cracking, *Practice Periodical on Structural Design and Construction*, **2**(3), 118-124.

Rashiddadash, P., Ramezanianpour, A. A., Mahdikhani, M. (2014). Experimental investigation on flexural toughness of hybrid fiber reinforced concrete (HFRC) containing metakaolin and pumice, *Construction and Building Materials*, **51**, 313-320.

Redon, C., Li, V. C., Wu, C., Hoshiro, H., Saito, T., Ogawa, A. (2001). Measuring and modifying interface properties of PVA fibers in ECC matrix, *Journal of materials in civil engineering*, **13**(6), 399-406.

Richard, W. B. (1998). The visible and invisible cracking of concrete, *ACI monograph*(11), 1-5.

Rossi, P., Acker, P., Malier, Y. (1987). Effect of steel fibres at two different stages: the material and the structure, *Materials and Structures*, **20**(6), 436-439.

Rougelot, T., Skoczylas, F., Burlion, N. (2009). Water desorption and shrinkage in mortars and cement pastes: experimental study and poromechanical model, *Cement and Concrete Research*, **39**(1), 36-44.

Şahmaran, M., Li, M., Li, V. C. (2007). Transport properties of engineered cementitious composites under chloride exposure, *ACI Materials Journal*, **104**(6), 604-611.

Şahmaran, M., Yaman, I. O. (2007). Hybrid fiber reinforced self-compacting concrete with a high-volume coarse fly ash, *Construction and Building Materials*, **21**(1), 150-156.

Şahmaran, M., Yildirim, G., Erdem, T. K. (2013). Self-healing capability of cementitious composites incorporating different supplementary cementitious materials, *Cement and Concrete Composites*, **35**(1), 89-101.

Şahmaran, M., Yucel, H. E., Demirhan, S., Arik, M. T., Li, V. C. (2012). Combined effect of aggregate and mineral admixtures on tensile ductility of engineered cementitious composites, *ACI Materials Journal*, **109**(6), 627-638.

Schmitt, T. R., Darwin, D. (1995). Cracking in concrete bridge decks, Project No. K-TRAN: KU-94-1, Report No. 39. Lawrence, Kansas, University of Kansas Center for Research, Inc.**:** 151.

Schmitt, T. R., Darwin, D. (1999). Effect of material properties on cracking in bridge decks, *Journal of Bridge Engineering*, **4**(1), 8-13.

Shah, H., Weiss, J. (2006). Quantifying shrinkage cracking in fiber reinforced concrete using the ring test, *Materials and Structures*, **39**(9), 887-899.

Shah, S., Krguller, M., Sarigaphuti, M. (1992). Effects of shrinkage-reducing admixtures on restrained shrinkage cracking of concrete, *ACI Materials Journal*, **89**(3), 289-295.

Shah, S., Ludirdja, D., Daniel, J., Mobasher, B. (1988). Toughness-durability of glass fiber reinforced concrete systems, *ACI Materials Journal*, **85**(5), 352-360.

Shah, S. P., Marikunte, S., Yang, W., Aldea, C. (1997). Control of cracking with shrinkage-reducing admixtures, *Transportation Research Record: Journal of the Transportation Research Board*(1574), 25-36.

Shaikh, F. (2013). Deflection hardening behaviour of short fibre reinforced fly ash based geopolymer composites, *Materials & Design*, **50**, 674-682.

Sherir, M. A., Hossain, K., Lachemi, M. (2015). Structural performance of polymer fiber reinforced engineered cementitious composites subjected to static and fatigue flexural loading, *Polymers*, **7**(7), 1299-1330.

Shilstone, J. S. (1990). Concrete mixture optimization, *Concrete International*, **12**(6), 33-39.

Snyder, M. J., Lankard, D. R. (1972). Factors affecting the flexural strength of steel fibrous concrete strength of steel fibrous concrete, *Journal Proceedings*, **69**(2), 96-100.

Song, P., Hwang, S. (2004). Mechanical properties of high-strength steel fiber-reinforced concrete, *Construction and Building Materials*, **18**(9), 669-673.

Song, P., Hwang, S., Sheu, B. (2005). Strength properties of nylon-and polypropylene-fiber-reinforced concretes, *Cement and Concrete Research*, **35**(8), 1546-1550.

Soroushian, P., Bayasi, Z. (1991). Fiber type effects on the performance of steel fiber reinforced concrete, *ACI Materials Journal*, **88**(2), 129-134.

Stähli, P., Sutter, M., Van Mier, J. (2007). Improving the mechanical properties of HFC by adjusting the filling method, *Fifth International RILEM Workshop on High*

Performance Fiber Reinforced Cement Composites-HPFRCC5, Mainz, Germany, 23-30.

Stock, A., Hannantt, D., Williams, R. (1979). The effect of aggregate concentration upon the strength and modulus of elasticity of concrete, *Magazine of Concrete Research*, **31**(109), 225-234.

Sun, W., Chen, H., Luo, X., Qian, H. (2000). Influence of hybrid fibers and expansive agent on the physical and mechanical properties of high performance concrete, *Proc. of the Int. Sym. on High Performance Concrete–Workability, Strength and Durability, Hong Kong*, 209-218.

Tangtermsirikul, S. (1995). Class C fly ash as a shrinkage reducer for cement paste, *Special Publication*, **5**(37), 385-402.

Tazawa, E.-i., Miyazawa, S. (1995). Influence of cement and admixture on autogenous shrinkage of cement paste, *Cement and Concrete Research*, **25**(2), 281-287.

Tia, M., Subramanian, R., Brown, D., Broward, C. (2005). Evaluation of shrinkage cracking potential of concrete used in bridge decks in Florida-UF Project No. 4910-4504-797-12, Final report for the Florida Department of Transportation. University of Florida, Department of Civil and Coastal Engineering, Gainesville, FL**:** 141.

TRB (2006). Control of cracking in concrete: State of the art, *Transportation Research Board-Transportation Research Circular E-C107*, 46.

Tritsch, N., Darwin, D., Browning, J. (2005). Evaluating shrinkage and cracking behavior of concrete using restrained ring and free shrinkage tests, SM Report No. 77. The Transportation Pooled Fund Program Project No. TPF-5 (051). Lawrence, Kansas, University of Kansas Center for Research, Inc.**:** 178.

Uotinen, L. K. T. (2011). Design of shotcrete rock reinforcement in hard rock according to Eurocode. *Proceeding of: Seminar on Geoengineering, Espoo, Finland*.

Van Gysel, A. (2000). Studie van het uittrekgedrag van staalvezels ingebed in een cementgebonden matrix met toepassing op staalvezelbeton onderworpen aan buiging.

Van Mier, J. G. (1997). Fracture process of concrete: Assessment of material parameters for fracture models. Boca Raton, Florida, USA: CRC Press.

Vandewalle, L. (2002). RILEM TC162-TDF: Test and design methods for Steel Fibre Reinforced Concrete: Bending test (final recommendation), *Materials and Structures*, **35**, 579-582.

VDOT. Virginia Department of Transportation. (2016). Road and bridge specifications, 1047.

Vogel, H. M., Svecova, D. (2012). Evaluation of elastic modulus for high-strength concrete, *ACI Materials Journal*, **109**(3).

Voigt, T., Bui, V. K., Shah, S. P. (2004). Drying shrinkage of concrete reinforced with fibers and welded-wire fabric, *ACI Materials Journal*, **101**(3), 233-241.

Wan, B., Foley, C., Komp, J. (2010). Concrete cracking in new bridge decks and overlays, Report No. WHRP 10-05. Milwaukee, Wisconsin, USA, Marquette University, Department of Civil, Construction, and Environmental Engineering**:** 142.

Wang, K., Jansen, D. C., Shah, S. P., Karr, A. F. (1997). Permeability study of cracked concrete, *Cement and Concrete Research*, **27**(3), 381-393.

Wei, S., Mandel, J. A., Said, S. (1986). Study of the interface strength in steel fiber-reinforced cement-based composites, *Journal Proceedings*, **83**(4), 597-605.

Weiss, J., Berke, N. (2003). Admixtures for reduction of shrinkage and cracking, *Report 25: Early Age Cracking in Cementitious Systems-Report of RILEM Technical committee TC 181-EAS: Early age cracking shrinkage induced stresses and cracking in cementitious systems*, **25**, 323.

Weiss, W., Yang, W., Shah, S. (2000). Factors influencing durability and early-age cracking in high-strength concrete structures, *Special Publication*, **189**, 387-410.

Weiss, W. J., Shah, S. P. (1997). Recent trends to reduce shrinkage cracking in concrete pavements, *Aircraft/Pavement Technology In the Midst of Change*, 217-228.

Weiss, W. J., Yang, W., Shah, S. P. (1998). Shrinkage cracking of restrained concrete slabs, *Journal of Engineering Mechanics*, **124**(7), 765-774.

Whiting, D. A., Detwiler, R. J., Lagergren, E. S. (2000). Cracking tendency and drying shrinkage of silica fume concrete for bridge deck applications, *ACI Materials Journal*, **97**(1).

Wiegrink, K., Marikunte, S., Shah, S. P. (1996). Shrinkage cracking of high-strength concrete, *ACI Materials Journal*, **93**(5), 409-415.

Yan, H., Sun, W., Chen, H. (1999). The effect of silica fume and steel fiber on the dynamic mechanical performance of high-strength concrete, *Cement and Concrete Research*, **29**(3), 423-426.

Yang, K.-H. (2011). Tests on concrete reinforced with hybrid or monolithic steel and polyvinyl alcohol fibers, *ACI Materials Journal*, **108**(6), 664-672.

Yao, W., Li, J., Wu, K. (2003). Mechanical properties of hybrid fiber-reinforced concrete at low fiber volume fraction, *Cement and Concrete Research*, **33**(1), 27-30.

Yap, S. P., Alengaram, U. J., Jumaat, M. Z. (2013). Enhancement of mechanical properties in polypropylene–and nylon–fibre reinforced oil palm shell concrete, *Materials & Design*, **49**, 1034-1041.

Yazıcı, Ş., İnan, G., Tabak, V. (2007). Effect of aspect ratio and volume fraction of steel fiber on the mechanical properties of SFRC, *Construction and Building Materials*, **21**(6), 1250-1253.

Yoo, D.-Y., Yoon, Y.-S., Banthia, N. (2015). Flexural response of steel-fiber-reinforced concrete beams: Effects of strength, fiber content, and strain-rate, *Cement and Concrete Composites*, **64**, 84-92.

Yücel, H. E. (2013). Design of crack-free, durable and ductile concrete for sustainable highway rigid pavement overlays. Ph.D. thesis. University of Gaziantep, Gaziantep, Turkey.

Yurtseven, A. E. (2004). Determination of mechanical properties of hybrid fiber reinforced concrete. M.Sc. thesis. Middle East Technical University,

Zhang, J., Li, V. C. (2001). Influences of fibers on drying shrinkage of fiber-reinforced cementitious composite, *Journal of Engineering Mechanics*, **127**(1), 37-44.

Zhang, M.-H. (1995). Microstructure, crack propagation, and mechanical properties of cement pastes containing high volumes of fly ashes, *Cement and Concrete Research*, **25**(6), 1165-1178.

PERSONAL INFORMATION

Name and Surname : Qais Sahib BANYHUSSAN
Nationality : Iraq
Birth place and date : Baghdad/1976
Marital status : Married – 4 kids
Mobile number : +90 5360734801 in Turkey
+964 7700198342 in Iraq
E-mail : qb19235@mail2.gantep.edu.tr
qaisbanyhussan@gmail.com
qaisalmusawi@yahoo.com

EDUCATION

Degree	Graduate School	Year
Master	University of Al-Mustansiriya	2005
Bachelor	University of Al-Mustansiriya	2001
High School	Al-Noor High School	1995

WORK EXPERIENCE

Year	Place	Enrollment
2005-2010	University of Al-Mustansiriya	Assistant Lecturer
2010-Present	University of Al-Mustansiriya	Lecturer
2010-2012	University of Al-Mustansiriya	Manger of registration and student offers

PUBLICATIONS

Banyhussan, Q. S. (2010a).Effect of Aggregate Gradation on Reducing Reflection Crack, *Journal of Engineering and Development*, Vol. **14**, No. 2,212-225.

Banyhussan, Q. S. (2010b).The importance of Traffic Studies in the New Construction Highways: Case Study Abu-Gar Highway, *Journal of Engineering and Development*, Vol. **14**, No. 4,32-52.

Asmael, N. M., Ahmed I. A., **Banyhussan, Q. S**. (2010).Effect of Additives Types and Contents on the Properties of Stone Matrix Asphalt Mixtures, *Engineering and Technology*, **28**(21), 6414-6426.

Banyhussan, Q. S. (2011). Evaluation and Improvement The Performance of Al-Qudus At-Grade Intersection in Baghdad city, *Journal of Engineering and Development*, Vol. **15**, No. 2,19-48.

Yousif, R. A., **Banyhussan, Q. S**., Ellk, D. S. (2012). Effect of Additives Types and Contents on Permanent Deformation, *Journal of Engineering and Development*, Vol. **16**, No. 3,225-268.

Yildirim, G., Aras, G. H., **Banyhussan, Q. S**., Şahmaran, M., Lachemi, M. (2015). Estimating the self-healing capability of cementitious composites through non-destructive electrical-based monitoring. *Ndt & E International*, **76**, 26-37.

Banyhussan, Q. S., Yıldırım, G., Bayraktar, E., Demirhan, S., Şahmaran, M. (2016). Deflection-hardening hybrid fiber reinforced concrete: The effect of aggregate content. *Construction and Building Materials*, **125**, 41-52.